MASSACHUSETTS INSTITUTE OF TECHNOLOGY
DEPARTMENT OF NUCLEAR ENGINEERING

Cambridge, Massachusetts 02139

MIT-2344-9 MITNE-79

HEAVY WATER LATTICE PROJECT
ANNUAL REPORT

September 30, 1966

Contract AT(30-1)-2344

U.S. Atomic Energy Commission

MASSACHUSETTS INSTITUTE OF TECHNOLOGY
DEPARTMENT OF NUCLEAR ENGINEERING
Cambridge, Massachusetts 02139

MIT-2344-9 MITNE-79
AEC Research and Development Report
UC-34 Physics
(TID-4500, 47th Edition)

HEAVY WATER LATTICE PROJECT ANNUAL REPORT

September 30, 1966

Contract AT(30-1)-2344
U.S. Atomic Energy Commission

Editors:

T. J. Thompson
I. Kaplan
M. J. Driscoll

Contributors:

J. H. Barch
N. L. Berube
H. E. Bliss
K. D. Bowles
E. J. Chase
H. S. Cheng
F. M. Clikeman
M. J. Driscoll
I. A. Forbes
D. Frech
J. W. Gosnell
T. L. Harper
J. Harrington, III
F. H. Hauck
M. G. Johnson
I. Kaplan
B. Kelley
L. T. Papay
E. E. Pilat
L. N. Price
N. C. Rasmussen
R. L. Ricketts
E. Sefchovich
S. S. Seth
A. T. Supple
T. J. Thompson
G. L. Woodruff

DISTRIBUTION

MIT-2344-9 MITNE-79

AEC Research and Development Report

UC-34 Physics

1. USAEC, New York Operations Office, Library
2-4. USAEC, Reactor Physics Branch, Division of Reactor Development and Technology
5. USAEC, New York Patents Office, Brookhaven National Lab.
6. USAEC, Cambridge Branch, New York Operations Office, Research Contracts Division
7. USAEC, Division of Reactor Development and Technology
8. USAEC, HWOCR Branch
9. USAEC, Water Projects Branch
10. USAEC, Core Design Branch
11. USAEC, Division of Naval Reactors
12. Advisory Committee on Reactor Physics (E. R. Cohen)
13. ACRP (G. Dessauer)
14. ACRP (R. Fluharty)
15. ACRP (E. Gaerttner)
16. ACRP (R. Ehrlich)
17. ACRP (F. C. Maienschein)
18. ACRP (J. Chernick)
19. ACRP (R. Avery)
20. ACRP (M. Nelkin)
21. ACRP (F. Dawson)

22. ACRP (G. Hansen)

23. ACRP (W. B. Loewenstein)

24. ACRP (L. W. Nordheim)

25. ACRP (T. M. Snyder)

26. ACRP (R. Bayard)

27-29. D. T. I. E., Oak Ridge, for Standard Distribution

30-100. Internal Distribution

101. Combustion Engineering (S. Visner)

102. Brookhaven National Laboratories (H. Kouts)

ABSTRACT

An experimental and theoretical program on the physics of heavy water moderated, slightly enriched lattices is being conducted at the Massachusetts Institute of Technology. During the past year, work was completed on studies of fast neutron distributions, lattices with added neutron absorbers, miniature lattices, two-region lattices, pulsed neutron source methods, and single-rod experiments. In the past year, measurements were also completed on six lattices: three spacings each for 0.75-inch- and 0.387-inch-diameter, 0.947% enriched, uranium metal fuel.

TABLE OF CONTENTS

1. Introduction 1
    1. Forward 1
    2. Staff 1
    3. References 3

2. Material Buckling Measurements 4
    1. Introduction 4
    2. Experimental Methods 4
    3. Results 5
    4. References 5

3. Measurement of Integral Parameters 13
    1. Parameter Measurements 13
    2. Foil Correction Factors 21
        2.1 δ_{28} Correction Factor 21
        2.2 δ_{25} and ρ_{28} Correction Factors 23
    3. ρ_{28} Measurement Techniques 26
        3.1 Discussion 26
        3.2 Experimental Studies 26
            3.2.1 Test of Method B 29
            3.2.2 Test of Method A 30
    4. References 30

4. Pulsed Neutron Studies 31
    1. Introduction 31
    2. Theory 31
    3. Experimental Equipment 34
    4. Analysis of Data 37
    5. Results and Conclusions 38
    6. References 46

5. Use of Neutron Absorbers in the Determination of Lattice Parameters 48
    1. Introduction 48
    2. Theory 49

2.1 The Multiplication Factor k_∞ and the Four-Factor Formula 49
2.2 The PCTR Technique 51
2.3 The Material Buckling 52
2.4 The Subcritical Technique for Measuring k_∞ 53
3. Experiments 54
4. Calculation of the Spatially-Dependent Thermal Neutron Spectrum 56
5. Results 56
5.1 Measurement of k_∞ 56
5.2 Measurement of L^2 61
5.3 Measurement of η 62
6. Reduction of the Amount of Fuel Required: Suggestion for Future Research 63
7. Conclusions 63
8. References 64

6. Buckling Methods 67
1. Moments Analysis 67
1.1 Axial Buckling 67
1.2 Radial Buckling 68
2. Diagonal Buckling 68
2.1 Experiments 71
2.2 Data Analysis 71
3. References 74

7. Intracellular Flux Traverses with Lutetium 75
1. Introduction 75
2. Experimental Procedures 75
3. Results 75
4. References 79

8. Miniature Lattice Studies 80
1. Introduction 80
2. Experimental Techniques and Facilities 82
2.1 Experimental Facilities 82
2.2 Experimental Techniques 83

3. Theoretical Methods 83
3.1 Subcritical Assemblies 84
3.2 Critical and Infinite Assemblies 85
3.3 Test of the Theory 87
3.4 Correction Procedures for Lattice Parameters 88
4. Results 92
4.1 Axial and Radial Traverses of R_{Au}-1 92
4.2 Intracellular Activity Distribution of Gold 101
4.3 The Parameters ρ_{28}, δ_{28}, δ_{25} and C^* 105
5. Nuclear Constants Which Appear in the Theory and Extrapolation Corrections 116
5.1 Thermal Energy Parameters for the Lattice-Born Neutrons 116
5.2 Nuclear Parameters for Source Neutrons 117
5.3 Value of k_∞ 117
5.4 Values of S_{Au}, S_{28} and S_{25} 118
6. Discussion of Results 121
7. Conclusions 123
8. References 124

9. Fast Neutron Distributions 126

10. Noise Analysis 128
1. Introduction 128
2. Noise Analysis System 128
3. Detector Studies 129
4. References 133

11. Void Reactivity Measurements 136
1. Introduction 136
2. Simulated Fuel Assembly 136
3. Test Procedure 136
4. Interpretation of Results 136
5. Conclusions 140
6. References 140

12. Gamma-Ray Spectra of Lattice Fuel 141
1. Introduction 141
2. Description of Apparatus 141
3. Results and Applications 143
4. Conclusions 146
5. References 146

13. Two-Region Lattices 148
1. Gold-Cadmium Ratios 148
2. δ_{28} Measurements 148
3. R_{28} Measurements 155
4. Present Work 155

14. Single Rod Studies 156
1. Introduction 156
2. Theoretical Methods 158
3. Applications in the Thermal Region 159
4. The Resonance Region 162
5. The Fast Region 169
6. Conclusions 174
7. References 178

Appendix A. Bibliography of Heavy Water Lattice Project Publications 180
1. Doctoral Theses on MITR Heavy Water Lattice Project 180
2. M.S. Theses on MITR Heavy Water Lattice Project 182
3. Lattice Project Publications 184
3.1 Prior to September 30, 1965 184
3.2 Publications (including theses) Since September 30, 1965 187

LIST OF FIGURES

3.1.1 Variation of δ_{28} with Volume Fraction Fuel 16

3.1.2 Variation of ρ_{28} with Volume Fraction Fuel 17

3.1.3 Variation of δ_{25} with Volume Fraction Fuel 18

3.1.4 Variation of C^* with Volume Fraction Fuel 19

3.2.1 Comparison of Theory and Experiment for δ_{28} Correction Factor 24

3.3.1 Schematic Representations of the Epicadmium and Subcadmium Np^{239} Activity Distribution in a Fuel Rod 27

3.3.2 Two Variations of the ADM Procedure for ρ_{28} 28

4.1 Schematic of Overall Pulsing, Detection and Analysis Circuitry 36

4.2 Measured Decay Constant λ for the 500 Lattice as a Function of Geometric Buckling B^2 39

5.1 Neutron Life Cycle in a Thermal Neutron Reactor (Infinite Medium) 50

5.2 Relative Activation Distribution in 250B1 Assembly as a Function of Radial Position 57

5.3 Relative Activation Distribution in Four 250 Assemblies as a Function of Axial Position 58

5.4 Relative Thermal Activation Distribution Near Center Fuel Rod in 250A2 Assembly 59

6.1 Foil Holder Position for Diagonal Traverse 72

6.2 Diagonal Activation Traverses 73

7.1 Lu^{177} Activity Distribution in a Lattice of 0.25-Inch-Diameter, 1.143% U-235 Rods on a 1.75-Inch Triangular Pitch 76

7.2 Lu^{177} and Au^{198} Activity Distributions in a Lattice of 0.75-Inch-Diameter, 0.947% U-235 Rods on a 2.5-Inch Triangular Pitch 77

7.3 Lu^{177} Activity Distribution in a Lattice of 0.75-Inch-Diameter, 0.947% U-235 Rods on a 5-Inch Spacing 78

8.1 Axial Distribution for Cadmium Ratio of Gold in ML2 93

8.2 Axial Distribution of Cadmium Ratio of Gold in ML7 94

8.3 Axial Distribution of Cadmium Ratio of Gold in ML3 95

8.4 Axial Distribution of Cadmium Ratio of Gold in ML4 96

8.5 Axial Distribution of Cadmium Ratio of Gold in ML6 97

8.6	Axial Distribution of Cadmium Ratio of Gold in ML5	98
8.7	Radial Distribution of Cadmium Ratio of Gold in ML2	100
8.8	Relative Radial Activity Distribution of Gold in ML7, 9.75 Inches from Source End	102
8.9	Subcadmium Activity Distribution in ML7 Before and After Correction to Infinite System	103
8.10	Intracellular Activity Distribution of Gold in ML2	104
8.11	Intracellular Activity Distribution of Gold in ML4, 9 Inches from Source End	106
8.12	Intracellular Activity Distribution of Gold in ML4, 13 Inches from Source End	107
8.13	Intracellular Activity Distribution of Gold in ML7	108
8.14	Intracellular Activity Distribution of Gold in ML6	109
8.15	Intracellular Activity Distribution of Gold in ML3	110
8.16	Intracellular Activity Distribution of Gold in ML5	111
8.17	Variation of the Function $\psi = pq/\xi\Sigma_s\phi_T$ with Z for ML2 and the Corresponding Exponential Assembly	112
8.18	Variation of the Function $\psi = pq/\xi\Sigma_s\phi_T$ with Z for ML5 and the Corresponding Exponential Assembly	113
10.1	Schematic Circuit Diagram for Cross-Correlation Measurements	130
10.2	Auto-Spectral Density Measurements in M.I.T. Lattice	131
10.3	Detector Efficiencies Required vs. k_{eff} for Noise Spectral Analysis	132
10.4	Sketch of Liquid Scintillation Detector	134
11.1	Simulated Pressure Tube and Fuel Bundle in Lattice	138
12.1	Block Diagram of Compton Suppression Apparatus	142
12.2	Schematic Diagram of Vacuum Dewar and Electronics for Use with Ge(Li) Gamma-Ray Detector	144
12.3	UO_2 Spectrum Number 60611 Using Compton Suppression	145
13.1	Gold Foil Activities in Assembly XI	150
13.2	Gold-Cadmium Ratios in Assembly XI	151
13.3	δ_{28} in Assembly III, 1.027% Enriched, 1/4-Inch Diameter	153
13.4	δ_{28} in Assembly IX, 2-1/2-Inch Spacing	154
14.1	Relative Np^{239} Activity in Depleted Uranium Foils of Various Sizes in Heavy Water	163
14.2	The Ratio C^* of Captures in U-238 to Fissions in U-235 vs. Volume Fraction of Fuel in Unit Cell for 1/4-Inch-Diameter, 1.027% Enriched Uranium Metal Rods in D_2O	165

14.3 Functions $C_N(z)$ Appearing in Integrated Form of Line, Annular, and Rod First Flight Kernels 171

14.4 The Single Rod Kernel Giving the Uncollided Flux Around a Single, 0.25-Inch-Diameter, Uranium Rod in Heavy Water 172

14.5 Relative Activity in Triangular Lattice of 0.25-Inch-Diameter, 1.027% Enriched Uranium Metal Fuel Rods on a 1.75-Inch Spacing in D_2O 173

14.6 Fast Fission Ratio vs. Ratio of Fuel Volume to Unit Cell Volume for 1/4-Inch-Diameter Fuel Rods in D_2O 176

14.7 Fast Fission Ratio, δ_{28}, vs. Volume Fraction of Fuel in Cell for Slightly Enriched Uranium Rods of 1/4-Inch Diameter in Light Water 177

LIST OF TABLES

2.1	Buckling Values for 0.75-Inch-Diameter, 0.947% U^{235} Enriched, Uranium Rods (Density of 18.9 gm/cm^3) in a 3.5-Inch Triangular Pitch Lattice	6
2.2	Buckling Values for 0.75-Inch-Diameter, 0.947% U^{235} Enriched, Uranium Rods (Density of 18.9 gm/cm^3) in a 5.0-Inch Triangular Pitch Lattice	7
2.3	Buckling Values for 0.387-Inch-Diameter, 0.947% U^{235} Enriched, Uranium Rods (Density of 18.9 gm/cm^3) in a 1.5-Inch Triangular Pitch Lattice	9
2.4	Buckling Values for 0.387-Inch-Diameter, 0.947% U^{235} Enriched, Uranium Rods (Density of 18.9 gm/cm^3) in a 2.25-Inch Triangular Pitch Lattice	10
2.5	Buckling Values for 0.387-Inch-Diameter, 0.947% U^{235} Enriched, Uranium Rods (Density of 18.9 gm/cm^3) in a 3.0-Inch Triangular Pitch Lattice	12
3.1	Integral Parameter Results for 0.75-Inch-Diameter, 0.947% Enriched Fuel	14
3.2	Integral Parameter Results for 0.387-Inch-Diameter, 0.947% Enriched Fuel	15
3.3	Single Rod Results	20
3.4	Comparison of Correction Factors for ρ_{28} and δ_{25}	25
3.5	Experimental Test of Method B	29
4.1	Description of Lattices Studied	35
4.2	Values of the Infinite Medium Multiplication Factor k_∞	41
4.3	Values of the Absorption Cross Section $\overline{v\Sigma}_a$	42
4.4	Values of the Thermal Diffusion Area L^2	43
4.5	Values of the Multiplication Factor k_∞ in the Test Region of Two-Region Assemblies	44
4.6	Comparison of Values of the Multiplication Factor k_∞ and Absorption Cross Section $\overline{v\Sigma}_a$ in Unmodified Lattices	45
5.1	Lattices Studied	55
5.2	Values of k_∞ Obtained with Equations 5.1 and 5.10	60
5.3	Measured and Calculated Values of the Diffusion Area L^2	62
6.1	Comparison of Axial Buckling Calculations	69
6.2	Comparison of Radial Buckling Calculations	70
6.3	Diagonal Buckling Results	74
8.1	Lattices Investigated	82

8.2	Summary of Results for Subcritical Assemblies	86
8.3	Parameters Used in MINIFLUX Calculations	99
8.4	Experimental Data and Extrapolated Results for Lattices with 1.143% Enriched Fuel	114
8.5	Experimental Data and Extrapolated Results for Lattices with 1.027% Enriched Fuel	115
8.6	Progress of Iteration Procedure to Obtain k_∞	119
8.7	Relation Between the Values of S in Different Assemblies	120
8.8	Values of τ_{Au}, τ_{28} and τ_{25} in the Lattices Studied	122
11.1	Comparative HWOCR Fuel Assembly Parameters	137
11.2	Estimate of Reactivity Changes and Void Coefficients of the Test Assembly for 7- and 19-Rod Runs	139
12.1	Comparison of Theory and Experiment	147
13.1	Two-Region Assemblies Tested in the M.I.T. Lattice Facility	149
13.2	δ_{28} Measurements	152
13.3	R_{28} Measurements	155
14.1	Values of the Thermal Utilization for Lattices of Slightly Enriched Uranium Rods in Heavy Water	161
14.2	Geometric and Nuclear Constants	166
14.3	Values of ρ_{28}, the Ratio of Epicadmium to Subcadmium Capture in U-238, and of C^*, the Ratio of Capture in U-238 to Fission in U-235, for 1/4-Inch-Diameter, Uranium Metal Rods in D_2O	167
14.4	Values of Resonance Integrals for Fission in U^{235}, as Determined from Measurements of δ_{25}	168
14.5	Data Used in Calculations of δ_{28}	174
14.6	Values of δ_{28} for Slightly Enriched Uranium Rods in Heavy Water	175

1. INTRODUCTION

1. FORWARD

This report is the sixth annual progress report of the Heavy Water Lattice Project of the Massachusetts Institute of Technology. The first five progress reports describe development of the facility and experimental methods and give results for nine lattice spacings of three different sets of uranium metal fuel (1, 2, 3, 4, 5).

Work was completed on four major project areas during the past year: fast neutron distributions, lattices with added absorbers, pulsed neutron methods, and miniature lattice studies. This report contains brief summaries of the topical reports issued in these areas, plus progress reports on continuing work in a number of other areas. In addition, this report presents information on six more lattice spacings: three each for 0.75-inch- and 0.387-inch-diameter, 0.947% enriched, uranium metal fuel.

The report covers work done primarily in the period of October 1, 1965 through September 30, 1966. The terminal date also conveniently coincides with the end of the work phase concerned with metal-fueled lattices. Thus, while oxide-fueled lattice studies were also initiated in September, 1966, preceded by some preliminary investigations, it was convenient to limit this report to metal-fueled lattices.

2. STAFF

The project staff, including thesis students, during the report period was as follows:

*I. Kaplan, Professor of Nuclear Engineering
*T. J. Thompson, Professor of Nuclear Engineering
*M. J. Driscoll, Assistant Professor of Nuclear Engineering
*F. M. Clikeman, Assistant Professor of Nuclear Engineering

---

*Continuing on staff as of October 1, 1966.

[+]H. E. Bliss, Hertz Fellow (to Sept. 1966)
[+]K. D. Bowles, SM student (to Sept. 1966)
[*+]E. J. Chase, SM student (since June 1966)
[*]H. S. Cheng, Research Assistant, ScD student (since June 1966)
[*+]I. A. Forbes, Special project student
[*+]D. Frech, SM student
[*+]J. W. Gosnell, ScD student
[+]T. L. Harper, SM student
[+]J. Harrington, III, AEC Fellow, ScD student (to March 1966)
[+]F. H. Hauck, SM student (to Sept. 1966)
[+]M. G. Johnson, SM student (to Sept. 1966)
[*+]L. T. Papay, ScD student
[*]E. E. Pilat, Research Assistant, ScD student
[+]L. N. Price, SM student (to Sept. 1966)
[+]R. L. Ricketts, SM student (to Sept. 1966)
E. Sefchovich, Research Assistant, ScD student (to Oct. 1966)
[*]S. S. Seth, Research Assistant, SM student (since Feb. 1966)
C. Stassis, Research Assistant (to Feb. 1966)
[+]G. L. Woodruff, ScD student (to Jan. 1966)
J. H. Barch, Senior Technician (to Oct. 1966)
[*]A. T. Supple, Jr., Senior Technician
[*]N. L. Berube, Technician
[*]R. DiMartino, Technician (after Nov. 1966)
[*]Miss Barbara Kelley, Technical Assistant
[*]D. A. Gwinn, Part-time Electronics Supervisor

---

[*]Continuing on staff as of October 1, 1966.
[+]Salary not paid from contract funds.

3. REFERENCES

Previous Annual Reports:

(1) "Heavy Water Lattice Research Project Annual Report," NYO-9658, September 30, 1961.

(2) "Heavy Water Lattice Project Annual Report," NYO-10208 (MITNE-26), September 30, 1962.

(3) "Heavy Water Lattice Project Annual Report," NYO-10212 (MITNE-46), September 30, 1963.

(4) "Heavy Water Lattice Project Annual Report," MIT-2344-3 (MITNE-60), September 30, 1964.

(5) "Heavy Water Lattice Project Annual Report," MIT-2344-4 (MITNE-65), September 30, 1965.

Other Lattice Project publications are listed in Appendix A: section 3.2, in particular, lists all publications since September 30, 1965.

2. MATERIAL BUCKLING MEASUREMENTS

B. Kelley
J. H. Barch
A. T. Supple
N. L. Berube
F. M. Clikeman

1. INTRODUCTION

Standard methods have been developed to measure the material buckling and the intracellular thermal neutron distributions for the lattices studied in the M.I.T. Lattice Facility (1). Since the last annual report (2), results have been obtained by using these techniques on five lattices of uranium rods in D_2O. The results given in this report are for 0.947% U^{235} enriched, 0.75-inch-diameter rods in triangular lattice spacings of 3.5 and 5.0 inches, and 0.947% U^{235} enriched, 0.387-inch-diameter uranium rods in triangular lattice spacings of 1.5, 2.25 and 3.0 inches.

2. EXPERIMENTAL METHODS

Neutron flux distributions are measured throughout the lattice assembly by activating gold foils, both bare and cadmium-covered. Special aluminum foil holders are used to accurately position the foils throughout the lattice assembly. The relative gold activity is measured in both the radial and axial directions in the tank. The cadmium ratio of gold is then calculated as a function of position to locate that region of the lattice assembly which has an equilibrium neutron spectrum. The relative activities of both the bare and cadmium-covered foils from the equilibrium region are then fitted by least squares to the functional relationship:

$$\phi = AJ_o(\alpha r) \sinh \gamma(H-Z), \qquad (2.1)$$

where

α^2 is the radial buckling in the r direction,
γ^2 is the axial buckling in the Z direction,

and

H is the extrapolated height of the assembly.

The material buckling B_m^2 is then given by,

$$B_m^2 = \alpha^2 - \gamma^2 . \qquad (2.2)$$

Corrections to the measured foil activities for counter deadtime, activity decay times and foil weights, together with the least-squares fitting to Eq. 2.1, are accomplished using an IBM 7094 computer.

A more detailed account of the experimental techniques may be found in reference 1.

3. RESULTS

The results of the measurements of α^2 and γ^2 for five lattices are given in Tables 2.1 through 2.5.

The errors quoted for the buckling measurements are the standard deviation of the individual measurements of the buckling.

4. REFERENCES

(1) Palmedo, P. F., I. Kaplan and T. J. Thompson, "Measurements of the Material Bucklings of Lattices of Natural Uranium Rods in D_2O," NYO-9660 (MITNE-13), January 1962.

(2) "Heavy Water Lattice Project Annual Report," MIT-2344-4 (MITNE-65), September 30, 1965.

Table 2.1

Buckling Values for 0.75-Inch-Diameter, 0.947% U^{235} Enriched, Uranium Rods (Density of 18.9 gm/cm^3) in a 3.5-Inch Triangular Pitch Lattice

D_2O Temperature (°C)	Type of Run	Type of Detector	Run Number	Radial Buckling α^2 ($cm^{-2} \times 10^6$)	Axial Buckling γ^2 ($cm^{-2} \times 10^6$)	Material Buckling B_m^2 ($cm^{-2} \times 10^6$)
27*	Radial	Bare Au	K9	1399		
			L0	1416		
			L2	1398		
			L6	1382		
			L7	1425		
			Average	1404 ± 8		
		Cd-covered Au	L1	1398		
			L3	1380		
			L5	1412		
			L8	1388		
			Average	1395 ± 7		
26**	Axial	Bare Au	M0		5	
			M2		35	
			M4		45	
			Average		28 ± 12	
		Cd-covered Au	L9		40	
			M1		65	
			M3		48	
			M5		32	
			Average		46 ± 7	
Grand average of all axial measurements					39 ± 7	
Grand average of all radial measurements				1400 ± 5		
Material buckling = $\alpha^2 - \gamma^2$ =						1361 ± 9

* Average of temperatures ranging from 24-31°C

** Average of temperatures ranging from 24-27°C

Table 2.2

Buckling Values for 0.75-Inch-Diameter, 0.947% U^{235} Enriched Uranium Rods (Density of 18.9 gm/cm^3) in a 5.0-Inch Triangular Pitch Lattice

D_2O Temperature (°C)	Type of Run	Type of Detector	Run Number	Radial Buckling α^2 ($cm^{-2} \times 10^6$)	Axial Buckling γ^2 ($cm^{-2} \times 10^6$)	Material Buckling B_m^2 ($cm^{-2} \times 10^6$)
27° *	Radial	Bare Au	G9	1408		
			H2	1420		
			H5	1415		
			I1	1394		
			I2	1404		
			I3	1425		
			I4	1437		
			I5	1412		
			I6	1413		
			J2	1387		
			J4	1389		
			J5	1388		
			J8	1428		
			K0	1418		
			Average	1410 ± 4		
		Cd.-covered Au	H3	1396		
			H4	1387		
			H7	1396		
			Average	1393 ± 3		

* Average of temperatures ranging from 24-30°C.

Table 2.2 (continued)

Buckling Values for 0.75-Inch-Diameter, 0.947% U^{235} Enriched, Uranium Rods (Density of 18.9 gm/cm^3) in a 5.0-Inch Triangular Pitch Lattice

D_2O Temperature (°C)	Type of Run	Type of Detector	Run Number	Radial Buckling α^2 ($cm^{-2} \times 10^6$)	Axial Buckling γ^2 ($cm^{-2} \times 10^6$)	Material Buckling B_m^2 ($cm^{-2} \times 10^6$)
27°C**	Axial	Bare Au	H6		255	
			H9		261	
			I0		275	
			J9		260	
			K1		298	
			K4		250	
			K6		300	
			K7		285	
			Average		273 ± 7	
		Cd.-covered Au	H8		288	
			J1		305	
			J3		310	
			J7		268	
			K3		247	
			K5		273	
			Average		282 ± 10	
Grand average of all axial measurements					277 ± 6	
Grand average of all radial measurements				1407 ± 4		
Material buckling = $a^2 - \gamma^2$ =						1130 ± 7

** Average temperature ranging from 24-29°C.

Table 2.3

Buckling Values for 0.387-Inch-Diameter, 0.947% U^{235} Enriched, Uranium Rods (Density of 18.9 gm/cm^3) in a 1.5-Inch Triangular Pitch Lattice

D_2O Temperature (°C)	Type of Run	Type of Detector	Run Number	Radial Buckling α^2 ($cm^{-2} \times 10^6$)	Axial Buckling γ^2 ($cm^{-2} \times 10^6$)	Material Buckling B_m^2 ($cm^{-2} \times 10^6$)
26° *	Radial	Bare Au	N4	2375		
			N6	2373		
			N7	2382		
			N9	2373		
			P3	2390		
			P6	2374		
			Average	2378 ± 3		
		Cd.-covered Au	N3	2364		
			N5	2347		
			P0	2335		
			P2	2342		
			P4	2354		
			Average	2348 ± 5		
27° **	Axial	Bare Au	O2		1397	
			O4		1403	
			O9		1381	
			Average		1394 ± 7	
		Cd.-covered Au	N8		1420	
			O3		1456	
			O5		1425	
			O6		1406	
			P1		1382	
			Average		1418 ± 12	
Grand average of all axial measurements					1409 ± 9	
Grand average of all radial measurements				2364 ± 5		
Material buckling = $\alpha^2 - \gamma^2$ =						955 ± 10

*
** Average of temperature ranging from 22-30°C.
** Average of temperature ranging from 25-29°C.

Table 2.4

Buckling Values for 0.387-Inch-Diameter, 0.947% U^{235} Enriched, Uranium Rods (Density of 18.9 gm/cm^3) in a 2.25-Inch Triangular Pitch Lattice

D_2O Temperature (°C)	Type of Run	Type of Detector	Run Number	Radial Buckling α^2 ($cm^{-2} \times 10^6$)	Axial Buckling γ^2 ($cm^{-2} \times 10^6$)	Material Buckling B_m^2 ($cm^{-2} \times 10^6$)
28°*	Radial	Bare Au	S1	2390		
			S3	2408		
			S5	2419		
			U3	2441		
			U4	2445		
			Average	2421 ± 10		
		Cd.-covered Au	S4	2395		
			S6	2379		
			S7	2401		
			S8	2376		
			T9	2392		
			U2	2419		
			Average	2394 ± 6		

* Average of temperatures ranging from 24-31°C.

Table 2.4 (continued)

Buckling Values for 0.387-Inch-Diameter, 0.947% U^{235} Enriched, Uranium Rods (Density of 18.9 gm/cm^3) in a 2.25-Inch Triangular Pitch Lattice

D_2O Temperature (°C)	Type of Run	Type of Detector	Run Number	Radial Buckling α^2 ($cm^{-2} \times 10^6$)	Axial Buckling γ^2 ($cm^{-2} \times 10^6$)	Material Buckling B_m^2 ($cm^{-2} \times 10^6$)
29°**	Axial	Bare Au	T1		1133	
			T2		1169	
			T4		1156	
			T5		1171	
			T7		1120	
			U0		1124	
			Average		1146 ± 9	
		Cd.-covered Au	S9		1177	
			T0		1138	
			T3		1205	
			T6		1171	
			T8		1208	
			U1		1176	
			Average		1179 ± 10	
Grand average of all axial measurements					1162 ± 8	
Grand average of all radial measurements				2406 ± 7		
Material buckling = $\alpha^2 - \gamma^2$ =						1244 ± 11

** Average of temperatures ranging from 25-31°C.

Table 2.5

Buckling Values for 0.387-Inch-Diameter, 0.947% U^{235} Enriched, Uranium Rods (Density of 18.9 gm/cm^3) in a 3.0-Inch Triangular Pitch Lattice

D_2O Temperature (°C)	Type of Run	Type of Detector	Run Number	Radial Buckling α^2 ($cm^{-2} \times 10^6$)	Axial Buckling γ^2 ($cm^{-2} \times 10^6$)	Material Buckling B_m^2 ($cm^{-2} \times 10^6$)
25°C*	Radial	Bare Au	Q9	2446		
			R1	2444		
			R3	2415		
			R6	2473		
			R8	2448		
			Average	2445 ± 9		
		Cd.-covered Au	Q4	2346		
			Q7	2420		
			R0	2375		
			R2	2399		
			R5	2348		
			R7	2427		
			Average	2386 ± 15		
24°C**	Axial	Bare Au	P9		1382	
			Q1		1332	
			Q5		1348	
			R4		1387	
			Average		1362 ± 13	
		Cd.-covered Au	Q0		1365	
			Q2		1386	
			Q6		1384	
			Q8		1394	
			Average		1382 ± 6	
Grand average of all axial measurements					1372 ± 8	
Grand average of all radial measurements				2413 ± 11		
Material buckling = $\alpha^2 - \gamma^2$ =						1041 ± 14

* Average of temperatures ranging from 23-27°C.
** Average of temperatures ranging from 23-26°C.

3. MEASUREMENT OF INTEGRAL PARAMETERS

S. S. Seth, L. N. Price and M. J. Driscoll

Work continues on the measurement of the integral parameters ρ_{28}, δ_{28}, δ_{25} and C^*. During the past year, measurements were completed on six lattices: 3 spacings for each of two sets of 0.947% enriched uranium metal rods, 0.387-inch diameter and 0.750-inch diameter (1). Work was also completed on a number of single rod measurements (1) and on the theoretical analysis of foil packet correction factors (2). A feasibility study was started on a new method for making ρ_{28} measurements (1, 2).

1. PARAMETER MEASUREMENTS (S. Seth)

The following integral parameters were measured using standard techniques (1, 3).

$$\rho_{28} = \frac{\text{epicadmium } U^{238} \text{ capture rate}}{\text{subcadmium } U^{238} \text{ capture rate}}$$

$$\delta_{25} = \frac{\text{epicadmium } U^{235} \text{ fission rate}}{\text{subcadmium } U^{235} \text{ fission rate}}$$

$$\delta_{28} = \frac{U^{238} \text{ fission rate}}{U^{235} \text{ fission rate}}$$

$$C^* = \frac{U^{238} \text{ capture rate}}{U^{235} \text{ fission rate}}$$

Tables 3.1 and 3.2 list the results for the two fuel diameters studied during the past year. Figures 3.1.1 through 3.1.4 show plots of the data versus volume fraction fuel in the unit cell. The expected linear variation is evident in all cases.

Table 3.3 presents the four sets of metal fuel single rod measurements made during 1966.

Table 3.1

Integral Parameter Results for 0.75-Inch-Diameter, 0.947% Enriched Fuel

Lattice Spacing[1] (Inches)	δ_{28}	ρ_{28}	δ_{25}	C*
2.5 [7]	0.0615 (3) ± 0.0021 (2)	1.358 (3) ± 0.026		
3.5 [4]	0.0516 ± 0.0032	0.6453 ± 0.0019	0.0528 ± 0.0035	0.786 ± 0.031
5.0 [6]	0.0489 ± 0.0017	0.3341 ± 0.0011	0.0270 ± 0.0020	0.650 ± 0.028
∞ [2] (single rod)	0.0463 ± 0.0023	0.0856 ± 0.0160	0.0060 ± 0.0012	0.537 ± 0.041
	0.0419 ± 0.0020 (3)			
	0.0431 ± 0.0012 (4)			

(1) Numbers in brackets in this column are the number of measurements made for each parameter.

(2) The standard deviations shown include Student's T factor.

(3) S. P. Hellman result, reference 4.

(4) L. T. Papay result, reference 5.

Table 3.2

Integral Parameter Results for 0.387-Inch-Diameter, 0.947% Enriched Fuel

Lattice Spacing (Inches)	δ_{28}	ρ_{28}	δ_{25}	C^*
1.5 [10]	0.0459 ± 0.0013	1.1515 ± 0.0012	0.0861 ± 0.0016	1.0018 ± 0.0082
2.25 [10]	0.0326 ± 0.0010	0.5184 ± 0.0017	0.0367 ± 0.0012	0.7339 ± 0.0067
3.0 [9]	0.0291 ± 0.0018	0.3108 ± 0.0021	0.0218 ± 0.0024	0.6399 ± 0.0018
∞ [2] (Single rod)	0.0259 ± 0.0020	0.0384 ± 0.0030	0.0030 ± 0.0019	0.5153 ± 0.0032

Same notation as Table 3.1 .

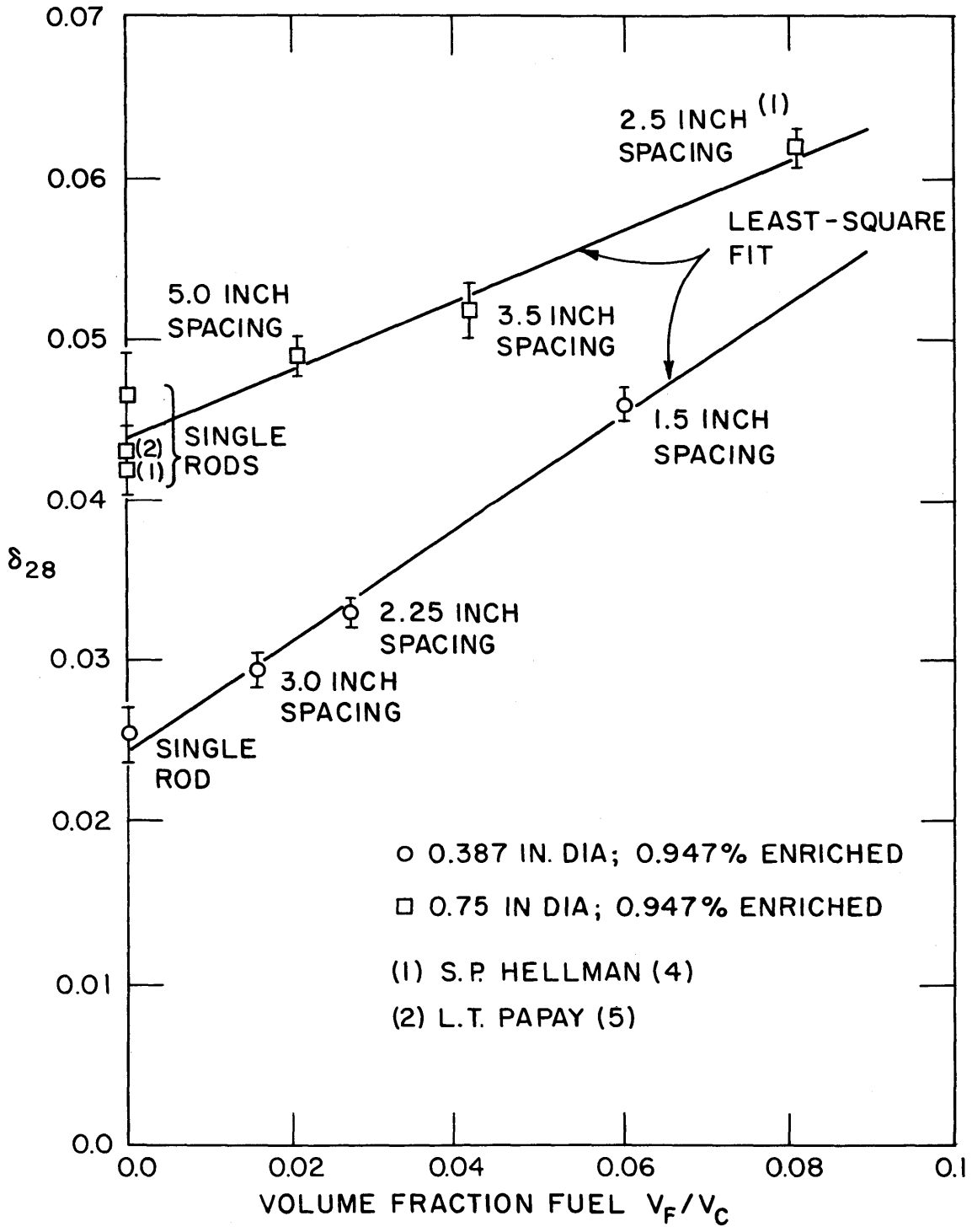

FIG. 3.1.1 VARIATION OF δ_{28} WITH VOLUME FRACTION FUEL

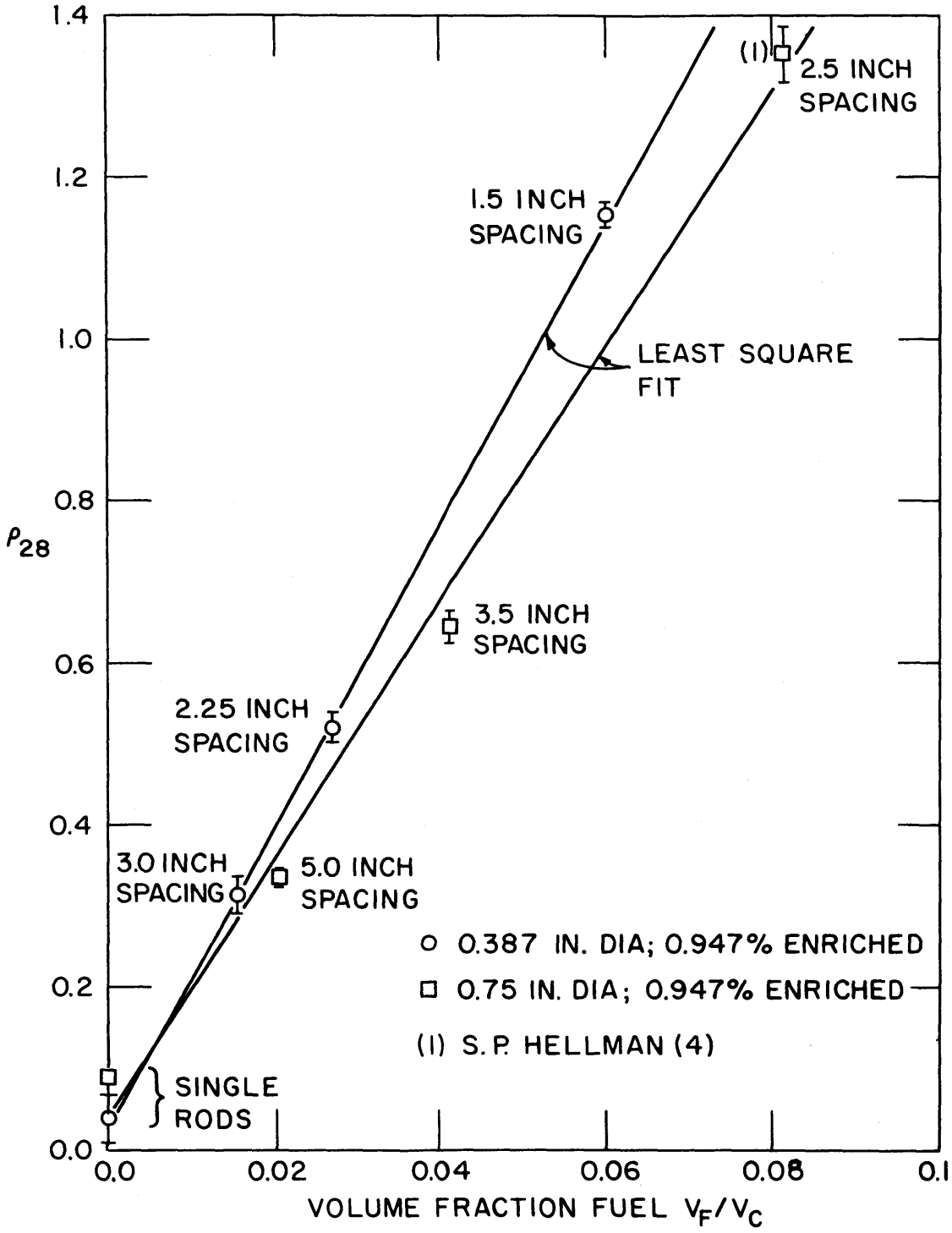

FIG. 3.1.2 VARIATION OF ρ_{28} WITH VOLUME FRACTION FUEL

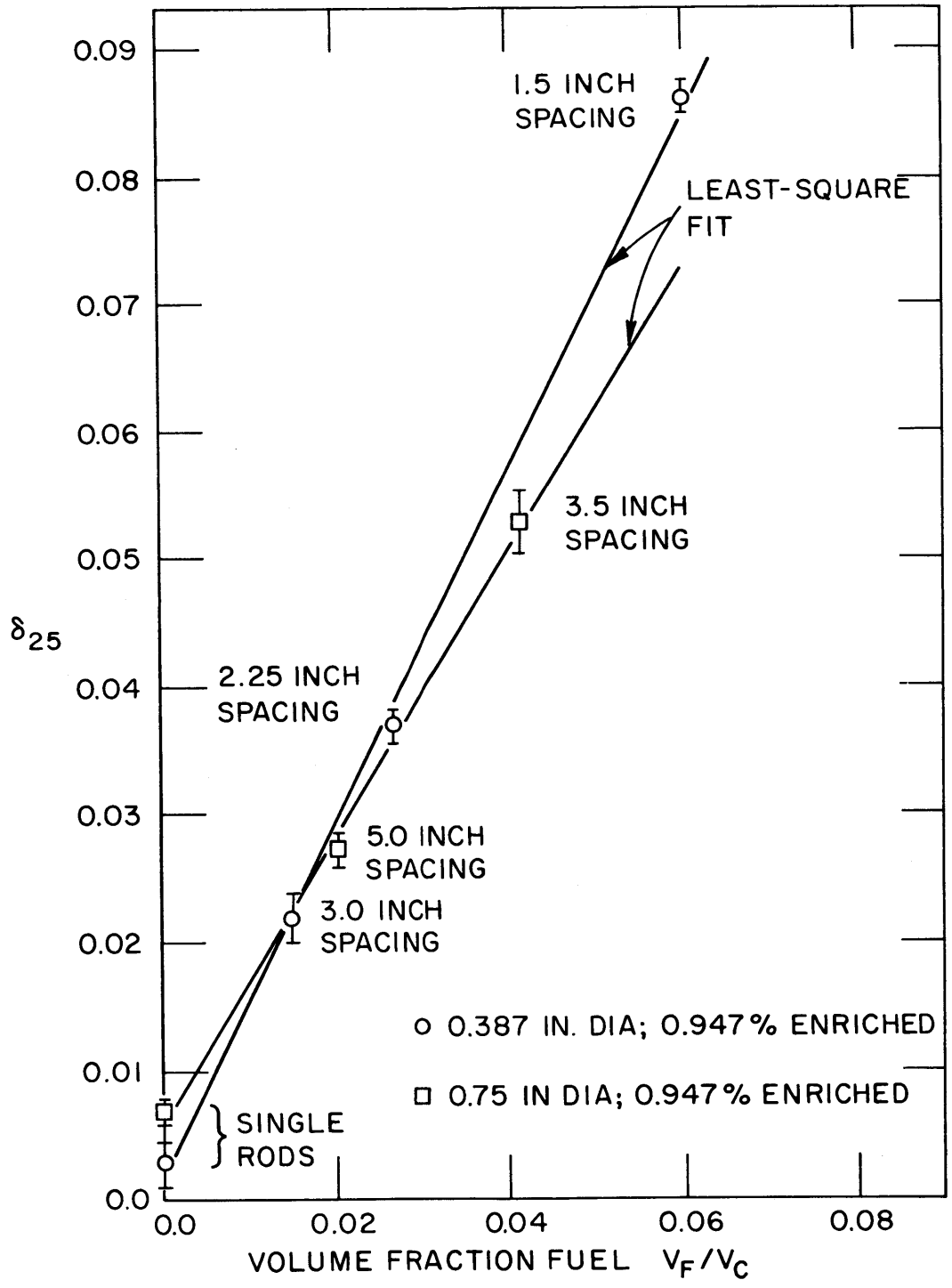

FIG. 3.1.3 VARIATION OF δ_{25} WITH VOLUME FRACTION FUEL

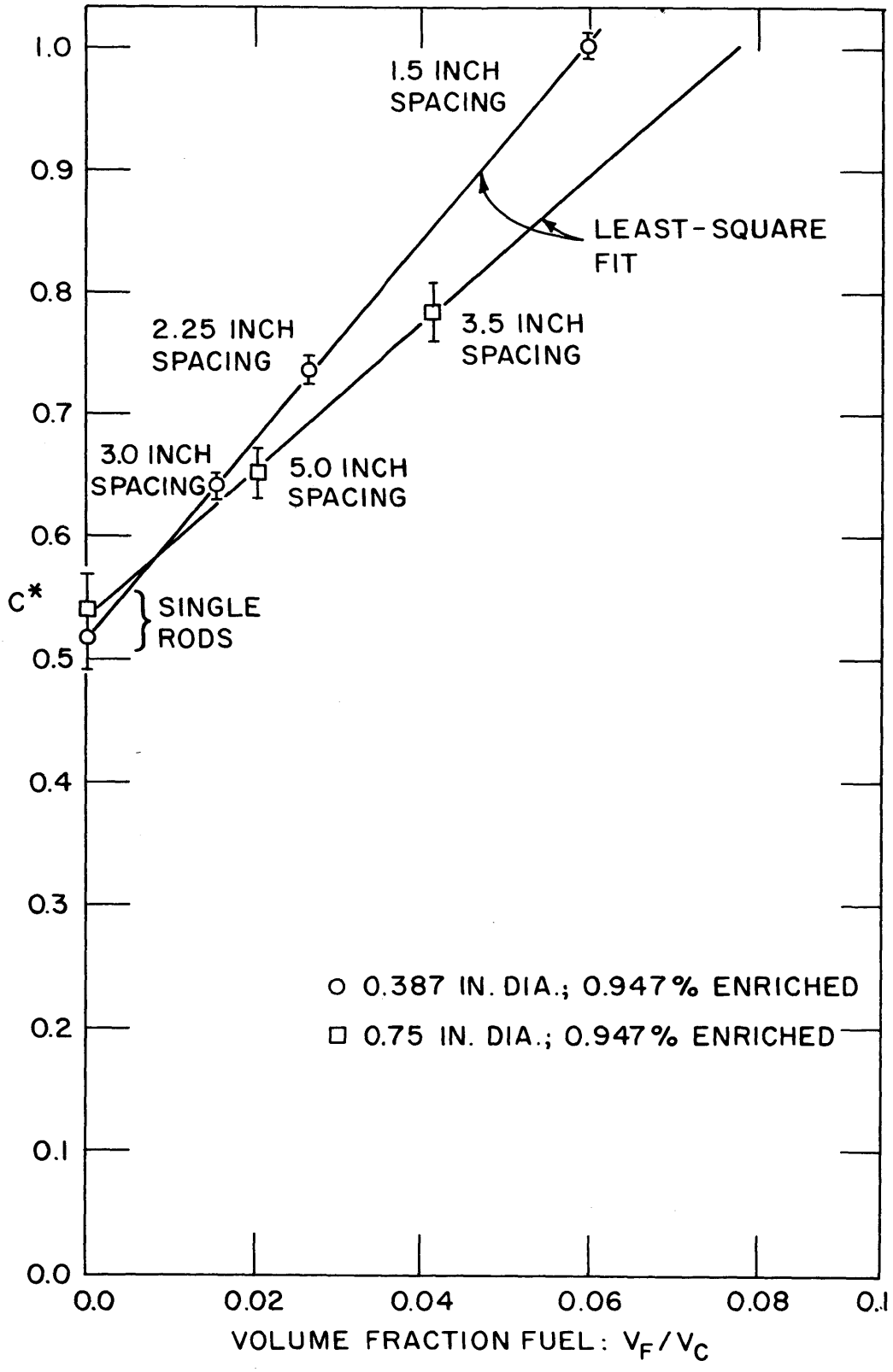

FIG. 3.1.4 VARIATION OF C^* WITH VOLUME FRACTION FUEL

Table 3.3

Single Rod Results

Rod Diameter (Inches)	Fuel Enrichment %	δ_{28}	ρ_{28}	δ_{25}	C^*
0.75 [2]	0.947	0.0463 ± 0.0023	0.0856 ± 0.0016	0.0066 ± 0.0012	0.537 ± 0.041
0.387 [2]	0.947	0.0259 ± 0.0020	0.0384 ± 0.0030	0.0030 ± 0.0019	0.5153 ± 0.0032
0.25 [2]	1.143	0.0197 ± 0.0031	0.028 ± 0.006	0.0011 ± 0.0012	0.420 ± 0.003
1.01 [2]	0.714 (natural)	0.0627 ± 0.0052	0.1066 ± 0.0083	0.0081 ± 0.0022	0.7302 ± 0.0095

Same notation as Table 3.1 .

2. FOIL CORRECTION FACTORS (L. Price)

The most important correction factors associated with the measurement of integral parameters are made necessary by the fast source depression and the corresponding decrease in foil activity due to the reduction in the number of first flight interactions:

a) in measurements of δ_{28}, a depleted uranium detector foil covered with aluminum catcher foils is used. The removal of U^{235} in and near the detector foil results in a decrease in the number of thermal fissions and therefore a decrease in the fast source, which reduces the number of U^{238} fissions;

b) in measurements of ρ_{28} and δ_{25}, the thermal fissions inside and near cadmium-covered foil packets are suppressed. There is consequently a decrease in the local fast source which reduces both the number of first flight captures in U^{238} and first flight fissions in U^{235}.

In most previous work at M. I. T. and elsewhere, the correction factors have been determined experimentally. Because the corrections are small, the experimental approach is difficult: for the same reason, however, it is possible to develop simple analytical methods for making the corrections which are sufficiently accurate (2).

2.1 δ_{28} Correction Factor

On the basis of the following assumptions, it is possible to calculate a correction factor for δ_{28}:

a) δ_{28} is a linear function of the volume fraction of fuel in the unit cell (V_f/V_c), with an ordinate intercept given by the single rod value and a slope approximated by a homogeneous model:

$$\delta_{28} = \delta_{28}(SR) + \bar{\nu} \frac{\Sigma_f^{28}}{\Sigma_r D_2O} \left(\frac{V_f}{V_c} \right), \tag{3.1}$$

where $\bar{\nu}$ is the mean number of neutrons per fission in U^{235}. Substituting $\bar{\nu} = 2.43$, $\Sigma_f^{28} = 0.0146\ cm^{-1}$, $\Sigma_r D_2O = 0.093\ cm^{-1}$:

$$\delta_{28} \approx \delta_{28}(SR) + 0.382\left(\frac{V_f}{V_c}\right), \tag{3.2}$$

which is in good agreement with experimental correlations.

b) $\delta_{28}(SR)$ depends upon the mean chord length, $\bar{\ell}$, of a neutron emitted inside a fuel rod.

$$\delta_{28}(SR) = \frac{\bar{\nu}\Sigma_f^{28}\bar{\ell}}{1 - \bar{\nu}\Sigma_f^{28} \cdot \bar{\ell}} = \frac{0.0355\,\bar{\ell}}{1 - 0.0355\,\bar{\ell}} . \tag{3.3}$$

Here $\bar{\ell}$ is given by the approximation:

$$\bar{\ell} \approx \left(\frac{2d}{3}\right) e^{-\frac{2d}{3\lambda u}} \tag{3.4}$$

in which

d = fuel rod diameter,

λu = removal mean free path for uranium metal $\approx$ 10 cm.

Equations 3.3 and 3.4 give good agreement with experiment:

Rod Diameter (Inches)	$\delta_{28}(SR)$ Theory	Experiment
0.25	0.0147	0.0151
0.75	0.0406	0.0409
1.01	0.0535	0.0551

With the above approximations, it is then possible to develop a multiplicative factor, M_{28}, to convert the measured δ_{28}^{o} value into the correct value:

$$\delta_{28} = M_{28} \cdot \delta_{28}^{o} ,$$

where

$$M_{28} = \left[1 - \frac{\bar{w}}{\bar{\ell} + \lambda_R^{D_2O}\left(\frac{V_f}{V_c}\right)\left[1 - \bar{\nu}\Sigma_f^{28}\bar{\ell}\right]} \right]^{-1} \tag{3.5}$$

The parameter $\overline{w}$ is the mean chord length which the fast neutrons would have had in the detector foil. It can be calculated from the following approximate expression:

$$\overline{w} = 3/4\ t_e + 1/2\ t_e \ln (d/2t_e) . \tag{3.6}$$

In Eq. 3.6, t_e is the effective thickness of the depleted detector foil:

$$t_e = T + Z_1 f_1 + Z_2 f_2 , \tag{3.7}$$

where

T = depleted foil thickness,

Z_1, Z_2 = spacer foil thicknesses,

f = weighting factor to account for fact that spacers are not as important as detectors in suppressing detector fissions:

$$f = 1 - \frac{[(T/Z)+2] \ln (1+Z/T) + (Z/T) \ln (1+T/Z)}{3 + 2 \ln (d/2T)} \tag{3.8}$$

One final correction remains. If one of the "spacers" is in part a natural uranium foil, as is usually the case for a δ_{28} measurement, then Z_2 is reduced:

$$Z_2^* = (Z_2 - T_n) + T_n \frac{\varepsilon - 0.7104}{\varepsilon} , \tag{3.9}$$

where

T_n = thickness of natural foil,

ε = enrichment of lattice fuel.

Equations 3.5 through 3.9 permit calculation of M_{28} for a variety of experimental conditions. Figure 3.2.1 shows a comparison between previous experimental work done at M.I.T. and the present theoretical expressions.

2.2 δ_{25} and ρ_{28} Correction Factors

Additive correction factors are easily determined in terms of δ_{28}(SR), the calculation of which was discussed in the preceding section:

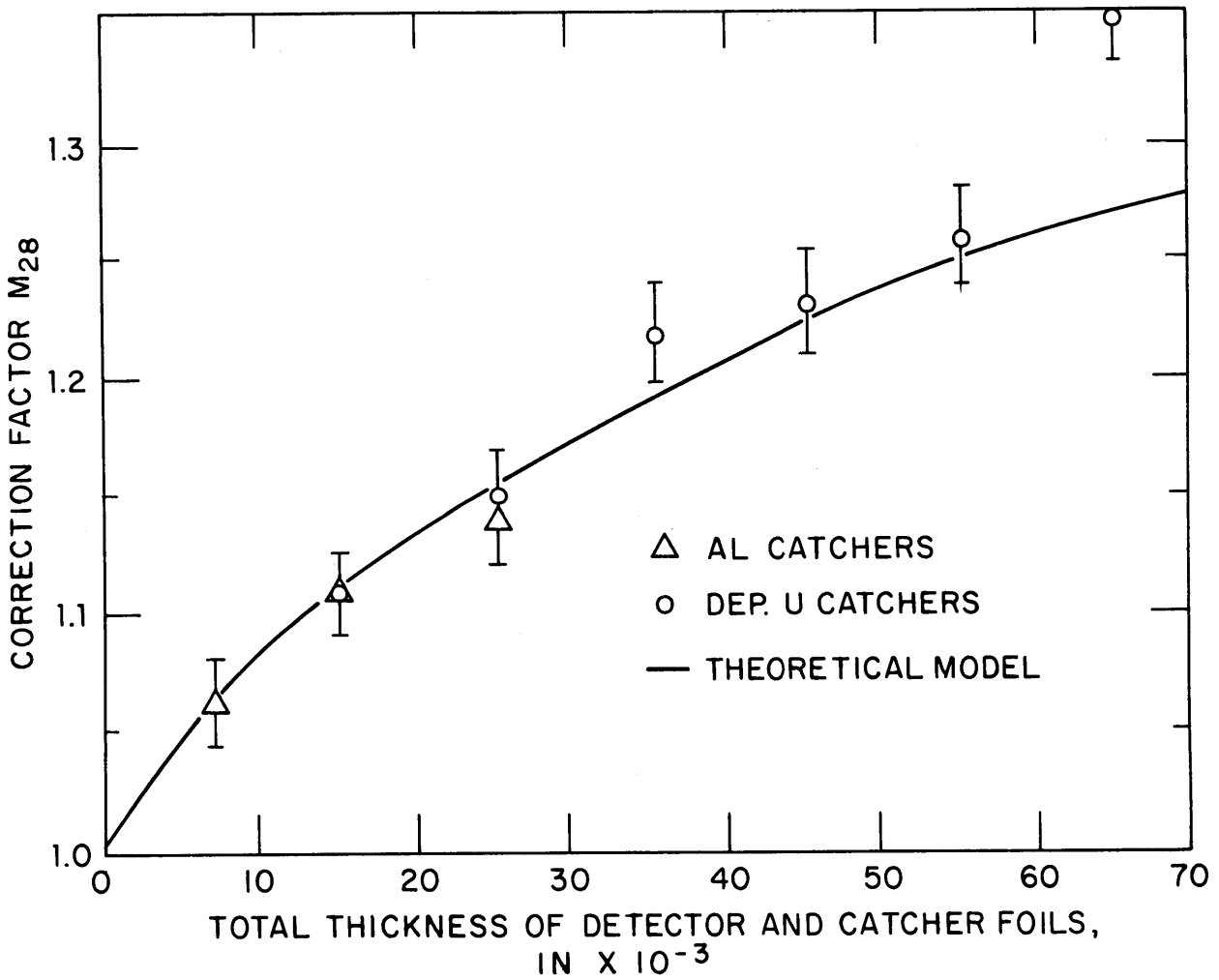

FIG. 3.2.1 COMPARISON OF THEORY AND EXPERIMENT FOR δ_{28} CORRECTION FACTOR

$$\rho_{28} = \rho_{28}^{o} + C_{28} ,$$
$$\delta_{25} = \delta_{25}^{o} + C_{25} . \qquad (3.10)$$

The correction factor C_{28} is given by (2):

$$C_{28} = \left(\frac{\sigma_{n,\gamma}^{28}}{\sigma_f^{28}} \right)_{FAST} \cdot \delta_{28}(SR) \cdot \left(\frac{\sigma_f^{25}}{\sigma_a^{28}} \right)_{MAXW} \cdot \frac{238}{235} \cdot \frac{\varepsilon}{1 - \varepsilon} . \qquad (3.11)$$

Substitution of fission spectrum and thermal (Maxwellian) avaraged cross sections gives:

$$C_{28} = 62.52 \; \delta_{28}(SR) \frac{\varepsilon}{1 - \varepsilon} . \qquad (3.12)$$

Similarly:

$$C_{25} = \left(\frac{\sigma_f^{25}}{\sigma_f^{28}} \right)_{FAST} \cdot \delta_{28}(SR) \cdot \frac{238}{235} \frac{\varepsilon}{1 - \varepsilon} , \qquad (3.13)$$

$$C_{25} = 4.435 \; \delta_{28}(SR) \frac{\varepsilon}{1 - \varepsilon} . \qquad (3.14)$$

In the above expressions, ε is the U^{235} concentration of the fuel.

There is very little previous work with which the results of this analysis can be compared. At M.I.T., D'Ardenne (3) used the GAM-1 code and homogenized the unit cell to compute correction factors. Table 3.4 compares his results with those from the present calculations. The agreement is reasonably good in view of the small corrections involved and the approximate nature of both methods, in particular of the homogenized treatment.

Table 3.4

Comparison of Correction Factors for ρ_{28} and δ_{25}
(0.250-Inch-Diameter, 1.027% Enriched Fuel)

Lattice Pitch	C_{28}/ρ_{28}		C_{25}/δ_{25}	
(Inches)	Ref. (3)	This Work	Ref. (3)	This Work
1.25	0.0024	0.0044	0.0053	0.0050
1.75	0.0058	0.0095	0.011	0.0085
2.50	0.013	0.016	0.021	0.014

3. ρ_{28} MEASUREMENT TECHNIQUES (S. Seth, L. Price, M. Driscoll)

3.1 Discussion

There has been considerable interest in avoiding the use of cadmium in the measurement of ρ_{28} in lattices. One procedure which has been developed is the thermal activation technique (6) in which U^{238} and Dy^{164} activations are compared. In this section, the preliminary results of a feasibility study into a new method are reported.

The spatial distributions of epicadmium and subcadmium U^{238} captures within a fuel rod are different, as shown schematically in Fig. 3.3.1. Hence, if one divides a foil into a central and an outer region, the ratio of their activities should be a function of the ratio of epicadmium to subcadmium activations — that is, ρ_{28}. Indeed, it can be shown (2) that:

$$\rho_{28} = \left(\frac{1+r_E}{1+r_S}\right)\left(\frac{r_L - r_S}{r_E - r_L}\right), \tag{3.15}$$

where

r_E = ratio of epicadmium activities: outer/inner parts of foils,

r_S = same ratio, subcadmium,

r_L = same ratio, in lattice fuel rod.

Under the assumption that the epicadmium and subcadmium activation shapes depend only on the fuel rod parameters, r_E and r_S can be determined once in a separate experiment; lattice measurements of r_L then yield ρ_{28} directly.

The method embodied in Eq. 3.15 has several interesting features, the most important of which is that it involves only counting ratios and should thus lead to cancellation of a number of errors.

3.2 Experimental Studies

There are two possible variations of the activity distribution method (called ADM hereafter). As shown in Fig. 3.3.2, the foils can be cut into two parts (Method A); or a one-piece foil can be used and

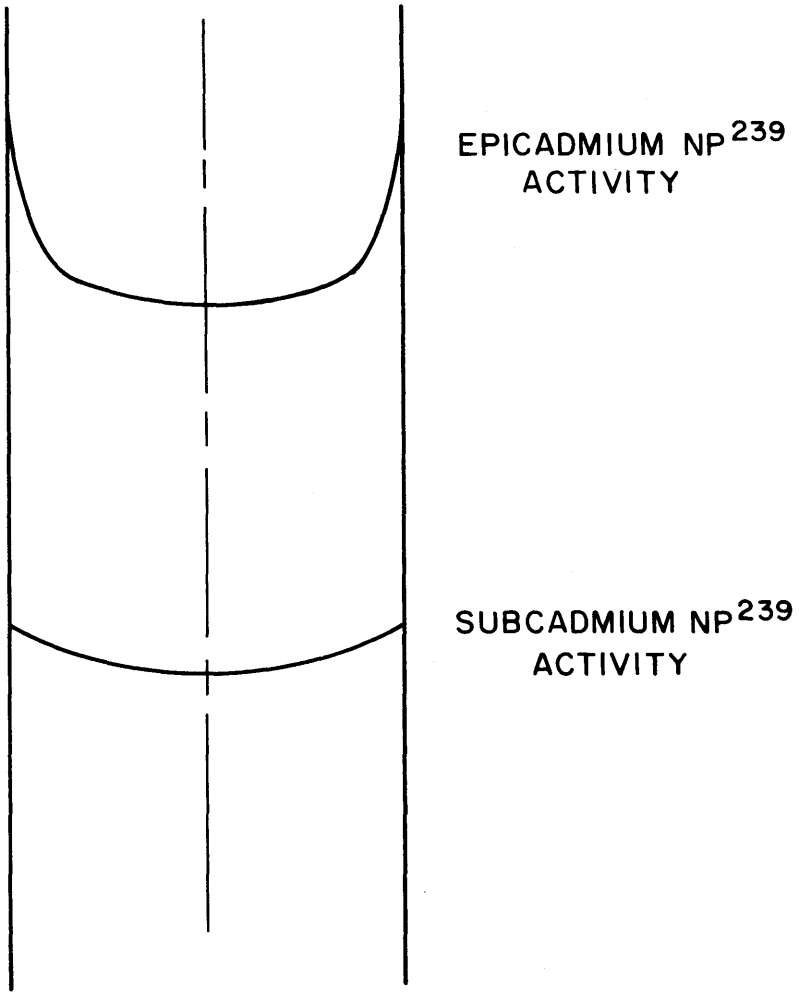

FIG. 3.3.1 SCHEMATIC REPRESENTATIONS OF THE EPICADMIUM AND SUBCADMIUM NP^{239} ACTIVITY DISTRIBUTION IN A FUEL ROD

METHOD A: 2 PIECE FOIL

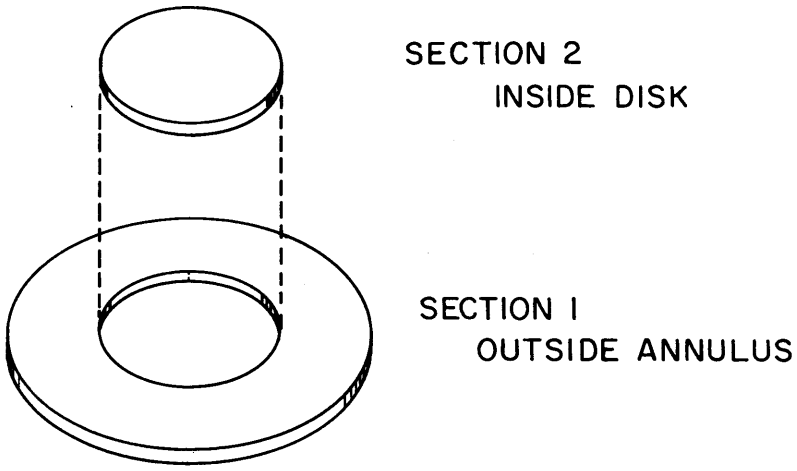

METHOD B: SHIELDED FOIL

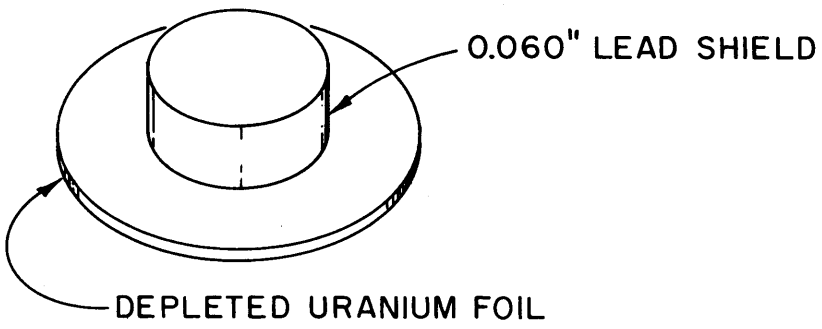

FIG. 3.3.2 TWO VARIATIONS OF THE ADM PROCEDURE FOR ρ_{28}

counted twice, once bare and once with a thin lead shield (Method B). Method B is possible because the 100-kev Np^{239} gamma rays are easily absorbed.

3.2.1 Test of Method B

Since Method B involves changing counting procedures only, it was tested first by using foils already irradiated as part of the standard ρ_{28} measurement program. The measurements were made on a lattice of 0.947% enriched, 0.387-inch-diameter rods, having a 2.25-inch spacing. The results are shown in Table 3.5.

Table 3.5

Experimental Test of Method B

Foil Diameter: 0.387-inch depleted U (18 ppm U^{235})
Shield: 0.246-inch-diameter, 0.060-inch-thick Pb

Run	r_E	r_S	r_L	ADM*	Standard Method*
1	3.4809	1.3095	1.7399	0.4796	–
2	2.9424	1.4878	1.8132	0.4537	–
3	1.7829	1.3936	1.5165	0.5363	0.5255
4	1.8140	1.3310	1.4750	0.4998	0.4626
			Mean	0.492	0.494
			$\pm\sigma$	$\pm$ 0.020	$\pm$ 0.022

* Comparable values, both uncorrected for foil perturbations.

While the ADM results are in good agreement with the ρ_{28} results determined by the standard cadmium ratio technique, the close correspondence must be regarded as somewhat fortuitous, particularly since r_E, which should be constant, varies considerably from run to run. Some of this variation is attributed to unperfected experimental technique for the first two runs, mainly in the accurate placement of the lead counting shield. Since this preliminary study gave promising but inconclusive results, a second experiment was made using Method A.

3.2.2 Test of Method A

Another test of the ADM was performed, this time using Method A in which a two-piece annular test foil was employed. In addition, r_E and r_S were separately determined: r_S was measured inside a rod in a highly thermalized spectrum (near the bottom of the exponential facility) where the epithermal correction was small; r_E was measured high in the lattice where the epithermal component was appreciable.

The measurements were made in an oxide lattice of 1.099% enriched fuel having a 0.431-inch rod diameter on a 2.25-inch spacing. Two ADM runs yielded $\rho_{28} = 0.393 \pm 0.026$, which compares favorably with the mean of four standard runs: $\rho_{28} = 0.412 \pm 0.008$.

Work will continue to determine whether the ADM offers worthwhile advantages over other ρ_{28} methods.

4. REFERENCES

(1) Seth, S. S., "Measurement of the Integral Parameters C^*, δ_{25}, δ_{28}, ρ_{28} in Single Rods and Lattices of Slightly Enriched Uranium in Heavy Water Moderator," S. M. Thesis, M. I. T. Nuc. Eng. Dept., under preparation.

(2) Price, L. N., "A Systematic Study of Foil Correction Factors in the Measurement of δ_{28}, δ_{25}, ρ_{28} and C^* in Slightly Enriched, D_2O Moderated Lattices," S. M. Thesis, M. I. T. Nuc. Eng. Dept., September 1966.

(3) D'Ardenne, W. H., T. J. Thompson, D. D. Lanning and I. Kaplan, "Studies of Epithermal Neutrons in Uranium, Heavy Water Lattices," MIT-2344-2, MITNE-53, August 1964.

(4) Hellman, S. P., "Measurements of δ_{28} and ρ_{28} in a 2.5-Inch Triangular Lattice of 0.75-Inch Metallic Uranium Rods (0.947 % U-235) in a Heavy Water Moderator," S. M. Thesis, M. I. T. Nuc. Eng. Dept., September 1965.

(5) Papay, L. T., "Fast Neutron Fission Effect for Single, Slightly Enriched Uranium Rods in Air and Heavy Water," S. M. Thesis, M. I. T. Nuc. Eng. Dept., June 1965.

(6) Lewis, R. H., T. C. Engelder, D. M. Roberts and D. B. Weyhmeyer, "Thermal Activation Method for ρ_{28} Measurements in Slightly Enriched Uranium Oxide Lattices," BAW-1268 (1963).

4. PULSED NEUTRON STUDIES

H. E. Bliss

This chapter contains a summary of the topical report: MIT-2344-7, MITNE-73 of September 1966, "Use of a Pulsed Neutron Source to Determine Nuclear Parameters of Lattices of Partially Enriched Uranium Rods in Heavy Water" by H. E. Bliss, I. Kaplan, and T. J. Thompson. Progress reports on this work were also contained in the 1964 and 1965 Annual Reports.

1. INTRODUCTION

The time dependence of the neutron density in a multiplying medium irradiated by bursts of fast neutrons has been investigated theoretically and experimentally. The theoretical work has concentrated on the development of expressions, developed on the basis of several simple models, relating the prompt neutron decay constant to the nuclear parameters of the medium. The experimental program has consisted of thermal die-away measurements in a number of subcritical lattices of partially enriched uranium rods and heavy water.

2. THEORY

Consider a cylindrical multiplying medium bombarded by a pulse of fast neutrons and subject to the following boundary conditions:

(a) The fast neutrons have been thermalized and a source of thermal neutrons appears in the assembly at $t = 0$, $(n(\vec{r}, 0) = n_o(\vec{r}))$.

(b) The neutron density vanishes at the extrapolated boundaries of the assembly.

(c) The slowing-down time for neutrons resulting from thermal fission is negligible.

(d) The effect of delayed neutrons is neglected except as applied to neutron multiplication.

The thermal neutron diffusion equation, according to age-diffusion theory, is:

$$\overline{vD}\nabla^2 n(\vec{r}, t) - \overline{v\Sigma}_a n(\vec{r}, t) + \overline{v\Sigma}_a (1-\beta) k_\infty P_1(B^2)\, n(\vec{r}, t-T_o) = \frac{\partial}{\partial t} n(\vec{r}, t), \tag{4.1}$$

where $\overline{vD}$ and $\overline{v\Sigma}_a$ are averages over the neutron density, and T_o is the slowing-down time. The Laplace transform of Eq. 4.1 with $T_o = 0$ (condition (c)) is:

$$\overline{vD}\nabla^2 \bar{n}(\vec{r}, s) - \overline{v\Sigma}_a \bar{n}(\vec{r}, s) + \overline{v\Sigma}_a (1-\beta) k_\infty P_1(B^2)\, \bar{n}(\vec{r}, s) = s\bar{n}(\vec{r}, s) - n_o(\vec{r}). \tag{4.2}$$

The functions $\bar{n}(\vec{r}, s)$ and $n_o(\vec{r})$ are expanded in terms of an infinite set of orthogonal functions:

$$\bar{n}(\vec{r}, s) = \sum_{n=1}^{\infty} \bar{Q}_n(s) F_n(\vec{r}), \tag{4.3a}$$

$$n_o(\vec{r}) = \sum_{n=1}^{\infty} C_n F_n(\vec{r}), \tag{4.3b}$$

where

$$\nabla^2 F_n(\vec{r}) + B_n^2 F_n(\vec{r}) = 0. \tag{4.4}$$

Equations 4.3a, 4.3b, and 4.4 are now inserted into Eq. 4.2; the result (for the n^{th} mode) is:

$$\bar{Q}_n(s) = \frac{C_n}{\lambda_n + s}, \tag{4.5}$$

where

$$\lambda_n = \overline{v\Sigma}_a + \overline{vD}\, B_n^2 - \overline{v\Sigma}_a (1-\beta) k_\infty P_1(B_n^2). \tag{4.6}$$

Equation 4.5 is inverted, giving the expression for the neutron density:

$$n(\vec{r}, t) = \sum_{n=1}^{\infty} C_n F_n(\vec{r})\, e^{-\lambda_n t}. \tag{4.7}$$

After a sufficiently long time, all modes but the fundamental have

decayed away and only one term is left in the sum on the right side of Eq. 4.7, for which the decay constant is:

$$\lambda_1 \equiv \lambda = \overline{v\Sigma}_a + \overline{vD}\,B^2 - \overline{v\Sigma}_a(1-\beta)\,k_\infty P_1(B^2)\,. \tag{4.8}$$

The quantity B^2 in Eq. 4.8 is the geometric buckling which, for a cylindrical assembly, is given by:

$$B^2 = \left(\frac{2.405}{R}\right)^2 + \left(\frac{\pi}{H}\right)^2 .$$

The expression for the fundamental mode decay constant may also be derived from other theoretical models. If the slowing-down time for fission neutrons is not neglected, the age-diffusion treatment (referred to hereafter as modified age diffusion) leads to the following expression:

$$\lambda = \frac{\overline{v\Sigma}_a + \overline{vD}\,B^2 - \overline{v\Sigma}_a(1-\beta)\,k_\infty P_1(B^2)}{1 + T_o\overline{v\Sigma}_a(1-\beta)\,k_\infty P_1(B^2)}\,. \tag{4.9}$$

A two-group treatment yields a slightly different expression for the decay constant:

$$\lambda = \frac{\overline{v\Sigma}_a + \overline{vD}\,B^2 - \overline{v\Sigma}_a(1-\beta)\,k_\infty P_1(B^2)}{1 + (\ell_1/\ell_2)}\,, \tag{4.10}$$

where ℓ_1 and ℓ_2 are the fast and thermal neutron lifetimes, respectively. A multigroup treatment leads to:

$$\lambda = \frac{\overline{v\Sigma}_a + \overline{vD}\,B^2 - \overline{v\Sigma}_a(1-\beta)\,k_\infty \prod_{i=1}^{I-1} P_i(B^2)}{1 + \dfrac{\sum_{i=1}^{I-1} \ell_i}{\ell_I}}\,, \tag{4.11}$$

where the index I refers to the thermal group.

The analysis of pulsed neutron measurements has been extended to several new experimental situations. First, the parameters of the

test region of a two-region assembly have been related to the decay constant for the two-region assembly on the assumption that the parameters of the reference region are known from previous pulsed neutron experiments on a lattice composed entirely of the reference region medium. Second, the analysis of experiments on a lattice modified by the insertion of successive amounts of a distributed neutron absorber has indicated the possibility of obtaining values of the parameters of the unmodified lattice more accurately than would be possible with measurements on the unmodified lattice alone. Finally, the effect of the absence of a cadmium plate at the bottom of the lattice tank, normally inserted to complete the "black boundary" requirement, has been analyzed in terms of an effective return coefficient.

3. EXPERIMENTAL EQUIPMENT

The lattices studied in this work consisted of uranium metal rods clad in Type 1100 aluminum, arranged on a triangular spacing, and immersed in heavy water. The absorber-modified lattices contained, in addition, thin OFHC (oxygen-free, high conductivity) copper rods which served as the distributed neutron absorber. A summary of the lattices is given in Table 4.1.

The normal arrangement of the Lattice Facility was modified by the insertion of a cadmium plate at the bottom of the lattice tank. The installation of the plate was undesirable for experimental reasons and experiments were made with and without the plate in an attempt to obviate the need for the plate.

A Type A-810 neutron generator built by Kaman Nuclear served as the pulsed neutron source. Approximately 10^7 neutrons per burst were produced by the D-T reaction. The thermalized neutrons were detected by a small BF_3 detector centered axially and radially in the assembly. The counts from the detector were amplified and then sent to an analyzer whose purpose was to map a time profile of the decaying neutron density by recording numbers proportional to the density at preset intervals of time. The analyzer was a TMC-256 channel analyzer with a Model CN-110 digital computer and a Type 212 pulsed neutron plug-in unit. A block diagram of the experimental arrangement and the data recording system is shown in Fig. 4.1.

Table 4.1

Description of Lattices Studied

Lattice Designator	Lattice Spacing (inches)	Fuel Slug Diameter (inches)	Air Gap (inches)	Clad Thickness (inches)	Fuel Rod Outer Diameter (inches)	Uranium Enrichment (weight %)	D_2O Purity (mole %)	Amount of Added Absorber (inches^2)
125	1.25	0.250	0.006	0.028	0.318	1.143	99.60	–
175	1.75	0.250	0.006	0.028	0.318	1.143	99.53	–
175A1[a]	1.75	0.250	0.006	0.028	0.318	1.143	99.53	0.0278
175A1B1	1.75	0.250	0.006	0.028	0.318	1.143	99.53	0.0441
250	2.50	0.250	0.006	0.028	0.318	1.143	99.56	–
250B1[a]	2.50	0.250	0.006	0.028	0.318	1.143	99.56	0.0163
250B2	2.50	0.250	0.006	0.028	0.318	1.143	99.56	0.0326
253	2.50	0.750	0.004	0.028	0.814	0.947	99.51	–
253A2B1	2.50	0.750	0.004	0.028	0.814	0.947	99.51	0.0718
350	3.50	0.750	0.004	0.028	0.814	0.947	99.47	–
500	5.00	0.750	0.004	0.028	0.814	0.947	99.47	–
175(2R)[b]	1.75	0.250	0.006	0.028	0.318	1.027	99.53	–
	1.75	0.250	0.006	0.028	0.318	1.143	99.53	–
500(2R)	5.00	1.010	0.014	0.028	1.094	0.710	99.47	–
	5.00	0.750	0.004	0.028	0.814	0.947	99.47	–
MOD[c]	∞	–	–	–	–	–	99.47	–

a) The symbol A1 refers to one 0.188-inch-diameter copper rod per unit cell; the symbol B1 refers to one 0.144-inch-diameter copper rod per unit cell.

b) Two-region assembly: the first set of values refers to the test lattice and the second set refers to the reference lattice.

c) Pure moderator.

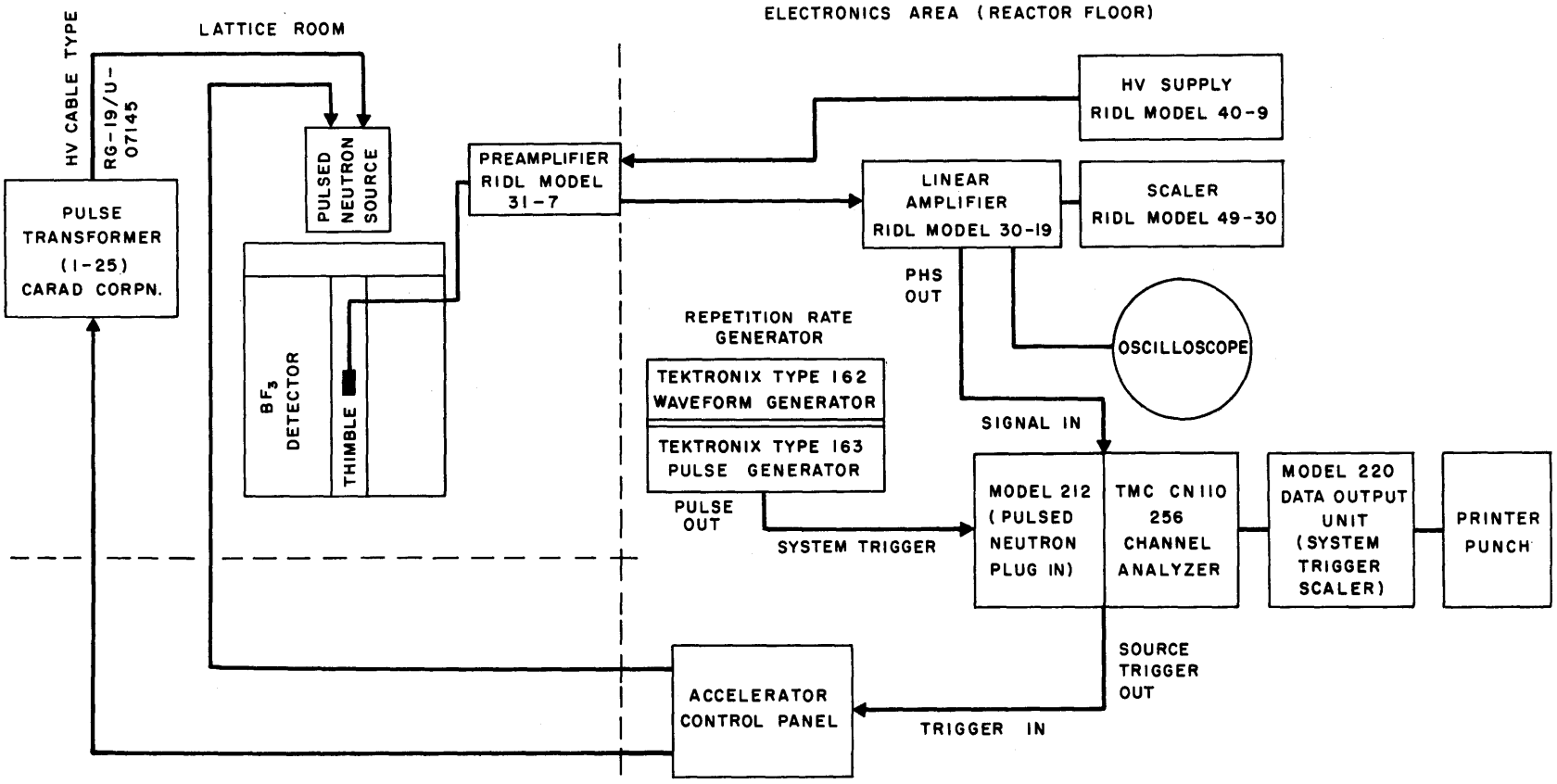

FIG. 4.1 SCHEMATIC OF OVERALL PULSING, DETECTION AND ANALYSIS CIRCUITRY

4. ANALYSIS OF DATA

Measurements of the neutron density as a function of time were made at several values of the moderator height in each lattice to vary the geometric buckling B^2. Three values of the fundamental mode decay constant were obtained from each measurement, one from each of three computer codes. Two of the codes, STRIP and FRAUD, were written as a part of this program, and the third, EXPO, was available from previous work (1). Agreement among the three codes, within experimental error, was obtained in over 90% of the cases analyzed.

The experimental values of λ and B^2 were analyzed on both the modified age-diffusion model and the two-group model to obtain values of the parameters k_∞ and $\overline{v\Sigma}_a$. The remaining quantities appearing in the expressions for λ, e.g., τ_o, $\overline{vD}$, β, T_o, L^2, and $\overline{v_1\Sigma_1}$, were presumed known either from calculations or from previous experiments. A short description of the two-group analysis is given from which the extension to a modified age-diffusion treatment is straightforward.

The ratio ℓ_1/ℓ_2 in Eq. 4.10 is written as:

$$\ell_1/\ell_2 = \alpha_{2G}(1+L^2B^2)\, P_1(B^2), \tag{4.12}$$

where

$$\alpha_{2G} = \frac{\overline{v\Sigma}_a}{\overline{v_1\Sigma_1}}, \tag{4.12a}$$

$$P_1(B^2) = \frac{1}{1+\tau_o B^2}. \tag{4.12b}$$

If Eqs. 4.12, 4.12a and 4.12b are substituted into Eq. 4.10, the result is:

$$\begin{aligned}\lambda' &= \overline{v\Sigma}_a - \overline{v\Sigma}_a(1-\beta)\, k_\infty P_1(B^2) \\ &= r - sP_1(B^2),\end{aligned} \tag{4.13}$$

where

$$\lambda' = \lambda[1+\alpha_{2G}(1+L^2B^2)P_1(B^2)] - \overline{vD}\,B^2. \tag{4.13a}$$

A least-squares fit is made to Eq. 4.13, with an assumed value for α_{2G}, to obtain the least-squares coefficients r and s which are then solved for k_∞ and $\overline{v\Sigma}_a$. This procedure is repeated for a predetermined range of values of α_{2G} until Eq. 4.12a is satisfied:

$$\overline{v\Sigma}_a = \alpha_{2G}\overline{v_1\Sigma_1} . \tag{4.14}$$

Since k_∞ is close to unity in practical cases of interest, a more accurate value of k_∞ is obtained if a least-squares fit is made to a modified version of Eq. 4.13:

$$\lambda' = r' - sP_1' , \tag{4.15}$$

where

$$r' = \overline{v\Sigma}_a[1-(1-\beta)k_\infty] , \tag{4.15a}$$

$$P_1' = P_1 - 1 . \tag{4.15b}$$

Then, k_∞ is derived as:

$$k_\infty = \frac{1}{(1-\beta)(1+r/s)} . \tag{4.16}$$

An IBM-7094 computer code, LSQHEB, has been written as a part of this program to aid in the analysis.

Measurements of λ as a function of B^2 were also made in pure moderator. The data were analyzed according to the method described in Ref. (1) to obtain values of the diffusion parameters of heavy water.

5. RESULTS AND CONCLUSIONS

The variation of λ as a function of B^2 in the 500 lattice, based on the results of FRAUD, is illustrated in Fig. 4.2. These data, together with those taken in the other lattices listed in Table 4.1, were analyzed according to the methods described in the preceding section. Three sets of values of k_∞ and $\overline{v\Sigma}_a$, one for each of the three computer codes, were obtained for each lattice. The three values of k_∞ were in agreement, within experimental error, for all but one lattice. This was also the case for the values of $\overline{v\Sigma}_a$; hence, the values of k_∞ and $\overline{v\Sigma}_a$ with the smallest percentage standard deviations were selected in each lattice.

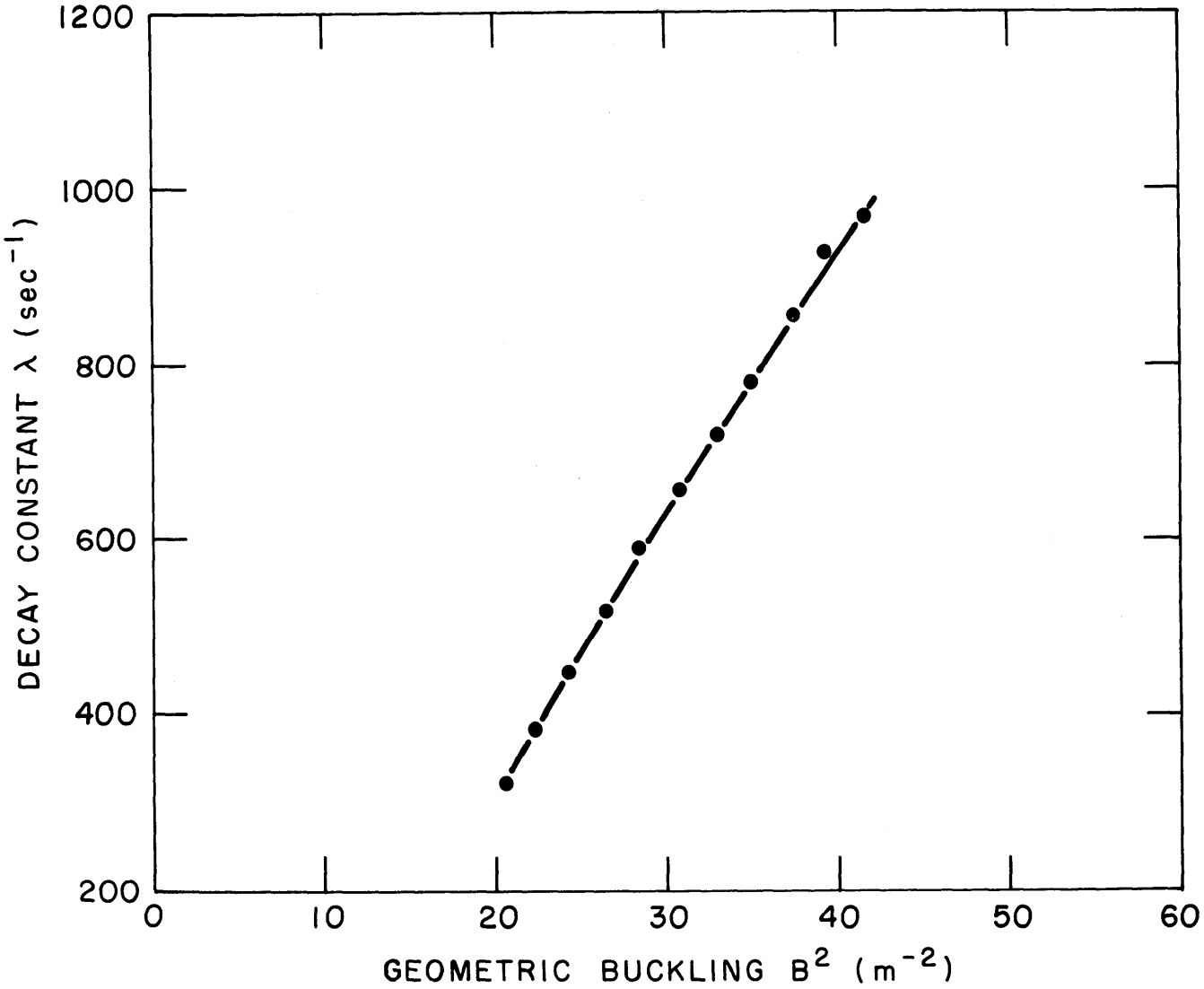

FIG. 4.2 MEASURED DECAY CONSTANT λ FOR THE 500 LATTICE AS A FUNCTION OF GEOMETRIC BUCKLING B^2

The first two columns of Table 4.2 contain values of k_∞ obtained with the pulsed neutron technique. Results of both the modified age-diffusion and two-group treatments are given. The uncertainties quoted are the total errors which reflect contributions from statistical fluctuations and known systematic sources of error. Columns 3 and 4 contain, for comparison, values of k_∞ obtained with the added-absorber technique (2) and the four-factor formula, respectively. Values of k_∞ obtained from the age-diffusion and two-group critical equations are listed in the last two columns of Table 4.2.

If the two pulsed neutron values of k_∞ are compared with the values obtained from their respective critical equations, the two-group results are in better agreement, within the quoted uncertainties, than the age-diffusion results. Comparison of the pulsed neutron results with the results of the added-absorber method and the four-factor formula yields similar conclusions. The percentage uncertainty in the two-group values of k_∞ is less than that in the corresponding modified age-diffusion value for all eleven lattices. It is concluded, therefore, that the two-group analysis is preferable to the age-diffusion analysis for determining values of k_∞ in lattices of uranium and heavy water by the pulsed neutron technique.

Uncertainties between 1.5% and 4.5% have been obtained in the values of k_∞ reported in this work. The smaller uncertainties are dominated by the contribution of known systematic sources of error which, at present, limit the precision of the pulsed neutron method to between 1.0% and 1.5%. The pulsed neutron method is attractive, therefore, as a means of comparison with the results of material buckling measurements. The accuracy of the pulsed neutron method should be as good as or better than that of the four-factor formula; of the two methods, the pulsed neutron method requires less time. The added-absorber method also requires considerably more time than the pulsed neutron method although somewhat better precision is possible with the former method.

Tables 4.3 and 4.4 contain experimental and theoretical values of the absorption cross section $\overline{v\Sigma}_a$ and the thermal diffusion area L^2, respectively. The theoretical values are based on the results of

Table 4.2

Values of the Infinite Medium Multiplication Factor k_∞

Lattice Designator	Source of Value for k_∞					
	Pulsed Source (Age-Diffusion)	Pulsed Source (Two-Group)	Added Absorber	Four-Factor Formula	Age-Diffusion Critical Equation	Two-Group Critical Equation
125	1.330 ± 0.035	1.315 ± 0.030		1.330 ± 0.027	1.338 ± 0.008	1.318 ± 0.008
175	1.437 ± 0.070	1.389 ± 0.054	1.416 ± 0.011	1.393 ± 0.026	1.419 ± 0.010	1.400 ± 0.010
175A1	1.006 ± 0.034	1.073 ± 0.033	1.004 ± 0.009	0.988 ± 0.018	1.004 ± 0.007	1.004 ± 0.007
175A1B1	0.704 ± 0.026	0.829 ± 0.022	0.871 ± 0.012	0.857 ± 0.017	0.831 ± 0.006	0.826 ± 0.006
250	1.445 ± 0.077	1.389 ± 0.064	1.429 ± 0.007	1.422 ± 0.028	1.432 ± 0.013	1.419 ± 0.013
250B1	1.074 ± 0.051	1.127 ± 0.047	1.148 ± 0.007	1.143 ± 0.023	1.142 ± 0.006	1.140 ± 0.006
250B2	0.743 ± 0.041	0.861 ± 0.037	0.963 ± 0.005	0.959 ± 0.020	0.963 ± 0.003	0.963 ± 0.003
253	1.097 ± 0.036	1.151 ± 0.036	1.187 ± 0.027	1.154 ± 0.023	1.190 ± 0.004	1.179 ± 0.004
253A2B1	0.834 ± 0.031	0.948 ± 0.028	1.003 ± 0.026	0.976 ± 0.020	1.002 ± 0.011	1.002 ± 0.011
350	1.351 ± 0.025	1.329 ± 0.021			1.331 ± 0.008	1.315 ± 0.008
500	1.427 ± 0.021	1.379 ± 0.020			1.390 ± 0.009	1.378 ± 0.009

Table 4.3

Values of the Absorption Cross Section $\overline{v\Sigma}_a$

Lattice Designator	Source of Value for $\overline{v\Sigma}_a$ (sec^{-1})		
	Pulsed Source (Age-Diffusion)	Pulsed Source (Two-Group)	Theoretical
125	2730.6 ± 89.6	3610.7 ± 121.9	3376.6
175	1303.8 ± 82.8	1818.0 ± 111.1	1716.4
175A1	2359.9 ± 134.4	2733.6 ± 92.5	2442.1
175A1B1	2141.6 ± 70.4	3056.0 ± 187.7	2834.5
250	631.4 ± 45.9	920.2 ± 70.5	840.9
250B1	656.9 ± 52.3	895.7 ± 75.0	1076.0
250B2	780.0 ± 48.0	1009.8 ± 73.1	1265.2
253	3667.0 ± 215.5	4867.5 ± 282.6	5312.5
253A2B1	4103.6 ± 176.7	5372.5 ± 252.6	6611.0
350	1790.4 ± 38.1	2189.2 ± 56.5	2530.3
500	927.9 ± 16.5	1159.3 ± 23.4	1182.4

Table 4.4
Values of the Thermal Diffusion Area L^2

Lattice Designator	Source of Value for L^2 (cm^2)		
	Pulsed Source (Age-Diffusion)	Pulsed Source (Two-Group)	Theoretical
125	93.2 ± 4.1	70.5 ± 2.7	76.7
175	175.0 ± 11.1	125.5 ± 7.7	135.6
175A1	102.4 ± 5.8	88.5 ± 3.0	98.5
175A1B1	114.6 ± 3.7	80.3 ± 4.9	86.5
250	342.3 ± 24.9	234.8 ± 18.0	260.9
250B1	331.9 ± 26.4	243.4 ± 20.4	206.3
250B2	278.8 ± 17.2	215.4 ± 15.6	177.4
253	73.4 ± 4.3	55.2 ± 3.2	50.7
253A2B1	66.4 ± 2.9	40.5 ± 1.9	42.2
350	132.8 ± 2.8	108.6 ± 3.8	99.7
500	237.4 ± 4.2	190.0 ± 3.8	186.6

THERMØS (3). With the exception of the 175A1 lattice, the values of $\overline{\nu\Sigma}_a$ and L^2 obtained from the two-group analysis are considerably closer to the theoretical values than are those obtained from the modified age-diffusion analysis. Furthermore, if an estimated 3% uncertainty is included in the theoretical values of L^2 (due to uncertainties in the nuclear cross sections used by THERMØS), the two-group pulsed source values of L^2 are in reasonable agreement with those from THERMØS. These observations reinforce the conclusion given earlier, with respect to values of k_∞, that the two-group analysis yields better results than the modified age-diffusion analysis.

The analysis of pulsed neutron experiments in two-region assemblies has shown that the parameters of the test region can be obtained if the parameters of the reference region are known. Experimental values of k_∞ in the test region of two-region assemblies are given in Table 4.5. Values of k_∞ based on the four-factor formula have previously been obtained for a lattice composed entirely of the test region of the 175(2R) lattice by D'Ardenne (4) and of the 500(2R) lattice by Weitzberg (5), and these results are also listed in Table 4.5. Agreement, within the quoted uncertainties, is excellent in both lattices.

Table 4.5
Values of the Multiplication Factor k_∞
in the Test Region of Two-Region Assemblies

	Source of Value for k_∞		
Lattice Designator	Pulsed Source (Two-Group)	Four-Factor Formula	
175 (2R)	1.350 ± 0.038	1.339 ± 0.020	(4)
500 (2R)	1.188 ± 0.024	1.219 ± 0.014	(5)

Values of k_∞ and $\overline{\nu\Sigma}_a$, obtained in three unmodified lattices before and after the application of measurements in absorber-modified lattices, are given in Table 4.6. In all cases, the uncertainties in the new values

Table 4.6

Comparison of Values of the Multiplication Factor k_∞ and Absorption Cross Section $\overline{v\Sigma}_a$ in Unmodified Lattices

Lattice Designator	Source of Value for k_∞		Source of Value for $\overline{v\Sigma}_a$ (sec^{-1})	
	New Value	Old Value	New Value	Old Value
175	1.390 ± 0.049	1.389 ± 0.051	1845.0 ± 72.0	1811.0 ± 111.1
250	1.387 ± 0.022	1.389 ± 0.062	839.8 ± 16.0	920.2 ± 70.5
253	1.143 ± 0.002	1.151 ± 0.032	4725.3 ± 51.3	4867.2 ± 282.6

of these parameters are smaller than those obtained from an analysis of pulsed neutron measurements on the unmodified lattices alone. These results indicate the usefulness of the method of analysis of the measurements in absorber-modified lattices.

The pulsed neutron measurements with and without a cadmium plate at the bottom of the lattice tank led to a value of 0.44 ± 0.05 for the return coefficient for thermal neutrons from the graphite-lined cavity below the tank. This value is independent of the moderator height and is an average of measurements made in one lattice and in pure moderator.

A value of $(2.088 \pm 0.018) \times 10^5$ cm^2 sec^{-1} was obtained for the diffusion coefficient in 100% D_2O at 20°C. This value is in good agreement with the recent value of $(2.09 \pm 0.02) \times 10^5$ cm^2 sec^{-1} obtained by Parks and Bauman (6) but disagrees with the weighted average of $(2.031 \pm 0.015) \times 10^5$ cm^2 sec^{-1} obtained from earlier measurements (1, 7, 8, 9, 10, 11, 12).

6. REFERENCES

(1) Malaviya, B. K., I. Kaplan, T. J. Thompson and D. D. Lanning, "Studies of Reactivity and Related Parameters of Slightly Enriched Uranium, Heavy Water Lattices," MIT-2344-1, MITNE-49 (May 1964).

(2) Harrington, J., D. D. Lanning, I. Kaplan and T. J. Thompson, "Use of Neutron Absorbers for the Experimental Determination of Lattice Parameters in Subcritical Assemblies," MIT-2344-6, MITNE-69 (February 1966).

(3) Honeck, H. C., "THERMØS, A Thermalization Transport Theory Code for Reactor Lattice Calculations," BNL-5826 (September 1961).

(4) D'Ardenne, W. H., T. J. Thompson, D. D. Lanning and I. Kaplan, "Studies of Epithermal Neutrons in Uranium, Heavy Water Lattices," MIT-2344-2, MITNE-53 (August 1964).

(5) Weitzberg, A., I. Kaplan and T. J. Thompson, "Measurements of Neutron Capture in U-238 Lattices of Uranium Rods in Heavy Water," NYO-9659, MITNE-11 (January 1962).

(6) Parks, P. B. and N. P. Bauman, "Pulsed Measurements of Neutron Diffusion Parameters in D_2O," Trans. Amer. Nuc. Soc., 8, 2, 436 (November 1965).

(7) Ganguly, N. K., F. C. Cobb and A. W. Waltner, "The Diffusion Parameters of Heavy Water," Nuc. Sci. Eng., 17, 223 (1963).

(8) Jones, H. G., A. Robeson and G. N. Salaita, "Diffusion Parameters of Mixtures of Light and Heavy Water at Several Temperatures," Trans. Amer. Nuc. Soc., 8, 2, 431 (November 1965).

(9) Kussmaul, G., and H. Meister, "Thermal Neutron Diffusion Parameters of Heavy Water," Journal of Nuclear Energy A/B 17, 411 (1963).

(10) Malaviya, B. K., and A. E. Profio, "Measurement of the Diffusion Parameters of Heavy Water by the Pulsed-Neutron Technique," Trans. Amer. Nuc. Soc., 6, 1, 58 (June 1963).

(11) Utzinger, E., W. Heer and H. R. Lutz, "Pulsed-Source Experiments with Multiplying and Non-Multiplying Heavy Water Systems," Proceedings of a Symposium on Pulsed Neutron Research, Karlsruhe, 10-14 May 1965, 2, 119 (Vienna: IAEA, August 1965).

(12) Westfall, F. R. and A. W. Waltner, "Measurements of Natural Uranium Heavy Water Lattices by the Pulsed Neutron Techniques," Trans. Amer. Nuc. Soc., 5, 2, 386 (November 1962).

5. USE OF NEUTRON ABSORBERS IN THE DETERMINATION OF LATTICE PARAMETERS

J. Harrington, III

This chapter contains a summary of the topical report: MIT-2344-6, MITNE-69 of February 1966, "Use of Neutron Absorbers for the Experimental Determination of Lattice Parameters in Subcritical Assemblies" by J. Harrington, D. D. Lanning, I. Kaplan and T. J. Thompson. Preliminary progress reports in this area were also presented in the 1964 and 1965 Annual Reports.

1. INTRODUCTION

The neutron multiplication factor for an infinite medium, k_∞, is a parameter central to reactor physics and reactor analysis. The present work concerns the development and application of a new technique for the measurement of k_∞. It is based on a technique developed at the Hanford Laboratories for the measurement of k_∞ in a critical facility such as the Physical Constants Testing Reactor (PCTR) (1, 2). Like the PCTR technique, it involves the addition of neutron absorbers to a test lattice. Both methods have the advantage that the values of k_∞ obtained are independent of a number of sources of error normally important in such measurements, and both can be interpreted as measurements of the neutron regeneration factor, η, a quantity otherwise difficult to measure in a lattice. Both methods are very nearly measurements of the quantity $(k_\infty-1)$ so that, in lattices with values of k_∞ near unity, relatively precise determinations of k_∞ can be made. The major advantage of the method developed in the present work is that a critical facility is not required. Its major disadvantage, in comparison with the PCTR technique, is that more test fuel is required.

2. THEORY

2.1 The Multiplication Factor k_∞ and the Four-Factor Formula

The multiplication factor k_∞ is here defined as the ratio of the number of neutrons produced, per unit time in an infinitely large assembly, to the number of neutrons absorbed. For the reactors considered here, the "life-cycle" formulation of k_∞, which results in the well-known "four-factor formula," is convenient and appropriate (3). Figure 5.1 shows the neutron life cycle in an infinite medium; for one U^{235} fission neutron absorbed, a total of $\epsilon\eta pf(1+\delta_{25})$ U^{235} fission neutrons are produced. Thus, the equation for k_∞ is:

$$k_\infty = \epsilon\eta pf(1+\delta_{25}). \tag{5.1}$$

It is important that the factors in Eq. 5.1 be defined consistently and that each process be counted once and only once in the neutron life cycle.

One way to obtain "measured" values of k_∞ is to construct a critical or subcritical lattice, make foil activation measurements of various quantities, and then calculate values for each of the factors on the right-hand side of Eq. 5.1 based on the experimental results (4, 5). Quantities measured in the lattice include:

- δ_{28}, the ratio of fissions in U^{238} to fissions in U^{235},
- δ_{25}, the ratio of epithermal fissions in U^{235} to thermal fissions in U^{235}, and
- ρ_{28}, the ratio of epithermal absorptions in U^{238} to thermal absorptions in U^{238}.

In addition, the fine structure of the thermal neutron distribution is usually measured. Quantities measured in independent experiments include:

- ν_{25}, the average number of neutrons released in a single U^{235} fission,
- ν_{28}, the average number of neutrons released in a single U^{238} fission,

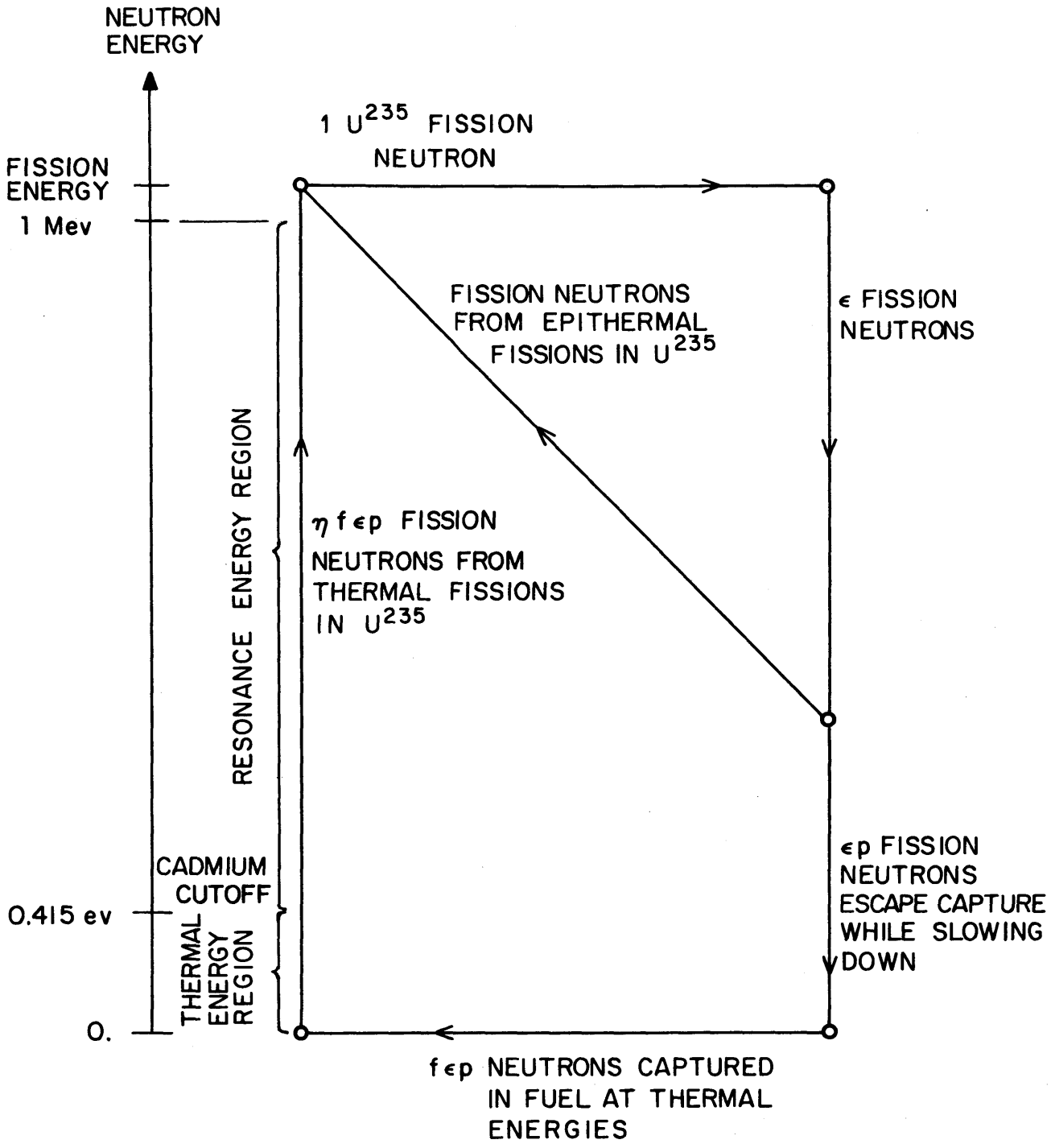

FIG. 5.1. NEUTRON LIFE CYCLE IN A THERMAL NEUTRON REACTOR (INFINITE MEDIUM)

α_{25}, the capture-to-fission ratio for U^{235}, and

α_{28}, the capture-to-fission ratio for U^{238}.

There are many ways to obtain values of ϵ, η, p, and f from these quantities and measured cross sections. In doing so, account must be taken of the effect of neutron leakage from the finite assembly in which the measurements are made. A self-consistent scheme, appropriate to the lattices studied here, is given in sections 2.2 and 2.3 of the topical report. Uncertainties in the values of ν_{25} and certain of the cross sections generally result in uncertainties between 1% and 2% in k_∞.

2.2 The PCTR Technique

Values of k_∞ measured with the PCTR are independent of some of the sources of error in values determined with Eq. 5.1. The PCTR is a cube of graphite, 7 ft on a side, with a cavity, 2 by 2 by 7 ft, located at its center. It is made critical by enriched uranium distributed outside the boundary of the central cavity. Several cells of the lattice to be tested are placed in the cavity, together with a quantity of a distributed neutron absorber sufficient to make the reactivity of the resulting assembly the same as that of the reactor with the cavity. Such a sample is held to have a value of k_∞ equal to unity. An attempt is made to ensure that the energy spectrum of the neutrons incident on the test sample, as defined by some suitable spectral index, is the same as the spectrum that would exist in an infinitely large sample of the medium.

If the assumption is made that the added absorber absorbs thermal neutrons only and causes no appreciable spectral perturbation, Eq. 5.1 for the test sample may be written:

$$1 = \epsilon\eta p f^{O}(1+\delta_{25}), \tag{5.2}$$

where the superscript (^{O}) indicates a medium with $k_\infty=1$. The value of k_∞ for the unmodified cell is then:

$$k_\infty = \frac{f}{f^{O}} . \tag{5.3}$$

The significance of this expression may most easily be shown by assuming the test cell to be homogeneous; Eq. 5.3 may then be written

as follows:

$$k_\infty - 1 = \frac{\Sigma^a_{absorber}}{\Sigma^a_{fuel} + \Sigma^a_{moderator}} \quad . \tag{5.4}$$

Here, Σ^a_i denotes the macroscopic thermal neutron absorption cross section for material i. The PCTR technique at its simplest consists of a determination of the amount of added neutron absorber necessary for Eq. 5.2 to be satisfied; this amount is used to calculate $\Sigma^a_{absorber}$, and the value of k_∞ is obtained with Eq. 5.4. Note that ν_{25} does not appear in the formula for k_∞ and that no particular "model" or form of reactor theory is necessary for the interpretation of the experiment.

2.3 The Material Buckling

The spatial distribution of the neutron flux, $\phi(\vec{r})$, in a bare, homogeneous, critical reactor is given by the fundamental mode solution of the Helmholtz equation,

$$\nabla^2\phi(\vec{r}) + B^2\phi(\vec{r}) = 0, \tag{5.5}$$

under the assumption that the flux goes to zero at the extrapolated boundaries of the system, assumed independent of energy (3). Here, the constant B^2 may be identified with the geometric buckling, B^2_g; it is a function only of the extrapolated dimensions of the critical reactor. The material buckling, B^2_m, is a characteristic of a given neutron-multiplying medium; in the absence of pronounced anisotropies, such as those caused by voids, it is a function only of the materials involved and not of the size of the assembly (4). It is defined to be equal to the geometric buckling of a critical reactor composed of the given material. The larger the material buckling, the smaller will be the critical reactor. It may be seen that k_∞ and B^2_m are related; there are a number of ways to do this, based on various "models" or reactor theories. The relationships derived from two-group theory and age-diffusion theory are, respectively (6):

$$k_\infty = \left(1+L^2B^2_m\right)\left(1+\tau B^2_m\right), \tag{5.6}$$

$$k_\infty = \left(1+L^2B_m^2\right)e^{\tau B_m^2}. \qquad (5.7)$$

Here, L^2 is the diffusion area for thermal neutrons, and τ is the Fermi age. Common to these relationships, and in fact to all such relationships, is the association of the value of unity for k_∞ with a zero material buckling. This follows from definitions already stated, upon noting that a reactor with a multiplication constant equal to unity is just critical by definition, since a steady-state chain reaction can then be maintained without external neutron sources. If the value of k_∞ for a given medium is equal to unity, a reactor composed of the medium, infinite in extent, would be just critical. The value of the geometric buckling of such a reactor would be zero, and it follows from the equivalence of geometric and material buckling for a critical reactor that the material buckling would also be zero.

For many types of reactors, particularly those with relatively low material buckling values, the material buckling may be measured in a subcritical assembly. In such an assembly, the fundamental mode solution to Eq. 5.5, with B^2 now associated with the material buckling, governs the spatial distribution of the neutron flux, far from the source and the boundaries (3). Measurements are made of the macroscopic spatial activation distribution with neutron-detecting foils; this distribution is taken to be proportional to the flux distribution. By comparing the observed distribution with the one predicted with Eq. 5.5, the "best value" of the material buckling is obtained, usually by a least-squares fitting technique. The assumptions made in the course of the development just summarized are discussed at length in Refs. (7), (8) and (9). The material buckling measurements made in the course of this work did not differ in any fundamental way from those used in unmodified lattices.

2.4 The Subcritical Technique for Measuring k_∞

It is clear from the foregoing discussion that a critical reactor is not required for the determination of the amount of added neutron absorber necessary to reduce the value of k_∞ to unity. Neutron absorbers in varying concentrations may be added to a subcritical

lattice, and the material buckling may be measured for each concentration. If the absorber concentrations are carefully chosen, a least-squares fit or similar interpolation may be used to find the amount of absorber which would reduce the material buckling value to zero exactly. Under the assumption that all the quantities in Eq. 5.1 are affected by the added absorber, Eq. 5.2 is replaced by the equation:

$$1 = \epsilon^{o}\eta^{o}p^{o}f^{o}\left(1+\delta_{25}^{o}\right). \tag{5.8}$$

If the thermal utilization is defined as follows:

$$f = \left[1 + \sum_{i} \frac{\overline{\phi}_i \overline{\Sigma}_i V_i}{\overline{\phi}_o \overline{\Sigma}_o V_o}\right]^{-1} = \left(1 + \sum_{i} A_i\right)^{-1}, \tag{5.9}$$

with summation over all materials in the lattice except the fuel, Eq. 5.4 is replaced by the equation:

$$k_{\infty} = \left(\frac{\epsilon}{\epsilon^{o}}\right)\left(\frac{\eta}{\eta^{o}}\right)\left(\frac{p}{p^{o}}\right)\left(\frac{1+\delta_{25}}{1+\delta_{25}^{o}}\right)\left[1+fA_a^{o}+f\sum_{i}\left(A_i^{o}-A_i\right)\right]. \tag{5.10}$$

Here, the summation is over all materials in the lattice except the fuel, and the absorber, which is denoted with the subscript "a". If the added absorber displaces little or no moderator and if it is predominantly a thermal neutron absorber, the first four factors in parentheses on the right-hand side of Eq. 5.10 will all be near unity. Furthermore, the difference between A_i^{o} and A_i can be made small.

The subcritical measurement may thus be seen to possess all the advantages attributed to the Hanford technique. In order to verify its usefulness in practice, the method was applied to three lattices.

3. EXPERIMENTS

The lattices studied are described in Table 5.1. All were fueled with uranium metal and moderated with heavy water. The rods were clad in aluminum. The lattices were arranged on a triangular spacing and were approximately 35 inches in diameter. The tank used was 36 inches in diameter; it was wrapped in cadmium 0.020 inch thick.

Table 5.1
Lattices Studied

Arbitrary Designator	Spacing (inches)	Fuel Rod Diameter (inches)	Uranium Enrichment (wt %)	Moderator-to-Fuel Volume Ratio
250	2.50	0.250	1.143	108.6
175	1.75	0.250	1.143	52.40
253	2.50	0.750	0.947	11.07

Solid copper rods were used as thermal neutron absorbers. Copper was chosen because of its favorable thermal neutron absorption cross section, its small resonance absorption integral, its availability at low cost in the form and purity desired, and its low specific activation. The rods were 0.144 inch and 0.188 inch in diameter and were clad in 0.0005 inch of KANIGEN nickel plating. Dissolved absorbers, such as boric acid, were considered but not used; use of homogeneous poison would simplify the analysis but raise the question of permanent contamination of the heavy water. Further, determination of the absorber concentration is not straightforward as is the case with heterogeneous absorbers.

Activation experiments with bare and cadmium-covered metallic gold foils were done to determine the relative neutron flux distribution throughout the assembly, away from sources and boundaries, as well as the fine structure of the thermal neutron distribution in the neighborhood of the fuel and copper rods. From these measurements, the material buckling and the thermal utilization were determined. The use of both bare and cadmium-covered foils allowed an experimental determination of the region of the assembly where the cadmium ratio was constant. This region was taken to be the region of spectral equilibrium, and all experiments were done in it. The experimental techniques did not differ in any fundamental way from those developed for use in the unmodified lattices.

Measurements were made by coworkers (10, 11, 12) of the quantities ρ_{28}, δ_{25} and δ_{28} in modified and unmodified lattices. Measurements

were also made of the ratio of epithermal absorptions in copper to thermal absorptions in copper.

4. CALCULATION OF THE SPATIALLY-DEPENDENT THERMAL NEUTRON SPECTRUM

The THERMØS code (13, 14, 15) has been found to be useful for calculating the thermal neutron spectrum in unmodified lattices of the type considered here (16, 17). The Wigner-Seitz approximation is made, and the problem is treated as a one-dimensional one in cylindrical geometry. The THERMØS code was not directly applied for the calculation of the spatial dependence of the spectrum in lattices modified by the addition of heterogeneous absorbers; a separate calculation was done for a cylindrical "cell" about each fuel rod and copper rod, the cell sizes being determined by a method derived by means of source-sink theory by J. E. Suich (18). Use was made of the fine structure measurements to normalize the two decoupled calculations. The results were used to calculate various quantities averaged over the thermal neutron spectrum, such as the diffusion coefficient $\overline{D}$, the macroscopic absorption cross section of the lattice $\overline{\Sigma}^a$, the absorption cross sections of all materials, and the fission cross section of the fuel.

It was found that the values of various ratios of epithermal events to thermal events (such as δ_{25} and ρ_{28}) could be calculated with satisfactory accuracy from measurements in similar assemblies, under the assumption that the neutron energy spectrum consisted of the THERMØS-calculated spectrum in the energy region below 0.78 ev, and a neutron flux proportional to E^{-1} in the epithermal energy region.

5. RESULTS

5.1 Measurement of k_∞

Figures 5.2, 5.3 and 5.4 give the results of some of the activation experiments. The values of η, ϵ, p, f and $(1+\delta_{25})$ typical of an infinite lattice, and the value of k_∞ derived from them with Eq. 5.1, are given in Table 5.2. The value of k_∞ derived with Eq. 5.10 is also given. Experimental difficulties were encountered in the buckling measurements in the 253 assemblies, and comparatively large uncertainties had to be

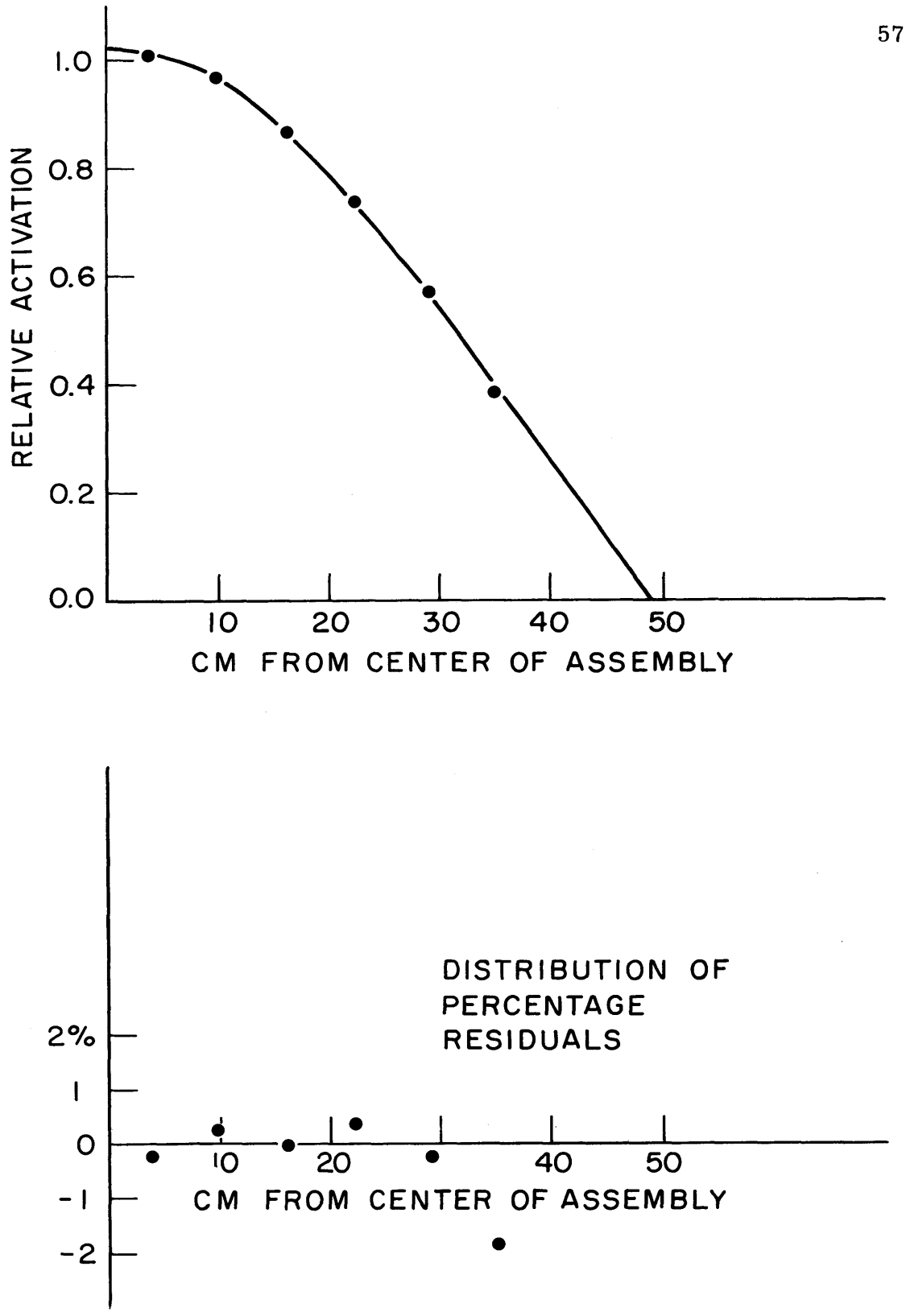

FIG. 5.2 RELATIVE ACTIVATION DISTRIBUTION IN 250BI ASSEMBLY AS A FUNCTION OF RADIAL POSITION (RUN 19, BARE FOILS; RADIAL BUCKLING IS 2418 μB.)

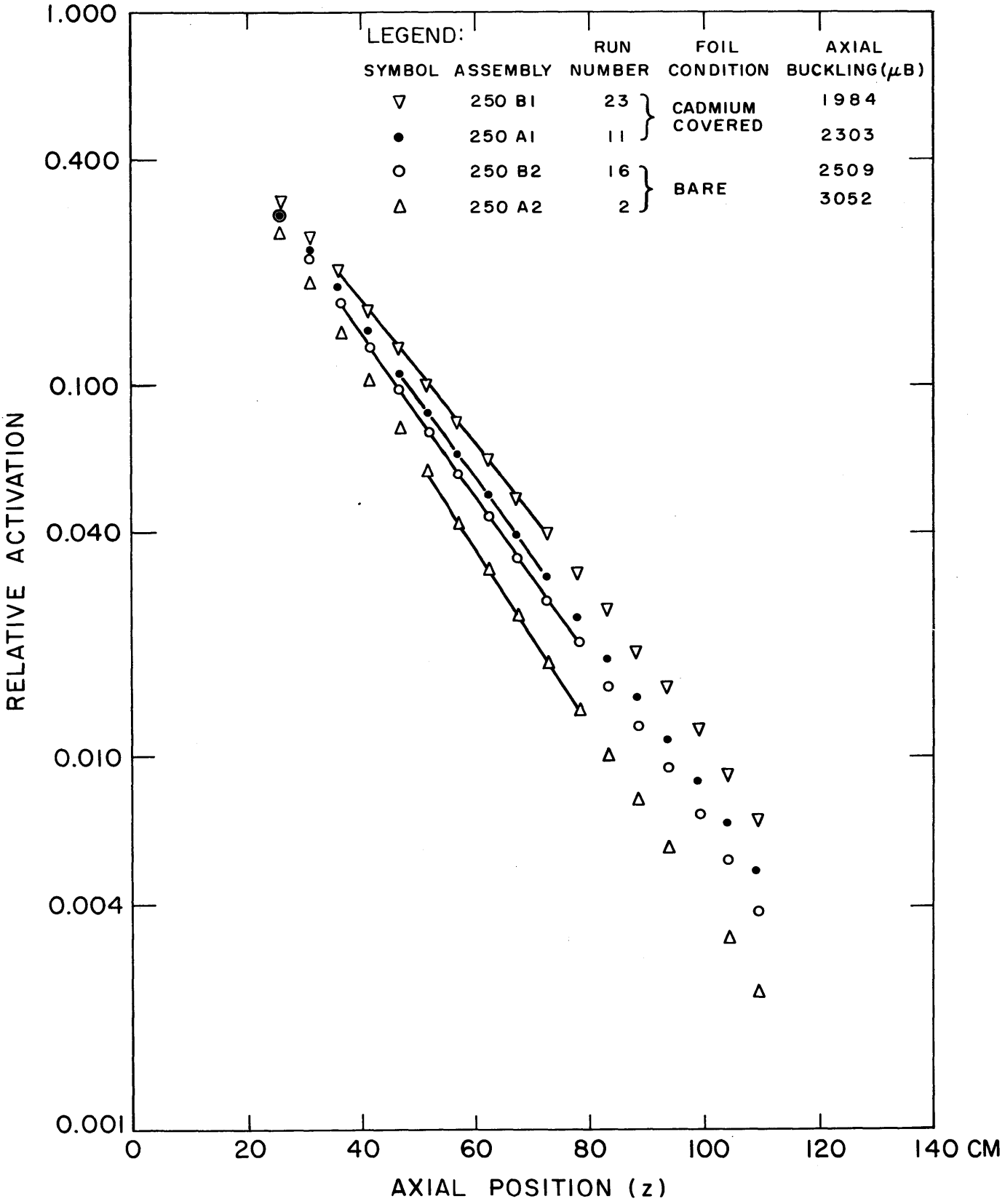

FIG. 5.3 RELATIVE ACTIVATION DISTRIBUTION IN FOUR 250 ASSEMBLIES AS A FUNCTION OF AXIAL POSITION. (GOLD FOILS USED WERE 0.010 INCHES THICK, 0.125 INCHES IN DIAMETER. UNCERTAINTY DUE TO COUNTING STATISTICS 0.2% TO 0.4%)

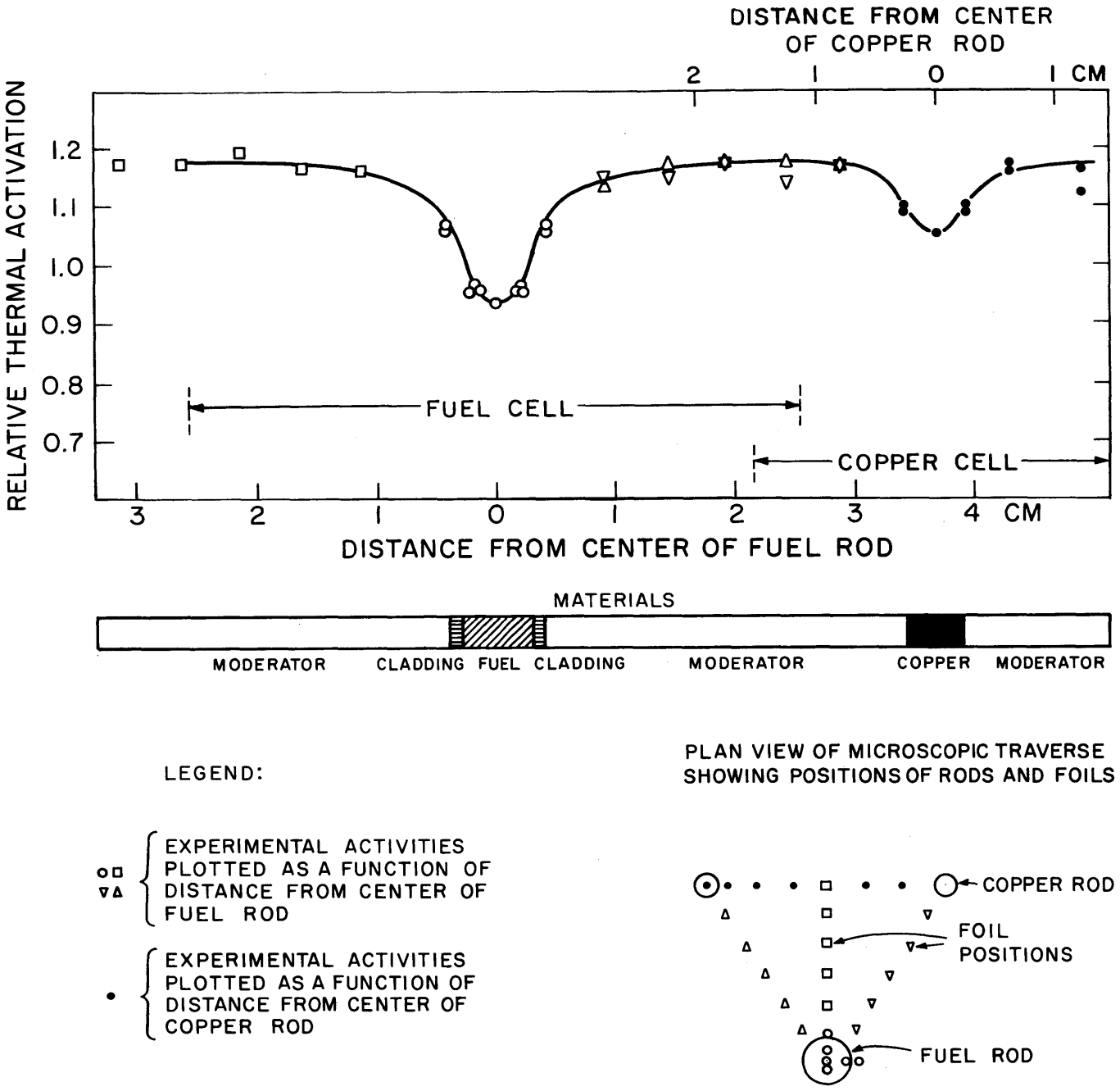

FIG. 5.4 RELATIVE THERMAL ACTIVATION DISTRIBUTION NEAR CENTER FUEL ROD IN 250A2 ASSEMBLY (RUN 7). (GOLD FOILS USED WERE 0.010 INCHES THICK, 0.0625 INCHES IN DIAMETER. UNCERTAINTY DUE TO COUNTING STATISTICS 0.28%. SOLID LINES SHOW THERMOS-CALCULATED RELATIVE THERMAL ACTIVATION DISTRIBUTION.)

Table 5.2

Values of k_∞ Obtained with Equations 5.1 and 5.10

Designator	Neutron Regeneration Factor (η)	Fast Fission Factor (ϵ)	Resonance Escape Probability (p)	Thermal Utilization (f)	Resonance Fission Factor ($1+\delta_{25}$)	Neutron Multiplication Factor, k_∞ (Eq. 5.1)	Neutron Multiplication Factor, k_∞ (Eq. 5.10)
250	1.532 ± 28	1.0117 ± 4	0.953 ± 4	0.9520 ± 15	1.012 ± 5	1.422 ± 0.028	1.429 ± 0.007
175	1.530 ± 28	1.0147 ± 5	0.906 ± 5	0.9678 ± 8	1.024 ± 2	1.393 ± 0.026	1.416 ± 0.011
253	1.441 ± 26	1.0439 ± 20	0.711 ± 5	0.9885 ± 3	1.093 ± 5	1.154 ± 0.023	1.187 ± 0.027

Note: Uncertainties shown for first five columns of the table refer to the least significant digits reported (i.e., 1.532 ± 28 ≡ 1.532 ± 0.028).

assigned to the measured buckling values. Consequently, the amount of added absorber necessary for a zero buckling value (A_a^o) is not known as precisely for the 253 lattice as it is for the others, and this affects the uncertainty in the value of k_∞ obtained with Eq. 5.10 markedly. The efficacy of the subcritical technique is demonstrated, however, by the results of the measurements in the 250 and 175 lattices; the uncertainties in $(k_\infty-1)$ are 1.6% and 2.6%, respectively. The PCTR technique yields about a 3% uncertainty in $(k_\infty-1)$. (See Refs. 19, 20.)

The uncertainties in the values of k_∞ obtained with Eq. 5.1 are calculated from the uncertainties in ν_{25}, ν_{28}, δ_{25}, δ_{28}, ρ_{28} and the uncertainties in the absorption cross sections for all materials. The uncertainties in the values of k_∞ obtained with Eq. 5.10, on the other hand, are almost completely determined by the uncertainty in the value of A_a^o, which is calculated from the standard deviations of the measured buckling values, the counting statistics in the fine structure measurement, and the uncertainties in the thermal neutron absorption cross sections of the fuel and added absorber. Strong efforts have been made by various workers to eliminate sources of systematic error from both methods for determining k_∞; the two values of k_∞ given for each lattice in Table 5.2 are in good agreement. This result lends confidence in both methods for measuring k_∞, at least for lattices like those studied here. However, because there are fewer sources of error in the measurement of k_∞ by the subcritical technique, and because the uncertainties are smaller in cases free of experimental difficulties, the results based on Eq. 5.10 are believed to be more trustworthy.

5.2 Measurement of L^2

The measured values of k_∞ have been used to calculate values of the diffusion area, L^2 (see Table 5.3). Equations 5.6 and 5.7 were used, together with measured buckling values and calculated values of the Fermi age (21). These values may be compared with values of L^2 calculated from the equation (6):

$$L^2 = \frac{\bar{D}}{\bar{\Sigma}^a}, \tag{5.11}$$

Table 5.3
Measured and Calculated Values of the Diffusion Area (L^2)

Designator	Material Buckling B_m^2 (μB)	Fermi Age (τ) (cm^2)	Source of Value of L^2		
			Equation 5.6 (cm^2)	Equation 5.7 (cm^2)	Equation 5.11 (cm^2)
250	1007 ± 17	123 ± 3	269 ± 8	261 ± 9	264
175	1405 ± 13	125 ± 3	145 ± 7	134 ± 7	136
253	969 ± 11	128 ± 3	58 ± 25	51 ± 25	51

where $\overline{D}$ and $\overline{\Sigma}^a$ are the diffusion coefficient and absorption cross section previously defined. The calculated values of L^2 are in slightly better agreement with values obtained with Eq. 5.7. In cases free of experimental difficulties (250, 175), use of the measured values of k_∞ (Eq. 5.10) in place of the values obtained with Eq. 5.1 results in a threefold reduction in the uncertainty in the value of L^2.

5.3 Measurement of η

It was noted earlier that values of the neutron regeneration factor, η, can be obtained from the results of the experiments. The formula for η is:

$$\eta = \left(\frac{\eta}{\eta^o}\right)\left[\frac{1 + \sum_i A_i^o}{\epsilon^o p^o (1+\delta_{25}^o)}\right]. \qquad (5.12)$$

It may be derived from Eqs. 5.8 and 5.9. The summation is over all materials except the fuel. The correction factor in parentheses accounts for the small change in η due to spectral hardening and deviates from unity by only a few tenths of a percent in the present work. The values of η for the 250 and 175 lattices are 1.525 ± 0.014 and 1.555 ± 0.008, respectively; they are in good agreement with the values given in Table 5.2, which were calculated with the THERMØS-averaged absorption and fission cross sections.

6. REDUCTION OF THE AMOUNT OF FUEL REQUIRED: SUGGESTION FOR FUTURE RESEARCH

It has been shown that approximately equal precision in the measurement of $(k_\infty - 1)$ may be expected from the Hanford technique and the subcritical measurement described here. The Hanford technique requires a critical facility, but much less test fuel is necessary. If the material buckling of a small sample of a test lattice with and without added absorber can be measured in a subcritical two-region measurement, there is an excellent chance that the fuel requirements of the subcritical measurement of k_∞ can be greatly reduced. Two-region buckling measurements in subcritical assemblies are the subject of a separate study by another worker at M. I. T. (22); final conclusions must await completion of that study. Exploratory experiments done as part of the present work give grounds for thinking that measurements of the thermal utilization, and ratios like ρ_{28} and δ_{25}, can be made in and near the central fuel rod of a two-region assembly. Further experiments will be necessary to verify the usefulness of the technique, but it appears to be a promising area for future research.

7. CONCLUSIONS

The most important conclusion to be drawn from the results just given is that values of k_∞ and η can be measured, with uncertainties between 0.5% and 1.0%, by making use of thermal neutron absorbers in subcritical assemblies in the manner described. The measured values of the multiplication factor are independent or nearly independent of many parameters associated with values of the multiplication factor calculated with the four-factor formula; among these are ν_{25}, ν_{28}, δ_{25}, δ_{28}, ρ_{28}, the macroscopic fission cross section of the fuel, and all absorption cross sections except that of the fuel. The measured values and the values obtained with Eq. 5.1 are in good agreement. Because the sources of uncertainty in the measured values are fewer in number, and because the uncertainties associated with them are smaller (in cases free of experimental difficulties), the measured values are believed to be more trustworthy.

The measured values of η are independent of the value of ν_{25} and of the fission cross section of the fuel; they are in agreement, within

experimental uncertainties, with values of η calculated from values of ν_{25} and the ratio of the fission and absorption cross sections of the fuel, averaged over the spectrum calculated with a multigroup transport theory code (THERMØS).

Exploratory experiments were made, with the ultimate objective of doing the measurements in two-region subcritical assemblies. No grounds for belief that the experiments could not be done in this way were discovered; there is considerable reason to believe that this can, in fact, be done if the material buckling can be measured in a two-region subcritical experiment. More experiments will be necessary before a conclusion can be definitely established.

"Experimental" values of the diffusion area computed with the age-diffusion criticality equation are in slightly better agreement with values of L^2 calculated with Eq. 5.11 than are those obtained with the two-group criticality equation. In the case of the 250 and 175 lattices, use of the measured values of k_∞ in place of the values obtained with Eq. 5.1 results in a threefold reduction in the uncertainty in the value of L^2.

8. REFERENCES

(1) Donahue, D. J., D. D. Lanning, R. A. Bennett, and R. E. Heineman, "Determination of k_∞ from Critical Experiments with the PCTR," Nuclear Sci. Eng., 4, 297 (1958).

(2) Heinemann, R. E. et al, "Experience in the Use of the Physical Constants Testing Reactor," Proceedings of the Second International Conference on the Peaceful Uses of Atomic Energy, 12, 650 (1958).

(3) Weinberg, A. M. and E. P. Wigner, The Physical Theory of Neutron Chain Reactors, The University of Chicago Press, Chicago (1958).

(4) Crandall, J. L., "Efficacy of Experimental Physics Studies on Heavy Water Lattices," Heavy Water Lattices, Second Panel Report, Technical Report Series No. 20, p. 503 (Vienna: IAEA, September 1963).

(5) Kaplan, I., "Measurements of Reactor Parameters in Subcritical and Critical Assemblies, A Review," NYO-10, 207, MITNE-25, August 1962.

(6) Glasstone, S. and M. C. Edlund, The Elements of Nuclear Reactor Theory, D. Van Nostrand Company, Inc., Princeton, New Jersey (1952).

(7) Cohen, E. R. et al., "Exponential Experiments on D_2O Uranium Lattices," Proceedings of the International Conference on the Peaceful Uses of Atomic Energy, 5, 268 (1955).

(8) Palmedo, P. F., I. Kaplan and T. J. Thompson, "Measurements of the Material Bucklings of Lattices of Natural Uranium Rods in D_2O," NYO-9660, MITNE-13, January 1962.

(9) Harrington, J., "Measurement of the Material Buckling of a Lattice of Slightly Enriched Uranium Rods in Heavy Water," SM Thesis, M.I.T. Nucl. Eng. Dept., July 1963.

(10) Thompson, T. J., I. Kaplan, F. M. Clikeman, M. J. Driscoll, "Heavy Water Lattice Project Annual Report," MIT-2344-4, MITNE-65, September 1965.

(11) Hellman, S. P., "Measurements of δ_{28} and ρ_{28} in a 2.5-Inch Triangular Lattice of 0.75-Inch Metallic Uranium Rods (0.947 wt % U^{235}) in a Heavy Water Moderator," SM Thesis, M.I.T. Nucl. Eng. Dept., September 1965.

(12) Robertson, C. G., "Measurements of Neutron Utilization for Lattices of Slightly Enriched Uranium Rods," SM Thesis, M.I.T. Nucl. Eng. Dept., June 1965.

(13) Honeck, H. C., "The Distribution of Thermal Neutrons in Space and Energy in Reactor Lattices. Part I: Theory," Nucl. Sci. and Eng., 8, 193 (1960).

(14) Honeck, H. C., "THERMØS, A Thermalization Transport Theory Code for Reactor Lattice Calculations," BNL-5826, September 1961.

(15) Honeck, H. C., "Some Methods for Improving the Cylindrical Reflecting Boundary Condition in Cell Calculations of the Thermal Neutron Flux," Trans. Amer. Nucl. Soc., 5, No. 2, 350 (1962).

(16) Brown, P. S., T. J. Thompson, I. Kaplan and A. E. Profio, "Measurements of the Spatial and Energy Distribution of Thermal Neutrons in Uranium, Heavy Water Lattices," NYO-10205, MITNE-17, August 20, 1962.

(17) Simms, R., I. Kaplan, T. J. Thompson and D. D. Lanning, "Analytical and Experimental Investigations of the Behavior of Thermal Neutrons in Lattices of Uranium Metal Rods in Heavy Water," NYO-10211, MITNE-33, October 1963.

(18) Suich, J. E., "Calculation of Neutron Absorption Ratios in D_2O-Moderated Mixed Lattices," Trans. Amer. Nucl. Soc., 7, No. 1, 32 (1964).

(19) Heinemann, R. E., "Role of Exponential and PCTR Experiments at Hanford in the Design of Large Power Reactors," Proceedings of the Symposium on Exponential and Critical Experiments, Amsterdam, September 2-6, 1963, I, p. 65 (Vienna: IAEA, February 1964).

(20) Engelder, T. C., N. L. Snidow, D. M. Roberts and G. T. Fairburn, "Measurement of k_∞ from Critical Experiments with the PCTR," Nuc. Sci. Eng., 4, 297 (1958).

(21) Bliss, H. E., I. Kaplan and T. J. Thompson, "Use of a Pulsed Neutron Source to Determine Nuclear Parameters of Lattices of Partially Enriched Uranium Rods in Heavy Water," MIT-2344-7, MITNE-73, September 1966.

(22) Gosnell, J., ScD Thesis, M.I.T. Nuclear Engineering Department, forthcoming.

6. BUCKLING METHODS

H. S. Cheng and I. A. Forbes

During the past year, progress has been made in two areas: moments analysis of buckling data and development of a diagonal buckling method.

1. MOMENTS ANALYSIS (H. S. Cheng)

In analogy to the alternative kernel and moments methods for defining age, one can also determine B_m^2 from moments of the foil activation data instead of by fitting a curve to the data.

1.1 Axial Buckling

Define the n^{th} moment of the axial activity distribution A(Z) as:

$$M_n = \int_0^b Z^n A(Z)\, dZ. \tag{6.1}$$

If $A(Z) \propto \sinh \gamma(H-Z)$,

$$\gamma^2 = \frac{12M_2 - 12bM_1 + b^2M_o}{M_4 - 2bM_3 + b^2M_2}, \tag{6.2}$$

where

b = axial distance between bottom and top foils in the traverse,

H = extrapolated height of the assembly.

The value of H may be determined by a separate experiment, or by calculation, or determined from the moments:

$$H = Z_o + \frac{1}{\gamma} \tanh^{-1} \left\{ \gamma b \left[\frac{\gamma^2(M_3 - 2bM_2 + b^2M_1) + (4bM_o - 6M_1)}{\gamma^2(2M_3 - 3bM_2 + b^3M_o) + 6(bM_o - 2M_1)} \right] \right\}, \tag{6.3}$$

where Z_o is the distance from the bottom of the exponential tank to the first foil.

A computer code was prepared, based on numerical quadrature (Simpson's rule), to evaluate the required moments. Some typical gold foil traverse data were analyzed to compare the results obtained with the moments method to the results of the standard AXFIT code in which γ^2 is determined by least-squares curve fitting. Table 6.1 shows the results of the comparison; the agreement is quite good.

1.2 Radial Buckling

Define the n^{th} moment:

$$M_n = \int_0^R r^n A(r)\, dr. \tag{6.4}$$

If it is assumed that $A(r) \propto J_o(\alpha r)$,

$$\alpha^2 = \frac{2RM_o - 4M_1}{M_3 - 2RM_2 + R^2 M_1}. \tag{6.5}$$

Table 6.2 shows a comparison of the results obtained with moments and curve-fit methods. The agreement is not as good as in the axial case. This is apparently due to the sensitivity of Eq. 6.5: the numerator involves finding small differences between quantities of like magnitudes.

The use of moments analysis of buckling data appears to be a useful alternative to the conventional curve-fitting method. More work is needed, particularly on error analysis, before it will be possible to determine if one method is superior.

2. DIAGONAL BUCKLING (I. A. Forbes)

Conventionally, B_m^2 is measured by performing separate radial and axial traverses in an assembly. It is theoretically possible, however, to determine B_m^2 directly from a single diagonal traverse. If this could be done, in practice it would be possible to automate the taking of buckling data using a counter traversing a lattice in a single direction. The idea of using a diagonal traverse was therefore considered worthy of further evaluation.

Table 6.1

Comparison of Axial Buckling Calculations

Fuel Enrichment (%)	Lattice Triangular Pitch (inches)	Run Number	Axial Buckling, γ^2 (μB)		Extrapolated Height, H (cm)	
			Moments Method	AXFIT Code	Moments Method	AXFIT Code
1.15	1.75	D-2	1015.79	1012	132.12	128
1.15	2.50	92	1390.63	1390	126.68	127.9
1.15	1.25	81	975.86	987	128.904	128
0.947	2.50	D-8	1388.62	1405*	132.34	134*
				1389		132.6
0.947	5.00	H-9	254.11	260	123.89	124
0.947	5.00	J-1	305.87	304	120.09	120.2

*The top values were obtained from the D-8 run, while the bottom values were obtained from the D-9 run which was made in the same lattice as D-8.

Table 6.2

Comparison of Radial Buckling Calculations

Fuel Enrichment (%)	Lattice Triangular Pitch (inches)	Run Number	Radial Buckling, α^2 (μB)		Extrapolated Radius (cm)	
			Moments Method	RADFIT Code	Moments Method	RADFIT Code
1.15	1.25	83	2612.31	2440	47.051	48.684
1.15	1.75	B-4	2681.9	2475	46.43	48.34

2.1 Experiments

A standard radial foil holder was modified to hang diagonally instead of horizontally in the lattice, and the foils were spaced so as to occupy equivalent positions in the unit cells traversed. Aside from this, all experimental procedures, foil counting, and raw data processing were exactly the same as for standard radial measurements.

Figure 6.1 shows the foil holder positioned in a lattice, and Fig. 6.2 shows activity traverses measured along the diagonal for the 2.25-inch-spacing lattice of 0.387-inch-diameter, 0.947% enriched fuel rods.

2.2 Data Analysis

The data are analyzed by using a computer program in the following iterative procedure:

(a) A value is assumed for α^2. This is easy to do with good accuracy because α^2 changes only slightly from lattice to lattice.

(b) A radial distribution, $\phi(r) = J_o(\alpha r)$, is computed and divided into the experimental data to obtain a trial axial distribution.

(c) The axial data are then processed by the moments technique described in section 1 to obtain γ^2 (and also H if it is not otherwise specified).

(d) The value of γ^2 is used to compute an axial distribution, $\phi(Z) = \sinh \gamma(H-Z)$, which is divided into the experimental data to give a trial radial distribution.

(e) A value of α^2 is determined, again using the moments method described in section 1.

(f) Steps (a) through (e) are repeated until α^2 changes by less than 0.1%.

Table 6.3 shows the results of analyzing the data for the runs plotted in Fig. 6.2, together with the results of a conventional run in which separate axial and radial measurements were made.

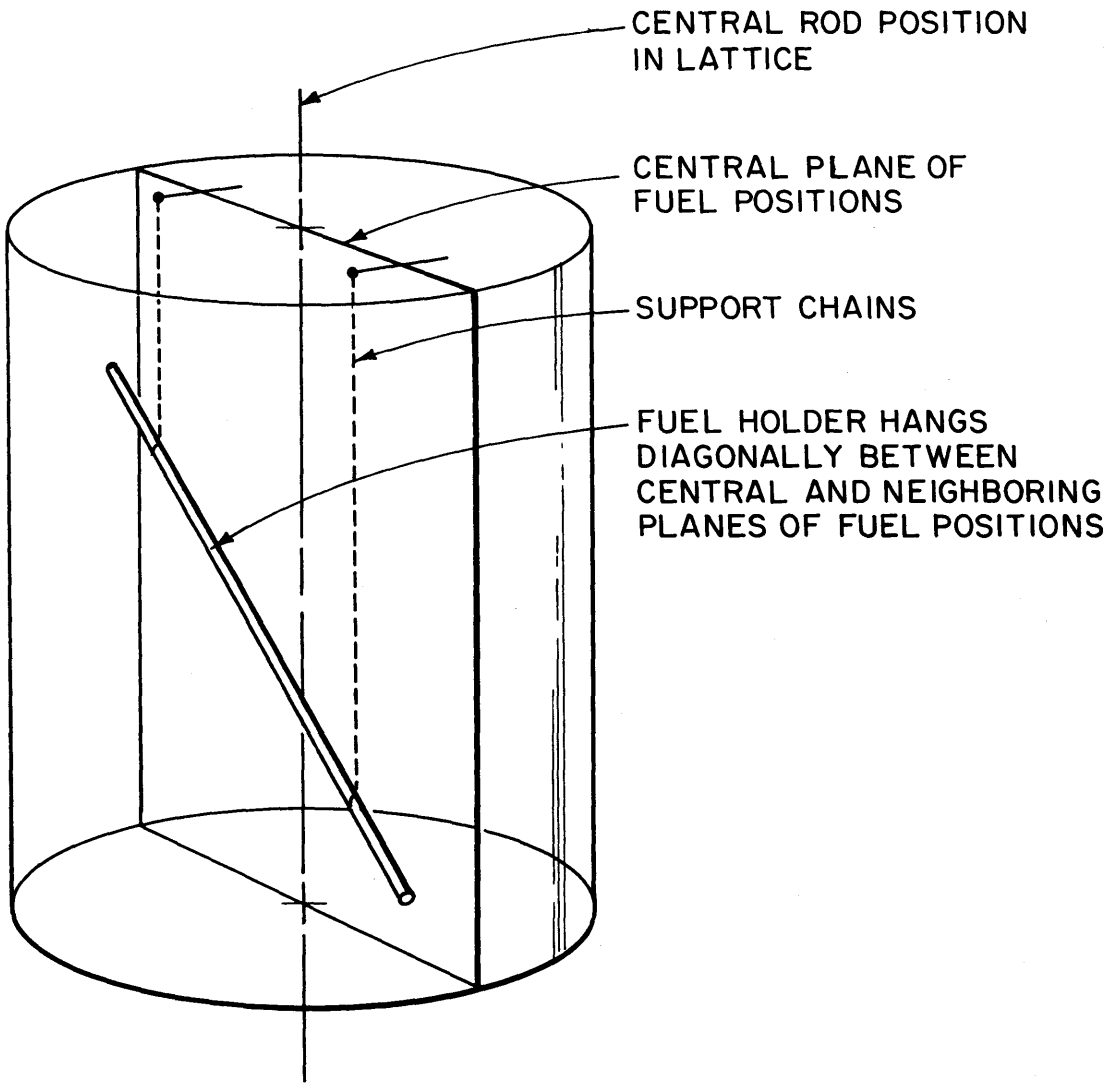

FIGURE 6.1 FOIL HOLDER POSITION FOR DIAGONAL TRAVERSE

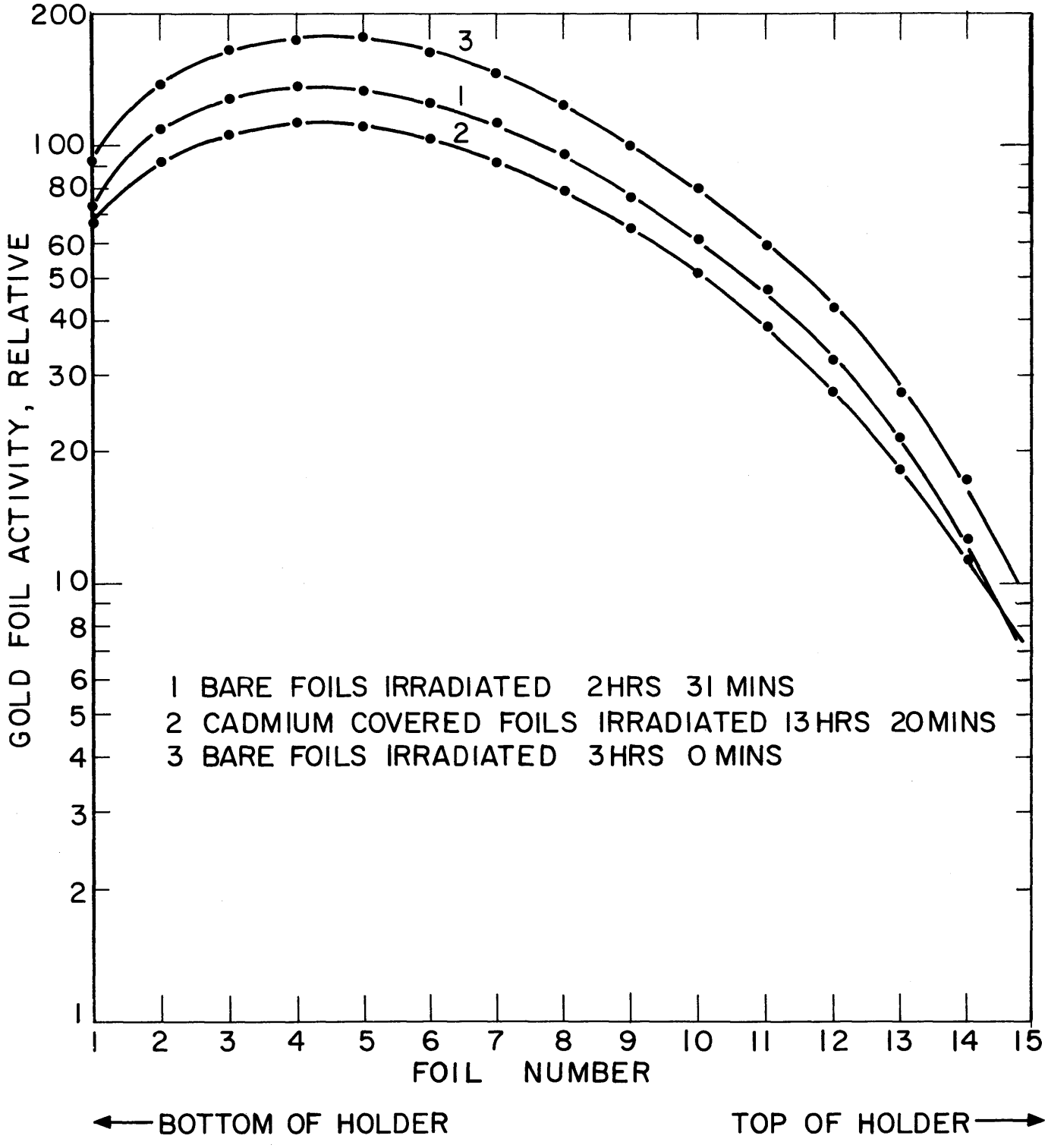

FIG. 6.2 DIAGONAL ACTIVATION TRAVERSES

Table 6.3

Diagonal Buckling Results

Run Number	Number of Points Fitted	α^2	γ^2	B_m^2 (μB)
1	13	2385.7	1147.5	1238.2
	11	2421.7	1176.2	1245.5
2	13	2370.1	1148.4	1221.7
Cadmium-covered foils	11	2263.7	1061.4	1202.3
3	11	2525.8	1238.7	1287.1
4 (mean of 1, 2, 3)		2393.0	1154.0	1239.0
5*		2404.0	1148.0	1256.0

*Conventional data taken, using separate radial and axial traverses analyzed with the AXFIT and RADFIT codes.

As can be seen from Table 6.3, the agreement between diagonal and conventional values of B_m^2 is good. In view of this result, future B_m^2 measurements on lattices will include diagonal traverses for comparison with the standard axial-radial results. In addition, more theoretical work is needed on error analysis and computer code development.

3. REFERENCES

(1) Palmedo, P. F., I. Kaplan and T. J. Thompson, "Measurements of the Material Bucklings of Lattices of Natural Uranium Rods in D_2O," NYO-9660, MITNE-13, January 1962.

7. INTRACELLULAR FLUX TRAVERSES WITH LUTETIUM

D. Frech and J. Barch

1. INTRODUCTION

Standard methods have been developed to measure the intracellular thermal neutron distributions for lattices studied in the M. I. T. Lattice Facility (1, 2). The results given here are for lutetium irradiations in lattices of 1.143% U^{235} enriched, 0.25-inch-diameter rods in a triangular spacing of 1.75 inches; and 0.947% U^{235} enriched, 0.75-inch-diameter uranium rods in 2.5-inch and 5.0-inch triangular spacings. A gold traverse is also reported for the 2.5-inch lattice.

2. EXPERIMENTAL PROCEDURES

The foils used as detectors were bare, 1/16-inch-diameter, 0.010-inch-thick, 10% Lu_2O_3 by weight in aluminum; and 1/16-inch-diameter, bare and cadmium-covered gold, 0.005 inch thick. The lutetium alloy foils were allowed to decay at least two days before counting to eliminate the 3.75-hour Lu^{176m} activity. The foils were counted on automatic sample-changing scintillation counters. Axial and radial leakage corrections were made as well as routine counting corrections. The activities of all foils irradiated in the same relative position in the cell were averaged together and the results are plotted in Figs. 7.1, 7.2 and 7.3. The errors due to counting statistics are about the size of the points.

3. RESULTS

The results are compared with distributions predicted by the modified one-dimensional THERMØS computer code (3). Both the THERMØS and the experimental distributions were normalized to 1.0 at the edge of the cell. The experimental lutetium activities generally exceed the theoretical activities slightly, indicating either that the amount of spectral hardening may be slightly greater than predicted by THERMØS or that

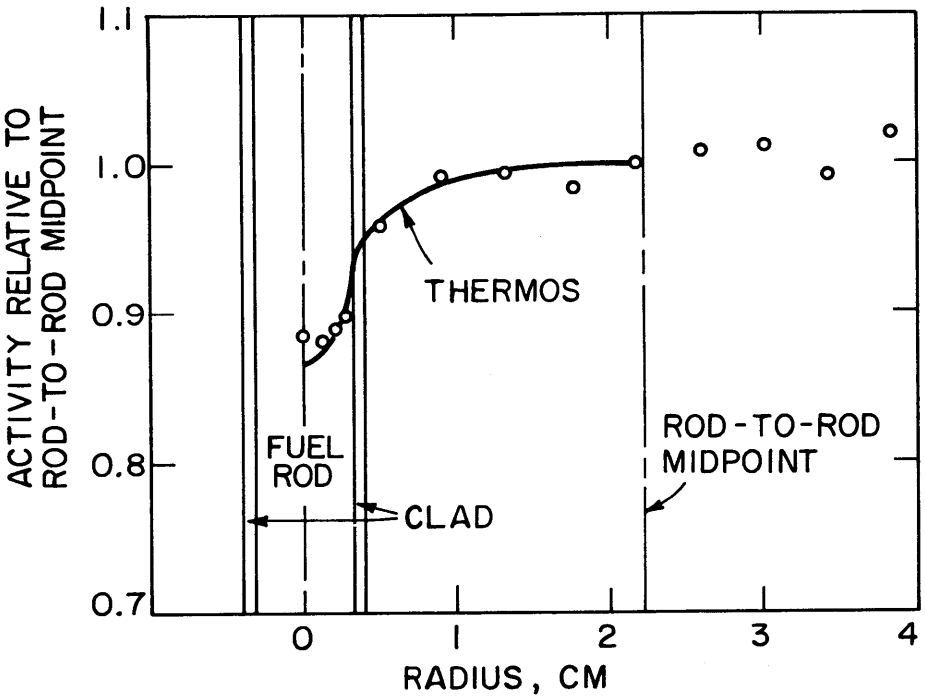

FIG. 7.1 Lu^{177} ACTIVITY DISTRIBUTION IN A LATTICE OF 0.25-INCH DIAMETER, 1.143% U^{235} RODS ON A 1.75-INCH TRIANGULAR PITCH

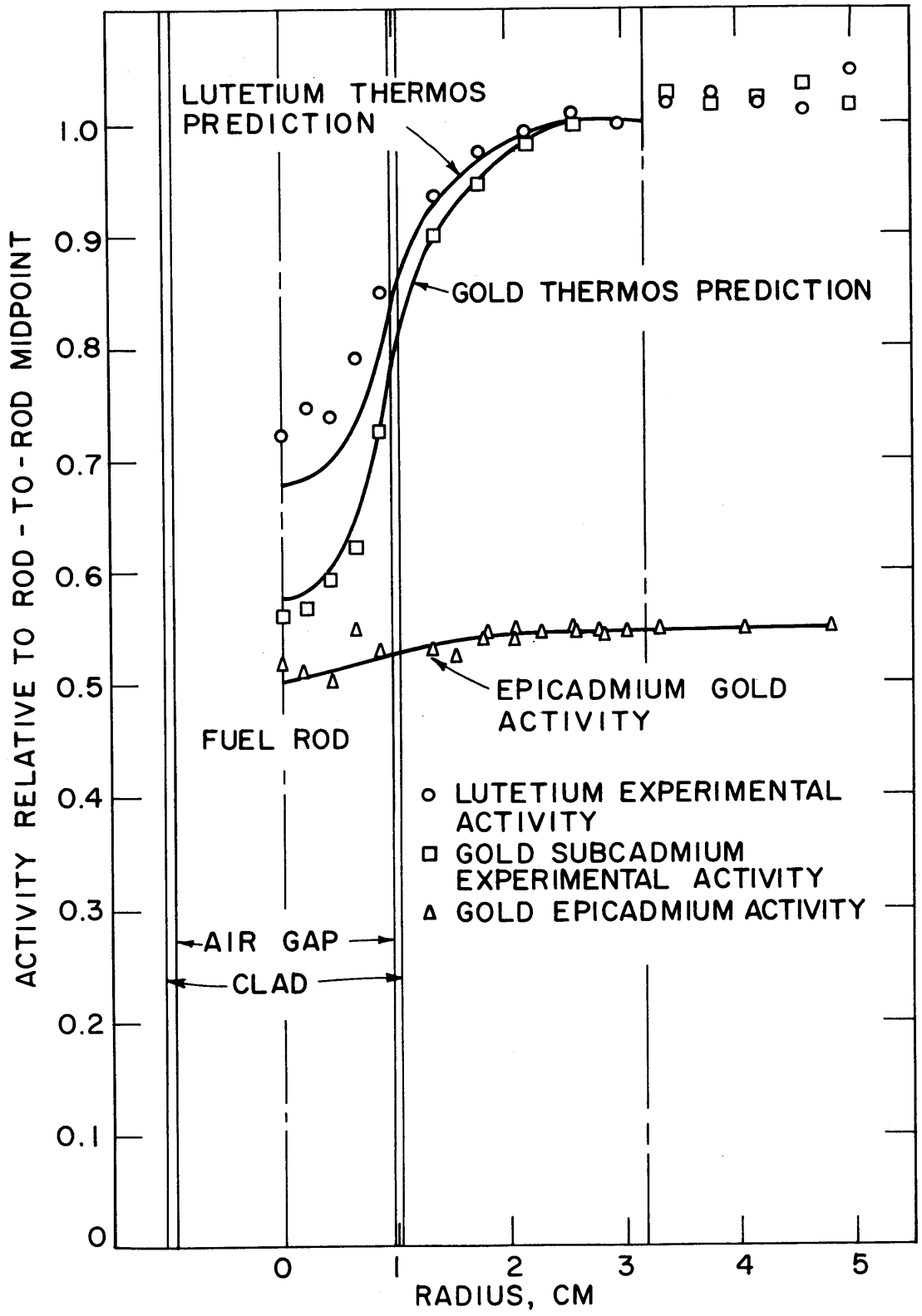

FIG. 7.2 Lu^{177} AND Au^{198} ACTIVITY DISTRIBUTIONS IN A LATTICE OF 0.75-INCH DIAMETER, 0.947% U^{235} RODS ON A 2.5-INCH TRIANGULAR PITCH

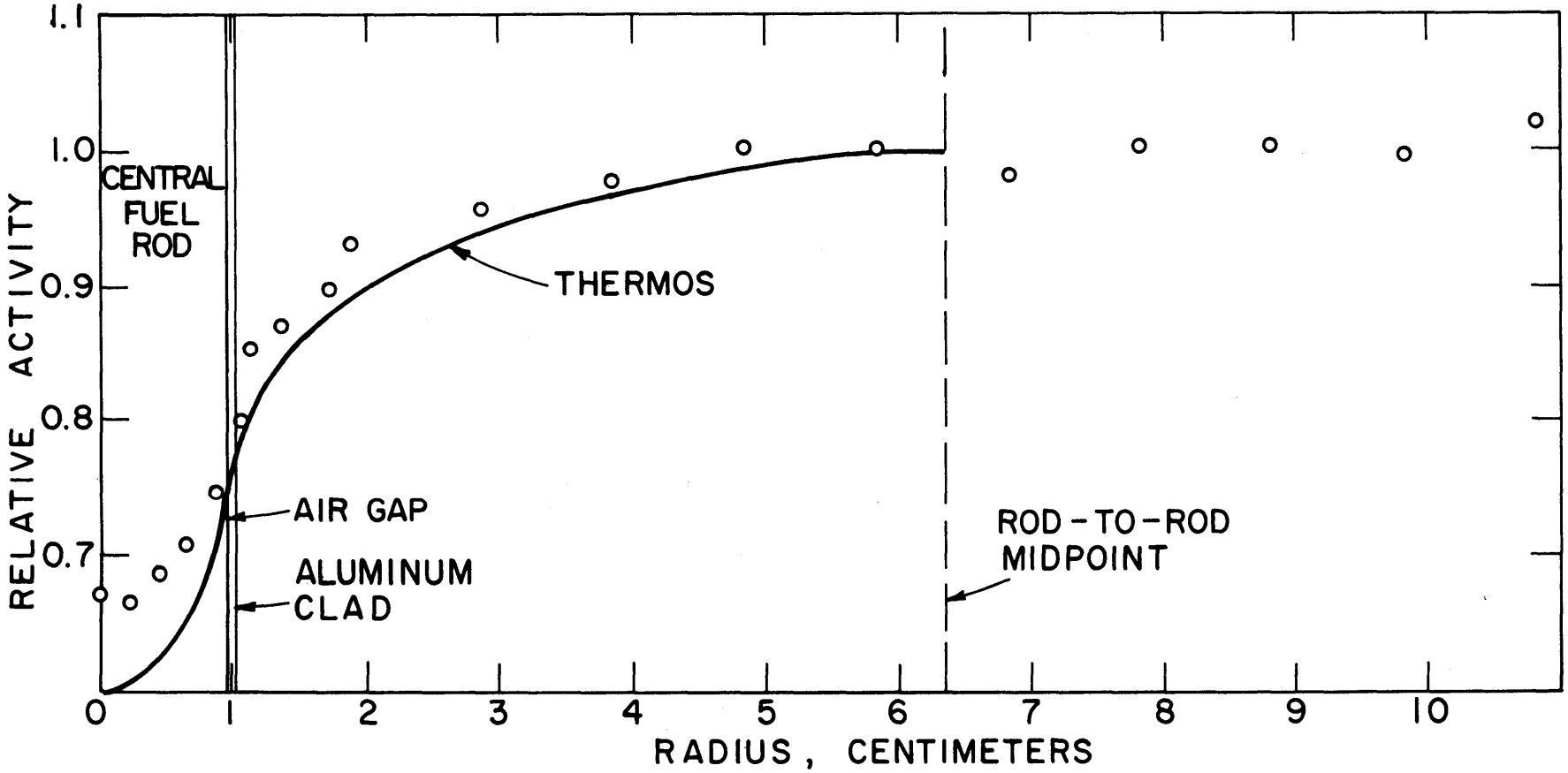

FIG. 7.3 Lu^{177} ACTIVITY DISTRIBUTION IN A LATTICE OF 0.75-INCH DIAMETER, 0.947% U-235 RODS ON A 5-INCH SPACING

the lutetium cross-section data are slightly in error. These results are consistent with those reported by Brown (2) for other M.I.T. lattices, in that experimental data generally exceed the THERMØS prediction by a few percent if both are normalized to agree at the cell edge.

As noted in the last annual report, gold traverses are predicted extremely well by THERMØS: a conclusion substantiated by the gold foil data in Fig. 7.2.

More in-fuel lutetium measurements are planned to examine spectral hardening, primarily to determine fuel-averaged neutron temperatures for comparison with THERMØS results. On the other hand, less emphasis will be placed on measurement of intracellular traverses because of the demonstrated accuracy of the THERMØS code in calculating such traverses for the lattices under investigation at M.I.T.

4. REFERENCES

(1) "Heavy Water Lattice Research Project Annual Report," NYO-10212, MITNE-46, September 30, 1963.

(2) Brown, P. S., T. J. Thompson, I. Kaplan and A. E. Profio, "Measurements of the Spatial and Energy Distribution of Thermal Neutrons in Uranium, Heavy Water Lattices," NYO-10205, MITNE-17, August 20, 1962.

(3) Honeck, H. C., "THERMØS, A Thermalization Transport Theory Code for Reactor Lattice Calculations," BNL-5826, September 1961.

8. MINIATURE LATTICE STUDIES

E. Sefchovich

This chapter contains a summary of the topical report: MIT-2344-8, MITNE-76 of October 1966, "The Measurement of Reactor Parameters in Slightly Enriched Uranium, Heavy Water Moderated Miniature Lattices," by E. Sefchovich, I. Kaplan and T. J. Thompson. A preliminary progress report was also contained in the 1965 Annual Report.

1. INTRODUCTION

Miniature lattices are being studied because if they can provide results that are useful in the design of full-scale reactor lattices, they offer the possibility of a large saving in cost and an increase in flexibility as compared with large subcritical or critical facilities. To establish their utility, it is necessary to show that they can provide reactor physics data comparable to those obtained in the larger assemblies.

The objective of the present work was to investigate the possibility of using miniature lattices for the measurement of lattice parameters. The following quantities, which are related either to k_∞ or the initial conversion ratio C, were measured: the ratio of epicadmium to subcadmium capture rates in U^{238} (ρ_{28}); the ratio of epicadmium to subcadmium fission rates in U^{235} (δ_{25}); the U^{238}-to-U^{235} fission ratio (δ_{28}); the ratio of the total capture rate in U^{238} to the total fission rate in U^{235} (C^*); the intracellular activity distribution of bare and cadmium-covered gold foils; and the axial and radial activity distributions of bare and cadmium-covered gold foils.

Although the determination of k_∞ by means of the four-factor formula requires that the various factors be determined for an infinite assembly, the parameters related to the four factors in k_∞ cannot, of course, be measured in an infinite assembly. Hence, lattice parameters are always measured in finite assemblies, either critical or subcritical

lattices, and corrections for leakage must be applied.

When these parameters are measured in a critical assembly, corrections for neutron leakage are smaller than those needed for subcritical assemblies, and the energy spectrum resembles closely the spectrum of neutrons in the reactor of interest. Critical assemblies have, however, several disadvantages: first, they require elaborate safety provisions; second, they need a larger investment in materials than do subcritical assemblies; and third, their use becomes cumbersome when many lattices are to be investigated.

Subcritical assemblies circumvent some of the difficulties inherent in critical assemblies but they present some disadvantages. Source effects, which are absent in critical assemblies, may be troublesome in an exponential experiment. The higher leakage rate as compared with that in critical assemblies may necessitate corrections in some of the measurements. Nevertheless, exponential assemblies remain useful tools for the testing of reactor theory and for reactor design. When subcritical assemblies are used, experimenters prefer lattices that are not far from critical. Over a large portion of such an assembly, the neutron spectrum resembles closely that in a critical assembly. Moreover, the measurements can be made far enough from the source and the boundaries so that corrections for neutron leakage and source neutrons are not much larger than in critical assemblies. The values of the parameters that are measured in this region, the equilibrium or "asymptotic" region, are therefore close to their value in a critical assembly.

In contrast with the determination of lattice parameters in critical assemblies and in the equilibrium region of an exponential assembly, the effects of source neutrons and boundaries are very important in the interpretation of data from miniature lattices. A theoretical model, which is an extension of that of Peak (1), has been developed to correct for source and boundary effects. This model permits the extrapolation of miniature lattice data to exponential, critical and infinite assemblies and, by so doing, a comparison can be made between results obtained in lattices of different dimensions. To test the validity of the methods described here, measurements were made in six lattices which are

Table 8.1
Lattices Investigated*

U^{235} Concentration of Fuel (percent)	Rod-to-Rod Distance (inches)	Denomination of Lattice
1.143	1.25	ML2
1.143	1.75	ML7
1.143	2.50	ML3
1.027	1.25	ML4
1.027	1.75	ML6
1.027	2.50	ML5

*All lattices are moderated by 99.75 mole percent D_2O. Fuel rods are 0.25-inch diameter in aluminum tubes of 0.318-inch O.D.

miniature versions of lattices investigated in the exponential assembly at M. I. T. The lattices studied are described in Table 8.1. The validity of the extrapolation methods was tested by comparing the results of correcting miniature lattice data to exponential assemblies with the results obtained from measurements in the exponential facility at M. I. T. This summary describes the measurements made, the extrapolation techniques used, and the results obtained in this research.

2. EXPERIMENTAL TECHNIQUES AND FACILITIES

2.1 Experimental Facilities

The source of neutrons for the present study was the neutron beam in the Medical Therapy Facility at the M. I. T. Reactor. The nominal power in the course of these experiments was 5 MW. The miniature lattice tank is a right circular cylinder, 21 inches high and 20 inches in diameter, with a removable base plate of 1/2-inch-thick aluminum. The tank is equipped with a wheeled stand to provide mobility and with appropriate piping to allow filling and draining. The fuel elements are 16-inch-long, U-metal rods and the required lattice spacings

are obtained through the use of different grid plates.

The shielding consists of successive laminae of 1/4-inch borated plastic, three inches of paraffin, a layer of cadmium and three more inches of paraffin. The shielding is completely lined with cadmium to minimize the reflection of thermal neutrons back into the lattice. The tank itself is surrounded on the outside and bottom by cadmium to approximate as closely as possible a bare assembly.

In the course of this work, it was necessary to add a collimator to the beam port to modify the radial and azimuthal dependence of the neutrons entering the miniature lattice.

2.2 Experimental Techniques

One objective of the present study was to improve on the techniques used by Peak (1). Since the time of his research, much work at the M. I. T. Lattice Project has been devoted to improving the accuracy of the techniques used for the measurement of lattice parameters. Hence, except for changes made necessary by the small size of the assembly, axial and radial traverses were made according to the procedure of Palmedo (2) as improved by Harrington (3); the methods of Simms (4) were used for intracellular measurements; and the techniques developed by D'Ardenne (5) were used to measure δ_{28}, ρ_{28}, δ_{25} and C^*.

3. THEORETICAL METHODS

In contrast with exponential assemblies, in miniature lattices an equilibrium region is, in general, not achieved, and source and boundary effects are of great importance. Corrections for these effects must therefore be applied to the parameters measured in the miniature lattice.

Source effects are generally of three kinds. First, the spectrum of source neutrons is different from the spectrum of neutrons born in the lattice. Second, the anisotropy of the source results in the presence of harmonics. Third, the source may be asymmetric. This latter problem was avoided by placing a source collimator under the neutron beam.

Boundaries also cause several difficulties: first, they introduce spatial harmonics; second, in contrast with larger assemblies, the

increased leakage during slowing down in the miniature lattice results in a harder spectrum; third, the extrapolated dimensions of the assembly must be defined accurately. The latter problem was solved by designing the shielding as described in section 2.1.

The theory developed in this work was aimed at taking into account the effects discussed above.

3.1 Subcritical Assemblies

To calculate the thermal flux and slowing-down density in subcritical assemblies, the following assumptions are made:

1. Age-diffusion theory is applicable.

2. The thermal flux has two components: one due to neutrons coming from the source ϕ_s and the second due to neutrons born in the lattice ϕ_ℓ; Σ_a^s, D^s and L_s are, respectively, the thermal absorption cross section, the diffusion coefficient, and the thermal diffusion length of source neutrons; Σ_a^ℓ, D^ℓ and L_ℓ are the corresponding parameters for the spectrum characteristic of the lattice-born neutrons.

3. The thermal flux due to source neutrons satisfies the equation:

$$D^s\nabla^2\phi_s(r,z) - \Sigma_a^s\phi_s(r,z) = 0. \tag{8.1}$$

The boundary conditions are:

$$\phi_s(r,H) = \phi_s(R,z) = 0\,; \qquad -D^s\left[\frac{\partial\phi_s(r,z)}{\partial z}\right]_{z=0} = S(r), \tag{8.2}$$

where R and H are the extrapolated dimensions and S(r) is the neutron source as a function of the radius.

4. The flux of lattice-born neutrons satisfies the equation:

$$D^\ell\nabla^2\phi_\ell(r,z) - \Sigma_a^\ell\phi_\ell(r,z) + pq(r,z,\tau_t) = 0, \tag{8.3}$$

where p is the resonance escape probability and $q(r,z,\tau_t)$ is the slowing-down density at τ_t, the age to thermal energies.

5. The slowing-down density satisfies the age equation:

$$\nabla^2 q(r,z,\tau) = \frac{\partial}{\partial\tau}\, q(r,z,\tau), \tag{8.4}$$

without absorption, absorption being included in p. The initial condition for q is:

$$q(r, z, \tau=0) = \frac{k_\infty}{p}\left[\Sigma_a^s \phi_s(r, z)+\Sigma_a^\ell \phi_\ell(r, z)\right]. \tag{8.5}$$

The only boundary conditions that can be specified for q and ϕ_ℓ are:

$$q(r, H, \tau) = q(r, z, \tau) = \phi_\ell(r, H) = \phi_\ell(R, z) = 0. \tag{8.6}$$

Near the source end, one is faced with a problem in which the energy and space dependence of ϕ_ℓ and q are not separable. Thus, the extrapolation length at z=0 will depend on the age. To approximate the solution of the nonseparable problem in subcritical assemblies, it is assumed that q and ϕ_ℓ can be expanded in cylindrical harmonics. This approximation suggests itself because the fundamental modes of q and ϕ_ℓ are the solutions of the corresponding problem in a critical assembly. The results obtained by expanding the flux and slowing-down density in cylindrical harmonics are listed in Table 8.2. The quantities α_i in Table 8.2 are the solutions of the equation, $J_o(\alpha_i R) = 0$; J_1 is the Bessel function of order one.

3.2 Critical and Infinite Assemblies

The case of critical and infinite assemblies is simpler than that of subcritical assemblies. There are no external sources; all neutrons are born and slow down in the assembly. In critical assemblies, the thermal flux ϕ_c and the slowing-down density q_c vanish at approximately the same extrapolated dimensions and since only the fundamental mode is present, they are given by:

$$\phi_c(r, z) = \phi_o J_o(\alpha r) \sin \frac{\pi z}{H}, \tag{8.7}$$

and

$$q_c(r, z, \tau) = \phi_o \frac{k_\infty \Sigma_a}{p} J_o(\alpha r) \sin \frac{\pi z}{H} e^{-B_m^2 \tau}, \tag{8.8}$$

where ϕ_o is a constant of integration which denotes the thermal flux at the center of the lattice.

Table 8.2

Summary of Results for Subcritical Assemblies

$$\phi_s(r,z) = \frac{2S}{R^2 D^s} \sum_{i=1}^{\infty} \frac{\bar{f}_i}{\beta_i} \frac{\sinh \beta_i(H-z)}{\cosh \beta_i H} \frac{J_o(\alpha_i r)}{[J_1(\alpha_i R)]^2}$$

$$\phi_\ell(r,z) = \frac{4S}{R^2 D^s} \frac{\Sigma_a^s}{\Sigma_a^\ell} \sum_{i=1}^{\infty} \sum_{n=1}^{\infty} \frac{\bar{f}_i}{\beta_i} \frac{k_{in}}{1 - k_{in}} \frac{n\pi \tanh \beta_i H}{(n\pi)^2 + (\beta_i H)^2} \sin\left(\frac{n\pi z}{H}\right) \frac{J_o(\alpha_i r)}{[J_1(\alpha_i R)]^2}$$

$$pq(r,z,\tau) = \frac{4S}{R^2 D^s} k_\infty \Sigma_a^s \sum_{i=1}^{\infty} \sum_{n=1}^{\infty} \frac{\bar{f}_i}{\beta_i} \frac{1}{1 - k_{in}} \frac{n\pi \tanh \beta_i H}{(n\pi)^2 + (\beta_i H)^2} e^{-B_{in}^2 \tau} \sin\left(\frac{n\pi z}{H}\right) \frac{J_o(\alpha_i r)}{[J_1(\alpha_i R)]^2}$$

$$\phi_t(r,z) = \phi_s(r,z) + \phi_\ell(r,z)$$

$$S(r) = Sf(r) = \frac{2S}{R^2} \sum_{i=1}^{\infty} \bar{f}_i \frac{J_o(\alpha_i r)}{[J_1(\alpha_i R)]^2}$$

$$\bar{f}_i = \int_0^R r f(r) J_o(\alpha_i r)\, dr$$

$$\beta_i^2 = \frac{\Sigma_a^s}{D^s} + \alpha_i^2 = \frac{1}{L_s^2} + \alpha_i^2$$

$$B_{in}^2 = \alpha_i^2 + \left(\frac{n\pi}{H}\right)^2$$

$$k_{in} = \frac{k_\infty e^{-B_{in}^2 \tau_t}}{1 + L_\ell^2 B_{in}^2}$$

In an infinite assembly, there is neither leakage nor spatial variation in either q_∞ or ϕ_∞; the energy dependence is included in p. The solutions are:

$$\phi_\infty = \phi_o \tag{8.9}$$

and

$$q_\infty = \frac{k_\infty \Sigma_a}{p} \phi_o . \tag{8.10}$$

3.3 Test of the Theory

The model whose derivation was outlined above, was used to correct ρ_{28}, δ_{25} and C^*, all of which are related to cadmium ratios. It is, therefore, necessary that the model described be able to predict the values of cadmium ratios. The extrapolations to infinite assemblies of δ_{28} and the intracellular distribution of the subcadmium activation of gold required a different treatment, described in sections 3.4.2 and 3.4.3.

The axial and radial distributions of the activity of bare and cadmium-covered gold foils were measured with two objectives in mind: first, the distributions made it possible to relate measurements made at different positions within an assembly; second, they provided a means of testing the model just derived through the axial distribution of the cadmium ratio of gold.

Assuming that the thermal flux has a Maxwellian energy distribution M(E) which joins the epithermal 1/E flux at about 0.12 ev ($\sim$5kT), and that the cadmium cutoff energy is 0.4 ev which corresponds to a cadmium thickness of 0.20 inch, the following expressions are obtained for the subcadmium saturated activity per unit nuclide of gold A_b-A_c and the epicadmium saturated activity per unit nuclide A_c:

$$A_b(r,z) - A_c(r,z) = 0.886\, \sigma_o \phi_t(r,z) + 0.414\, \sigma_o \frac{pq(r,z,\tau_{28})}{\xi \Sigma_s} \tag{8.11}$$

and

$$A_c(r,z) = S_{Au} \sigma_o \frac{pq(r,z,\tau_{28})}{\xi \Sigma_s}, \tag{8.12}$$

where

$$S_{Au} = \frac{ERI_{Au}}{\sigma_o} + 0.5, \tag{8.13}$$

σ_o is the 2200 m/sec absorption cross section of gold, and ERI_{Au} is the effective resonance integral of gold. The cadmium ratio of gold $R_{Au}(r, z)$ is readily obtained from Eqs. 8.11 and 8.12 as:

$$R_{Au}(r, z) - 1 = \frac{0.886 + 0.414\ \psi(r, z)}{S_{Au}\psi(r, z)}, \tag{8.14}$$

where

$$\psi(r, z) = \frac{pq(r, z, \tau_{28})}{\xi \Sigma_s \phi_t(r, z)}. \tag{8.15}$$

In the preceding derivation, it has been assumed that epicadmium capture in U^{238} takes place at an effective age τ_{28}. Equation 8.14 was used to test the theory in all the lattices investigated. The results are discussed in section 4.1.

3.4 Correction Procedures for Lattice Parameters

In the derivations below, the indices ML, EX, C and ∞ will denote the value of a quantity in a miniature, an exponential, a bare critical, and an infinite assembly, respectively.

3.4.1 The Parameters ρ_{28}, δ_{25} and C^*

The correction factors for ρ_{28}, δ_{25} and C^* can be obtained by an analysis similar to that used to obtain R_{Au}-1. It must be noticed, however, that since these parameters are determined inside the fuel, σ_a^{28} and σ_f^{25} must be defined as the average thermal cross sections for absorption in U^{238} and fission in U^{235}, respectively, as obtained with the THERMØS (6) code which takes into account the hardening of the neutron spectrum. Since ρ_{28} is given by

$$\rho_{28} = \frac{1}{R_{28} - 1}, \tag{8.16}$$

then

$$\rho_{28}(r, z) = S_{28}\psi(r, z), \tag{8.17}$$

where

$$S_{28} = \frac{ERI_{28}}{\sigma_a^{28}} + 0.5 \ .$$

To relate the value of ρ_{28} measured in the miniature lattice to that measured in the equilibrium region of an exponential assembly, Eq. 8.17 is written for both assemblies and the ratio is taken. The relation is:

$$\rho_{28}^{EX} = \left(S_{28}^{EX}\psi_{EX}(r^E, z^E)/S_{28}^{ML}\psi_{ML}(r, z)\right)\rho_{28}^{ML}(r, z), \qquad (8.18)$$

where (r^E, z^E) denotes a position in the equilibrium region of the exponential assembly. The value of (r^E, z^E) is evidently immaterial since the equilibrium region is defined to be that in which ψ is constant to a first approximation. To obtain the extrapolation factors to critical and infinite assemblies, it is sufficient to change the index EX to C and ∞, respectively.

The quantity δ_{25} is defined in a similar way but for fissions in U^{235}. By similarity with ρ_{28}, the extrapolation factor for δ_{25} can be written as:

$$\delta_{25}^{EX} = \frac{S_{25}^{EX}}{S_{25}^{ML}} \frac{\psi_{EX}(r^E, z^E)}{\psi_{ML}(r, z)} \delta_{25}^{ML}(r, z), \qquad (8.19)$$

where

$$S_{25} = \frac{ERI_{25}}{\sigma_f^{25}} + 0.5 \ , \qquad (8.20)$$

in which ERI_{25} is the effective resonance integral for fissions in U^{235}.

The parameter C^* can be obtained in two independent ways. The definition,

$$C^* = \frac{1 + \rho_{28}}{1 + \delta_{25}} \left(\frac{\Sigma_a^{28}}{\Sigma_f^{25}}\right)_{sc} , \qquad (8.21)$$

can be corrected immediately with the aid of Eqs. 8.19 and 8.20. Thus,

$$C^*_{EX} = \frac{1 + \rho_{28}^{EX}}{1 + \rho_{28}^{ML}(r,z)} \frac{1 + \delta_{25}^{ML}(r,z)}{1 + \delta_{25}^{EX}} C^*_{ML}(r,z). \tag{8.22}$$

In the same way, the definition,

$$C^* = C^*_M R_N / R_F, \tag{8.23}$$

must be extrapolated according to the relation,

$$C^*_{EX} = \frac{1 + S_{28}^{EX}\psi_{EX}(r^E, z^E)}{1 + S_{28}^{ML}\psi_{ML}(r,z)} \frac{1 + S_{25}^{ML}\psi_{ML}(r,z)}{1 + S_{25}^{EX}\psi_{EX}(r^E, z^E)} C^*_{ML}(r,z). \tag{8.24}$$

3.4.2 The Fast Fission Ratio δ_{28}

According to the definition of δ_{28} given in section 1, δ_{28} can be written as:

$$\delta_{28} \simeq \frac{\bar{\sigma}_f^{28}}{\bar{\sigma}_f^{25}} \frac{\phi_F}{\phi_t}, \tag{8.25}$$

where σ_f^{28} and σ_f^{25} are the average fission cross sections of U^{238} and U^{235}, respectively; ϕ_F and ϕ_t are the average fast flux and thermal flux in the fuel, respectively. If the measurements in assemblies of different sizes are normalized to the same thermal flux, the required extrapolation correction is:

$$\delta_{28}^{EX} = \frac{\phi_F^{EX}}{\phi_F^{ML}} \delta_{28}^{ML}. \tag{8.26}$$

The difference between ϕ_F^{EX} and ϕ_F^{ML} comes from the interaction effect which depends: first, on the number of rings of fuel rods contributing to the fast flux in the fuel rod under consideration; and second, on the number of fission neutrons produced in these rods, i.e., the fission rate in U^{235} in the surrounding rods which is approximately proportional to the thermal flux. In miniature lattices, the number of contributing rods is smaller than in the larger assemblies; moreover,

the thermal neutron flux goes to zero more rapidly than in the larger assemblies because the boundaries are closer to the centermost rod. Thus, the correction factor in Eq. 8.26 is always greater than unity.

To calculate the ratio ϕ_F^{EX}/ϕ_F^{ML}, the theory developed by Woodruff (7) was used. The computation consists in integrating the single collision transport kernel for cylindrical shell sources. The integration is over the volume of each fuel rod in the assembly. The results are multiplied by the appropriate weighting factor (for cylinders: a J_o function) and then added to give the relative fast flux at the points of interest. Finally, the average over the fuel rod is computed.

3.4.3 Intracellular Subcadmium Activity Distribution of Gold

In determining k_∞, the value of the thermal utilization, f, must be determined for an infinite assembly. Hence, the intracellular thermal flux distribution of interest in calculating f is that in an infinite lattice.

Consider an infinite array of fuel rods placed periodically in an assembly. The thermal neutron flux distribution may be written as:

$$\phi(r) = \phi_M \phi_f(r), \tag{8.27}$$

where ϕ_M denotes the macroscopic flux distribution — in this case, a constant; ϕ_f, the intracellular flux distribution, represents the perturbation due to the rods and is the flux distribution of interest.

When the measurement is made in an infinite assembly, ϕ_M is no longer a constant. For a cylindrical lattice, it is given by:

$$\phi_M(r, z) = A' J_o(\alpha r)\, f(z), \tag{8.28}$$

where A′ is a constant; f(z) gives the axial variation of the flux. The measured subcadmium activity distribution at a given height, $z=z_o$, is given by:

$$A(r) = C J_o(\alpha r)\, \phi_f(r), \tag{8.29}$$

where C is a constant. Since C is the same for all the foils in an intracellular traverse, it can be set equal to unity. To obtain $\phi_f(r)$, the fine structure, the measured subcadmium activity must be corrected for the

macroscopic flux distribution. Thus,

$$\phi_f(r) = \frac{A(r)}{J_o(\alpha r)}, \tag{8.30}$$

where $\alpha = 2.405/R$. The experimental results indicate that the macroscopic subcadmium activity distribution of gold – at least, within the cell in which the measurements were made – has, indeed, a J_o-functional dependence.

4. RESULTS

4.1 Axial and Radial Traverses of R_{Au}-1

The distribution of the cadmium ratio of gold permitted the testing of the model derived in section 3.2 as discussed in section 3.3. The axial distribution of R_{Au}-1 in the six lattices investigated is shown in Figs. 8.1 through 8.6. The solid curve represents the value predicted by Eq. 8.14. The theoretical calculations were made with the MINIFLUX computer program. The parameters required for the use of MINIFLUX are listed in Table 8.3. The analytical methods used to obtain these quantities are discussed in section 5. It is evident that in all the lattices, the computed value of R_{Au}-1 agrees well with the measured value, at least over the bottom half of the assembly. There are two reasons for the discrepancy between measured and calculated values of R_{Au}-1 near the source end. First, the diffusion approximation fails near the source end. Second, the expansion in axial (Fourier) harmonics fails near the discontinuity at z=0. This is the result of fitting a discontinuous function with a finite number of continuous functions.

For the purpose of this work, the important result is that the theory predicts R_{Au}-1 over the region where ρ_{28}, δ_{25}, δ_{28} and C^* were measured. Hence, the theory can be used to extrapolate the values of these parameters obtained in the miniature lattice to exponential, critical, and infinite assemblies.

A typical radial distribution of R_{Au}-1 is shown in Fig. 8.7. Since each data point corresponds to a position halfway between adjacent rings of rods, it follows that R_{Au}-1 is constant over a portion of the lattice

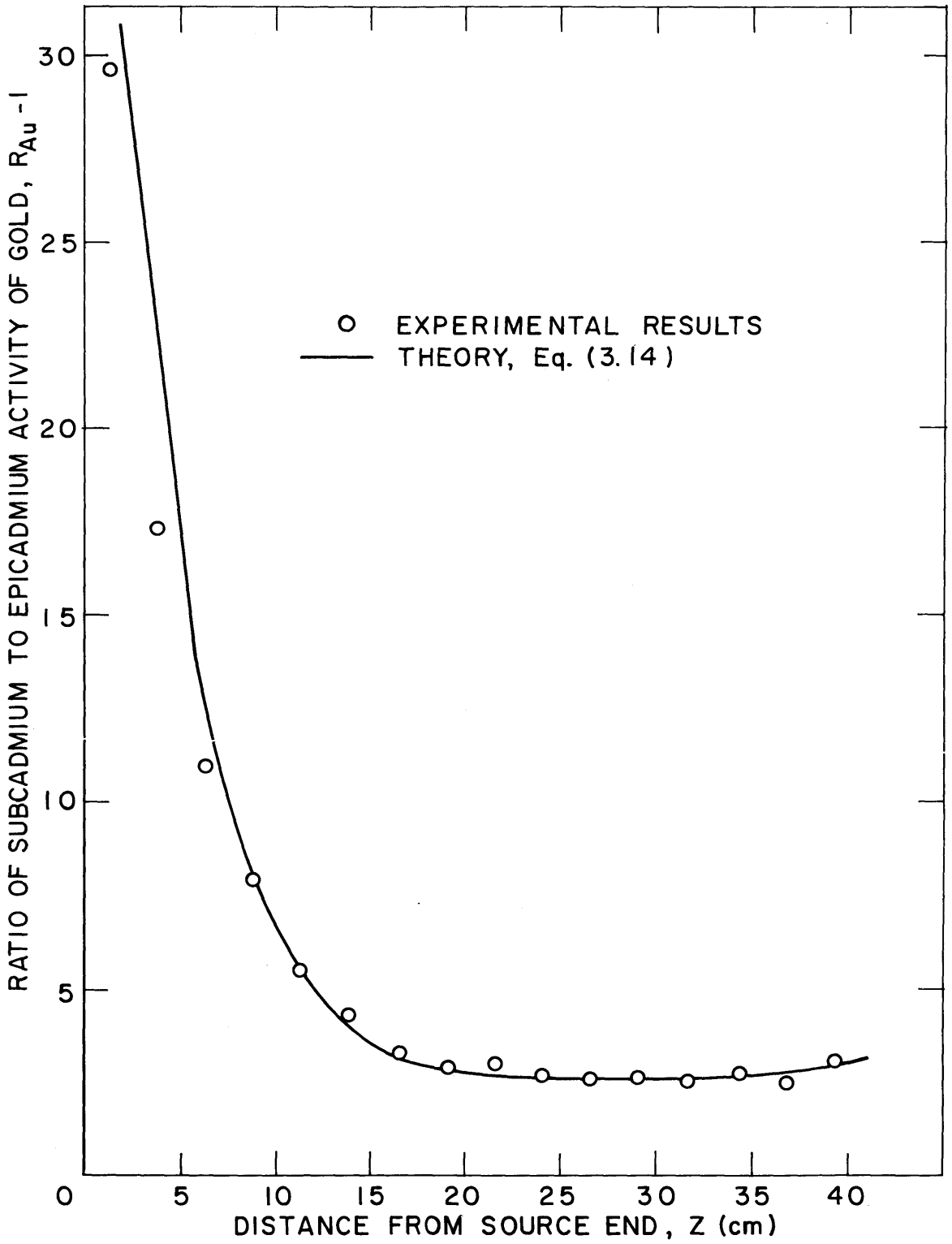

FIG. 8.1 AXIAL DISTRIBUTION FOR CADMIUM RATIO OF GOLD IN ML2
ML2: 1.143% ENRICHED FUEL, D_2O MODERATED,
1.25-INCH SPACING

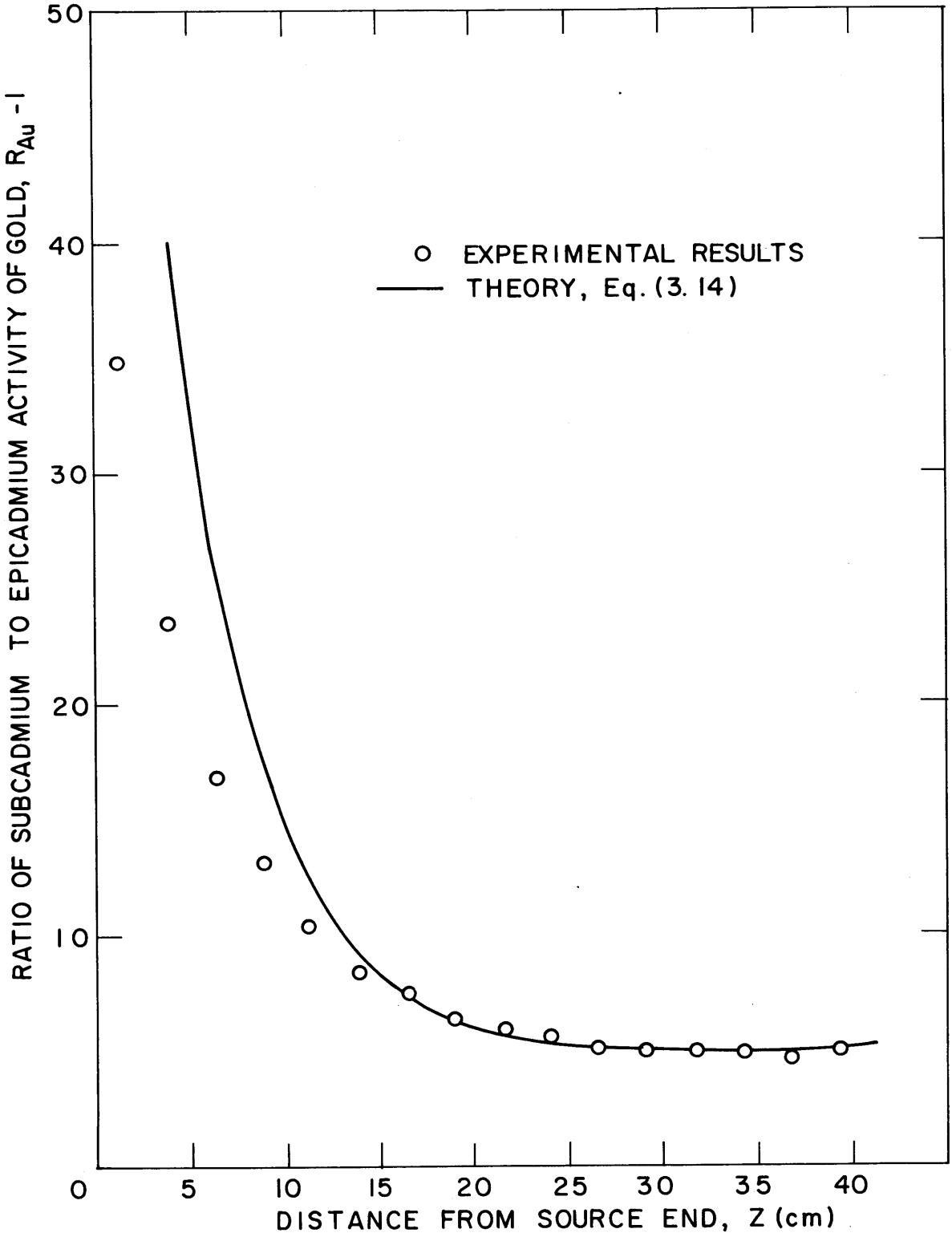

FIG. 8.2 AXIAL DISTRIBUTION OF CADMIUM RATIO OF GOLD IN ML7
ML7: 1.143 % ENRICHED FUEL, D_2O MODERATED
1.75 - INCH SPACING

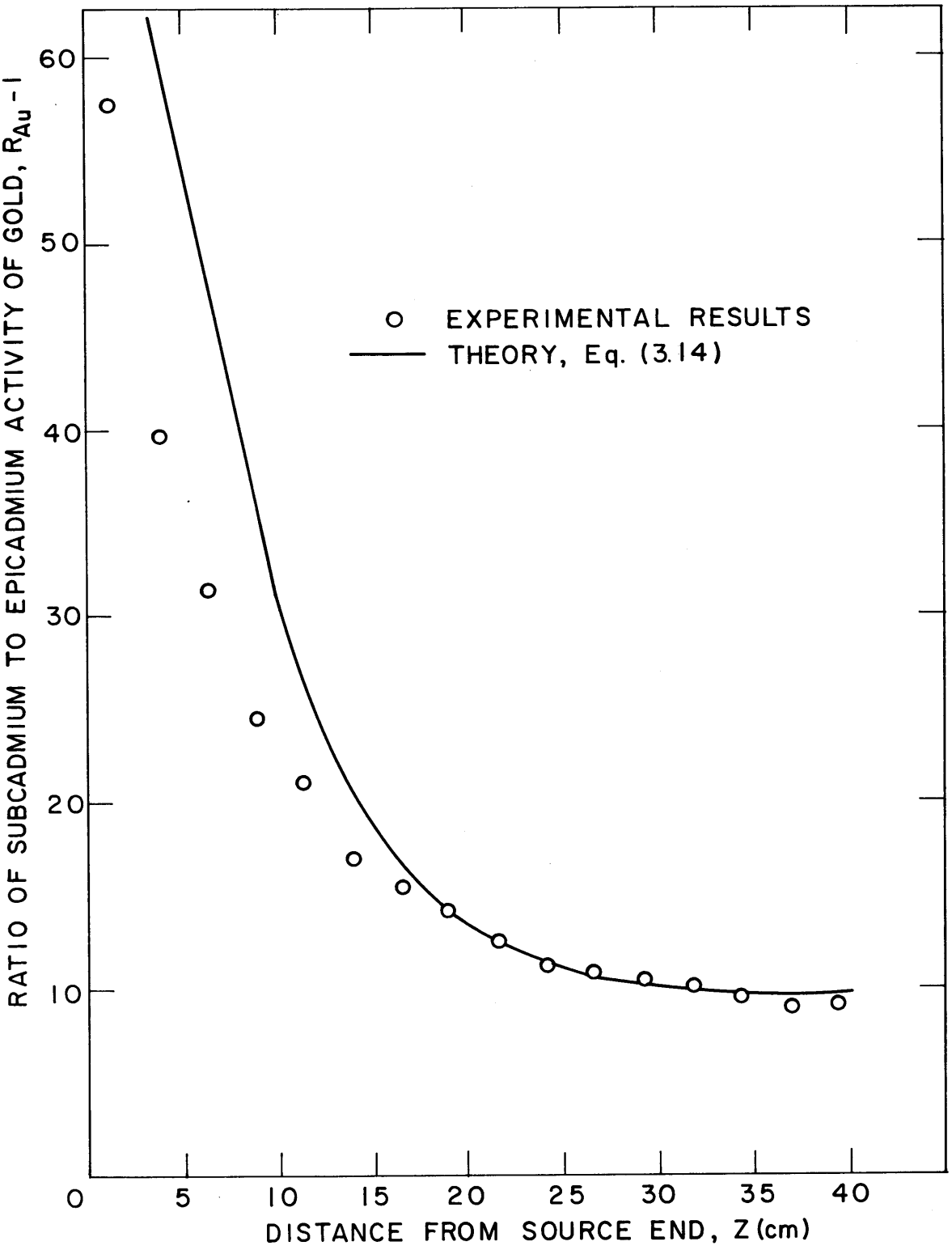

FIG. 8.3 AXIAL DISTRIBUTION OF CADMIUM RATIO OF GOLD IN ML3
ML3: 1.143% ENRICHED FUEL, D_2O MODERATED,
2.50 - INCH SPACING

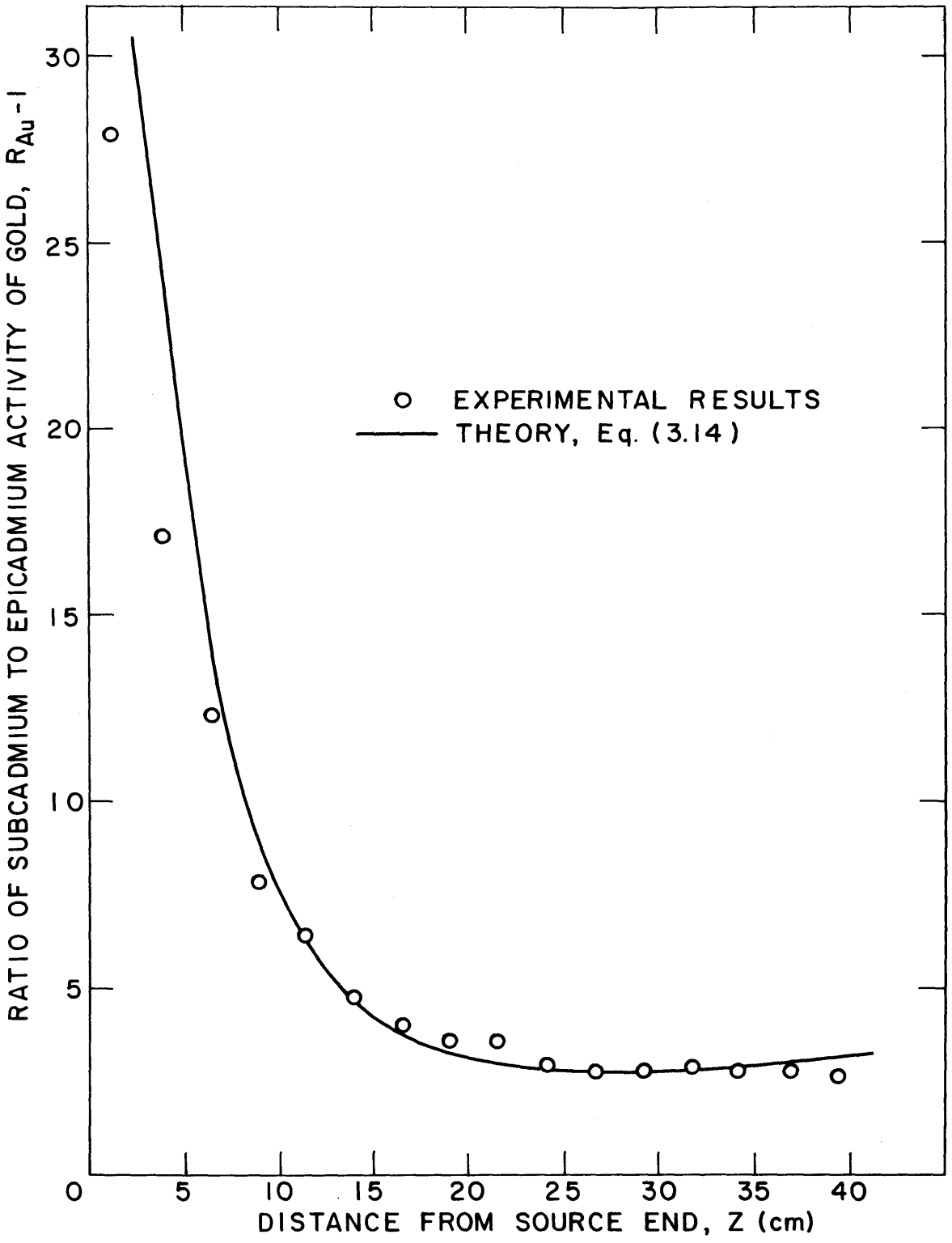

FIG. 8.4 AXIAL DISTRIBUTION OF CADMIUM RATIO OF GOLD IN ML4
ML4 : 1.027 % ENRICHED FUEL, D_2O MODERATED,
1.25 - INCH SPACING

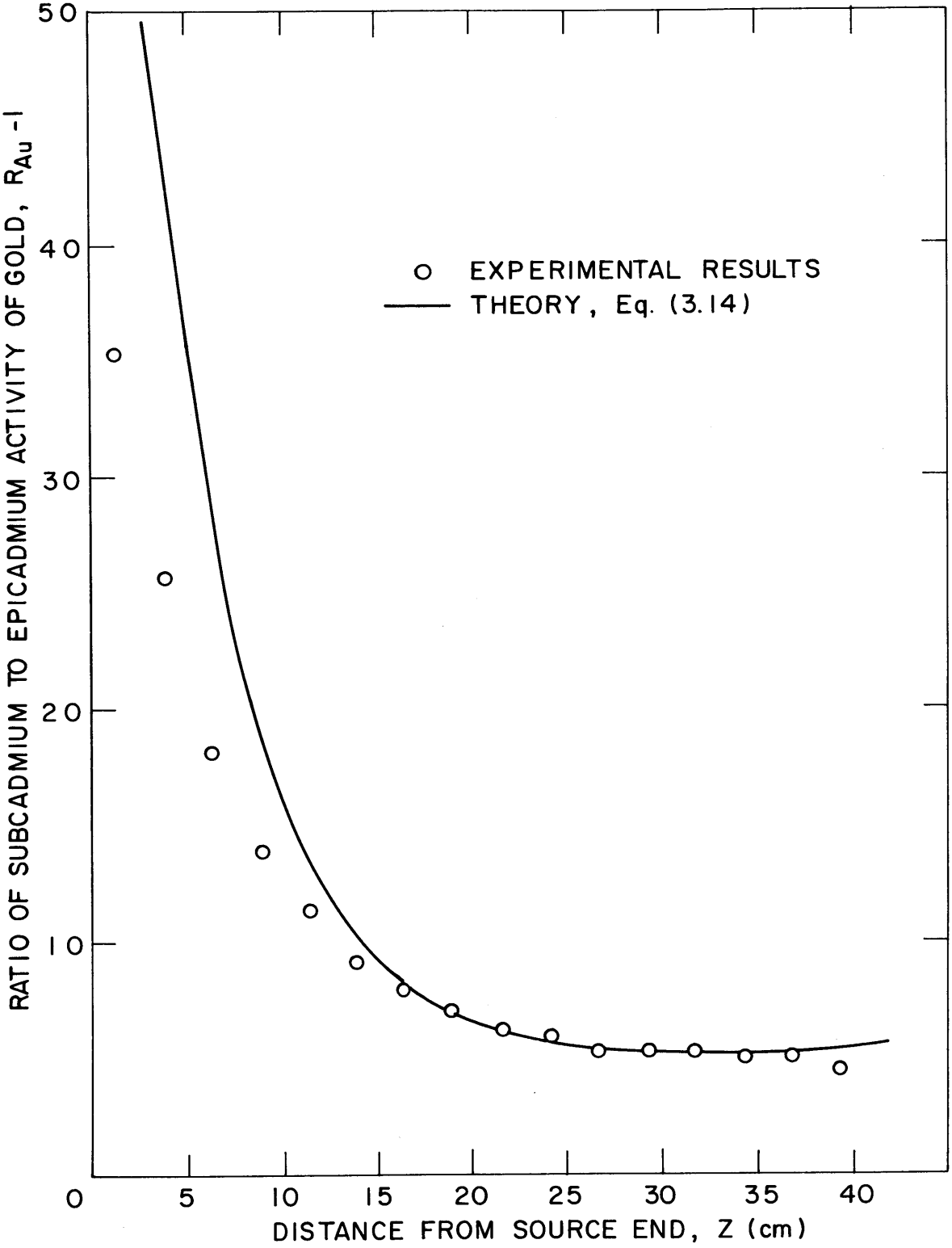

FIG. 8.5 AXIAL DISTRIBUTION OF CADMIUM RATIO OF GOLD IN ML 6
ML6: 1.027% ENRICHED FUEL, D_2O MODERATED
1.75 - INCH SPACING

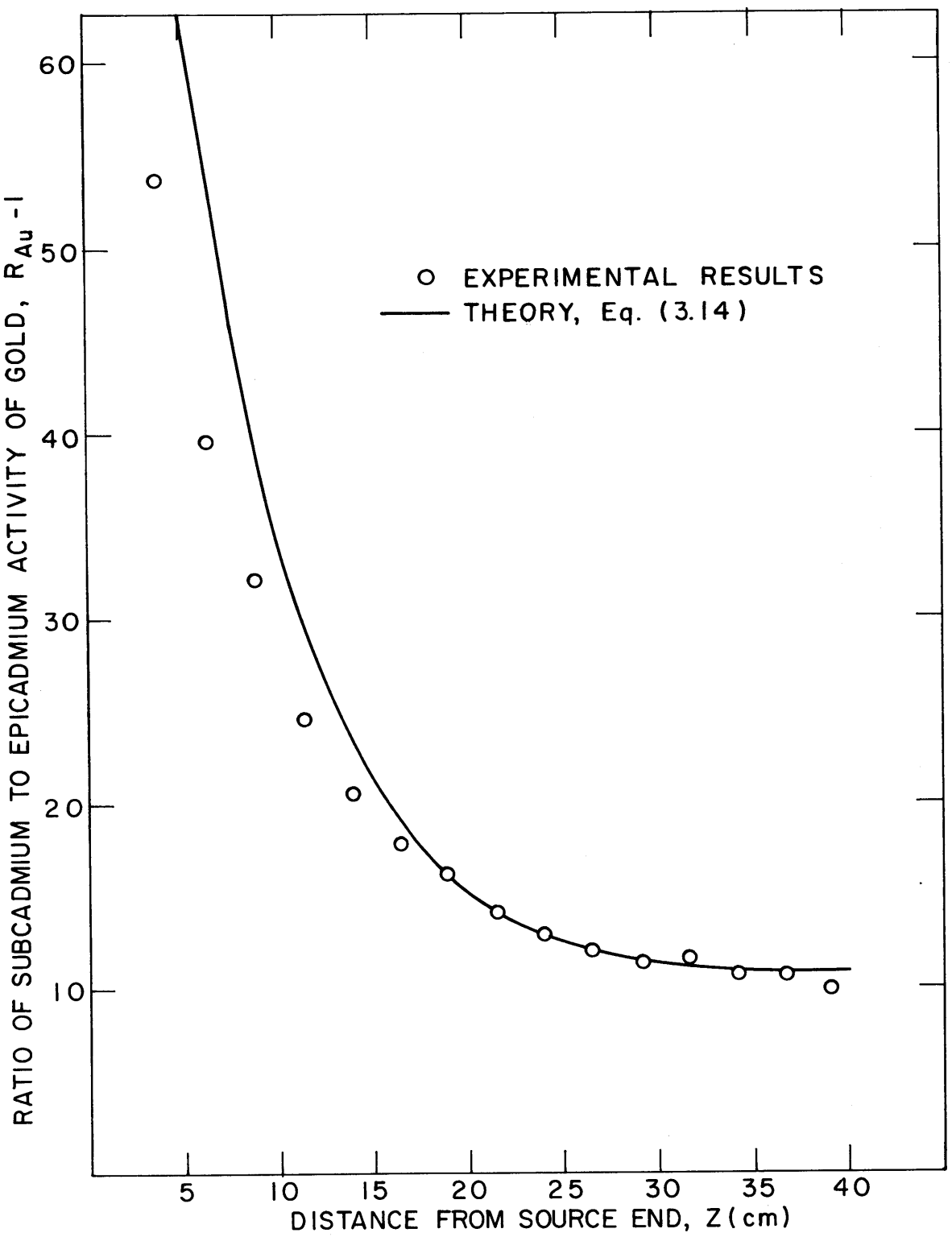

FIG. 8.6 AXIAL DISTRIBUTION OF CADMIUM RATIO OF GOLD IN ML5
ML5 : 1.027% ENRICHED FUEL, D_2O MODERATED,
2.50 - INCH SPACING.

Table 8.3

Parameters Used in MINIFLUX Calculations

Lattice[1]	Spacing (inches)	Enrichment (%)	V_M/V_F	Radius (cm)	Height (cm)	Σ_a^{ℓ}[4] (cm^{-1})	L_ℓ[4] (cm)
ML2	1.25	1.143	25.833	27.641	49.421	0.01191	8.493
ML7	1.75	1.143	52.164	27.576	47.366	0.00640	11.382
ML3	2.50	1.143	108.304	27.522	48.476	0.00326	15.705
ML4	1.25	1.027	25.833	27.617	49.421	0.01131	8.661
ML6	1.75	1.027	52.164	27.573	47.366	0.00608	11.668
ML5	2.50	1.027	108.304	27.528	48.476	0.00308	16.186

Lattice	Σ_a^s[4] (cm^{-1})	L_s[4] (cm)	k_∞	τ_{28}[5] (cm^2)	τ_t[4] (cm^2)	$\xi\Sigma_s$ (cm^{-1})	S_{Au}[5]
ML2	0.01072	8.952	1.328[2]	82.30	128.55	0.17455	2.851
ML7	0.00576	11.950	1.416[2]	81.34	124.90	0.17700	2.807
ML3	0.00326	15.705	1.419[2]	79.20	123.69	0.18206	2.787
ML4	0.00961	9.396	1.304[3]	82.30	128.55	0.17455	2.848
ML6	0.00547	12.310	1.375[3]	81.34	124.90	0.17700	2.806
ML5	0.00293	16.595	1.395[3]	79.20	123.69	0.18206	2.788

(1) All lattices have 0.25-inch-diameter rods clad in 0.318-inch-O.D. aluminum tubes in 99.75% D_2O.
(2) Ref. (8).
(3) Ref. (5), values corrected for epicadmium fission in U^{235}.
(4) Definitions in section 3.1.
(5) Definitions in section 3.3.

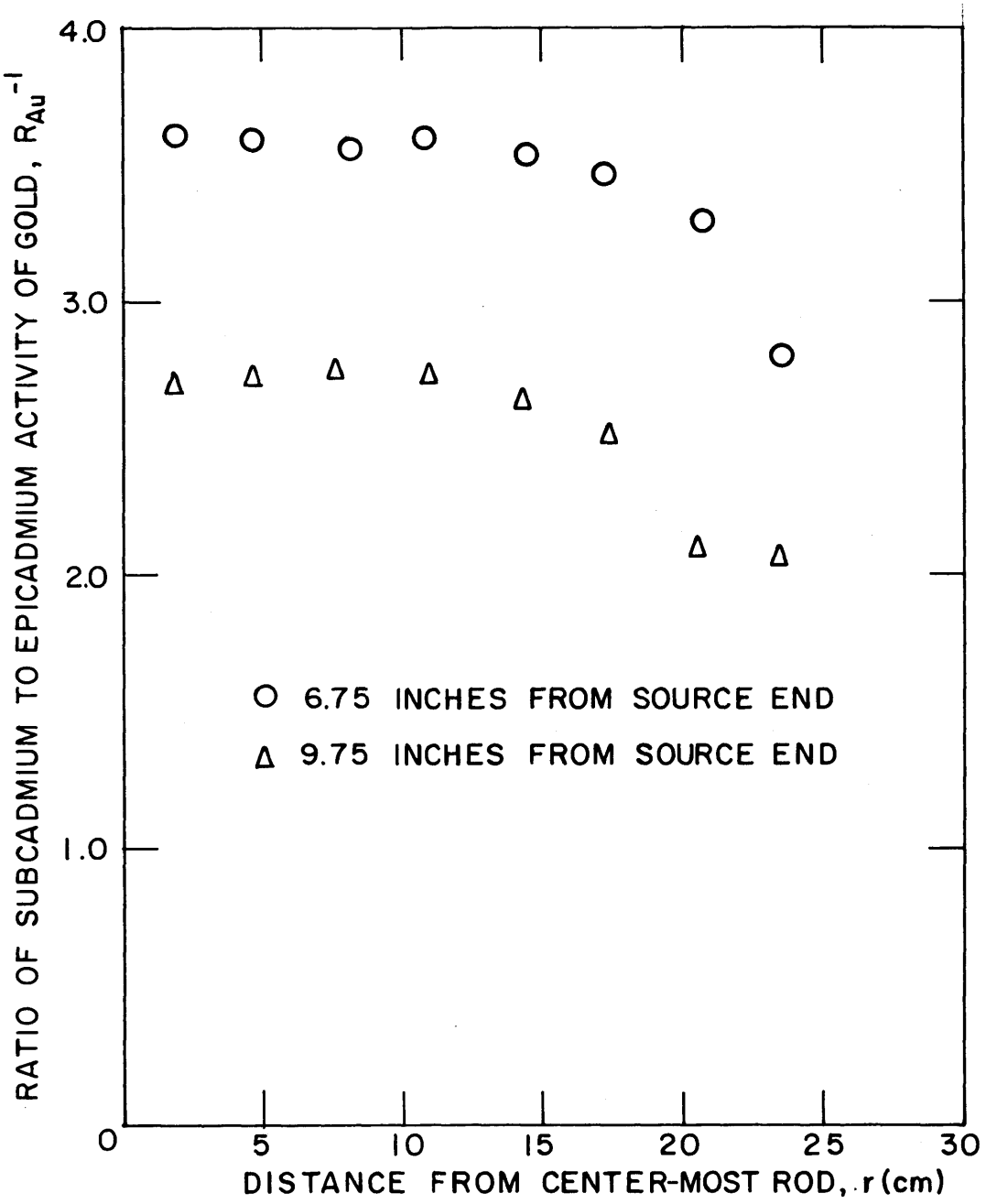

FIG. 8.7 RADIAL DISTRIBUTION OF CADMIUM RATIO OF GOLD IN ML2
ML2: 1.143% ENRICHED FUEL, D_2O MODERATED, 1.25 - INCH SPACING

comprising at least half the total number of rings in the lattice. The drop in the value of R_{Au}-1 near the boundary is mostly a consequence of the cadmium layer surrounding the assembly. The effect of the cadmium layer is better illustrated in Fig. 8.8, where the subcadmium and epicadmium activities of gold are shown for the lattice ML7. The results shown in Figs. 8.7 and 8.8 indicate: first, that the area corresponding to about half the number of rings in each lattice can be used to measure ρ_{28}, δ_{25} and C^*; second, that since the radial subcadmium activity distribution of gold follows closely a J_o function, the method used to correct the intracellular distribution of the activity of gold, described in section 3.4.3, is justified; and third, that to correct δ_{28}, as described in section 3.4.2, the interaction effect can be obtained by weighting the contribution of the surrounding rods with a J_o function.

4.2 Intracellular Activity Distribution of Gold

The magnitude of the correction required to extrapolate the measured distribution of the subcadmium activity of gold to an infinite assembly is illustrated in Fig. 8.9 for the case of ML7. The correction is, of course, larger, the farther the position of the foil is from the center of the rod. In the lattices with the 2.50-inch spacing, the correction is close to 7% for the foil position farthest from the center of the rod. If one considers only the foils placed between the center of the rod and the cell boundary, the correction is at most 2% to 3%.

In the lattice ML2, two independent measurements of the intracellular activity distribution were made. The results are shown in Fig. 8.10 and illustrate the spread observed in the data. The results obtained in the exponential assembly at M. I. T. are also shown in Fig. 8.10. It is evident from these results that the accuracies in activity distributions observed are not appreciably affected by being measured in a miniature lattice. The spread of the data in the fuel is most probably due to the difficulty of positioning foils accurately in a 1/4-inch-diameter fuel button. This is particularly true of the foils nearest the surface of the fuel rod where the flux gradient is large. The distributions obtained in both miniature and exponential lattices

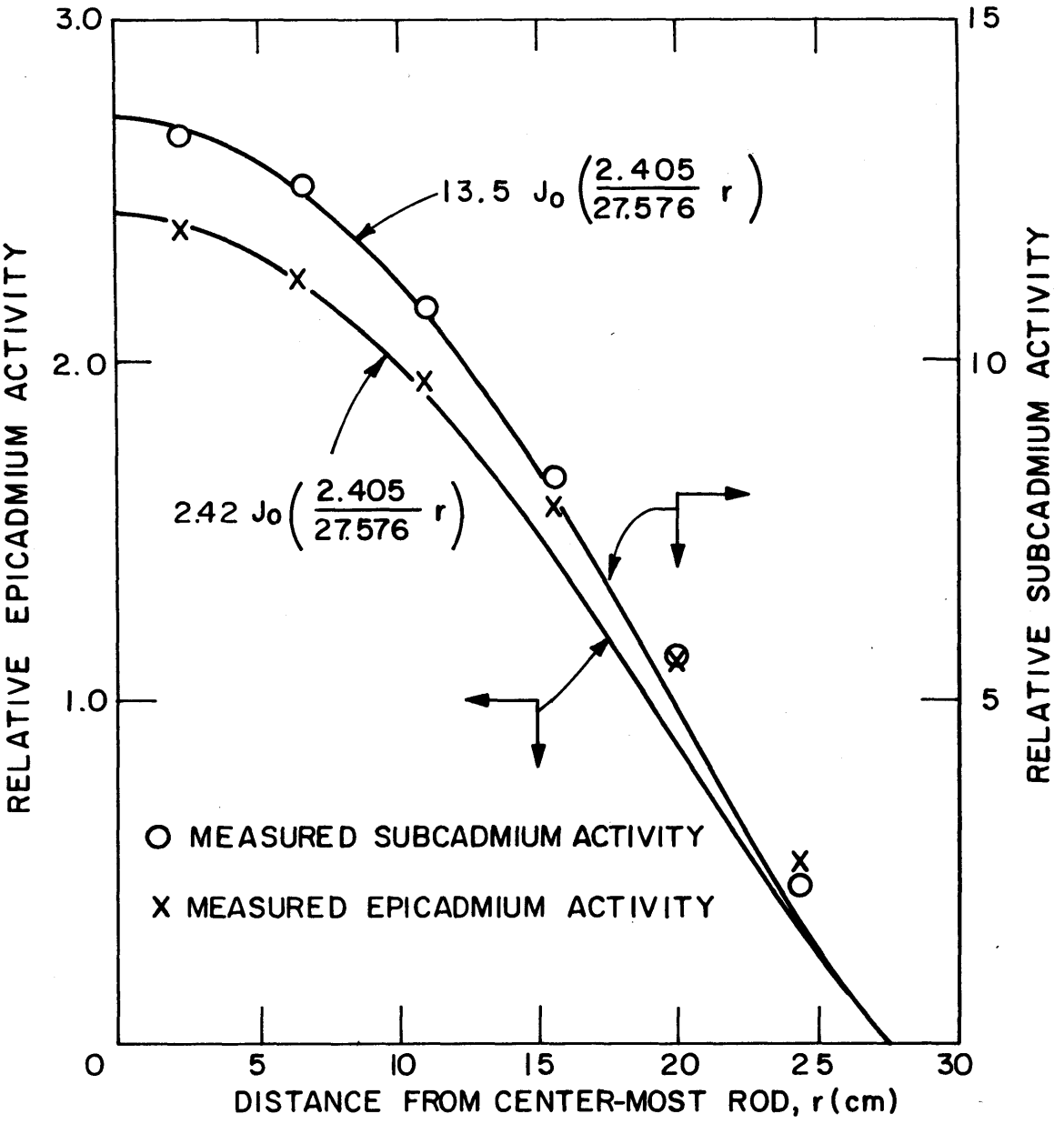

FIG. 8.8 RELATIVE RADIAL ACTIVITY DISTRIBUTION OF GOLD IN ML7, 9.75 INCHES FROM SOURCE END. ML7: 1.143% ENRICHED FUEL, D_2O MODERATED 1.75 - INCH SPACING

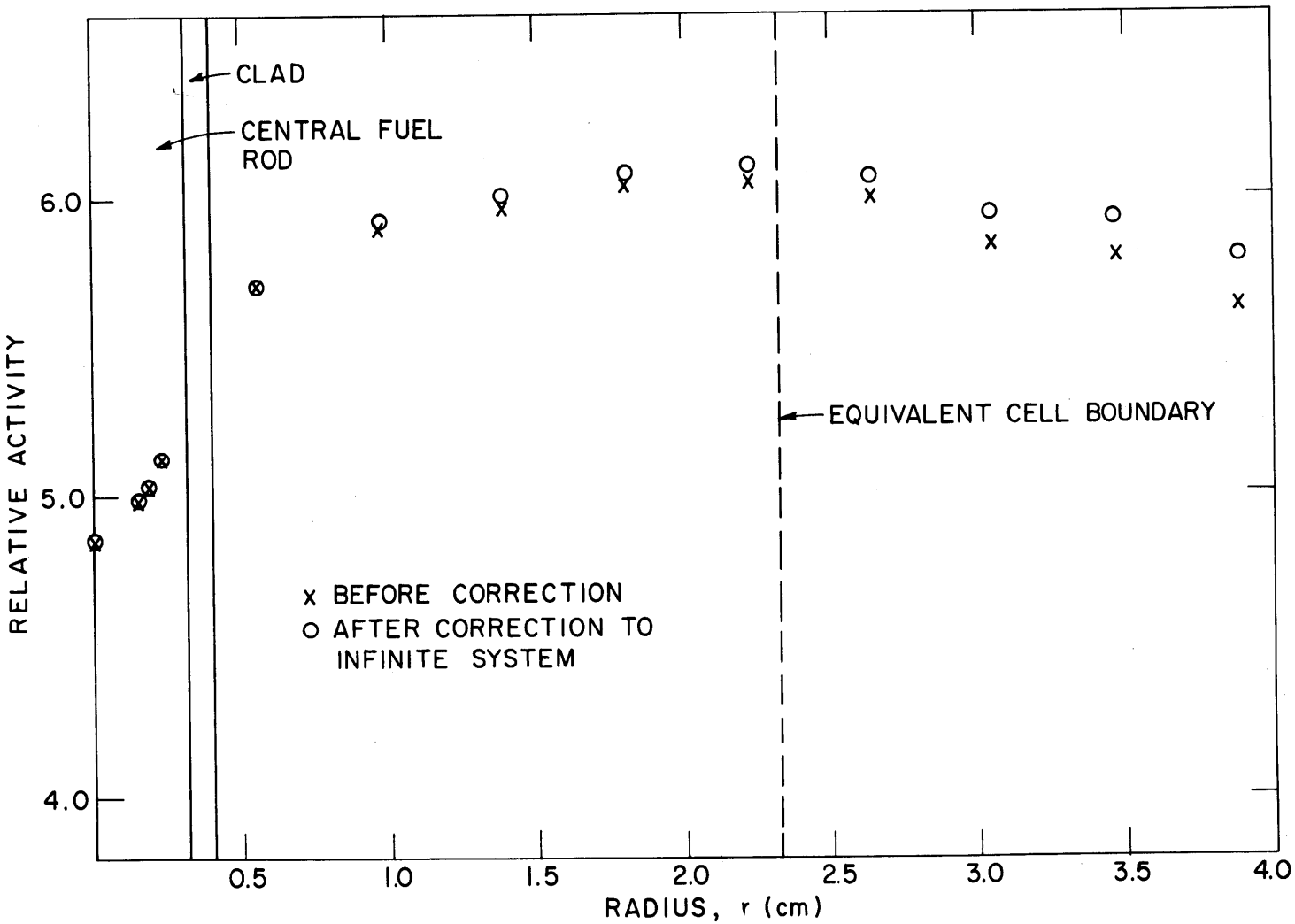

FIG. 8.9 SUBCADMIUM ACTIVITY DISTRIBUTION IN ML7 BEFORE AND AFTER CORRECTION TO INFINITE SYSTEM
ML7: 1.143% ENRICHED FUEL, D_2O MODERATED, 1.75-INCH SPACING

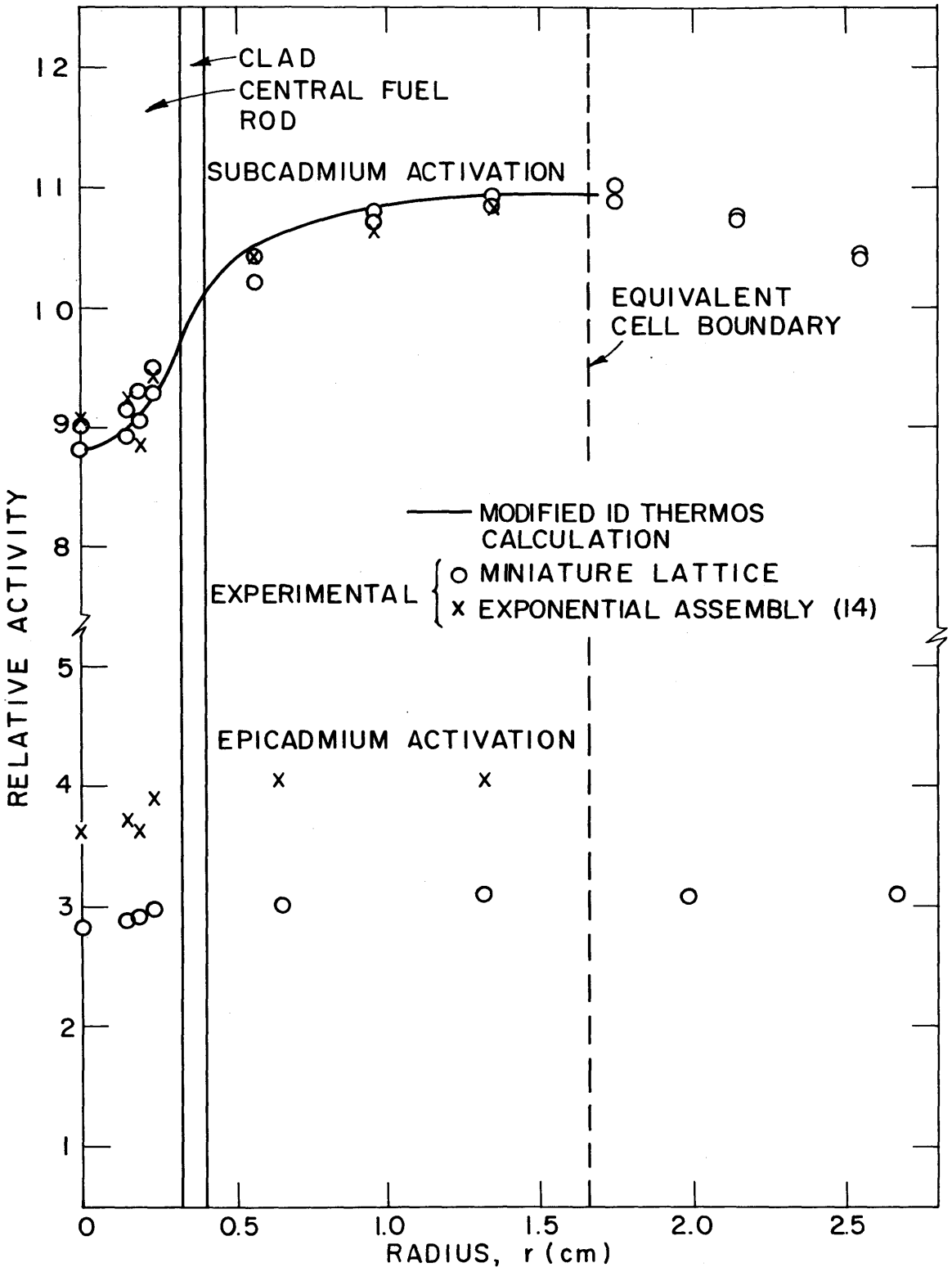

FIG. 8.10 INTRACELLULAR ACTIVITY DISTRIBUTION OF GOLD IN ML2
ML2: 1.143 % ENRICHED FUEL, D_2O MODERATED LATTICE
ON A 1.25-INCH TRIANGULAR SPACING

agree with those predicted by THERMØS (6).

In the lattice ML4, intracellular activity distributions were measured at two heights, 9 and 13 inches from the source end. See Figs. 8.11 and 8.12. In both cases, the agreement between the results obtained in miniature and exponential lattices is good, and both agree with the prediction of THERMØS (6).

Figures 8.13 through 8.16 show the subcadmium and epicadmium activity distributions in the rest of the lattices investigated. Again, the results obtained in miniature and exponential assemblies agree with each other and with the distributions predicted by THERMØS (6).

4.3 The Parameters ρ_{28}, δ_{28}, δ_{25} and C^*

The parameters ρ_{28}, δ_{28}, δ_{25} and C^* were measured in all the assemblies investigated. Application of the extrapolation methods obtained in sections 3.4.1 and 3.4.2 yielded the values of these parameters in exponential (EX), critical (C), and infinite (∞) assemblies. Except for the correction for δ_{28}, all corrections involve the function $\psi(r,z)$ defined by Eq. 8.15. The variation of $\psi(r,z)$ with z/H is illustrated in Figs. 8.17 and 8.18. Figure 8.17 shows $\psi(r,z)$ for ML2, the tightest lattice studied, and Fig. 8.18 shows $\psi(r,z)$ for ML5, the most dilute lattice investigated. The axial position in which the miniature lattice measurements were made is indicated in both cases. In the exponential assembly at M.I.T., the determinations were all made in the equilibrium region, i.e., the region where $\psi(r,z)$ is constant. It is apparent from these figures that in none of the miniature lattices studied is an equilibrium region attained.

The values of ρ_{28}, δ_{28}, δ_{25} and C^* measured in the miniature lattices are shown in Tables 8.4 and 8.5. Table 8.4 shows the results in the lattices with 1.143% enriched fuel, and Table 8.5, the results for the assemblies with 1.027% enriched fuel. Also shown are the values of these parameters extrapolated to exponential, critical, and infinite assemblies, as well as those obtained from measurements in the exponential assembly at M.I.T. The values to be compared are those measured in the exponential assembly (third row) and those extrapolated from miniature lattice data to exponential assemblies (second row). 'It

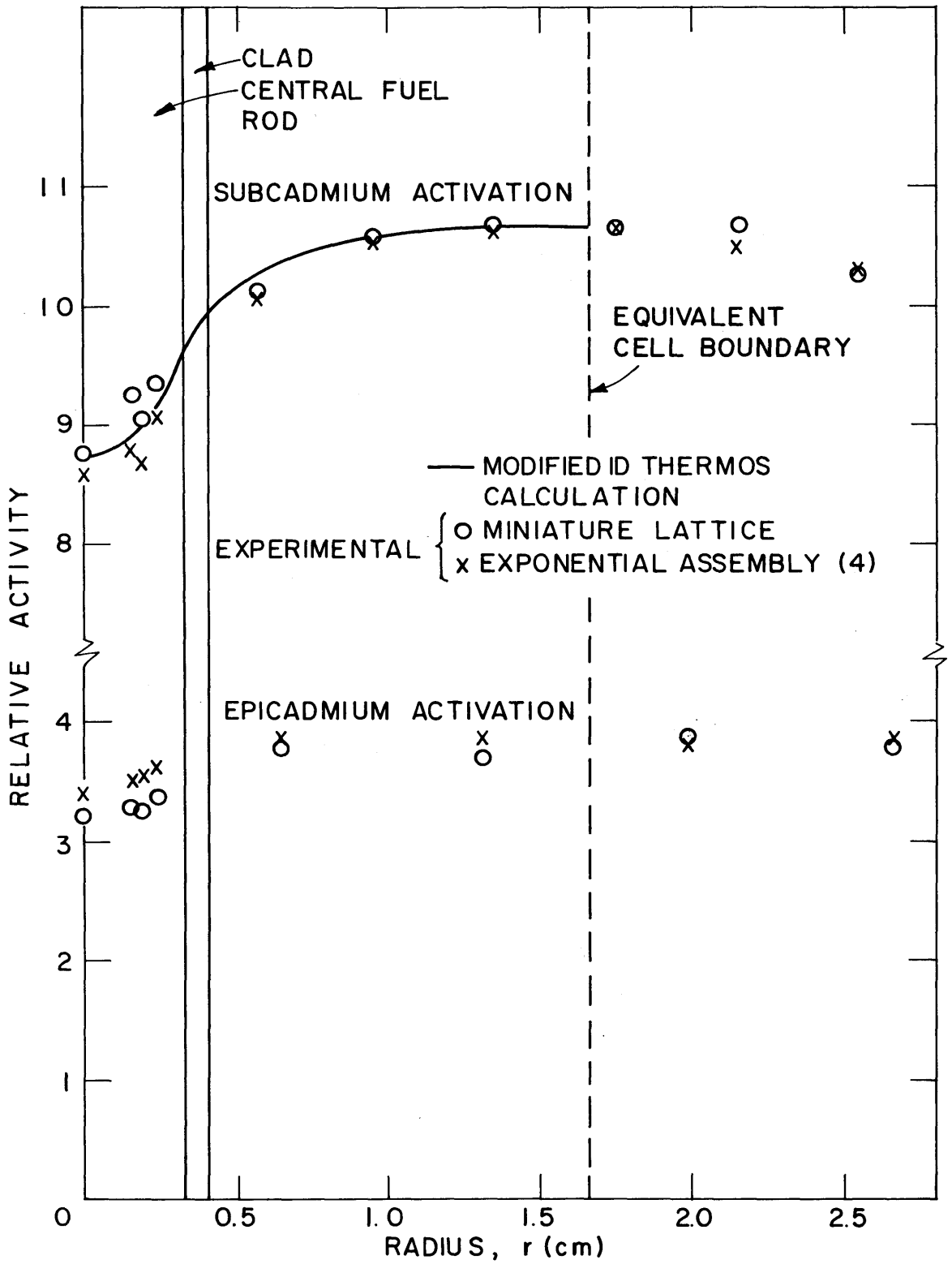

FIG. 8.11 INTRACELLULAR ACTIVITY DISTRIBUTION OF GOLD IN ML4; 9-INCHES FROM SOURCE END.
ML4: 1.027% ENRICHED FUEL, D_2O MODERATED LATTICE ON 1.25-INCH TRIANGULAR SPACING

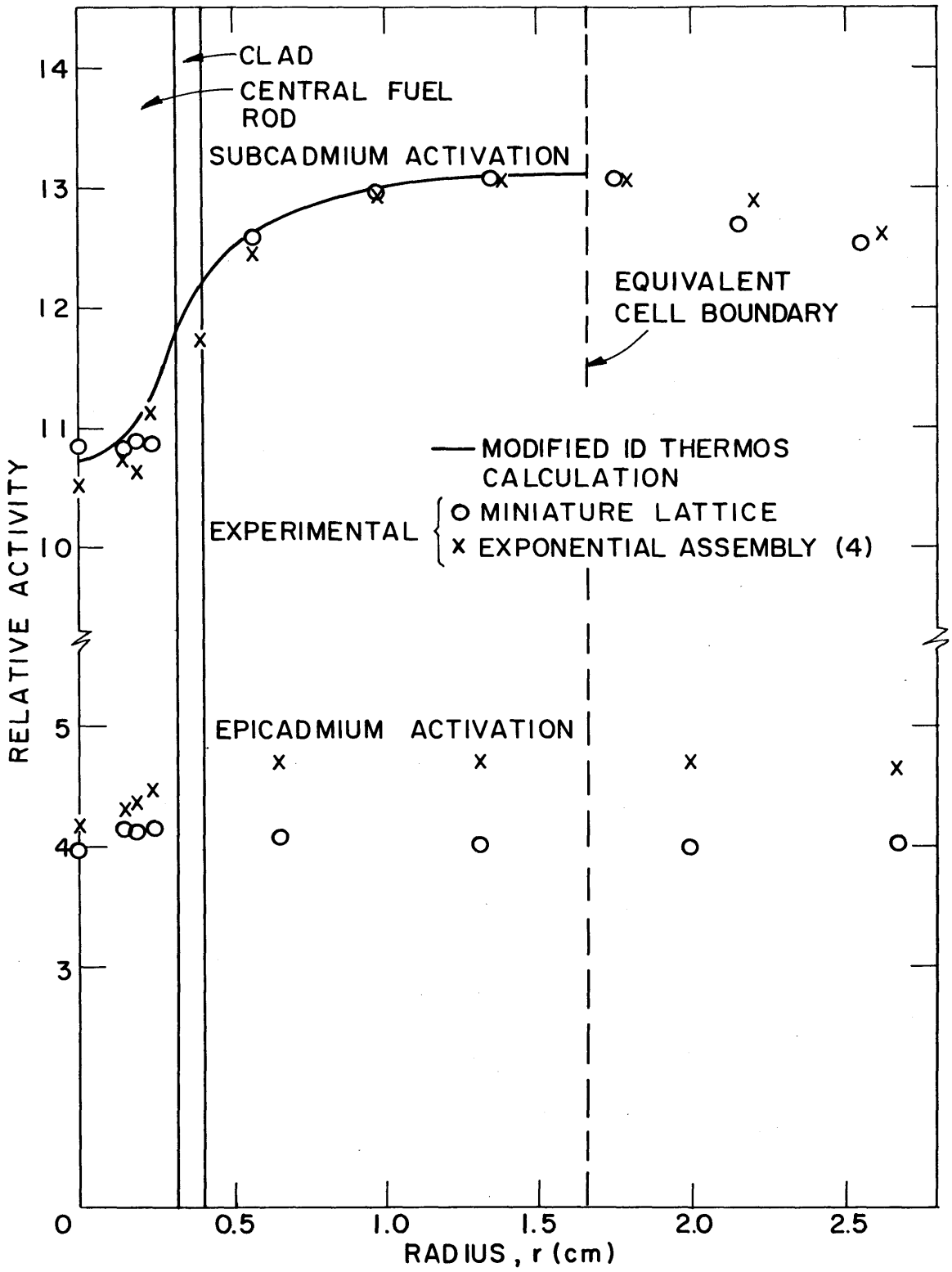

FIG. 8.12 INTRACELLULAR ACTIVITY DISTRIBUTION OF GOLD IN ML4; 13 INCHES FROM SOURCE END.
ML4: 1.027% ENRICHED FUEL, D_2O MODERATED LATTICE ON 1.25-INCH TRIANGULAR SPACING

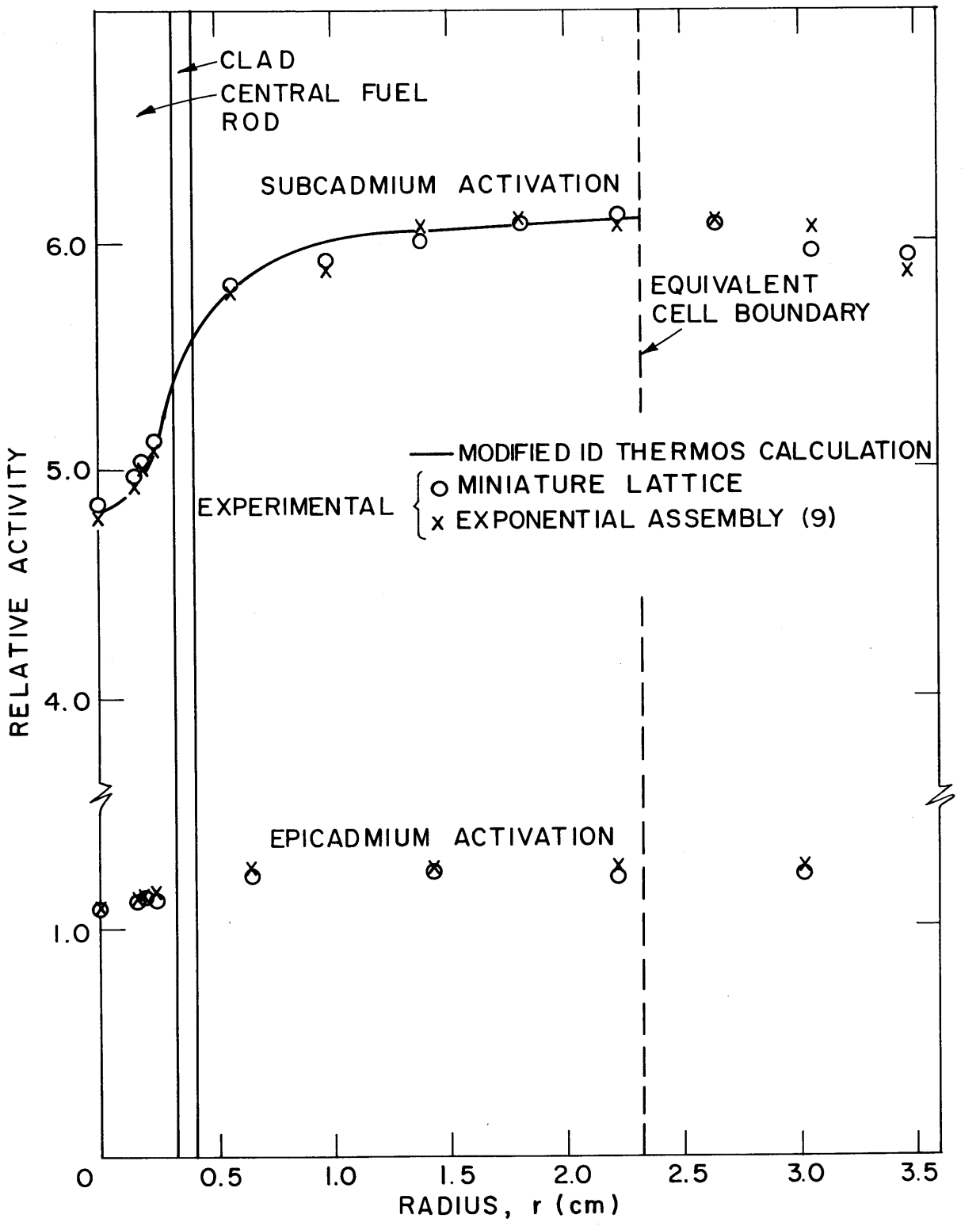

FIG. 8.13 INTRACELLULAR ACTIVITY DISTRIBUTION OF GOLD IN ML7
ML7: 1.143% ENRICHED FUEL, D_2O MODERATED LATTICE
ON A 1.75 -INCH TRIANGULAR SPACING

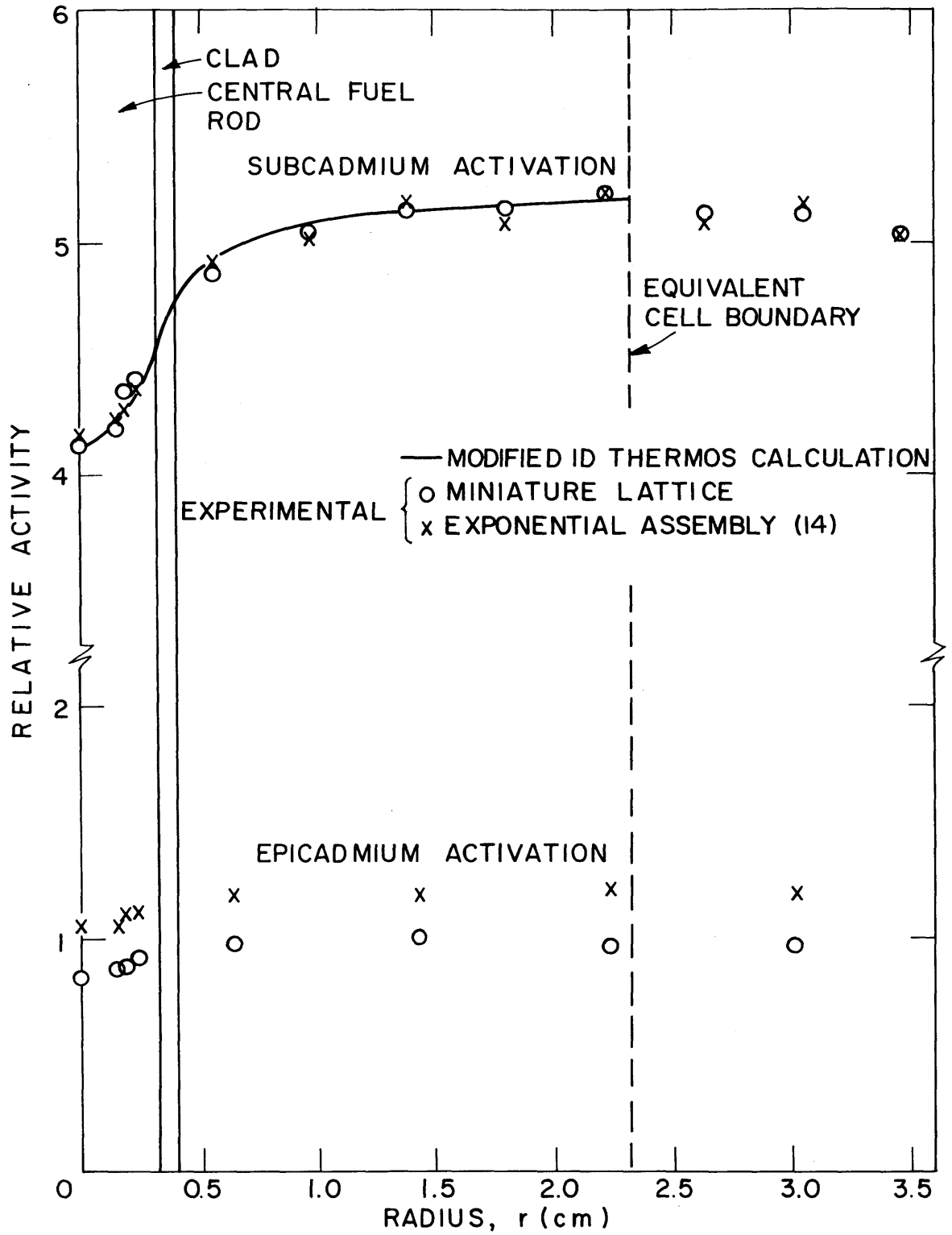

FIG. 8.14 INTRACELLULAR ACTIVITY DISTRIBUTION OF GOLD IN ML6
ML6: 1.027% ENRICHED FUEL, D_2O MODERATED LATTICE
ON A 1.75-INCH TRIANGULAR SPACING

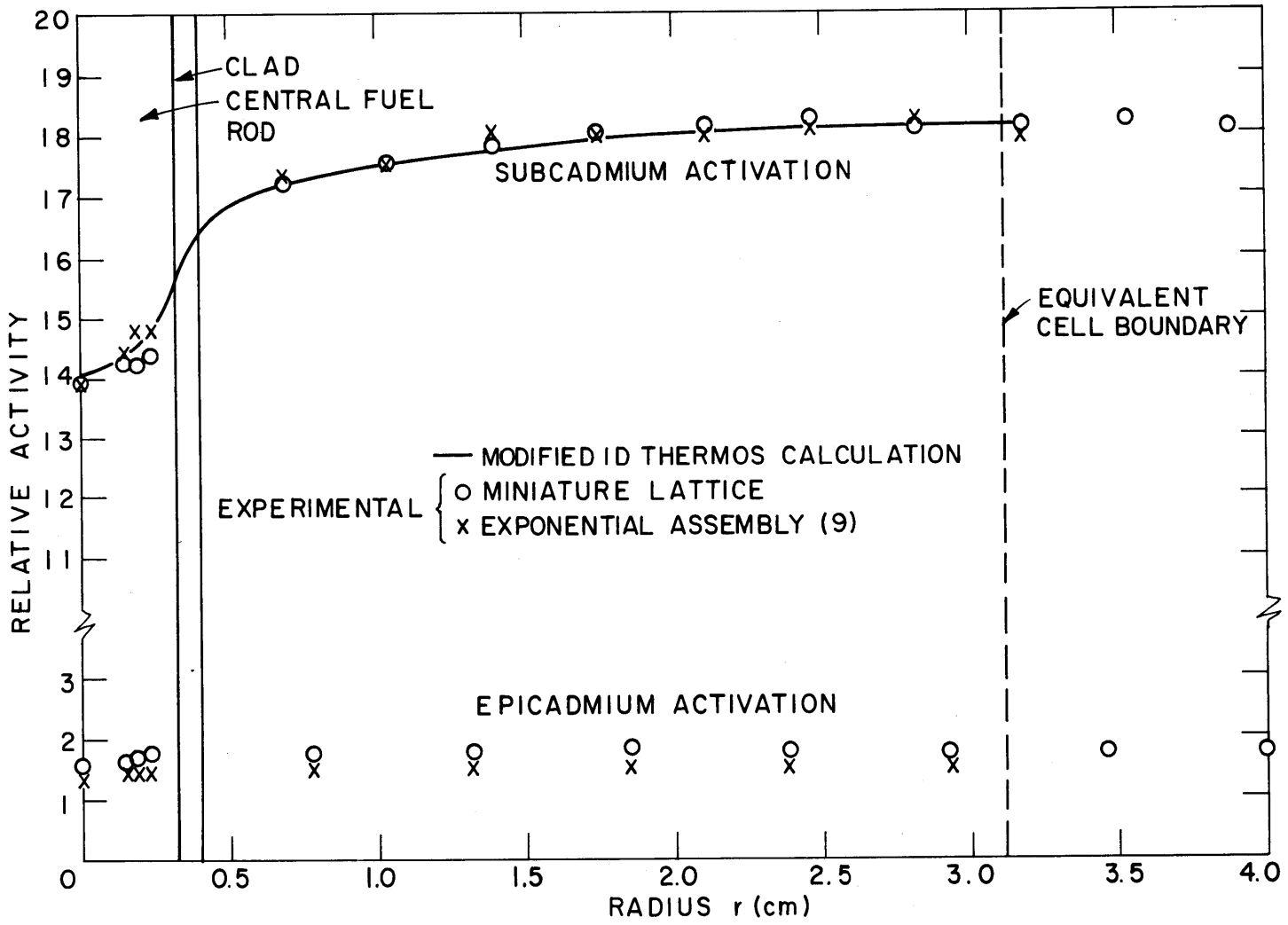

FIG. 8.15 INTRACELLULAR ACTIVITY DISTRIBUTION OF GOLD IN ML3
ML3: 1.143 % ENRICHED FUEL, D O MODERATED LATTICE ON A 2.50-INCH TRIANGULAR SPACING

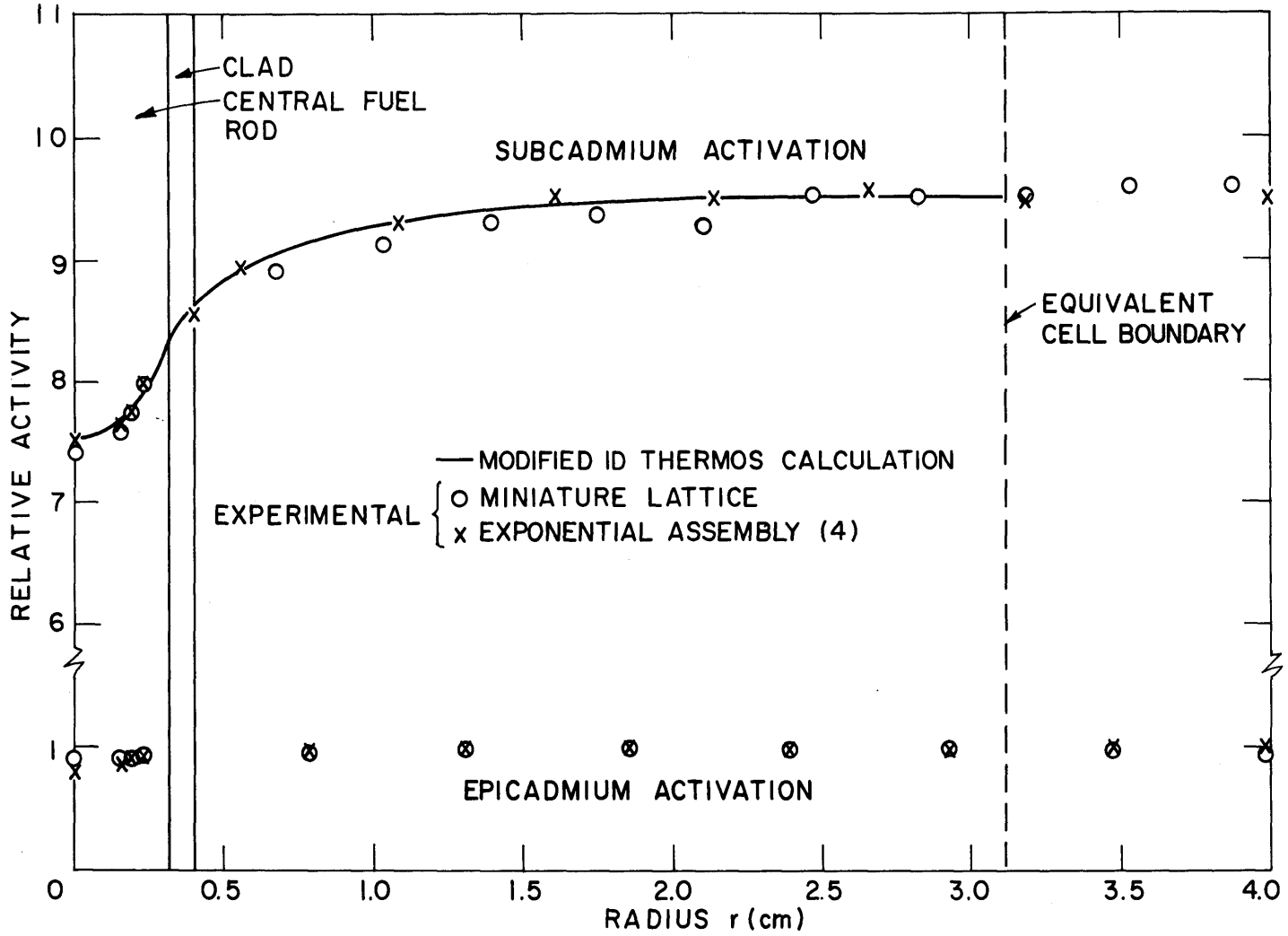

FIG. 8.16 INTRACELLULAR ACTIVITY DISTRIBUTION OF GOLD IN ML5
ML5 : 1.027% ENRICHED FUEL, D_2O MODERATED LATTICE ON A 2.50-INCH TRIANGULAR SPACING

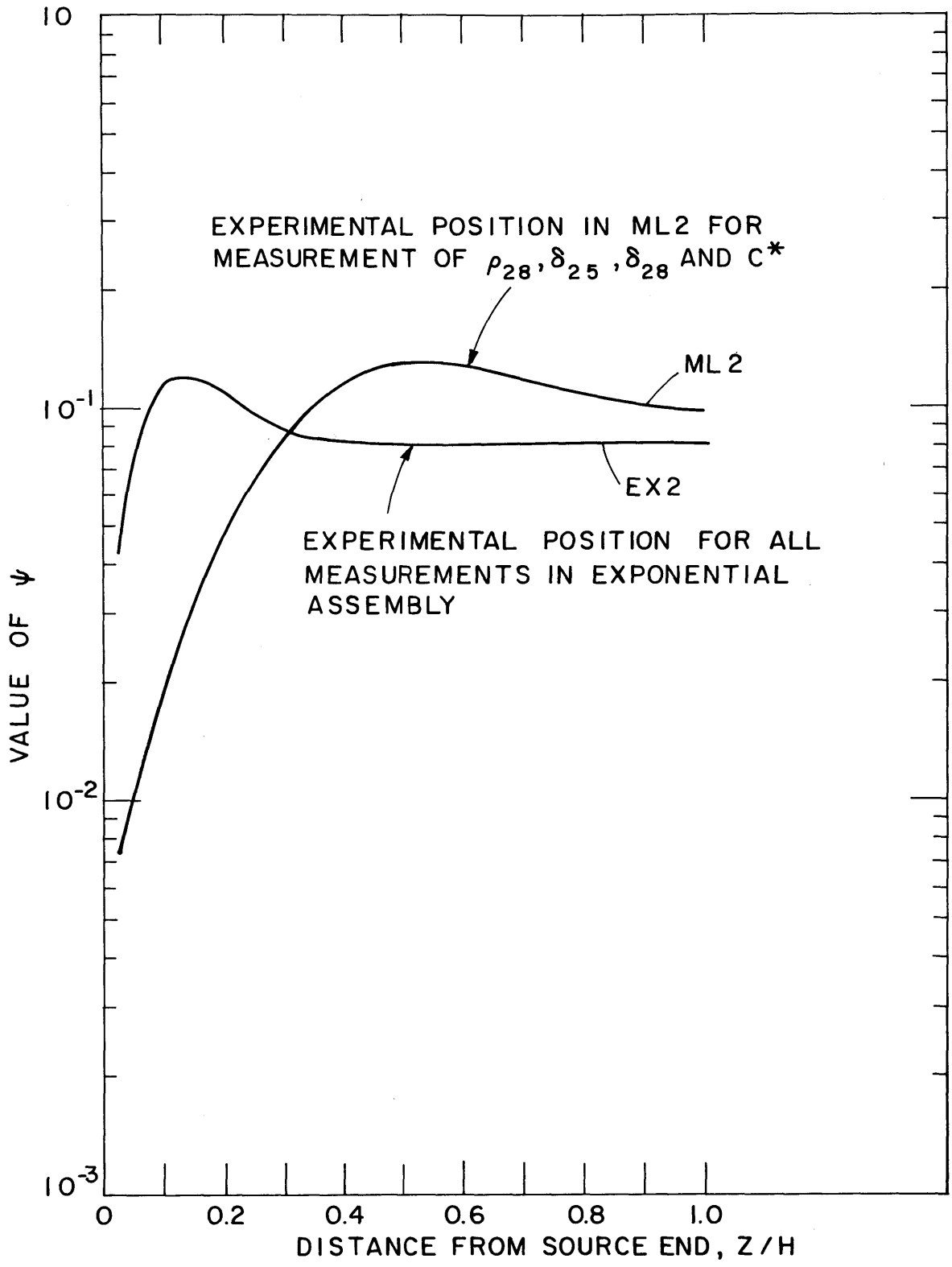

FIG. 8.17 VARIATION OF THE FUNCTION $\psi = pq/\zeta \Sigma_s \phi_f$ WITH Z, FOR ML2 AND THE CORRESPONDING EXPONENTIAL ASSEMBLY
ML2: 1.143% ENRICHED FUEL, D_2O MODERATED
1.25-INCH SPACING

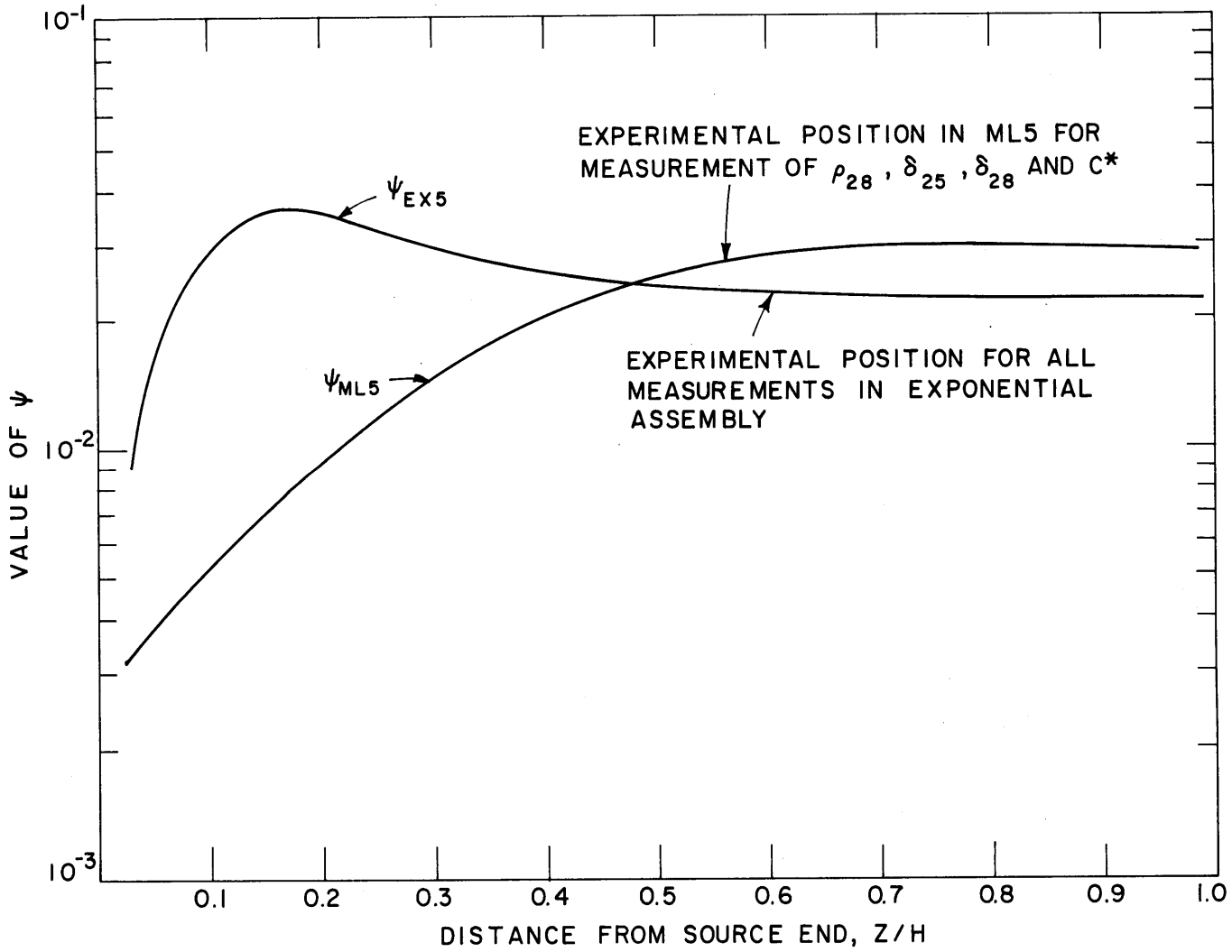

FIG. 8.18 VARIATION OF THE FUNCTION $\psi = pq/\xi\Sigma_s\phi_t$ WITH Z, FOR ML5 AND THE CORRESPONDING EXPONENTIAL ASSEMBLY.
ML5 : 1.027% ENRICHED FUEL, D_2O MODERATED, 2.5-INCH SPACING

Table 8.4

Experimental Data and Extrapolated Results for Lattices with 1.143% Enriched Fuel. Similar Data in Exponential Assemblies (EX)

Assembly	δ_{28}	ρ_{28}	δ_{25}	C^*_{MAX} (1)	C^*_{SC} (2)	ψ (3)
ML2	0.0252 ±.0010	0.916 ±.017	0.0863 ±.0033	0.740 ±.009	0.739 ±.007	0.1280
ML2 to EX	0.0268 ±.0011	0.861 ±.016	0.0609 ±.0023	0.732 ±.009	0.734 ±.007	0.0805
EX (meas.)	0.0264 (4) ±.0040	0.813 (5) ±.067	0.0584 (5) ±.0044	0.799 (5) ±.084	0.717 (5) ±.026	0.0805
ML2 to C		0.927 ±.017	0.0624 ±.0024	0.748 ±.009	0.759 ±.007	0.0809
ML2 to ∞	0.0278 ±.0011	1.111 ±.021	0.0716 ±.0027	0.802 ±.010	0.824 ±.008	0.0908
ML7	0.0195 ±.0007	0.395 ±.007	0.0398 ±.0010	0.571 ±.025	0.556 ±.003	0.05625
ML7 to EX	0.0204 ±.0007	0.476 ±.009	0.0364 ±.0009	0.597 ±0.26	0.591 ±.003	0.04562
EX (meas.)	0.0204 (4) ±.0030	0.471 (5) ±.017	0.0385 (5) ±.0099	0.630 (5) ±.051	0.589 (5) ±.010	0.04562
ML7 to C		0.514 ±.010	0.0374 ±.0009	0.606 ±.026	0.605 ±.003	0.04580
ML7 to ∞	0.0209 ±.0007	0.624 ±.012	0.0434 ±.0011	0.639 ±.028	0.644 ±.004	0.05230
ML3	0.0169 ±.0040	0.198 ±.002	0.0159 ±.0010	0.487 ±.017	0.488 ±.001	0.02780
ML3 to EX	0.0174 ±.0041	0.251 ±.003	0.0153 ±.0010	0.504 ±.018	0.509 ±.001	0.02380
EX (meas.)	0.0164 (4) ±.0010	0.222 (5) ±.026	0.0160 (5) ±.0056	0.492 (5) ±.050	0.498 (5) ±.011	0.02380
ML3 to C		0.272 ±.003	0.0156 ±.0010	0.511 ±.018	0.520 ±.001	0.02360
ML3 to ∞	0.0176 ±.0042	0.306 ±.004	0.0170 ±.0011	0.521 ±.018	0.531 ±.001	0.02540

(1) $C^*_{MAX} = C^*_M \frac{R_N}{R_F}$.

(2) $C^*_{SC} = \frac{1 + \rho_{28}}{1 + \delta_{25}} \left(\frac{\Sigma_a^{28}}{\Sigma_f^{25}} \right)_{SC}$.

(3) $\psi(r, z) = \frac{pq(r, z, \tau_{28})}{\xi \Sigma_s \phi_t(r, z)}$.

(4) Ref. (9).

(5) Data from Ref. (10) reanalyzed by present author.

Note: ±σ values for ML consider only counting statistics for the single measurement, while ±σ for EX is the SDM for a number of runs.

Table 8.5

Experimental Data and Extrapolated Results for Lattices with 1.027% Enriched Fuel. Similar Data in Exponential Assemblies (EX)

Assembly	δ_{28}	ρ_{28}	δ_{25}	C^*_{MAX} (1)	C^*_{SC} (2)	ψ (3)
ML4	0.0259 ±.0012	0.876 ±.024	0.0826 ±.0021	0.829 ±.060	0.804 ±.010	0.1160
ML4 to EX	0.0274 ±.0013	0.856 ±.023	0.0609 ±.0015	0.831 ±.060	0.809 ±.010	0.0758
EX (meas.)	0.0274 (4) ±.0012	0.845 (5) ±.007	0.0525 (4) ±.0100	0.814 (5) ±.007	0.792 (5) ±.002	0.0758
ML4 to C		0.937 ±.026	0.0631 ±.0016	0.856 ±.062	0.842 ±.010	0.0766
ML4 to ∞	0.0285 ±.0013	1.087 ±.030	0.0705 ±.0018	0.900 ±.065	0.901 ±.011	0.0844
ML6	0.0200 ±.0008	0.345 ±.005	0.0336 ±.0007	0.631 ±.035	0.601 ±.002	0.0515
ML6 to EX	0.0209 ±.0008	0.425 ±.006	0.0318 ±.0007	0.655 ±.036	0.637 ±.003	0.0427
EX (meas.)	0.0217 (4) ±.0007	0.437 (5) ±.003	0.0310 (4) ±.0013	0.625 (5) ±.016	0.644 (5) ±.003	0.0427
ML6 to C		0.462 ±.007	0.0328 ±.0007	0.669 ±.037	0.652 ±.003	0.0429
ML6 to ∞	0.0215 ±.0009	0.534 ±.008	0.0367 ±.0008	0.692 ±.038	0.680 ±.004	0.0473
ML5	0.0159 ±.0015	0.156 ±.002	0.0148 ±.0005	0.552 ±.017	0.525 ±.011	0.0214
ML5 to EX	0.0163 ±.0015	0.242 ±.003	0.0174 ±.0006	0.574 ±.018	0.563 ±.012	0.0224
EX (meas.)	0.0183 (4) ±.0007	0.227 (5) ±.0014	0.0188 (4) ±.0023	0.551 (5) ±.002	0.547 (5) ±.003	0.0224
ML5 to C		0.260 ±.003	0.0175 ±.0006	0.580 ±.018	0.570 ±.012	0.0219
ML5 to ∞	0.0165 ±.0015	0.290 ±.004	0.0193 ±.0007	0.588 ±.018	0.583 ±.012	0.0236

(1) $C^*_{MAX} = C^*_M \frac{R_N}{R_F}$.

(2) $C^*_{SC} = \frac{1 + \rho_{28}}{1 + \delta_{25}} \left(\frac{\Sigma_a^{28}}{\Sigma_f^{25}} \right)_{SC}$.

(3) $\psi(r, z) = \frac{pq(r, z, \tau_{28})}{\xi \Sigma_s \phi_t(r, z)}$.

(4) Ref. (11).

(5) Ref. (5).

Note: ±σ values for ML consider only counting statistics for the single measurement, while ±σ for EX is the SDM for a number of runs.

is evident from these results that the values of the parameters extrapolated from miniature lattice results generally lie within the range given by the experimental uncertainties of the value of the parameters obtained in exponential assemblies.

In Tables 8.4 and 8.5, the values of ψ for each condition are also quoted. In all cases, the value of ψ_{EX} is different from ψ_C. This difference indicates that the spectrum of neutrons in the equilibrium region of the exponential assemblies at M.I.T. is not quite that which would be observed in a critical assembly. If only the values of ψ entered into the extrapolation of the parameters ρ_{28}, δ_{25} and C^*, the difference between ψ_{EX} and ψ_C would have no significant effect in the extrapolation because this difference is smaller than the experimental errors in these parameters. The quantity S which will be discussed in section 5 does, however, affect the extrapolation factors significantly. The results listed in Tables 8.4 and 8.5 indicate that there should be an appreciable difference between the values of these parameters obtained by extrapolation of the miniature lattice data to an exponential and a critical assembly. At the present time, this result cannot be substantiated experimentally. Although there are indications that there may be a difference between material bucklings measured in exponential and critical assemblies, there are questions as to whether these discrepancies are real or represent experimental uncertainties (12). Unfortunately, measurements of ρ_{28}, δ_{25} and C^* in exponential and critical assemblies of the same composition are scarce and a definite conclusion cannot be reached until this information becomes available.

5. NUCLEAR CONSTANTS WHICH APPEAR IN THE THEORY AND EXTRAPOLATION CORRECTIONS

5.1 Thermal Energy Parameters for the Lattice-Born Neutrons

The agreement observed between the measured intracellular distributions of the activity of gold and those predicted by THERMØS indicates that the results of this program can be used to obtain Σ_a^ℓ, D^ℓ and L_ℓ^2. The latter was defined as:

$$L_\ell^2 = \frac{1}{3\Sigma_a^\ell \Sigma_{tr}^\ell}, \qquad (8.31)$$

where the macroscopic absorption and transport cross sections are obtained from THERMØS as volume and flux weighted averages over the various regions in the unit cell. The values of Σ_a^{ℓ} and L_{ℓ} for all the lattices studied are listed in Table 8.3.

5.2 Nuclear Parameters for Source Neutrons

To obtain Σ_a^s and L_s, two difficulties are encountered: first, the energy spectrum of source neutrons is not really known; and second, there is a rapid variation in the spectrum of the source neutrons as these diffuse through the lattice. Because of these difficulties, it was decided to use, as a first approximation, the same absorption cross section and diffusion length as for lattice-born neutrons. The values of Σ_a^s and L_s were then varied about these values to obtain the best agreement between the measured distribution of R_{Au}-1 and that calculated by MINIFLUX. The source constants were, however, the only parameters that were permitted to vary; all other quantities which appear, either in theory or the correction factors, are calculated. The values of Σ_a^s and L_s for the lattices studied are listed in Table 8.3.

5.3 Value of k_∞

In the six lattices investigated, the values of k_∞ were known since these lattices had been investigated in the exponential assembly at M.I.T. The function ψ, which appears in the correction factors for the parameters ρ_{28} and δ_{25} measured in the miniature lattice, depends on the value of k_∞. Hence, to determine k_∞ from measurements made in the miniature lattice, an iterative procedure must be used. A brief description of the iteration process follows.

1. The factors f and η are obtained from the THERMØS code. The fast fission factor ϵ is obtained by extrapolating δ_{28} to an infinite assembly (since it does not require the knowledge of k_∞).

2. A first value of k_∞ is obtained by neglecting epicadmium fissions in U^{235} and calculating p from simple theory (see, for example, Ref. (13)).

3. The value of k_∞ obtained in step 2 is used to correct ρ_{28} and δ_{25}, and a new value of k_∞ is obtained.

4. The new value of k_∞ is used to correct ρ_{28} and δ_{25}, leading to a new value of k_∞.

5. The iteration process concludes when the repeated use of steps 3 and 4 converges.

The iterative process just described was tested in the six lattices investigated. The results, shown in Table 8.6, indicate that the iteration procedure converges rapidly and, for the lattices investigated, leads to values of k_∞ which are in agreement with those obtained from measurements made in the exponential assembly at M.I.T.

5.4 Values of S_{Au}, S_{28} and S_{25}

The values of S_{28} and S_{25} in the assemblies of various sizes are required to extrapolate ρ_{28}, δ_{25} and C^*. The value of S_{Au} in the miniature lattices is needed to calculate R_{Au}-1. Since the leakage of neutrons while slowing down is larger in miniature lattices than in any of the corresponding larger assemblies, the epithermal cross sections in the miniature lattice must be averaged over a harder spectrum than in a larger assembly.

If it is assumed that age theory may be used and that epicadmium capture in U^{238} and Au and epicadmium fission in U^{235} each occurs at an effective energy which depends on the process under consideration, the relations shown in Table 8.7 are obtained. In these expressions, B_g^2 is the geometric buckling which was found to be approximated adequately by the expression:

$$B_g^2 = \left(\frac{2.405}{R}\right)^2 + \left(\frac{\pi}{H}\right)^2 . \qquad (8.32)$$

The ages τ_{28}, τ_{Au} and τ_{25} denote the effective ages for capture in U^{238}, capture in Au and fission in U^{235}, respectively. The quantities $\Delta\tau_x$ are given by:

$$\Delta\tau_x = \tau_t - \tau_x , \qquad (8.33)$$

Table 8.6

Progress of Iteration Procedure to Obtain k_∞

Iteration Step	Value of k_∞					
	ML2	ML7	ML3	ML4	ML6	ML5
k_∞ calculated as in steps 1 and 2	1.254	1.363	1.413	1.205	1.313	1.362
1st iteration	1.307	1.390	1.405	1.245	1.341	1.379
2nd iteration	1.307	1.422	1.406	1.295	1.375	1.383
3rd iteration		1.422		1.295	1.375	1.383
MEASURED	1.330[1] ±.027	1.416[1] ±.011	1.419[1] ±.007	1.304[2] ±.020	1.375[2] ±.021	1.395[2] ±.021

(1) Ref. (8).

(2) Ref. (5); values corrected for epithermal fission in U^{235}.

Table 8.7

Relation Between the Values of S in Different Assemblies

Assembly (x)	Value of $\frac{S^x}{S^{ML}}$		
	$\frac{S^x_{28}}{S^{ML}_{28}}$	$\frac{S^x_{25}}{S^{ML}_{25}}$	$\frac{S^x_{Au}}{S^{ML}_{Au}}$
Exponential[1] Assembly (EX)	$\exp\left\{\left(B_g^{ML^2}-B_g^{EX^2}\right)\cdot\Delta\tau_{28}\right\}$[3]	$\exp\left\{\left(B_g^{ML^2}-B_g^{EX^2}\right)\cdot\Delta\tau_{25}\right\}$	$\exp\left\{\left(B_g^{ML^2}-B_g^{EX^2}\right)\cdot\Delta\tau_{Au}\right\}$
Critical[2] Assembly (C)	$\exp\left\{\left(B_g^{ML^2}-B_m^2\right)\cdot\Delta\tau_{28}\right\}$	$\exp\left\{\left(B_g^{ML^2}-B_m^2\right)\cdot\Delta\tau_{25}\right\}$	$\exp\left\{\left(B_g^{ML^2}-B_m^2\right)\cdot\Delta\tau_{Au}\right\}$
Infinite Assembly (∞)	$\exp\left(B_g^{ML^2}\cdot\Delta\tau_{28}\right)$	$\exp\left(B_g^{ML^2}\cdot\Delta\tau_{25}\right)$	$\exp\left(B_g^{ML^2}\cdot\Delta\tau_{Au}\right)$

(1) B_g^2 = geometric buckling.

(2) B_m^2 = material buckling.

(3) $\Delta\tau_x = \tau_t - \tau_x$.

where τ_t is the age to thermal energies (~5 kT). The ages τ_{28} and τ_{Au} were obtained semi-empirically and the value of τ_{25} was assumed to correspond to 0.5 ev. The values of τ_{28}, τ_{Au} and τ_{25} are listed in Table 8.8 for the various lattices investigated.

Values of the material buckling were obtained from the measurements of B_m^2 made in the exponential assemblies at M.I.T. From the present study, it is apparent that in miniature lattices it may be necessary to include transport effects in the theory derived in section 3.2: first, to define a material buckling (if this is possible), and second, to obtain its value. Transport theory expressions for the thermal flux and slowing-down density in small multiplying assemblies are not available at the present time and more work in this direction is needed before a final conclusion can be reached.

6. DISCUSSION OF RESULTS

It is apparent from the results obtained in this work that the intracellular activity distributions are not affected by being measured in the miniature lattice. Since the macroscopic flux gradients are large, however, the foil holders must be positioned as accurately as possible.

There are limitations on the measurements of ρ_{28}, δ_{25} and C^*. The most important limitation is related to the need to predict R_{Au}-1 accurately as a function of position, in order to extrapolate the values of these parameters meaningfully.

The main difficulty affecting the accuracy of the value of δ_{28} is related to the fact that δ_{28} is generally a small quantity (0.01 to 0.03 for the lattices investigated). The observed U^{238} fission product activity is therefore small and good statistical accuracy is difficult to attain. The experimental determination of δ_{25} involves the same difficulties as that of δ_{28}.

The accuracy of the correction factor for ρ_{28}, δ_{25} and C^* depends on the value of $\psi(r, z)$ at the experimental position. Examples of this function were shown in Figs. 8.17 and 8.18. It is evident that when the measurements are made in the equilibrium region of an exponential assembly, the actual experimental position has little, if any, influence, mainly because $\psi(r, z)$ is practically constant. In miniature lattices,

Table 8.8

Values of τ_{Au}, τ_{28} and τ_{25} in the Lattices Studied

Lattice Spacing (Inches)	U^{235} Concentration (Percent)	τ_{Au} (cm^2)	τ_{28} (cm^2)	τ_{25} (cm^2)
1.25	1.143	97.80	82.30	114.6
1.75	1.143	95.08	81.34	112.0
2.50	1.143	94.11	79.20	110.6
1.25	1.027	97.80	82.30	114.6
1.75	1.027	95.08	81.34	112.0
2.50	1.027	94.11	79.20	110.6

this is not the case. In fact, in miniature lattices it is often necessary, as in the case shown in Fig. 8.18, to make the measurements in positions where the gradient of $\psi(r, z)$ is large. Hence, great care must be exercized in carrying out the experiments.

7. CONCLUSIONS

The present work has shown that significant measurements of lattice parameters can be made in miniature lattices of slightly enriched uranium rods in heavy water. Corrections derived from theory must be made to account for the presence of the external source and boundaries. The theory developed by Peak has been improved, and correction factors have been obtained which permit the extrapolation of miniature lattice data to exponential, critical and infinite assemblies. The validity of the extrapolation methods was tested by comparing the miniature lattice data as extrapolated to exponential assemblies with the results of similar measurements made in the exponential assembly at M.I.T. The extrapolated and measured results agreed generally within the experimental uncertainties.

The parameters measured were ρ_{28}, δ_{28}, δ_{25}, C^* and the intracellular activity distributions of gold. It was shown that to extrapolate the values of ρ_{28}, δ_{25} and C^* measured in miniature lattices to larger assemblies, it is only necessary to describe theoretically the measured spatial distribution of the cadmium ratio of gold.

It is apparent that to determine the material buckling in miniature lattices, it may be necessary to include transport effects, first, to define B_m^2 (if this is, indeed, possible) and second, to obtain its value. It was shown that k_∞ can be determined through an iterative process. The iteration procedure was shown to converge rapidly and, for the lattices investigated, led to results that were in agreement with the values of k_∞ obtained from measurements made in the exponential assembly at M.I.T.

8. REFERENCES

(1) Peak, J. C., I. Kaplan and T. J. Thompson, "Theory and Use of Small Subcritical Assemblies for the Measurement of Reactor Parameters," NYO-10204, MITNE-16 (April 1962).

(2) Palmedo, P. F., I. Kaplan and T. J. Thompson, "Measurements of the Material Bucklings of Lattices of Natural Uranium Rods in D_2O," NYO-9660, MITNE-13 (January 1962).

(3) Harrington, J., "Measurement of the Material Buckling of a Lattice of Slightly Enriched Uranium Rods in Heavy Water," M.S. Thesis, M.I.T. Nuclear Engineering Dept. (July 1963).

(4) Simms, R., I. Kaplan, T. J. Thompson and D. D. Lanning, "Analytical and Experimental Investigations of the Behavior of Thermal Neutrons in Lattices of Uranium Metal Rods in Heavy Water," NYO-10211, MITNE-33 (October 1963).

(5) D'Ardenne, W. H., T. J. Thompson, D. D. Lanning and I. Kaplan, "Studies of Epithermal Neutrons in Uranium, Heavy Water Lattices," MIT-2344-2, MITNE-53 (August 1964).

(6) Honeck, H. C., "THERMØS, A Thermalization Transport Theory Code for Reactor Lattice Calculations," BNL-5826 (September 1961).

(7) Woodruff, G. L., I. Kaplan and T. J. Thompson, "A Study of the Spatial Distributions of Fast Neutrons in Lattices of Slightly Enriched Uranium Rods Moderated by Heavy Water," MIT-2344-5, MITNE-67 (November 1965).

(8) Harrington, J., D. D. Lanning, I. Kaplan and T. J. Thompson, "Use of Neutron Absorbers for the Experimental Determination of Lattice Parameters in Subcritical Assemblies," MIT-2344-6, MITNE-69 (February 1966).

(9) Thompson, T. J., I. Kaplan, F. M. Clikeman and M. J. Driscoll, "Heavy Water Lattice Project Annual Report," MIT-2344-4, MITNE-65 (September 1965).

(10) Robertson, C. G., "Measurements of Neutron Utilization for Lattices of Slightly Enriched Uranium Rods," M.S. Thesis, M.I.T., Nuclear Engineering Dept. (June 1965).

(11) Bliss, H. E., "Measurements of the Fast Effect in Heavy Water, Partially Enriched Uranium Lattices," M.S. Thesis, M.I.T., Nuclear Engineering Dept. (May 1964).

(12) Kaplan, I., "Measurements of Reactor Parameters in Subcritical and Critical Assemblies: A Review," NYO-10207, MITNE-25 (August 1962).

(13) Glasstone, S. and M. C. Edlund, The Elements of Nuclear Reactor Theory (Princeton, New Jersey: D. Van Nostrand Company, Inc., 1952).

(14) Lanning, D. D., I. Kaplan and F. M. Clikeman, "Heavy Water Lattice Project Annual Report," MIT-2344-3, MITNE-60 (September 1964).

9. FAST NEUTRON DISTRIBUTIONS

G. L. Woodruff

Work in this area was completed prior to, and discussed in, the 1965 Annual Report, followed shortly by issuance of the topical report: MIT-2344-5, MITNE-67 of November 1965, "A Study of the Spatial Distributions of Fast Neutrons in Lattices of Slightly Enriched Uranium Rods Moderated by Heavy Water," by G. L. Woodruff, I. Kaplan and T. J. Thompson.

The work will, therefore, not be discussed further in this report except to call attention to an erratum in the topical report.

In the cylindrical shell kernel discussed on page 47, Eqs. 3.1 and 3.2:

$$\overline{T}_c(r, r') = \left\{ \begin{array}{ll} \frac{\Sigma}{2\pi} \int_1^\infty K_o(\Sigma r y)\, I_o(\Sigma r' y)\, dy & r > r' \\ \\ \frac{\Sigma}{2\pi} \int_1^\infty K_o(\Sigma r' y)\, I_o(\Sigma r y)\, dy & r < r' \end{array} \right\},$$

$\overline{T}_c(r, r')$ is the flux and not the collision density, so that the above expression should not be divided by Σ as described on page 47. The UNCOL code is corrected by removing Σ from the denominator of five expressions corresponding to Eqs. 3.14 and 3.15 on page 49. These expressions are located in the listing of the UNCOL code in Appendix A as follows:

Page	Line	Remarks
130	38	Statement preceding statement number 25
131	22	Statement following statement number 63
131	26	Statement following statement number 65
132	8	Statement preceding statement number 125
133	4	Statement preceding statement number 135

In each of the above steps, the variable C should be replaced by the variable Y at the end of the statement.

The results of the UNCOL calculations given in the topical report are not significantly affected, provided the value of the effective removal cross section for D_2O, Σ_m, is reduced from 0.093 cm^{-1} to give good agreement with the calculated value of 0.0899 cm^{-1}. It is also found that the results of UNCOL calculations are very insensitive to changes in the fuel removal cross section, Σ_f, after making the above change. The value of Σ_f used in the report, 0.100 cm^{-1}, should not, therefore, be interpreted as an experimental value for the fast neutron removal cross section for uranium metal as suggested in the topical report.

The above results will be discussed further in a forthcoming paper by the author.

10. NOISE ANALYSIS

F. H. Hauck, M. G. Johnson and F. M. Clikeman

1. INTRODUCTION

Some preliminary work has been completed (1, 2) evaluating the application of noise analysis techniques (3, 4, 5, 6) to subcritical assembly studies. The ultimate objective of this work is to develop an alternative method for measuring the prompt neutron decay constant, α, thereby supplementing or supplanting the pulsed neutron source techniques described in Chapter 4 of this report.

2. NOISE ANALYSIS SYSTEM

In the initial phase of this work, apparatus was assembled and debugged for measuring both auto- and cross-correlation functions of the neutron density in a lattice in the M. I. T. exponential facility. Actually, the Fourier transforms of the respective functions were determined to give the corresponding power-spectral-density functions.

For single-detector autocorrelation, one obtains (1):

$$\left\langle \left| I(w) \right|^2 \right\rangle = 2Q^2 \varepsilon F_o \left[1 + \frac{K}{\omega^2 + \alpha^2} \right], \tag{10.1}$$

where

I = detector current,

Q = charge collected per fission detected,

ε = fraction of fissions detected,

F_o = fission rate,

ω = frequency,

α = prompt neutron decay constant,

and

$$K = \frac{\varepsilon k_p}{\bar{\nu} \ell^2} \left[2 - \frac{k_p}{\bar{\nu}} + k_p + \frac{k_p^2}{\bar{\nu}} \right] \left(\overline{\nu^2} - 2\bar{\nu} + 1 \right),$$

with

k_p = prompt multiplication constant = $k(1-\beta)$,

$\bar{\nu}$ = average number of neutrons emitted per fission,

ℓ = prompt neutron lifetime.

Equation 10.1 shows that a measurement of I(w) versus ω can, in theory, permit determination of α. In practice, however, K is so small for a subcritical system and low efficiency detectors that this is impracticable.

For two-detector cross correlation one obtains, on the other hand, a response whose shape is not dependent upon detector efficiency:

$$\langle |I(w)|^2 \rangle = 2\varepsilon_1\varepsilon_2 F_o Q^2 \frac{\overline{\nu(\nu+1)}}{(\bar{\nu})^2} \frac{k_p^2}{\ell^2} \cdot \frac{1}{\omega^2 + \alpha^2}, \qquad (10.2)$$

where the nomenclature is the same as before, except that we now have the product of two detector efficiencies, ε_1 and ε_2, entering.

Figure 10.1 shows the circuit diagram of the analog system used to process cross-correlation results. The portion outside the dotted lines was used for the one-detector autocorrelation measurements: a typical plot of output data is shown in Fig. 10.2. As can be seen, the spectrum is a flat, white-noise-like response except for a high frequency roll-off due to equipment limitations. No break point is detectable in the 100-1000 cps region where it would occur for the lattice studied. This result is as anticipated and is due to the low efficiency of the detection system used. Figure 10.3 shows estimated detector efficiencies required for lattice studies: it is clear that only a high efficiency system employing cross correlation of two detector outputs offers any promise of success. Therefore, once a workable electronics system for noise analysis was assembled, the emphasis was shifted to detector development.

3. DETECTOR STUDIES

As shown by Eqs. 10.1 and 10.2 and Fig. 10.3, high detection efficiency is essential for noise analysis in far subcritical systems. In autocorrelation, the shape of the response is particularly sensitive; while, for cross correlation, the amplitude depends on the square of the detector efficiency. In the electronics de-bugging experiments described

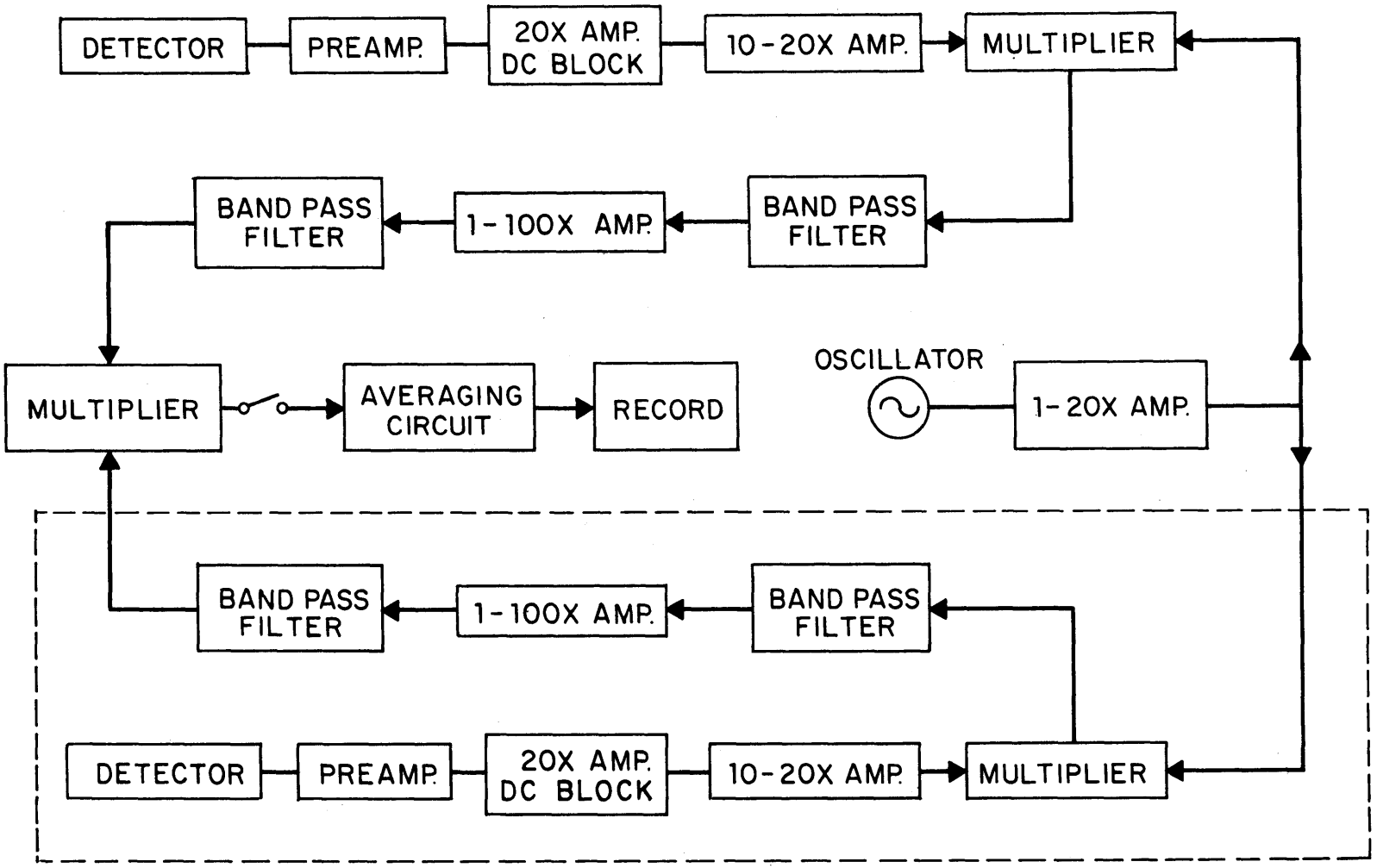

FIGURE 10.1 SCHEMATIC CIRCUIT DIAGRAM FOR CROSS-CORRELATION MEASUREMENTS

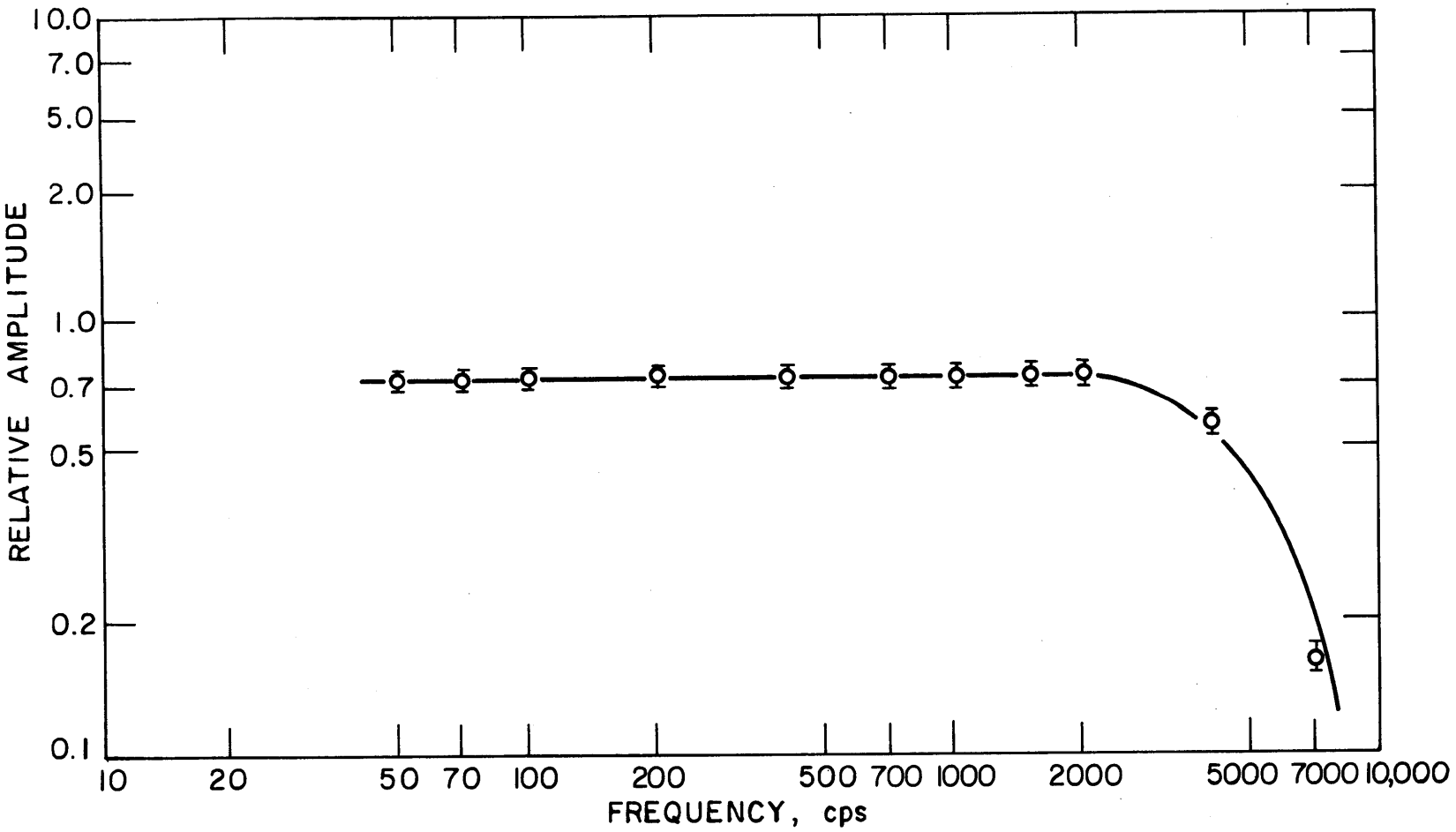

FIG. 10.2 AUTO-SPECTRAL DENSITY MEASUREMENTS IN MIT LATTICE

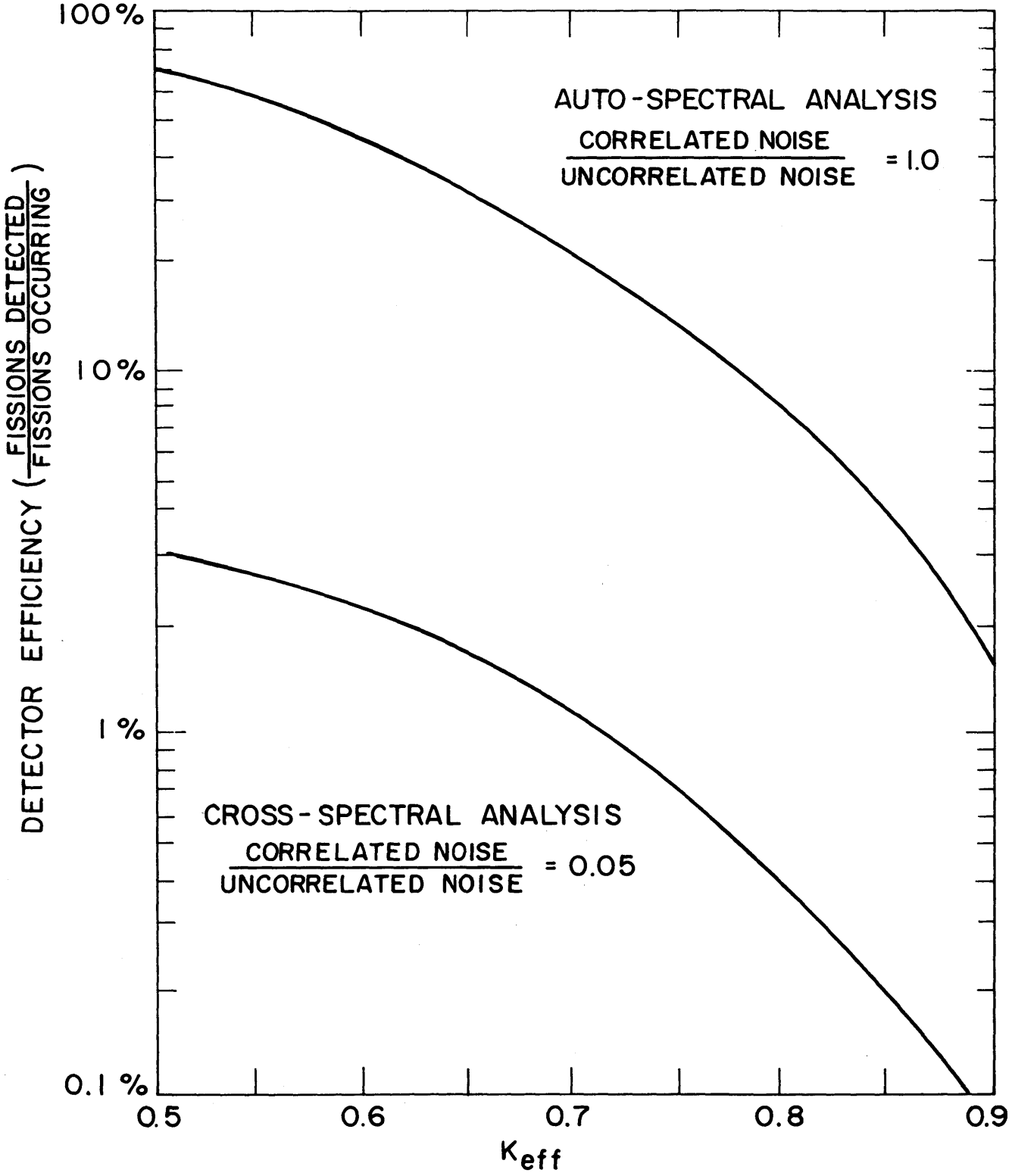

FIG. 10.3 DETECTOR EFFICIENCIES REQUIRED VS k_{eff} FOR NOISE SPECTRAL ANALYSIS

in section 2, a low efficiency detector was used; too low for either auto- or cross correlation.

In designing a high efficiency detector system, one is severely limited by the requirement that the detector not perturb the system being studied. Hence, attention was focused, at first, on detecting neutrons or gamma photons (7) which leak out of the lattice tank. Since the exponential tank is wrapped in cadmium, very few thermal neutrons escape, so that gamma detection appeared most promising. A large liquid scintillation detector, shown in Fig. 10.4, was assembled and placed next to the lattice tank. The major unconventional feature is the use of a photomultiplier, voltage divider, and pre-amp submerged in the scintillating fluid.

The scintillation detector was tested with the lattice facility in operation and the efficiency of the detector determined to be 2.2×10^{-4} detections per fission. It is evident from Fig. 10.3 that use of a bank of ten such detectors might permit cross-correlation studies for $k \approx 0.9$, but in general, the efficiency is too low to be really useful.

At present, an alternative photon detection system, based on the Cerenkov glow in the lattice D_2O, is under consideration.

4. REFERENCES

(1) Hauck, F., "Investigation of Noise Analysis Techniques for the M. I. T. Heavy Water Lattice," M.S. Thesis, M. I. T. (1966).

(2) Johnson, M. G., "A Radiation Detector for Noise Analysis on the MITR Subcritical Assembly," S.M. Thesis, M. I. T. (1966).

(3) Bierman, S. R., K. L. Garlid and R. W. Albrecht, "Complementary Use of Pulsed-Neutron and Reactor Noise Measurements," Nuclear Science and Engineering, 22, 206-214 (1965).

(4) Thie, J. A., Reactor Noise, Rowman and Littlefield, Inc., New York (1963).

(5) Cohn, C. E., "A Simplified Theory of Pile Noise," Nuclear Science and Engineering, 7, 472-475 (1960).

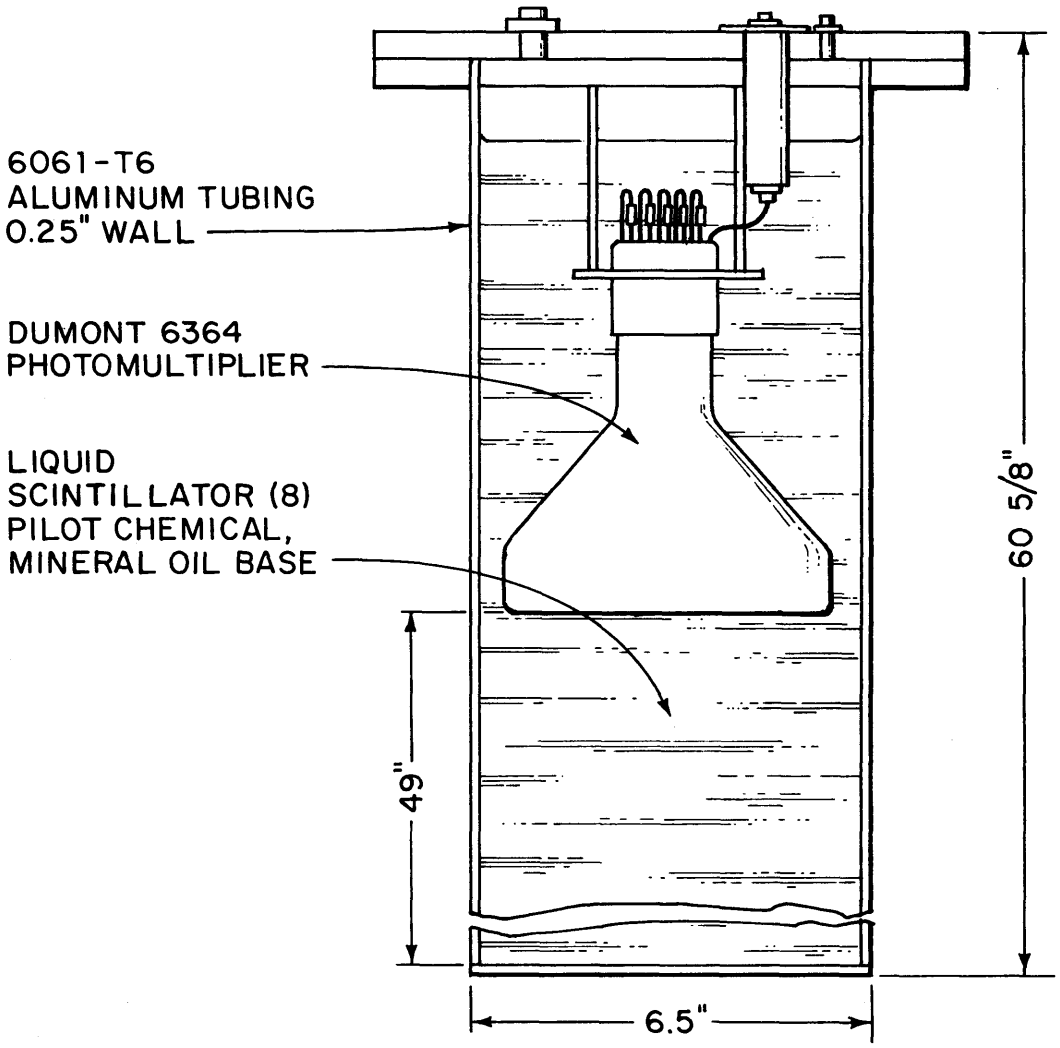

FIGURE 10.4 SKETCH OF LIQUID SCINTILLATION DETECTOR

(6) Seifritz, W., D. Stegemann and W. Vath, "Two Detector Cross-Correlation Experiments in the Fast-Thermal Argonaut Reactor STARK," Int. Symp. on Neutron Noise, Waves and Pulse Propagation, Gainesville, Florida, February 14-16, 1966.

(7) Gelinas, R. J. and R. K. Osborn, "Reactor Noise Analysis by Photon Observation," Nuc. Sci. Eng., 24 (February 1966).

(8) Reines, F. and T. L. Jenkins, "A Large Scintillator for the Detection of Antineutrino Reactions," I.E.E.E. Trans. Nuc. Sci., NS-11, 1 (1964).

11. VOID REACTIVITY MEASUREMENTS

L. Papay and K. Bowles

1. INTRODUCTION

A feasibility study was completed (1) evaluating the use of pulsed neutron source methods for measuring coolant void coefficients in heavy water moderated, organic cooled (i.e., HWOCR type) fuel bundles. The pulsed neutron system and experimental procedures employed were as already described in Chapter 4 of this report.

2. SIMULATED FUEL ASSEMBLY

The first aim of this study was to build a test assembly having parameters reasonably close to those of typical pressure tubes and fuel bundles considered for HWOCR-type reactors. The dimensions finally chosen for the test assembly are shown in Table 11.1, together with some other similar assemblies for comparison. As can be seen, the important coolant and insulating-gap to fuel ratios have been matched quite well, considering that the assembly was fabricated from available off-the-shelf materials. Figure 11.1 shows the completed fuel assembly inserted in place in the center of the lattice facility's large exponential tank.

3. TEST PROCEDURE

The pulsed neutron source technique was used to measure the prompt neutron decay constant, λ, for three conditions: assembly voided, assembly filled with simulated organic coolant, and assembly flooded with D_2O. The equipment, procedures, and data analysis methods were exactly the same as described in Chapter 4 and reference (2).

4. INTERPRETATION OF RESULTS

The codes developed to process pulsed neutron data provide $\lambda \pm \sigma$ for each experimental run. Differences between the various experimental states can then be described in terms of the change in decay

Table 11.1

Comparative HWOCR Fuel Assembly Parameters

Experiment	Coolant	Fuel Rods	Rod Pitch (Inches)	Lattice Pitch (Inches)	Calandria OD/ID (Inches)	Pressure Tube OD/ID (Inches)	Cross-Sectional Ratios* Structure / Fuel	Void / Fuel	Coolant / Fuel
Whiteshell WR-1	Santowax	UO_2 (18)			3.79/3.69	3.33/3.25	.298	.461	.887
CEND Design Study		UO_2 (37)	.513	9.75	4.038/3.966	3.766/3.642	.179	.174	.514
DOR Design	Diphyl	UO_2 (19)			4.57/4.33	3.94/3.57	.710	.485	.881
Savannah River	Dowtherm A	UO_2 (19)	.598		2.679 (Hex Geometry)		.0806		.767
		(19)	.607		3.086		.0827		1.05
		(31)	.607		4.00		.055		1.141
Pawling Test Rig	Dowtherm A	UC (7)	.58	7.5	1.615 Hex		.164		.437
		(19)	.58	8.46	2.619 Hex		.0935		.385
		(19)	.648	10.46	2.995 Hex		.1096		.197
		(31)	.648	10.46	4.096 Dia		.0672		1.670
Test Assembly	Monoiso-propyl-biphenyl	UO_2 (7)	.565	6.2	4.0/3.75	3.5/2.9	1.93	.603	2.240
		(19)	.565	6.2	4.0/3.75	3.5/2.9	1.22	.379	.782

*Cross-sectional ratios shown are the ratios of the areas of aluminum, void (air gap), or coolant to the area of fuel plus clad in a cross-sectional cut through the active volume of the test assembly.

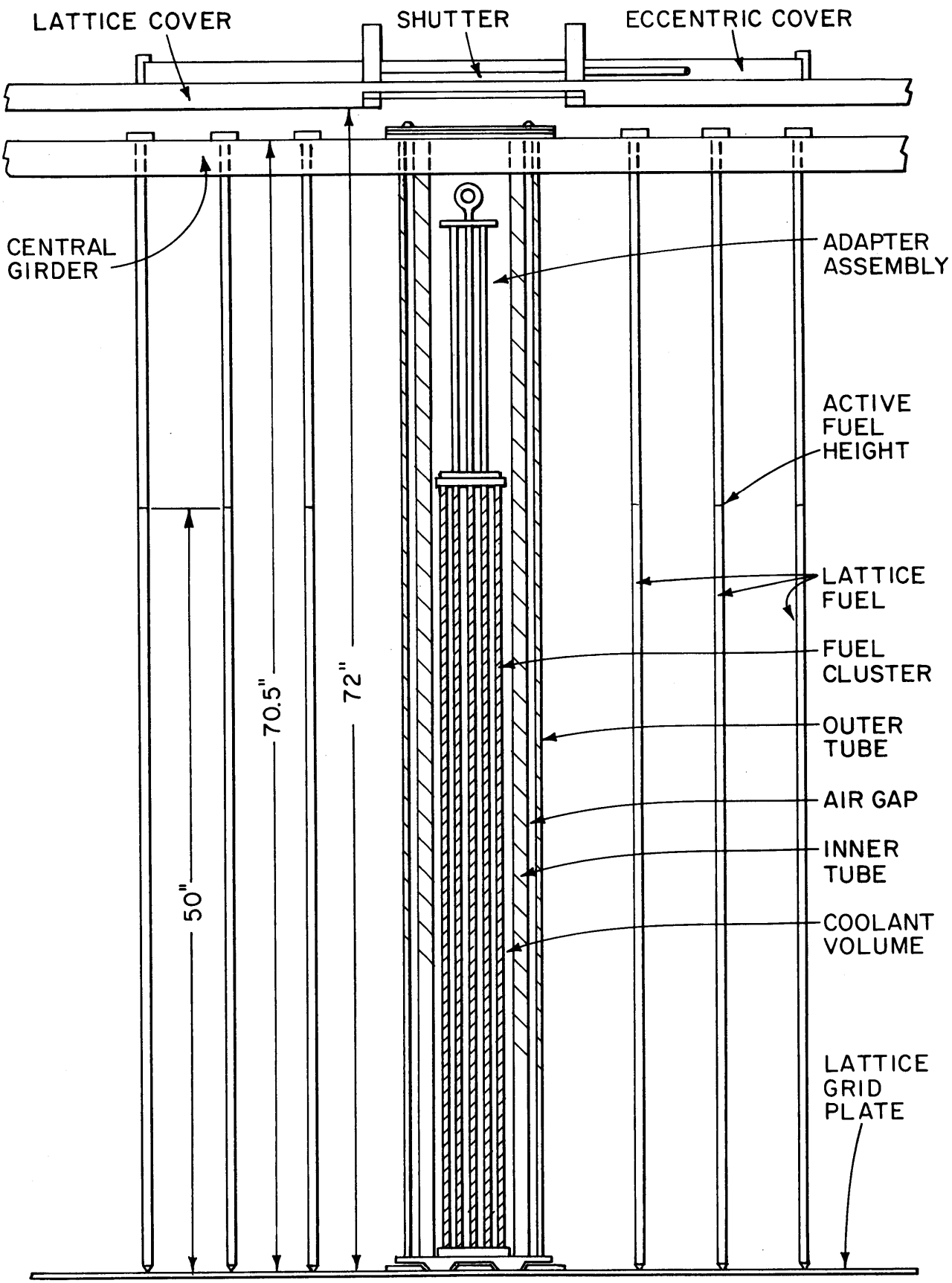

FIGURE 11.1 SIMULATED PRESSURE TUBE AND FUEL BUNDLE IN LATTICE

constant, $\Delta\lambda \pm \sigma$.

It is necessary to relate $\Delta\lambda$ to a reactivity change $\Delta\rho$. For this feasibility study, a simple model was used. Assuming the effective neutron generation time, $\Lambda \equiv \ell/k$, remains constant, one can show that (1):

$$\Delta\rho = -\frac{\ell}{k}\Delta\lambda, \tag{11.1}$$

where

ℓ = neutron lifetime,

k = effective multiplication constant.

With k = 0.65 and $\ell = 4.35 \times 10^{-4}$ sec,

$$\Delta\rho = -0.67 \times 10^{-3}\,\Delta\lambda. \tag{11.2}$$

Equation 11.2 was used to effect the transformation between the experimental $\Delta\lambda$ values and reactivity.

Table 11.2 shows the experimental void coefficients determined in this manner. It is evident that the results are statistically significant only for the longest runs with the 19-rod fuel bundles. For that particular configuration, the fuel bundle appeared to have a negative voiding coefficient in the M.I.T. lattice facility.

Table 11.2

Estimate of Reactivity Changes and Void Coefficients of the Test Assembly for 7- and 19-Rod Runs

Coolants Compared	$\Delta\rho \pm \sigma$* ($\times 10^{-3}$)	ΔV (cm^3)	$\Delta\rho/\Delta V \pm \sigma$ ($\times 10^{-3}\,\ell^{-1}$)
	7-Rod Short Runs		
Void-MIPB	+10.05 ± 10.4	4430	+2.27 ± 2.35
Void-D_2O	-3.08 ± 11.62	4430	-0.70 ± 2.62
	19-Rod Short Runs		
Void-MIPB	-6.17 ± 9.27	2405	-2.56 ± 3.85
Void-D_2O	+2.88 ± 10.68	2405	+1.24 ± 4.44
	19-Rod Long Runs		
Void-MIPB	-13.72 ± 7.45	2405	-5.71 ± 3.10
Void-D_2O	-13.25 ± 7.53	2405	-5.51 ± 3.13

*$\Delta\rho$ measures the reactivity change in going from the state on the right in column 1 to the state on the left.

5. CONCLUSIONS

The results of the subject feasibility study are encouraging since the pulsed neutron source strength and detector efficiency can be optimized to increase the precision of the data.

A new task proposing development and use of the pulsed neutron source technique for measuring HWOCR void coefficients has been submitted to the AEC.

6. REFERENCES

(1) Bowles, K. D., "Investigations of the Void Effect in a Heavy Water Moderated, Organic Cooled Assembly by the Pulsed Neutron Source Technique," M.S. Thesis, M.I.T., Nuclear Engineering Dept., September 1966.

(2) Bliss, H. E., I. Kaplan and T. J. Thompson, "Use of a Pulsed Neutron Source to Determine Nuclear Parameters of Lattices of Partially Enriched Uranium Rods in Heavy Water," MIT-2344-7, MITNE-73, September 1966.

12. GAMMA-RAY SPECTRA OF LATTICE FUEL

T. L. Harper and N. C. Rasmussen

1. INTRODUCTION

Work at a number of laboratories in recent years has shown that Ge(Li) semiconductor radiation detectors have considerably better energy resolution than scintillation detectors. The availability of Ge(Li) detectors at M.I.T. (1) prompted an investigation of possible applications in radionuclide analysis of lattice fuel and foils (2). Ge(Li) detectors were used in three ways: as separate detectors, with NaI detectors in Compton suppression, and in coincidence-counting setups. Low efficiency limited the utility of coincidence counting, and high Compton background limited the usefulness of the single detectors. Thus, the Compton suppression apparatus, described in more detail elsewhere (3), proved most useful and will be discussed further herein.

2. DESCRIPTION OF APPARATUS

The Compton suppression apparatus is composed of three main systems:

1. The Ge(Li) detector, bias supply, preamplifier and amplifier.
2. The NaI scintillation detectors, photomultiplier tubes, preamplifiers, and amplifiers.
3. The coincidence logic unit, gating pulse circuit, 4096 channel analyzer, and data readout equipment.

Figure 12.1 shows a block diagram of the apparatus. The figure shows schematically the two 6-inch-diameter by 3-inch-thick NaI(Tl) scintillation detectors. They are placed in good geometry with relation to the 31.25-cc active volume Ge(Li) detector so as to detect the scattered photons with high efficiency while, at the same time, being shielded from the main gamma source.

The initial Compton interaction causes a pulse to appear in the

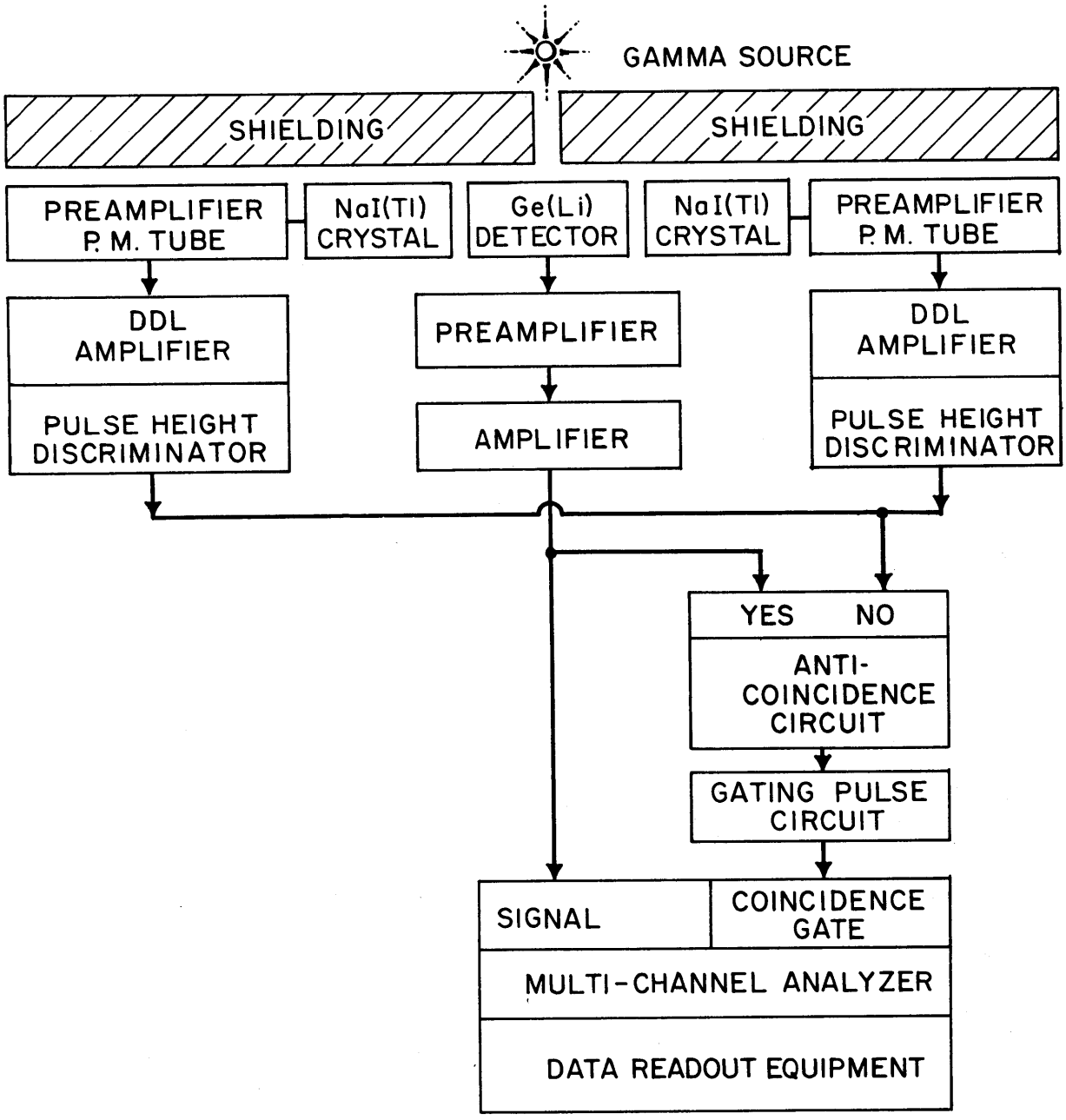

FIGURE 12.1 BLOCK DIAGRAM OF COMPTON SUPPRESSION APPARATUS

Ge(Li) detector, and the scattered photon has a good chance (~60% at 1 MeV) of being detected by the NaI(Tl) detectors. Both pulses are fed to the anticoincidence circuit, as shown, where the logic is arranged so as to gate the analyzer ON only if the Ge(Li) detector has registered a pulse, while during the same time interval, the Na(Tl) system has not registered a pulse. Thus, the initial Compton event in the Ge(Li) crystal will not be recorded by the analyzer, and the Compton contributions in the spectra will be reduced.

Figure 12.2 shows a typical detector assembly in more detail. This particular assembly was used for the single detector studies; slight modifications were employed in the other experiments.

3. RESULTS AND APPLICATIONS

Figure 12.3 shows a typical spectrum measured on a UO_2 fuel pellet irradiated in a lattice fuel rod using the Compton suppression apparatus. The high resolution, resulting in a large number of identifiable photopeaks, is evident.

Based upon the results obtainable with Ge(Li) detectors, it is possible to propose new methods for measurement of lattice parameters, not heretofore practicable. As an example, consider δ_{28}, the ratio of U^{238} to U^{235} fissions. Currently, δ_{28} is measured by comparing fission product activities in depleted and natural (or enriched) uranium foils. With Ge(Li) spectrometry, it appears possible to determine δ_{28} with a single foil of intermediate depletion (~ 200 ppm) by measuring relative activities due to fission products having a different yield for U^{238} and U^{235} fission. One can show that (2):

$$\delta_{28} = \frac{Y_1}{Y_2} \cdot \frac{R_{25} - R}{R - R_{28}} \frac{\varepsilon}{1 - \varepsilon} \cdot \frac{1 - \varepsilon_f}{\varepsilon_f}, \qquad (12.1)$$

where

Y_1/Y_2 = ratio of yields of fission products 1 and 2 for U^{235} fission,

R = ratio of the activity of fission product 2 to that of fission product 1 in the test foil irradiated in lattice fuel,

R_{25} = corresponding ratio for the U^{235} foil used to calibrate the apparatus initially,

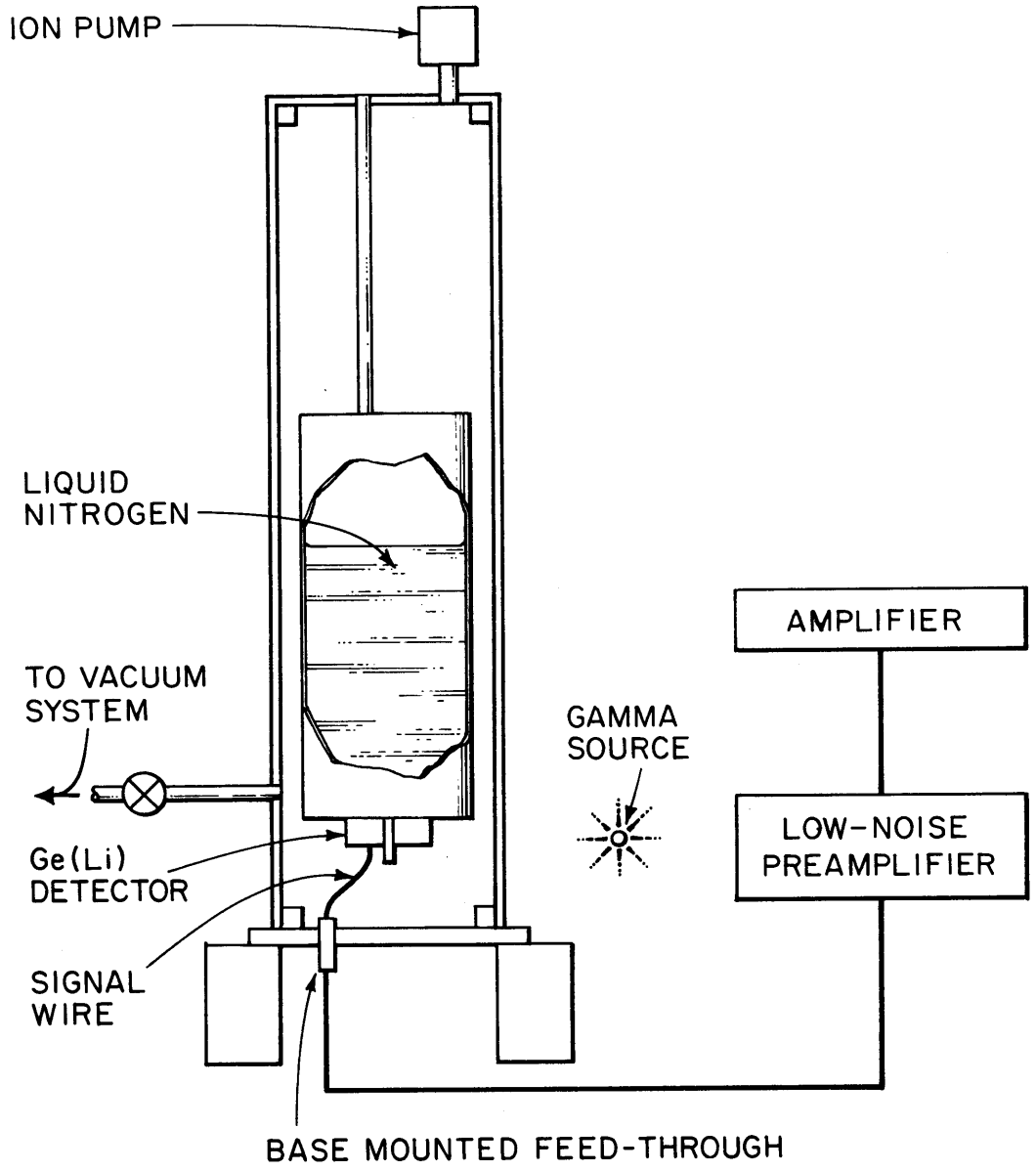

FIGURE 12.2 SCHEMATIC DIAGRAM OF VACUUM DEWAR AND ELECTRONICS FOR USE WITH Ge(Li) GAMMA RAY DETECTORS.

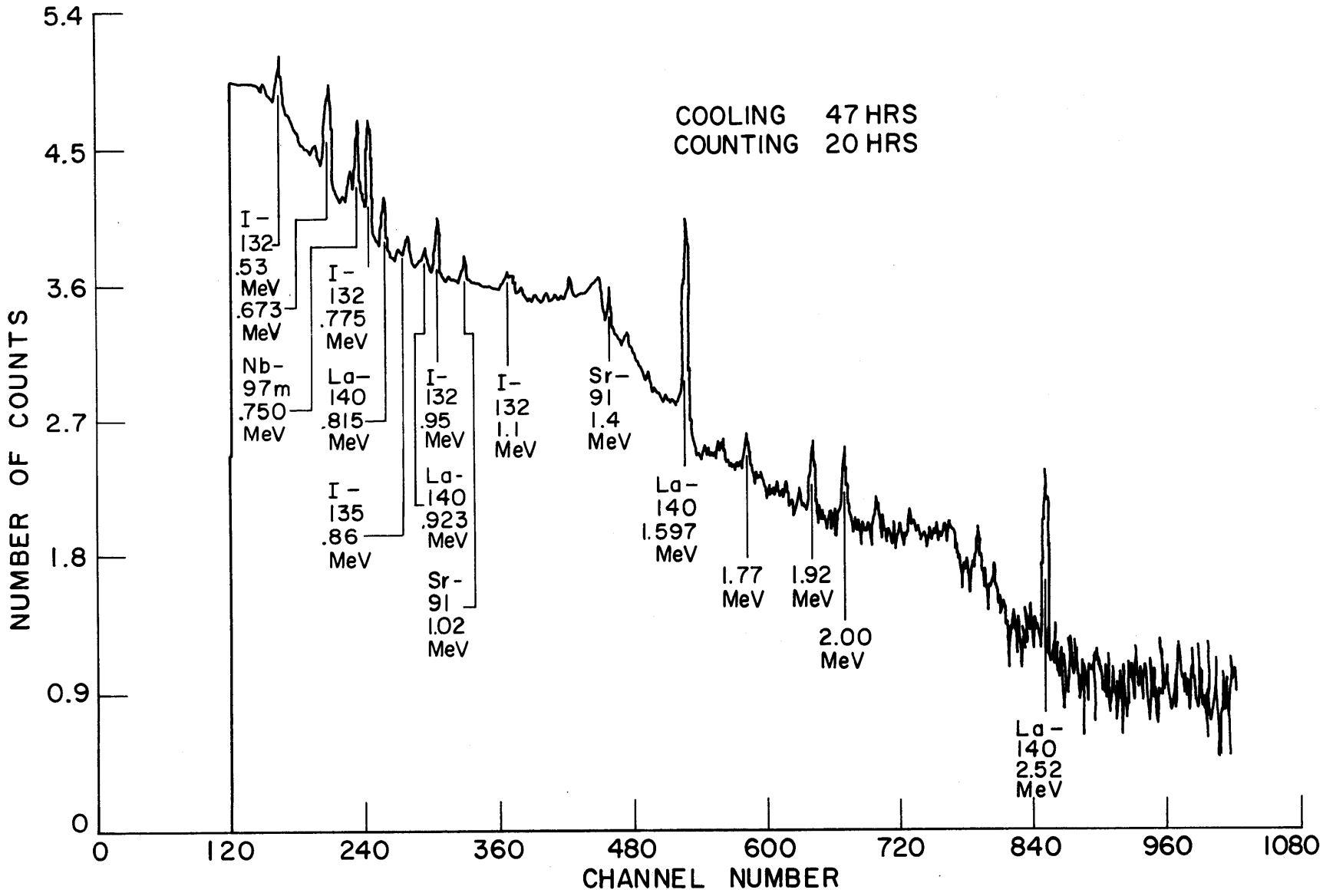

FIG. 12.3 UO_2 SPECTRUM NUMBER 60611 USING COMPTON SUPPRESSION

R_{28} = corresponding ratio for the U^{238} foil used to calibrate the apparatus initially,

ε = enrichment of test foil,

ε_f = enrichment of the lattice fuel.

In order to investigate the feasibility of the proposed method, the ratio R_{28}/R_{25} was measured with enriched (93.17% U^{235}) and depleted (18 ppm U^{235}) foils. In this part of the work, the Ge(Li) detector was used in the separate-detector mode. Table 12.1 shows the comparison between theoretical and experimental ratios for the fission products Sr-91, Sr-92, and I-135. As can be seen, agreement is within the experimental uncertainty in all cases. However, the experimental error is fairly large, primarily due to low count rates for the U^{238} foils.

4. CONCLUSIONS

Ge(Li) detection systems appear to have considerable promise for measurement of lattice physics parameters. The particular system employed in this study was limited by low detection efficiency, but this can be remedied by use of larger Ge(Li) detectors as they become available and by construction of counting setups specifically designed for this application.

5. REFERENCES

(1) Sovka, J. A. and N. C. Rasmussen, "Nondestructive Analysis of Irradiated MITR Fuel by Gamma-Ray Spectroscopy," AFCRL-65-787, MITNE-64, October 1965.

(2) Harper, T. L., "Analysis of Lattice Fuel Using Ge(Li) Gamma-Ray Spectrometry," M.S. Thesis, M.I.T., Nuclear Engineering Dept., September 1966.

(3) Rasmussen, N. C. and V. Orphan, "A Pair Spectrometer Using a Large Coaxial Lithium-Drifted Germanium Detector," Paper presented at I.E.E.E. Conference, October 1966.

Table 12.1

Comparison of Theory and Experiment

Fission Product 1	Gamma Energy (MeV)	Fission Product 2	Gamma Energy (MeV)	Theory R_{28}/R_{25}	Experiment R_{28}/R_{25}	Experimental Error $\pm\sigma$
Sr-91	1.025	Sr-92	1.37	0.802	0.874	± .109
Sr-91	1.025	I-135	1.14	1.335	1.306	± .170
Sr-91	1.025	I-135	1.275	1.335	1.465	± .183
Sr-92	1.37	I-135	1.14	1.660	1.500	± .190
Sr-92	1.37	I-135	1.275	1.660	1.685	± .204

13. TWO-REGION LATTICES

J. W. Gosnell

Investigation into methods of determining the properties of test lattices from measurements in two-region assemblies has continued. The assemblies investigated to date are listed in Table 13.1.

1. GOLD-CADMIUM RATIOS

Gold-cadmium ratios in the two regions have been given as a function of radius in previous annual reports for the first ten assemblies. The results of traverses made in Assembly XI with 0.125-inch-diameter, 0.010-inch-thick, gold foils are shown in Figs. 13.1 and 13.2. Two traverses were made with bare foils, and two with cadmium-covered foils. The standard deviation of the mean cadmium ratio is in most cases less than one percent.

The plots of epicadmium and subcadmium gold activities versus radius show a difference in shape, with the subcadmium activity having a greater tendency to flatten in the test region, as shown in Fig. 13.1. Although the two regions differed in both enrichment and fuel rod size, there are only small differences in the cadmium ratios measured in the moderator. This is attributed to the wide spacing common to both regions. However, the change in the ratio, though small, is evident in Fig. 13.2.

2. δ_{28} MEASUREMENTS

Measurements of δ_{28}, the ratio of the fission rate in U^{238} to that in U^{235}, were made in the center position of most of the assemblies studied using standard techniques.

In most cases, two independent determinations were made for each assembly. The results are shown in Table 13.2 along with previously reported values for the full lattice corresponding to the test region.

Table 13.1

Two-Region Assemblies Tested in the M.I.T. Lattice Facility

Assembly Designation	Properties Common to Both Regions	Outer Reference Region	Inner Test Region
I	0.25-in.-diameter, 1.027% U-235 fuel	9 rings – 1.25-in. spacing	2 rings* – 2.50-in. spacing**
II	0.25-in.-diameter, 1.027% U-235 fuel	7 rings – 1.25-in. spacing	3 rings – 2.50-in. spacing
III	0.25-in.-diameter, 1.027% U-235 fuel	5 rings – 1.25-in. spacing	4 rings – 2.50-in. spacing
IV	0.25-in.-diameter, 1.027% U-235 fuel	4 rings – 2.50-in. spacing	6 rings – 1.25-in. spacing
V	0.25-in.-diameter, 1.143% U-235 fuel	9 rings – 1.25-in. spacing	2 rings – 2.50-in. spacing
VI	0.25-in.-diameter, 1.143% U-235 fuel	5 rings – 1.25-in. spacing	4 rings – 2.50-in. spacing
VII	0.25-in.-diameter, 1.75-in. spacing	7 rings – 1.143% U-235 fuel	3 rings – 1.027% U-235 fuel
VIII	0.25-in.-diameter, 1.75-in. spacing	5 rings – 1.143% U-235 fuel	5 rings – 1.027% U-235 fuel
IX	2.50-in. spacing	3 rings – 0.25-in.-diameter, 1.027% U-235 fuel	4 rings – 0.75-in.-diameter, 0.947% U-235 fuel
X	2.50-in. spacing	5 rings – 0.25-in.-diameter, 1.027% U-235 fuel	2 rings – 0.75-in.-diameter, 0.947% U-235 fuel
XI	5.00-in. spacing	2 rings – 0.75-in.-diameter, 0.947% U-235 fuel	2 rings – 1.0-in.-diameter, natural uranium fuel

* Rings about the central rod.
** All spacings are the triangular lattice pitches used.

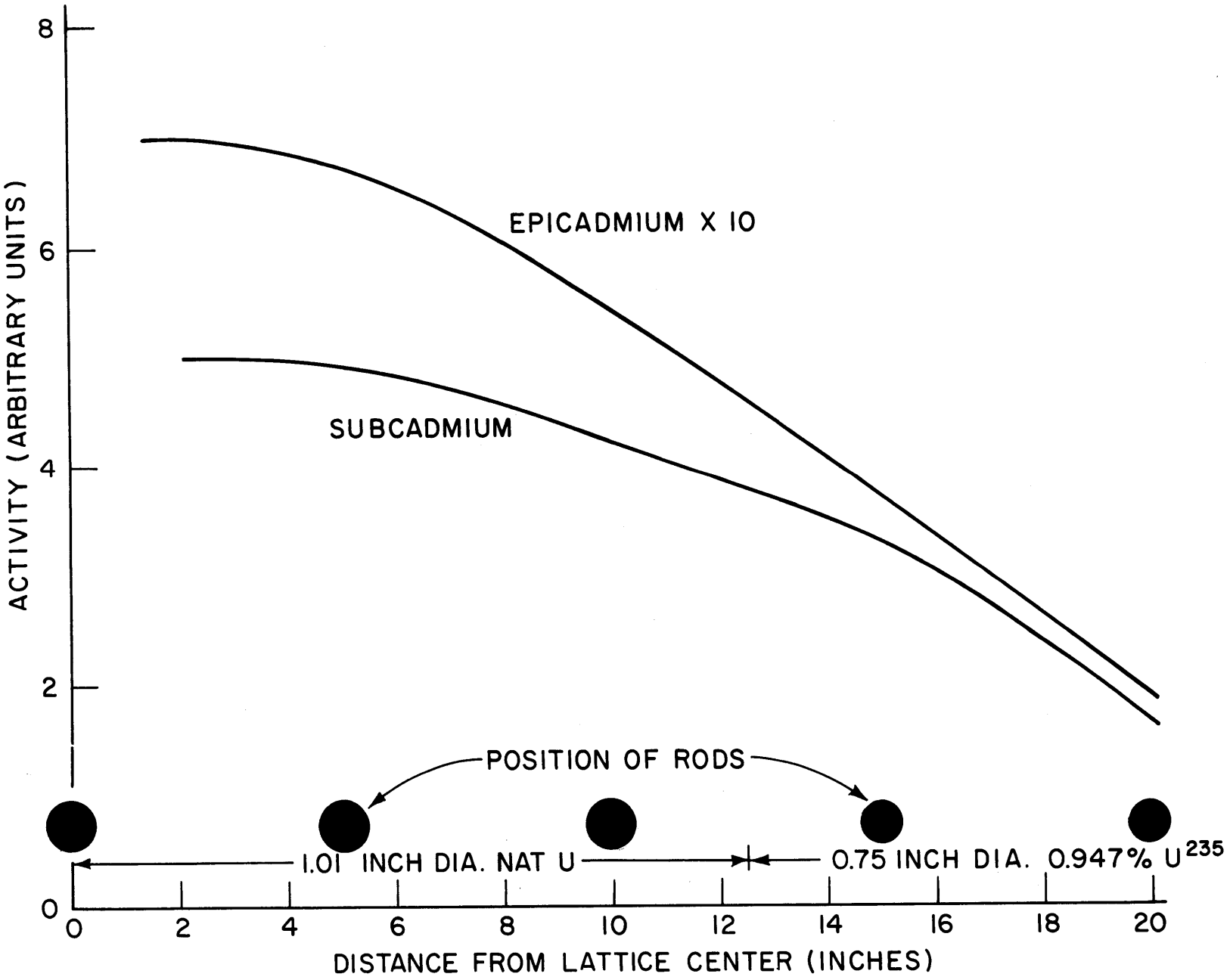

FIG. 13.1 GOLD FOIL ACTIVITIES IN ASSEMBLY XI

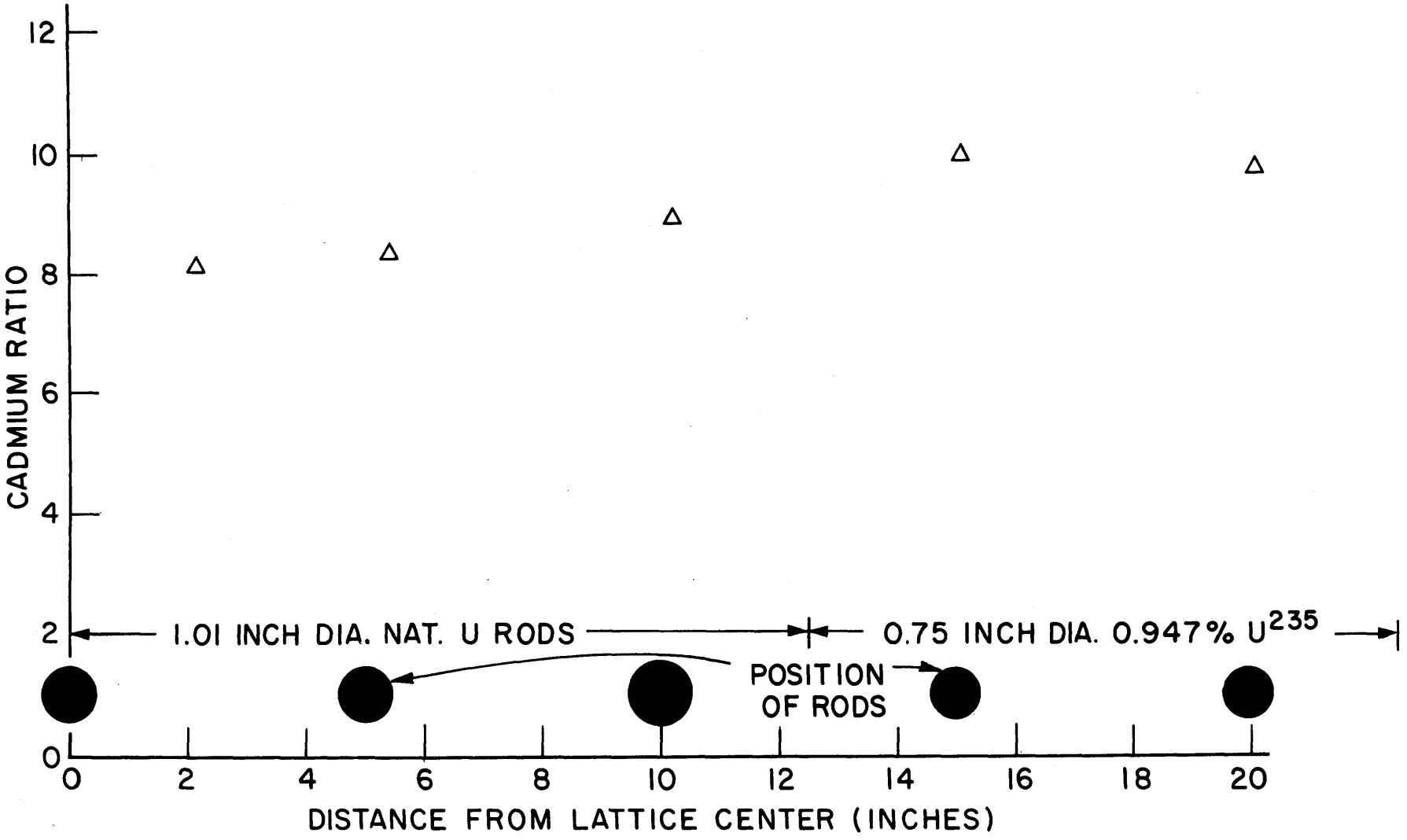

FIG. 13.2 GOLD CADMIUM RATIOS IN ASSEMBLY XI

Table 13.2

δ_{28} Measurements

Assembly	δ_{28} in Center Position		Full Lattice Value
II		0.0192	
		0.0188	
	Average	0.0190	0.0183 ± .0007
IV		0.0280	
		0.0272	
	Average	0.0276	0.0274 ± .0012
VII		0.0201	
		0.0201	
	Average	0.0201	0.0217 ± .0007
VIII	(one measurement)	0.0198	0.0217 ± .0007
X		0.0173	
		0.0193	
	Average	0.0183	0.0183 ± .0007
XI		0.0604	
		0.0595	
	Average	0.0600	0.0596 ± .0017

Good agreement between the test region values and those found in the full lattice of the same composition is evident, even for assemblies with small test regions such as Assemblies II and VII. It appears, then, that δ_{28} can validly be measured in the center of the assemblies considered, with little or no correction necessary.

The variation of δ_{28} across the two regions was investigated in two of the assemblies. In Assembly III (Fig. 13.3), the characteristics of the regions were not greatly different, and a gradual increase in δ_{28} with radius is evident. The regions of Assembly IX (Fig. 13.4) differ considerably in fuel rod size. A marked discontinuity is obvious between the two regions.

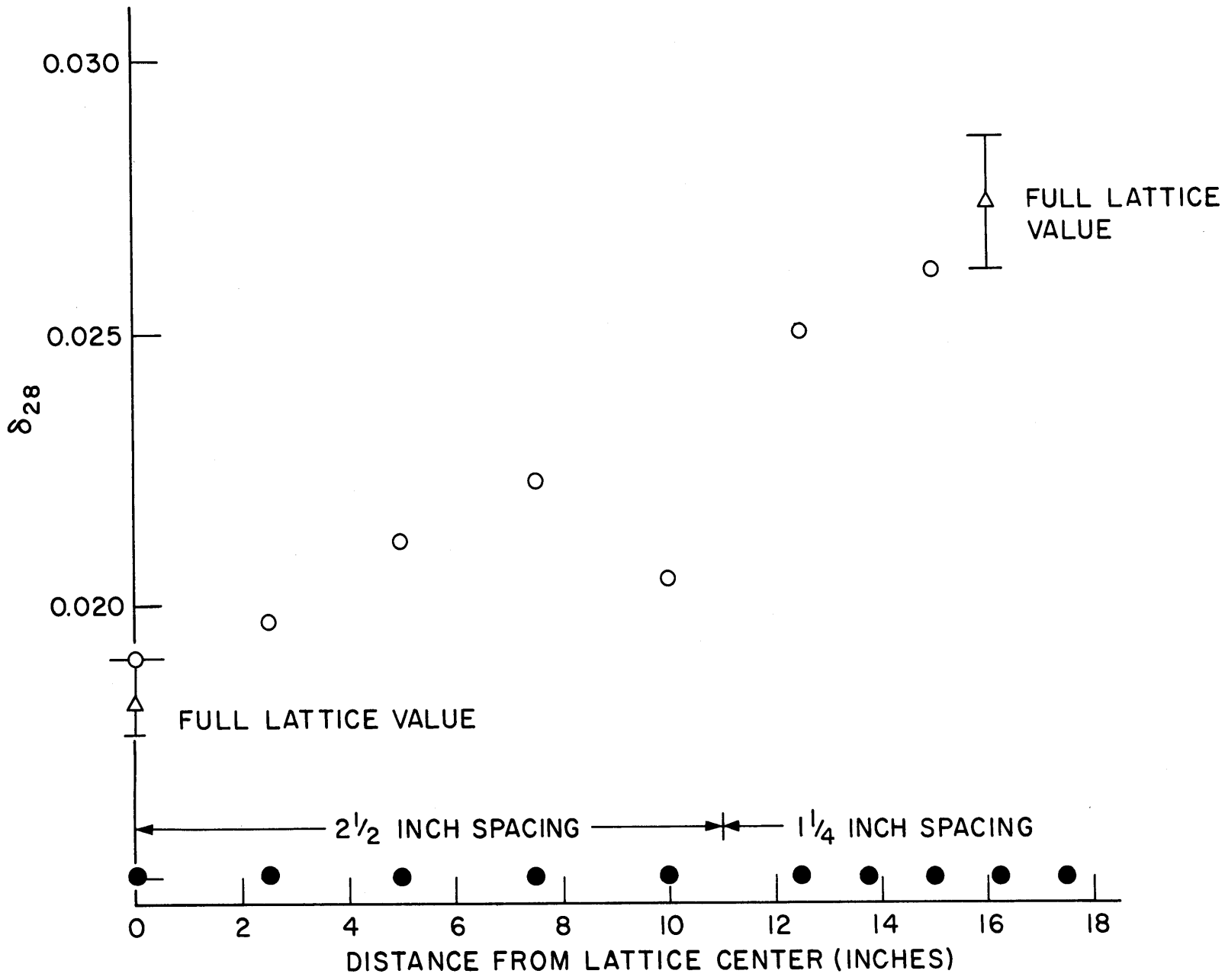

FIG. 13.3 δ_{28} IN ASSEMBLY III 1.027% ENRICHED 1/4 INCH DIAMETER

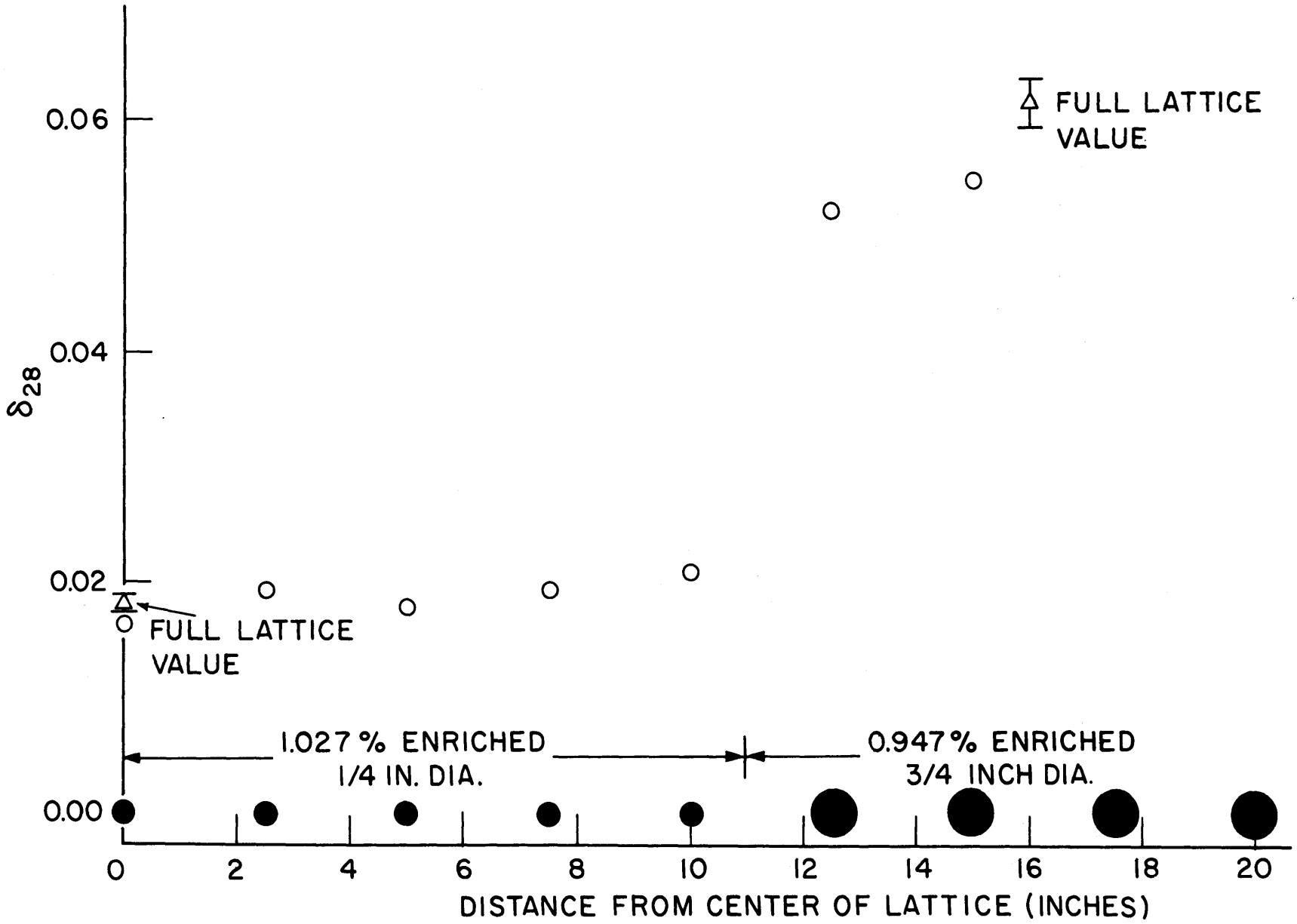

FIG. 13.4 δ_{28} IN ASSEMBLY IX 2 1/2 INCH SPACING

3. R_{28} MEASUREMENTS

The ratio, R_{28}, of total U^{238} activation to the epicadmium U^{238} activation, was measured in most of the assemblies with standard techniques developed previously by the Lattice Project. Each value shown in Table 13.3 is the average of two independent measurements in the center of the assembly; the standard deviation for each data set is also shown.

Table 13.3
R_{28} Measurements

Assembly	R_{28} in Center Fuel Position	Full Lattice Value
I	3.40 ± .04	5.40 ± .03
III	5.48 ± .06	5.40 ± .03
IV	2.28 ± .04	2.18 ± .01
V	4.07 ± .06	5.27 ± .10
VI	5.21 ± .08	5.27 ± .10
VII	3.08 ± .13	3.10 ± .02
VIII	3.43 ± .17	3.10 ± .02
IX	5.03 ± .10	5.40 ± .03
X	3.40 ± .07	5.40 ± .03

It is evident, and not surprising, that the size of the test region, given in Table 13.1, has a marked influence on the degree of agreement of the test region value with that of the full lattice.

4. PRESENT WORK

Correction factors to be applied to microscopic measurements made in the test region are being calculated, and work is continuing on methods of obtaining the material buckling of the test regions from the experimental data.

14. SINGLE ROD STUDIES

E. E. Pilat

1. INTRODUCTION

The nuclear parameters of a reactor lattice may be determined by critical experiments on that lattice, by theoretical calculations in which only cross sections are used as input, or by methods which combine theory and experiment. Of those methods which combine theory and experiment, the Single Element Method, abbreviated SEM, will be shown to have great usefulness. This method was introduced into reactor theory by Horning (1), Feinberg (2), and Galanin (3). Their developments of the method were restricted to the use of the age theory kernel and were mainly theoretical. Although the possibility of obtaining meaningful data from experiments on single fuel elements was pointed out, it was never seriously investigated in their work. The method used here combines experiments on the smallest meaningful unit of fuel – a single fuel element – with a theory which relates the behavior of a lattice of such elements to the experimentally determined behavior of the single element. This particular division of the problem into theory and experiment is useful for at least three reasons.

First, several parameters which characterize a reactor lattice – the thermal utilization and resonance escape probability, for example – often depend strongly and in a complicated manner on the properties of individual fuel elements, but only depend weakly or in a simple manner on interactions between the fuel elements. In the Single Element Method, the largest contribution to these parameters is determined by measurements on a single fuel element, and only a relatively small correction to account for the presence of the rest of the fuel elements need be estimated theoretically. Second, the determination of lattice parameters in this way represents a desirable saving of time, money, effort, and material over their determination in critical or exponential experiments. Third, it will be shown that the method provides an

excellent way of correlating the results of experimental measurements, since it shows what pertinent variables must be used to express the quantity of interest in a linear or nearly linear fashion.

The object of this investigation has been to develop workable Single Element Methods, to demonstrate their usefulness by applying them to lattices whose properties are already known from experiment, and to indicate how these methods may be applied to determine the parameters of new lattices. The achievement of these objectives will be demonstrated in the following sections.

The results shown here were obtained chiefly by applying the method to lattices of cylindrical, slightly enriched uranium, metal rods in heavy water. These lattices have been studied extensively in the large exponential facility at the M.I.T. Reactor, so that reliable, experimentally measured values of the various parameters defined below are available for comparison. To illustrate the generality of the method, a few applications will be made to lattices having different moderators or different fuel elements.

The parameters which will be studied are the thermal utilization, f:

$$f \equiv \frac{\text{subcadmium capture in fuel}}{\text{subcadmium capture in fuel and moderator}} ;$$

the ratio ρ_{28}, related to the cadmium ratio of U^{238}:

$$\rho_{28} \equiv \frac{\text{epicadmium capture in } U^{238}}{\text{subcadmium capture in } U^{238}} ;$$

the ratio C^*, related to the initial conversion ratio:

$$C^* \equiv \frac{\text{capture in } U^{238}}{\text{fission in } U^{235}} ;$$

the ratio δ_{25}, related to the epicadmium fission fraction:

$$\delta_{25} \equiv \frac{\text{epicadmium fission in } U^{235}}{\text{subcadmium fission in } U^{235}} ;$$

and the ratio δ_{28}, related to the fast fission factor:

$$\delta_{28} \equiv \frac{\text{fission in } U^{238}}{\text{fission in } U^{235}} .$$

2. THEORETICAL METHODS

In the Single Element Method, the reaction rate at any point in a unit cell is calculated as the sum of the reaction rates of neutrons originating at each separate fuel element of the system. To compute the neutron balance in this way, a tool is needed – the kernel $K(r, E)$ that gives the flux or reaction rate as a function of distance from the single fuel element in which the neutrons originate. The total flux or reaction rate at any point in a lattice of such fuel elements is then calculated by summing the values of the kernels appropriate to each of the fuel elements in the system, weighted with the relative source strength S of each element:

$$R(\vec{r}) = \sum_i K(|\vec{r} - \vec{r}_i|, E)\, S(\vec{r}_i)$$

$$= K(r, E)\, S(o) + K(|\vec{r} - \vec{r}_i|, E)\, S(\vec{r}_1) + K(|\vec{r} - \vec{r}_2|, E)\, S(\vec{r}_2) + \ldots \tag{14.1}$$

A remarkable property of this method, and the reason why it is especially useful, is that when the lattice is uniformly spaced and when the kernel $K(r)$ is a monotonically decreasing function of r, a detailed knowledge of the kernel is frequently unnecessary. It is found by Poisson summation (4) that in many cases of practical interest those neutrons that originate "far enough" away from a particular unit cell result in a net flux or reaction rate which is essentially constant across the cell. The profile of the total flux or reaction rate across the cell is then the sum of this constant "background" arising from distant neutron sources, plus one or more terms which vary rapidly in space and which represent the contribution of neutrons originating from the fuel element in the unit cell where the reaction rate is to be evaluated, and from fuel elements in nearby unit cells. The number of terms which must be summed explicitly equals the number of unit cells, surrounding and including the one of interest, in each of which the magnitude of the kernel $K(r)$ undergoes a large fractional change. Two special cases of this result are particularly simple and important.

In the first special case, there are no unit cells within which the kernel experiences a large change in magnitude; thus the total reaction

rate, R(r), as a function of position in the unit cell of interest is effectively constant. It may be shown (5) by Poisson summation (4) that in this case:

$$R(r) = \frac{PF}{V_c}, \tag{14.2}$$

where V_c is the volume of a unit cell, P is the nonleakage probability from fission to the energy at which R is calculated, and F is the integral of K(r) over all space. Equation 14.2 is a good representation of the slowing-down density in the epithermal energy region of many thermal reactors. The slowing-down density from the region of epithermal to that of thermal energies, for example, has often been assumed spatially constant.

The second special case is that in which the kernel's magnitude changes significantly only within the unit cell immediately surrounding the fuel element which provides the neutron source for the kernel. When this is so, Poisson summation may be applied to all the terms beyond the first one in Eq. 14.1, with the result (6):

$$R(r) = K(r) + \frac{F_1 P}{V_c}, \tag{14.3}$$

where F_1 is the integral of K over all space outside the unit cell at the origin. Equation 14.3 represents a separation of the total reaction rate into what are sometimes called "single rod" and "lattice" components. Its usefulness will appear when the fast effect is studied.

3. APPLICATIONS IN THE THERMAL REGION

The thermal utilization of an infinite, uniform lattice has been expressed (7) in terms of a parameter Γ, pertaining to an individual fuel element. A related, though not identical parameter was first introduced by Galanin (3). The parameter used here is the ratio of a flux to a current. The flux is that subcadmium flux which would exist at the center of the fuel element if all fast neutron sources in the system remained unchanged but if, in the calculation of the subcadmium neutron transport, all fuel elements were replaced by moderator. The

neutron current used is the net current of subcadmium neutrons into a unit length of the fuel element; this is, of course, equal to the net number of subcadmium neutrons absorbed by the fuel element. The advantage of defining Γ in terms of this effective subcadmium flux, first suggested by Klahr (8), is that diffusion theory is adequate to calculate the effective flux accurately because its definition removes all the strong absorption from the system. This simplifies the relation between the ratio Γ and the thermal utilization f to (7):

$$\frac{1}{f} = 1 + V_c \Sigma_{am} \Gamma , \qquad (14.4)$$

where Σ_{am} is the macroscopic absorption cross section of the moderator.

Values of Γ were deduced from subcadmium flux traverses around a single fuel rod immersed in heavy water. For this purpose, the net subcadmium current into the element and the effective subcadmium flux were obtained separately, but from the same flux traverse. Values of the net thermal neutron current were deduced by using the observed values of the subcadmium activities of gold foils around the fuel element in a least-squares fit to the neutron conservation equation in the diffusion approximation (9). Values of the effective thermal flux which would exist at the center of the fuel element, if its thermal properties were replaced by those of the moderator, were obtained by extrapolating the values of the subcadmium activities back to the center of the fuel element. This was done in such a way as to avoid the thermal flux dip near the element, thus effectively replacing the thermal neutron properties of the element by those of the moderator (10). Values of the macroscopic absorption cross section of the moderator were obtained from THERMØS (11). The resulting values of the thermal utilization are shown in Table 14.1, where they are compared with values obtained directly from THERMØS. It is evident that the agreement between the values of the thermal utilization obtained by the two methods is relatively good.

When values of the thermal utilization are obtained from the Single Element Method as expressed in Eq. 14.4, the only cross section required is that of the moderator. This is advantageous because moderator cross sections are usually much less hardened than fuel cross sections, so the values of the moderator cross section may be calculated more easily.

Table 14.1

Values of the Thermal Utilization for Lattices of Slightly Enriched Uranium Rods in Heavy Water

Concentration of U-235 in Rod Wt. %	Rod Diameter (Inches)	Lattice Spacing (Inches)	Value of the Thermal Utilization†		Percentage Difference	
			From Eq. 4.17*	From THERMØS	In f	In (1-f)
1.14	0.25	1.25	0.9935	0.9927	0.08	11
		1.75	0.9866	0.9852	0.14	9
		2.50	0.9701	0.9673	0.29	9
1.03	0.25	1.25	0.9939	0.9923	0.16	21
		1.75	0.9873	0.9844	0.29	19
		2.50	0.9735	0.9678	0.59	18
0.947	0.75	2.50	0.9935	0.9947	0.13	23
		3.50	0.9861	0.9884	0.23	20
		5.00	0.9708	0.9748	0.41	16
0.711	1.00	4.50	0.9910	0.9911	0.01	1
		5.00	0.9887	0.9890	0.03	3
		5.75	0.9848	0.9847	0.01	1

*Obtained from Eq. 14.4.

†Including the cladding with the fuel.

4. THE RESONANCE REGION

The value of the slowing-down density q(r) in a unit cell of a large uniform system may be calculated by the Single Element Method. When this is related to the flux by the assumption that:

$$\phi(r) = \frac{q(r)}{\xi \Sigma_s E} , \tag{14.5}$$

expressions for the ratios ρ_{28}, δ_{25}, and C^* in this lattice may be derived.

It has been shown experimentally (Fig. 14.1) that the kernel to be used in the SEM expression for q(r) may be approximately represented by the age theory kernel over much of its range. The data between 5 and 20 cm yields an effective age to resonance capture of 67 ± 3 cm^2. The D_2O moderated lattices investigated here are spaced such that the age theory kernel, when used with this value of the age, does not experience a large change within any unit cell. Thus the slowing-down density and, from Eq. 14.5, the flux in the resonance region are well represented by Eq. 14.2; they are constant within any one unit cell and are inversely proportional to the volume of a unit cell. From this representation of the flux, the following expressions have been derived for ρ_{28}, C^* and δ_{25} (12):

$$\rho_{28} = \frac{\eta\epsilon \frac{N_{28} V_F}{\xi \Sigma_s V_c} \{0.5\, \sigma_o p P_{1/v} + P_{Res} ERI^{28}\}}{\left(\frac{\Sigma_a^{28}}{\Sigma_a^{28} + \Sigma_a^{25}} \right)_{sc}} , \tag{14.6}$$

$$\delta_{25} = \frac{\eta\epsilon \frac{N_{25} V_F}{\xi \Sigma_s V_c} \{P_{25} p ERI^{25}\}}{\left(\frac{\Sigma_f^{25}}{\Sigma_a^{25} + \Sigma_a^{28}} \right)_{sc}} , \tag{14.7}$$

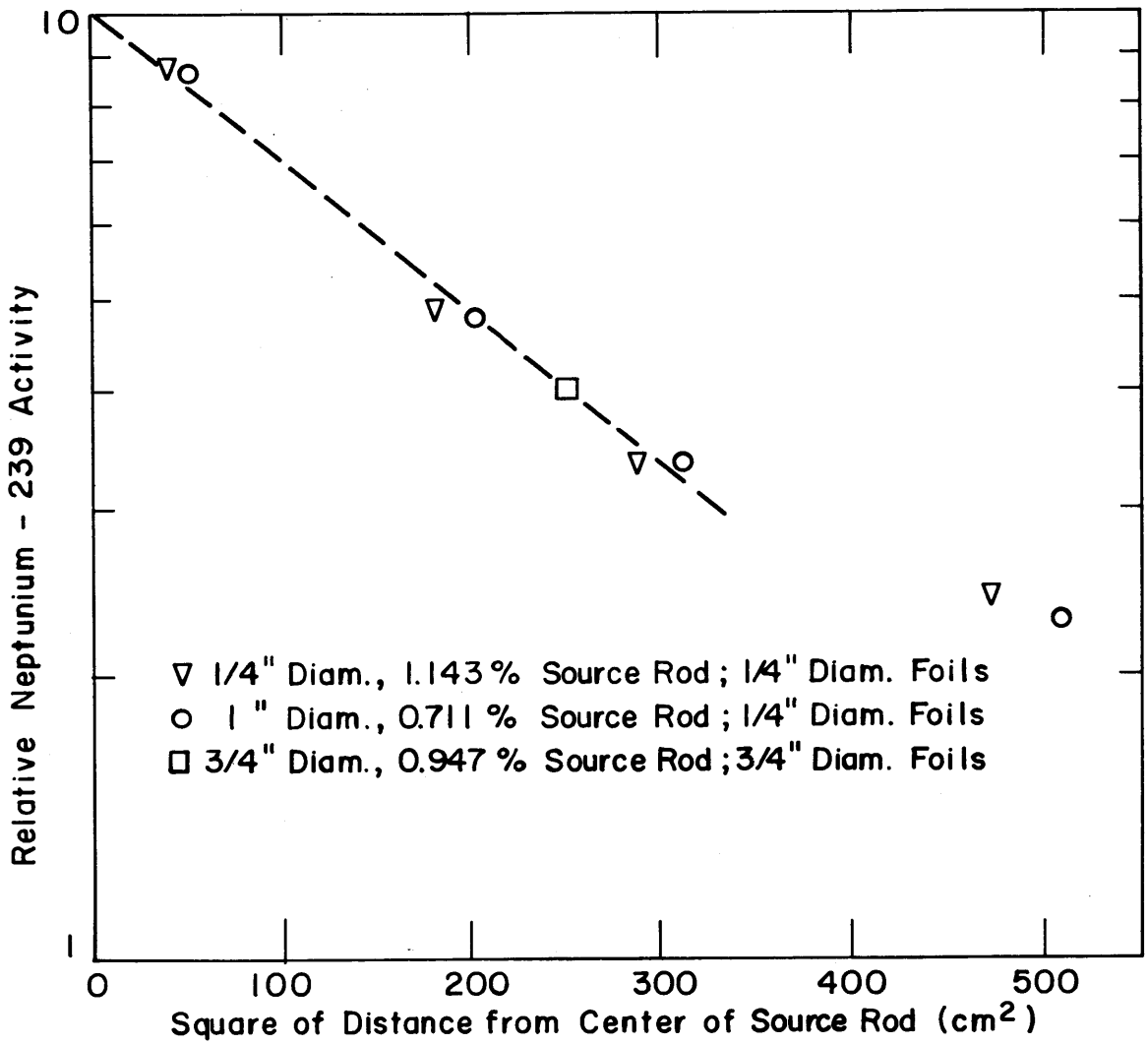

FIG. 14.1 RELATIVE NEPTUNIUM - 239 ACTIVITY IN DEPLETED URANIUM FOILS OF VARIOUS SIZES IN HEAVY WATER

$$C^* = \frac{\left(\frac{\Sigma_a^{28}}{\Sigma_a^{28} + \Sigma_a^{25}}\right)_{sc} + \frac{\eta\epsilon V_F}{\xi\Sigma_s V_c}\left[0.5\,\sigma_o p P_{1/v} + P_{Res} ERI^{28}\right]}{\left(\frac{\Sigma_f^{25}}{\Sigma_a^{28} + \Sigma_a^{25}}\right)_{sc}(1+\delta_{25})} . \tag{14.8}$$

In these equations:

η is the thermal regeneration factor;

ϵ is the fast fission factor;

p is the resonance escape probability;

P_x is the nonleakage probability from fission to the average energy at which capture in reaction x occurs;

N_{25} and N_{28} are the number densities of U^{235} and U^{238} in the fuel rods;

$(\ )_{sc}$ indicates a ratio of cross sections averaged over the sub-cadmium energy spectrum in the fuel rod;

Σ_a = macroscopic absorption cross section;

Σ_f = macroscopic fission cross section;

σ_o is the microscopic 2200 m/sec capture cross section of U^{238};

$\xi\Sigma_s$ is the slowing-down power of the unit cell medium;

ERI^{28} is the resonance integral for resonance capture in U^{238};

ERI^{25} is the resonance integral for epicadmium fission in U^{235}.

Equations 14.6 through 14.8 show that ρ_{28}, C^*, and δ_{25} are approximately inversely proportional to $1/V_c$, with constants of proportionality that vary only slightly as the lattice spacing (i.e., unit cell size) changes. This linear dependence on $1/V_c$ is shown for a typical set of lattices in Fig. 14.2. The solid curve was calculated from Eq. 14.8 using the nuclear constants from Table 14.2.

A comparison of values of ρ_{28} and C^* obtained by various methods is given in Table 14.3.

Equation 14.7 was used to calculate values of the fission resonance integral of U^{235} from the values of δ_{25} measured in lattices at M.I.T. These values are shown in Table 14.4; they are in approximate agreement

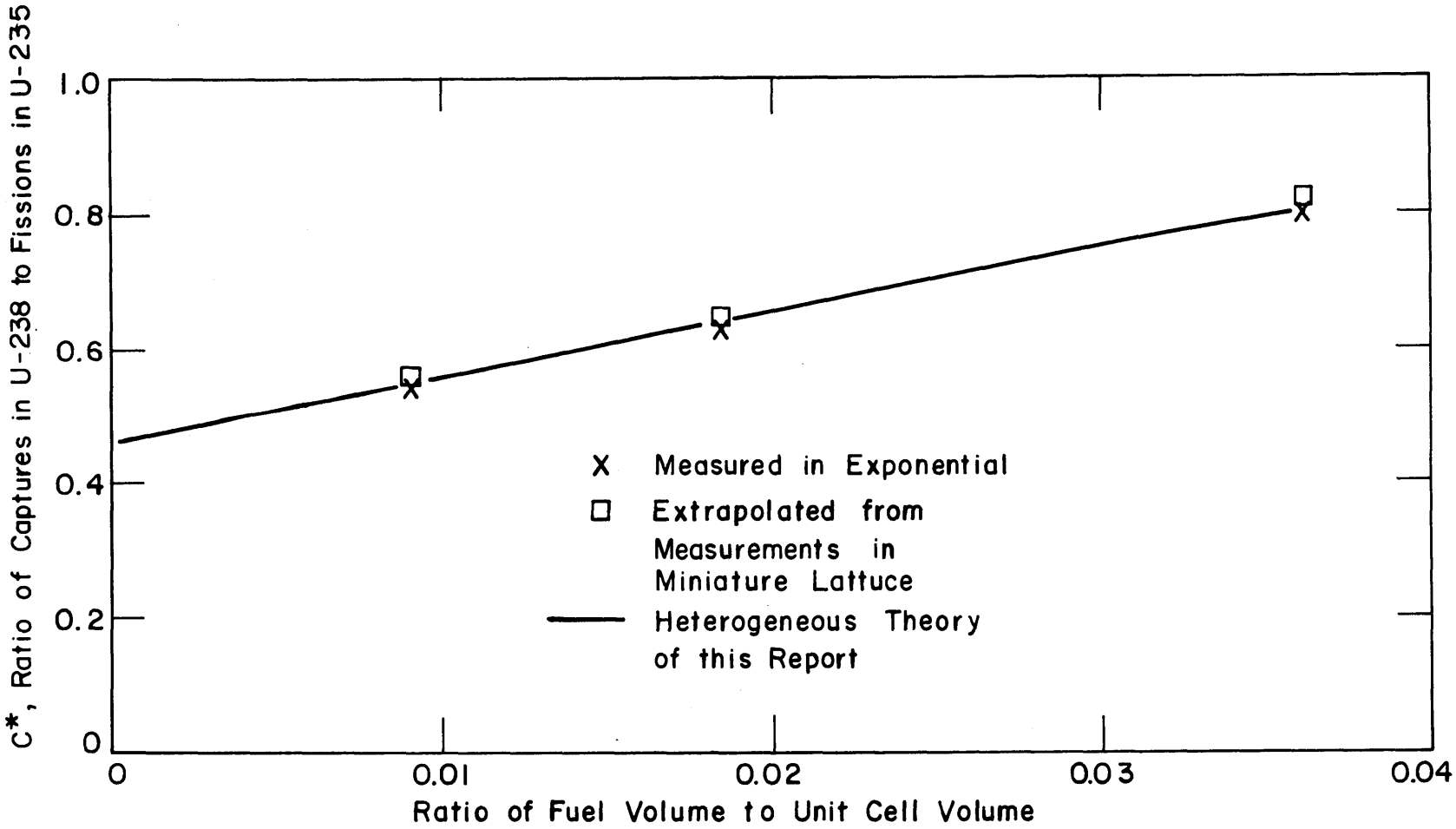

FIG. 14.2 THE RATIO, C* , OF CAPTURES IN U-238 TO FISSIONS IN U-235 VS. VOLUME FRACTION OF FUEL IN UNIT CELL FOR 1/4" DIAMETER, 1.027% ENRICHED URANIUM METAL RODS IN D_2O

Table 14.2

Geometric and Nuclear Constants

Concentration of U-235 in Rod (Wt. %)	Lattice Spacing (Inches)	Volume Ratio V_F/V_c	Slowing-Down Power of Cell, $\xi\Sigma_s$ (cm^{-1})	$\left(\frac{\Sigma_a^{28}}{\Sigma_a^{25}+\Sigma_a^{28}}\right)_{sc}$ †	$\left(\frac{\Sigma_f^{25}}{\Sigma_a^{25}+\Sigma_a^{28}}\right)_{sc}$ †	$\eta\epsilon$ †
1.027	1.25	0.03628	0.179	0.2873	0.6101	1.5192*
	1.75	0.01851	0.182	0.2852	0.6115	1.5164
	2.50	0.009069	0.184	0.2832	0.6122	1.5147
1.143	1.25	0.03628	0.179	0.2619	0.6282	1.5707*
	1.75	0.01851	0.182	0.2610	0.6296	1.5643
	2.50	0.009069	0.184	0.2606	0.6304	1.5607
0.711	4.50	0.0448	0.180	0.3646	0.5413	1.3663**
	5.00	0.0363	0.180	0.3649	0.5408	1.3661
	5.75	0.0274	0.180	0.3651	0.5404	1.3401

* Values of ϵ from reference 13.

** Values of ϵ from reference 14.

† Values of η and cross section ratios from THERMØS.

Table 14.3

Values of ρ_{28}, the Ratio of Epicadmium to Subcadmium Capture in U^{238}, and of C^*, the Ratio of Capture in U^{238} to Fission in U^{235}, for 1/4-Inch-Diameter, Uranium Metal Rods in D_2O

Concentration of U-235 in Fuel Rod (Wt. %)	Lattice Spacing (Inches)	Volume Ratio V_F/V_c	ρ_{28}			C^*		
			Direct Experiment (Exponential)	Extrapolation (Miniature Lattice)	Single Element Method	Direct Experiment (Exponential)	Extrapolation (Miniature Lattice)	Single Element Method
1.027	1.25	0.03628	0.8453(1)	0.856	0.7853	0.8028(1)	0.820	0.7991
	1.75	0.01851	0.4373	0.425	0.4207	0.6345	0.646	0.6433
	2.50	0.00907	0.2272	0.242	0.2170	0.5506	0.568	0.5527
1.143	1.25	0.03628	0.8130(2)	0.861	0.8750	0.773(2)	0.733	0.7391
	1.75	0.01851	0.471	0.476	0.4678	0.617	0.594	0.5888
	2.50	0.00907	0.222	0.251	0.2412	0.490	0.506	0.5049

(1) "Direct Experiment" values from reference 15.

(2) "Direct Experiment" values from reference 16.

Table 14.4

Values of Resonance Integrals for Fission in U^{235}, as Determined from Measurements of δ_{25}

Concentration of U-235 in Fuel Rod (Wt. %)	Lattice Spacing (Inches)	Volume Ratio V_F/V_c	ERI^{25}_{fiss} (Barns)
1.027(1)	1.25	0.03628	278 ± 50
	1.75	0.01851	300 ± 12
	2.50	0.009069	344 ± 41
1.143(2)	1.25	0.03628	286 ± 52
	1.75	0.01851	300 ± 14
	2.50	0.009069	275 ± 120
0.711(3)	4.50	0.0448	262 ± 10
	5.00	0.0363	256 ± 22
	5.75	0.0274	231 ± 19
Average (with observed standard deviation of the mean)			281 ± 11

(1) Values of δ_{25} from reference 15.
(2) Values of δ_{25} from reference 16.
(3) Values of δ_{25} from reference 14.

with the value of 274 ± 10 barns given for the infinite dilution resonance integral in the Second Supplement to the Second Edition of BNL-325.

The results of the SEM analysis in the resonance region are:

1) values of ρ_{28} can be calculated to about 8% accuracy and values of C^* to about 4% accuracy for uranium metal rods by means of the SEM;

2) the approximate linear dependence of ρ_{28}, δ_{25}, and C^* on $1/V_c$ is found both experimentally and theoretically; this linear dependence is of aid in extrapolating and interpolating values of these ratios to other lattice spacings;

3) the value of the fission resonance integral of U^{235} for rods of slightly enriched uranium is approximately the same as the infinite dilution value of this resonance integral.

5. THE FAST REGION

Semi-analytic expressions have been developed (17) for the first flight kernel for infinitely long, uniform neutron sources having the shape of a line, an annulus, or a solid rod. The structure of these expressions may be seen from an examination of the kernels for line and annular sources:

$$K_{line}(r) = \frac{C_2(\Sigma_R r)}{2\pi r}, \tag{14.9}$$

$$K_{annulus}(R, r) = \frac{1}{2\pi r}\left\{ I_o(\Sigma_R R)\, C_2(\Sigma_R r) + \left(\frac{R}{r}\right) I_o'(\Sigma_R R)\, C_3(\Sigma_R r) + \left(\frac{R}{r}\right)^2 I_o''(\Sigma_R R)\, C_4(\Sigma_R r) + \ldots \right\}, \quad r \geq R_o \tag{14.10}$$

where:

Σ_R is the macroscopic removal cross section of the medium;

R is the radius of the annular source;

r is the radius at which the flux is observed;

I_o is the modified Bessel function of the first kind.

Derivatives of the Bessel functions are to be taken with respect to their arguments.

$C_n(z) \equiv \int_1^\infty \frac{e^{-zt}\,dt}{t^{n-1}\sqrt{t^2-1}}$; these have been evaluated numerically and are shown in Fig. 14.3.

It is evident from Eq. 14.10 that the expansion converges very quickly except for $R = r$. The semi-analytic forms of the kernels also show clearly how the shape of the kernel for an annular source approaches that for a line source at large distances from the sources, when only the first term in Eq. 14.10 is important. This fact is not obvious from the integral expressions for the kernels given in Weinberg and Wigner (18).

The kernel for a solid rod has been developed by integrating the annular kernel over the fission source distribution within the rod. A typical single rod kernel so obtained is shown in Fig. 14.4. The magnitude of this kernel changes considerably within the unit cell surrounding the rod of interest, but it is slowly varying elsewhere. The total uncollided flux in a unit cell in a large lattice may therefore be approximated by Eq. 14.3. Values of the uncollided flux calculated in this way are shown in Fig. 14.5 for a typical lattice. The comparison with the experimentally measured values of Woodruff (19) shows good agreement.

A formula for the value of the fast fission ratio has been developed using the SEM approximation to the uncollided flux in the lattice. It has been assumed that only the uncollided flux contributes to fast fission and that later generations of fast fission have the same spatial shape as the first. The resulting expression for δ_{28} is (20):

$$\delta_{28} = \frac{\nu_{25}\mathrm{H}}{1 - \nu_{28}\mathrm{H}}\,, \tag{14.11}$$

where:

ν_{25} is the average number of fast neutrons produced per fission in U^{235};

ν_{28} is the average number of fast neutrons produced per fast fission in U^{238};

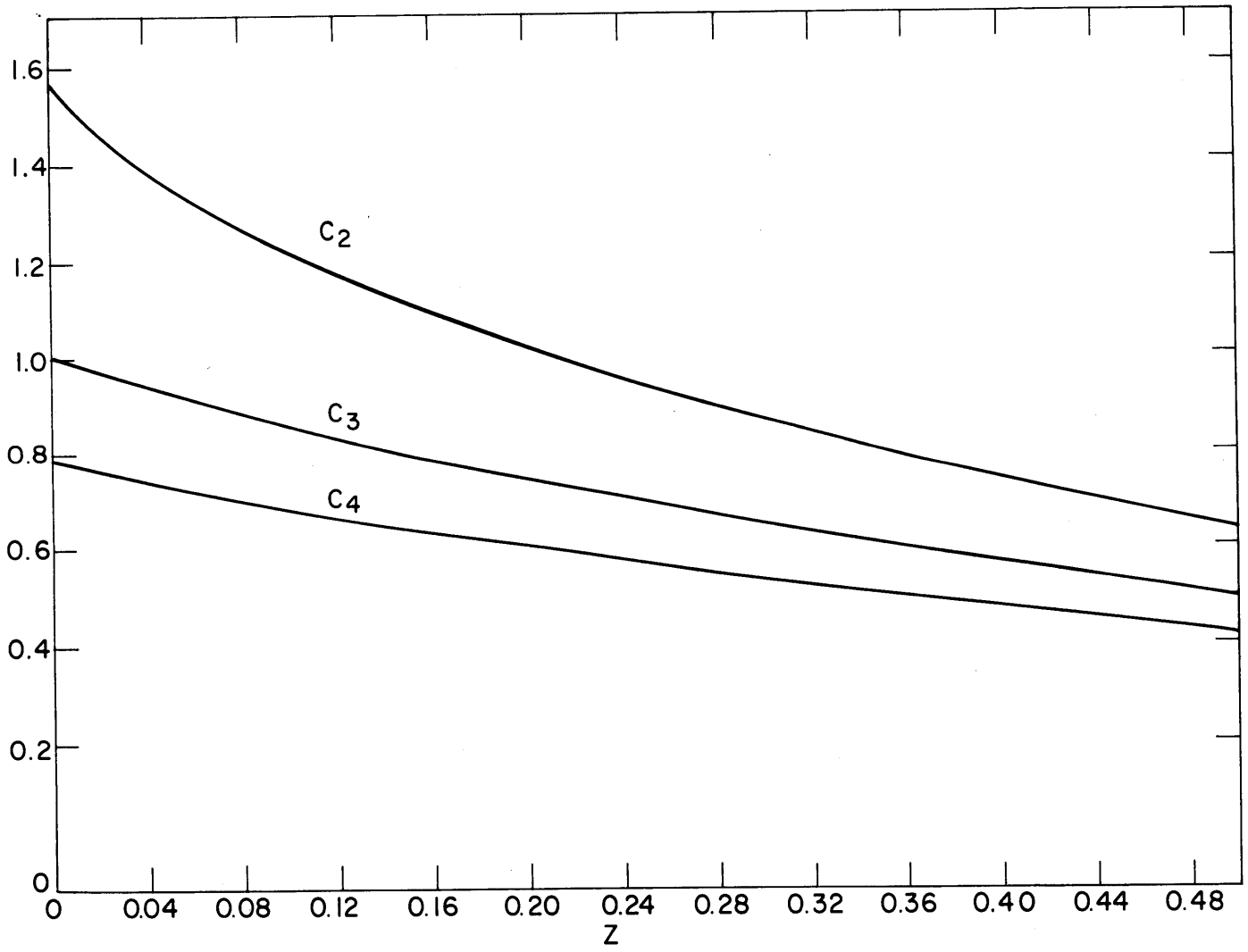

FIG. 14.3 FUNCTIONS $c_n(z)$ APPEARING IN INTEGRATED FORM OF LINE, ANNULAR, AND ROD FIRST FLIGHT KERNELS

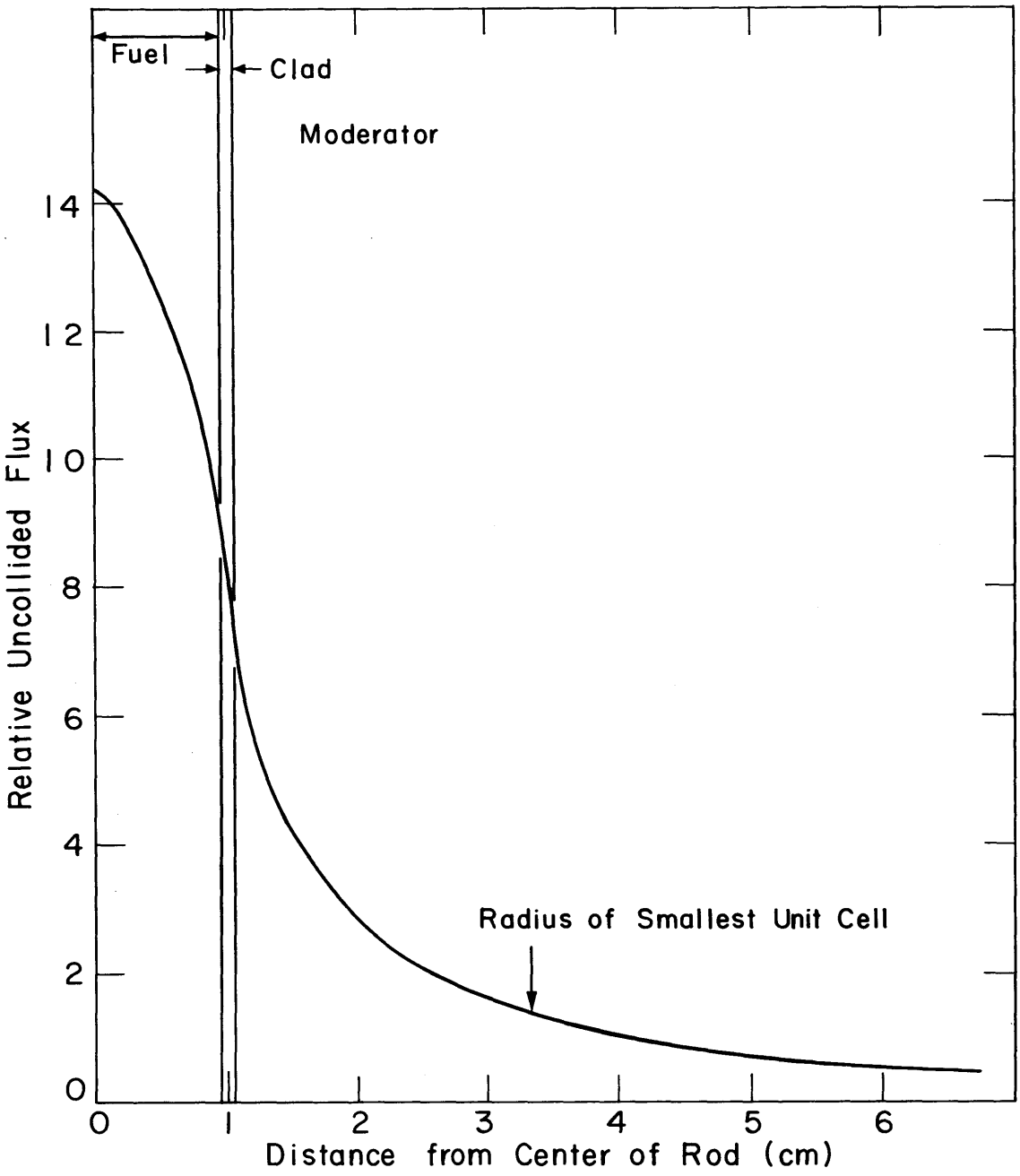

FIG. 14.4 THE SINGLE ROD KERNEL GIVING THE UNCOLLIDED FLUX AROUND A SINGLE, 0.75 INCH DIAMETER, URANIUM ROD IN HEAVY WATER

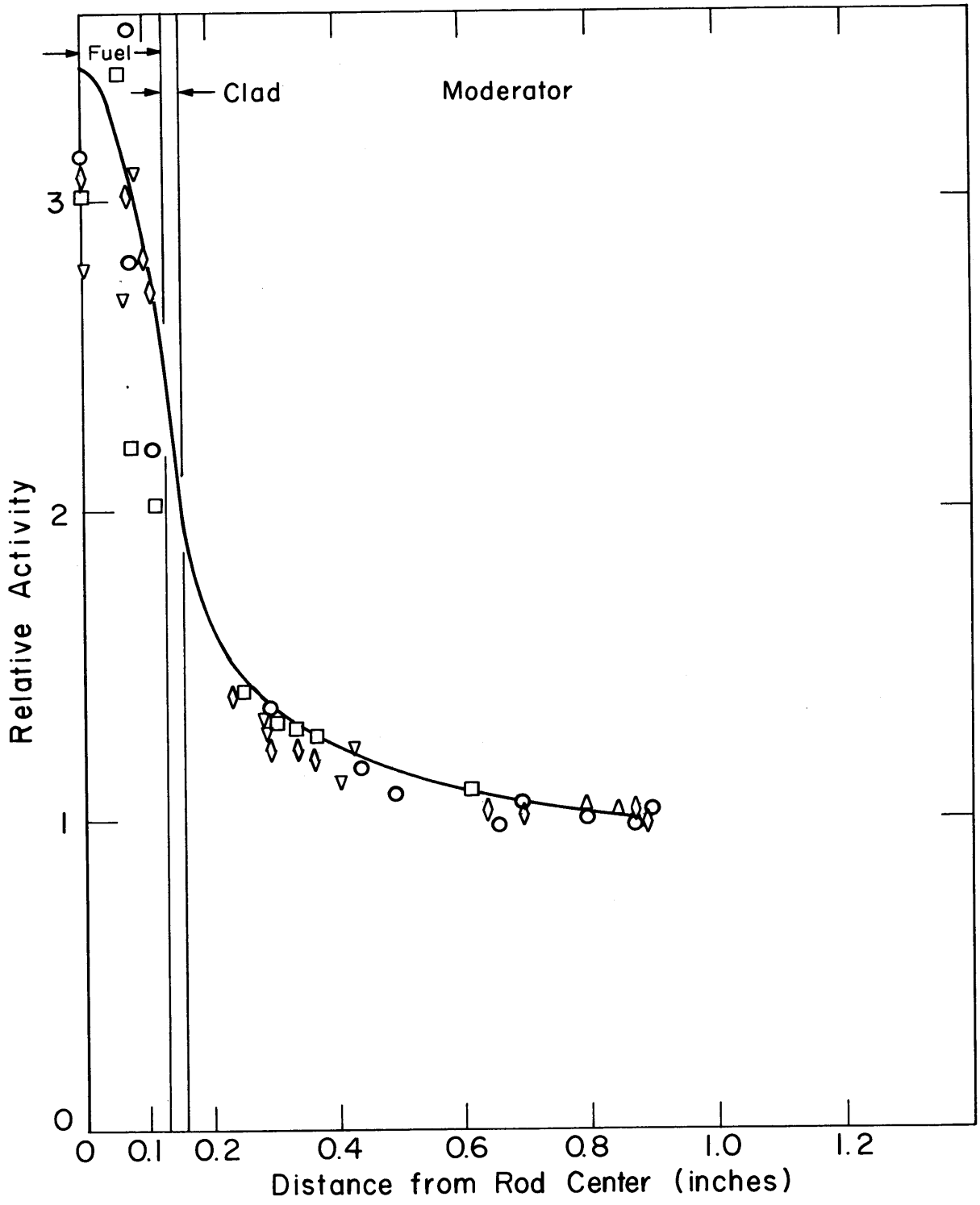

FIG. 14.5 RELATIVE ACTIVITY IN TRIANGULAR LATTICE OF 0.25 INCH DIAMETER, 1.027% ENRICHED URANIUM METAL FUEL RODS ON A 1.75 INCH SPACING IN D_2O

Σ_f is the macroscopic cross section of the fuel rod for fast fission;

H is Σ_f times the integral of the total uncollided flux over the fuel rod.

Equation 14.11 has been used with the nuclear constants of Table 14.5 to obtain values of δ_{28} in lattices of uranium metal rods in D_2O and H_2O. Calculated values for typical lattices are compared with measured values in Table 14.6 and are shown in Figs. 14.6 and 14.7. It is evident that good agreement has been obtained.

Table 14.5
Data Used in Calculations of δ_{28}

$(\Sigma_R)_{FUEL} = 0.100\ cm^{-1}$
$(\Sigma_R)_{D_2O} = 0.085\ cm^{-1}$
$(\Sigma_R)_{H_2O} = 0.105\ cm^{-1}$
$(\Sigma_R)_{CLAD} = 0.0$
$\nu_{25} = 2.45$
$\nu_{28} = 2.84$
$\Sigma_f = 0.0146\ cm^{-1}$

6. CONCLUSIONS

The Single Element Method has been used to develop formulas which relate the parameters of interest in reactor lattices to parameters obtainable in and near single fuel elements. The method shows how values of ρ_{28}, δ_{25}, or C^* in lattices of different spacings are related to each other and to the value of the ratio in a single, isolated fuel element. The correlations predicted for these ratios by the Single Element Method were checked by comparison with values measured in large lattices in the exponential assembly at the M.I.T. Reactor. The results showed that the correlations are accurate to within several

Table 14.6

Values of δ_{28} for Slightly Enriched Uranium Rods in Heavy Water

Fuel Rod Diameter (Inches)	Fuel Rod Enrichment (%)	Fuel Rod Spacing (Inches)	(V_F/V_c)	δ_{28} (Expt.) (a)	δ_{28} (Calc.) (b)	δ_{28}^{∞} (Calc.) (c)
0.25	1.03	∞	0	0.0133 ±0.0004	0.0140	0.0140
	1.14			0.0151 ±0.0004		
	1.03	2.50	0.009069	0.0183 ±0.0007	0.0166	0.0167
	1.14			0.0164 ±0.0010		
	1.03	1.75	0.01851	0.0217 ±0.0007	0.0200	0.0203
	1.14			0.0204 ±0.0030		
	1.03	1.25	0.03628	0.0274 ±0.0012	0.0265	0.0270
	1.14			0.0265 ±0.0070		
0.75	0.947	∞	0	0.0409 ±0.0012	0.0383	0.0383
		5.0	0.0204	0.0489 ±0.0017	0.0425	0.0428
		3.5	0.0416	0.0516 ±0.0032	0.0490	0.0494
		2.5	0.0816	0.0615 ±0.0021	0.0631	0.0640

(a) From references 13, 14 and 16.

(b) From calculations made with the semi-analytic method. Leakage in lattices of finite spacing assumed the same as in critical system.

(c) From calculations made with the semi-analytic method with zero leakage.

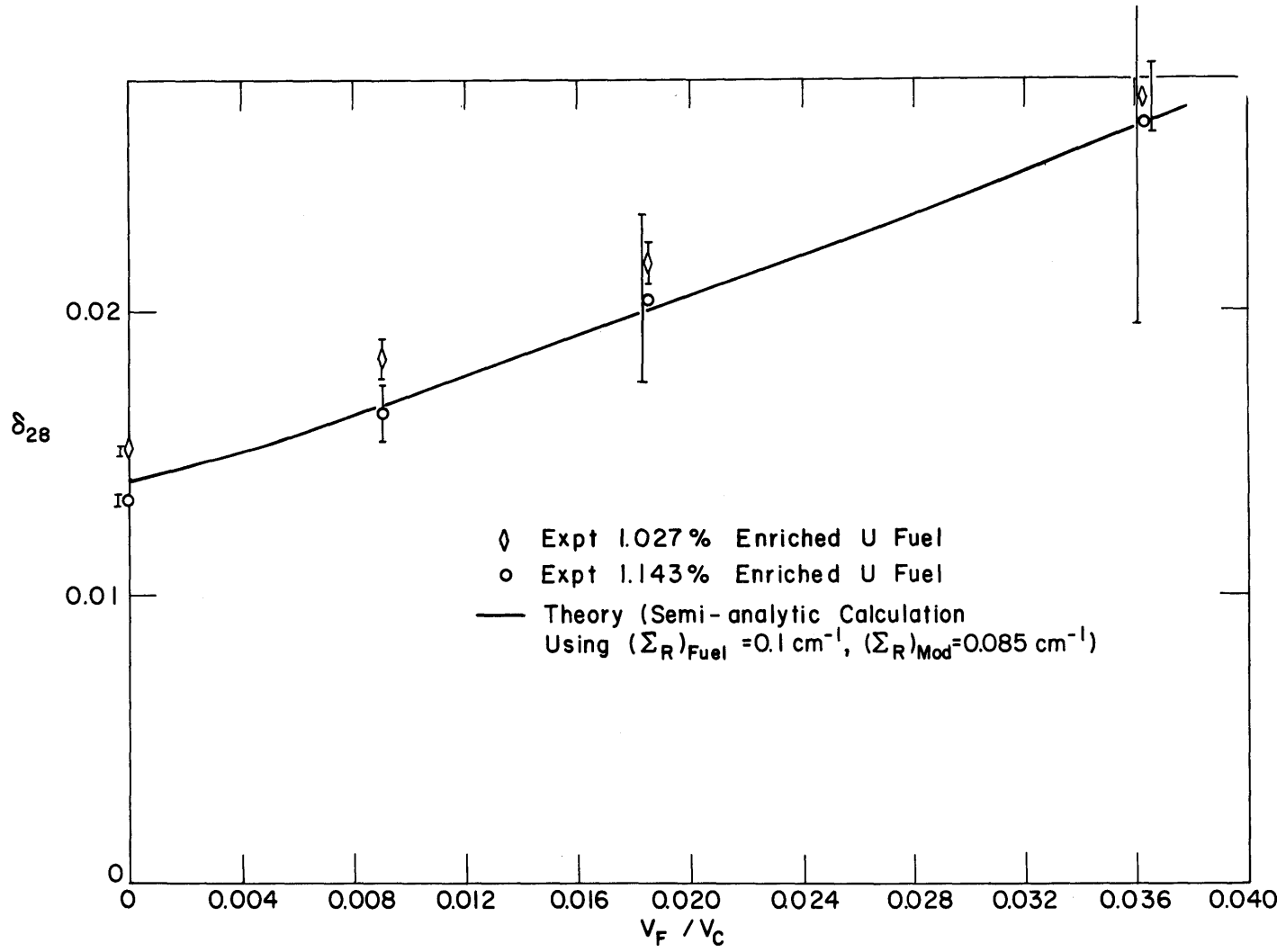

FIG. 14.6 FAST FISSION RATIO VS RATIO OF FUEL VOLUME TO UNIT CELL VOLUME FOR 1/4" DIAM FUEL RODS IN D_2O

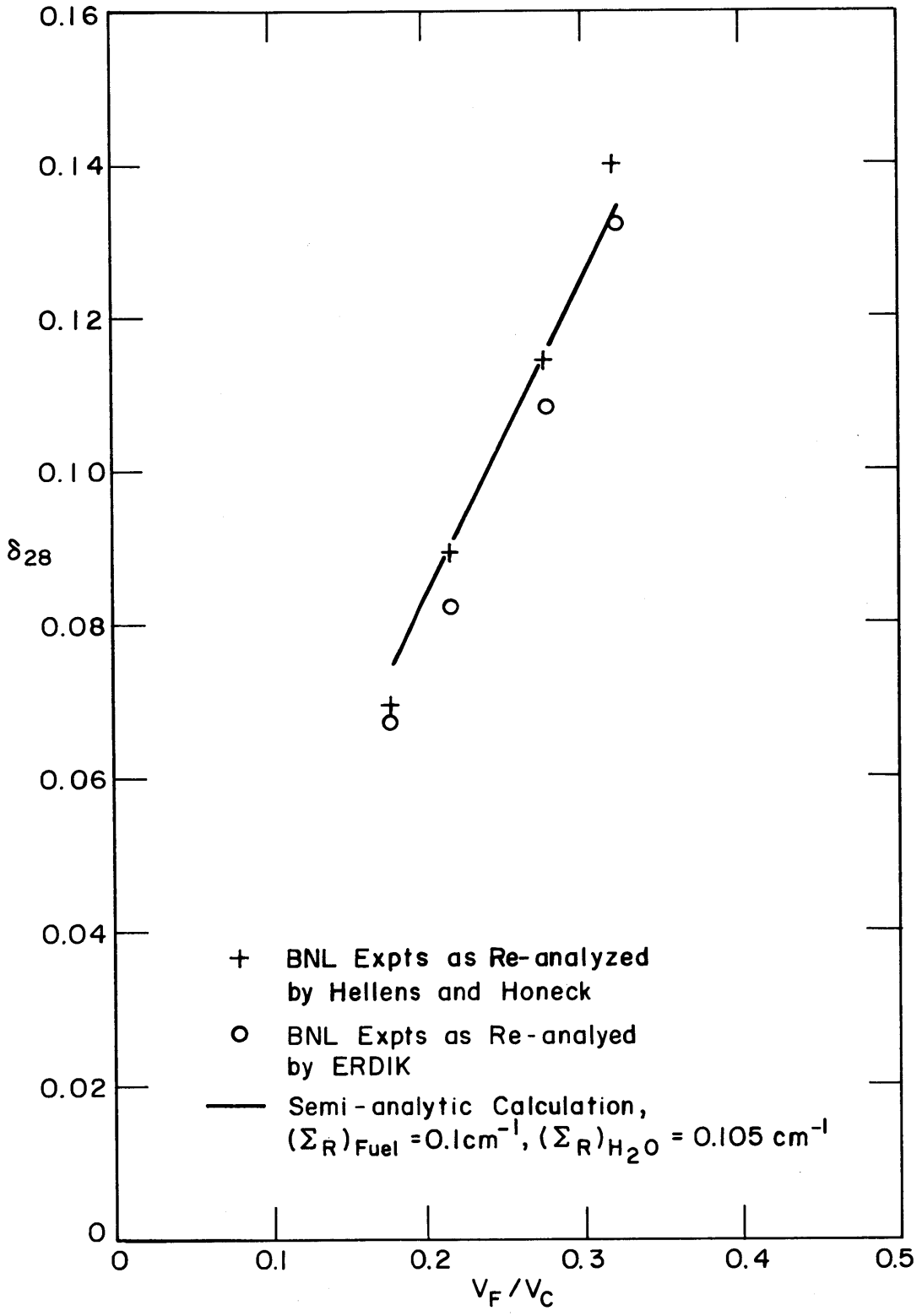

FIG. 14.7 FAST FISSION RATIO, δ_{28}, VS. VOLUME FRACTION OF FUEL IN CELL FOR SLIGHTLY ENRICHED URANIUM RODS, OF 1/4 INCH DIAMETER IN LIGHT WATER

percent and that they are useful in evaluating experimental data. It was also shown that values of these ratios and of the thermal utilization were indeed obtainable by experiments on single fuel elements.

It has thus been demonstrated that values of several important lattice parameters can be obtained by combining experiments on a single fuel element with a theory which accounts for the effect of the rest of the lattice. It is suggested that the method might be usefully applied in obtaining lattice parameters in this way and in correlating values of such parameters obtained from experiments in lattices. Further possible applications include the determination of the value of the thermal utilization in lattices composed of clusters of fuel rods and the determination of lattice parameters of partially burned-up fuel.

7. REFERENCES

(1) Horning, W. A., "A Summary of Small Source Theory Applied to Thermal Reactors," HW-34021 (1954).

(2) Feinberg, S. M., "Heterogeneous Methods for Calculating Reactors," PICG, P/669 (1956).

(3) Galanin, A. D., "Thermal Coefficient in a Heterogeneous Reactor," PICG, P/666 (1956).

(4) Morse, P. M., and H. Feshbach, "Methods of Theoretical Physics," pp. 453, 467, McGraw-Hill Book Co. (1953).

(5) Pilat, E. E., "The Use of Experiments on a Single Fuel Element to Determine Nuclear Parameters of Reactor Lattices," Sec. 2.2.3, Ph. D. Thesis, M. I. T. Nuc. Eng. Dept. (1967).

(6) Ibid., Sec. 2.2.5.

(7) Ibid., Sec. 4.2.2.

(8) Klahr, C. N., et al., "Heterogeneous Reactor Calculation Methods," NYO-2680 (1961).

(9) Ibid., Sec. 4.2.1.

(10) Ibid., Sec. 4.2.1.

(11) Honeck, H. C., "THERMØS, A Thermalization Transport Theory Code for Reactor Lattice Calculations," BNL-5826 (1961).

(12) Ibid., Sec. 5.2.2.

(13) Bliss, H. E., "Measurement of the Fast Fission Effect in Heavy Water, Partially Enriched Uranium Lattices," S.M. Thesis, M.I.T. Nuc. Eng. Dept. (1964).

(14) Weitzberg, A., I. Kaplan and T. J. Thompson, "Measurements of Neutron Capture in U-238 in Lattices of Uranium Rods in Heavy Water," NYO-9659, MITNE-11 (1962).

(15) D'Ardenne, W. H., T. J. Thompson, D. D. Lanning and I. Kaplan, "Studies of Epithermal Neutrons in Uranium Heavy Water Lattices," MIT-2344-2, MITNE-53 (1964).

(16) Thompson, T. J., I. Kaplan, F. M. Clikeman and M. J. Driscoll, "Heavy Water Lattice Project Annual Report," MIT-2344-4, MITNE-65 (1965).

(17) Pilat, E. E., loc. cit. ref. 5, Appendix B.

(18) Weinberg, A. M. and E. P. Wigner, "The Physical Theory of Neutron Chain Reactors," p. 217, University of Chicago Press (1958).

(19) Woodruff, G. W., et al., "A Study of the Spatial Distribution of Fast Neutrons in Lattices of Slightly Enriched Uranium Rods Moderated by Heavy Water," MIT-2344-5, MITNE-67 (1965).

(20) Pilat, E. E., loc. cit. ref. 5, sect. 6.2.3.

(21) Helmholtz, J., and W. Rothenstein, "Multigroup Calculations of the Fast Spectrum and Fast Fission Effect," Nuc. Sci. Eng., 24, 349 (1966).

Appendix A

BIBLIOGRAPHY OF HEAVY WATER LATTICE PROJECT PUBLICATIONS

In this appendix are tabulated all publications directly associated with work performed in the M.I.T. Heavy Water Lattice Project. Sc.D. theses are listed first, followed by M.S. theses, and then by other publications. For convenience, publications since the last annual progress report, dated September 30, 1965, are listed separately.

1. DOCTORAL THESES ON MITR HEAVY WATER LATTICE PROJECT

Madell, John T.
Spatial Distribution of the Neutron Flux on the Surface of a Graphite-Lined Cavity
Sc.D. Thesis, M.I.T. Nucl. Eng. Dept., January 1962
(Thesis Supervisors: I. Kaplan and T. J. Thompson)

Weitzberg, Abraham
Measurements of Neutron Capture in U-238 in Lattices of Uranium Rods in Heavy Water
Ph.D. Thesis, M.I.T. Nucl. Eng. Dept., January 1962
(Thesis Supervisors: I. Kaplan and T. J. Thompson)

Palmedo, Philip F.
Measurements of the Material Bucklings of Lattices of Natural Uranium Rods in D_2O
Ph.D. Thesis, M.I.T. Nucl. Eng. Dept., January 1962
(Thesis Supervisors: I. Kaplan and T. J. Thompson)

Wolberg, John R.
A Study of the Fast Fission Effect in Lattices of Uranium Rods in Heavy Water
Ph.D. Thesis, M.I.T. Nucl. Eng. Dept., February 1962
(Thesis Supervisors: I. Kaplan and T. J. Thompson)

Peak, John
Theory and Use of Small Subcritical Assemblies for the Measurement of Reactor Parameters
Ph.D. Thesis, M.I.T. Nucl. Eng. Dept., April 1962
(Thesis Supervisors: I. Kaplan and T. J. Thompson)

Brown, Paul S.
Measurements of the Spatial and Energy Distribution of Thermal Neutrons in Uranium, Heavy Water Lattices
Ph.D. Thesis, M.I.T. Nucl. Eng. Dept., August 1962
(Thesis Supervisors: I. Kaplan and T. J. Thompson)

Simms, Richard
Analytical and Experimental Investigations of the Behavior of Thermal Neutrons in Lattices of Uranium Metal Rods in Heavy Water
Ph.D. Thesis, M.I.T. Nucl. Eng. Dept., October 1963
(Thesis Supervisors: I. Kaplan and T. J. Thompson)

Malaviya, Bimal K.
Studies of Reactivity and Related Parameters in Subcritical Lattices
Ph.D. Thesis, Physics Dept., Harvard University, May 1964
(Thesis Supervisors: I. Kaplan and D. D. Lanning
T. J. Thompson, on sabbatical leave)

D'Ardenne, Walter H.
Studies of Epithermal Neutrons in Uranium Heavy Water Lattices
Ph.D. Thesis, M.I.T. Nucl. Eng. Dept., August 1964
(Thesis Supervisors: I. Kaplan and D. D. Lanning
T. J. Thompson, on sabbatical leave)

Woodruff, Gene L.
A Study of the Spatial Distributions of Fast Neutrons in Lattices of Slightly Enriched Uranium Rods Moderated by Heavy Water
Ph.D. Thesis, M.I.T. Nucl. Eng. Dept., November 1965
(Thesis Supervisors: I. Kaplan and T. J. Thompson)

Harrington, Joseph
Use of Neutron Absorbers for the Experimental Determination of Lattice Parameters in Subcritical Assemblies
Sc.D. Thesis, M.I.T. Nucl. Eng. Dept., February 1966
(Thesis Supervisors: I. Kaplan and T. J. Thompson)

Bliss, Henry E.
Use of a Pulsed Neutron Source to Determine Nuclear Parameters of Lattices of Partially Enriched Uranium Rods in Heavy Water
Sc.D. Thesis, M.I.T. Nucl. Eng. Dept., September 1966
(Thesis Supervisors: I. Kaplan and T. J. Thompson)

Sefchovich, Elias
The Measurement of Reactor Parameters in Slightly Enriched Uranium, Heavy Water Moderated Miniature Lattices
Sc.D. Thesis, M.I.T. Nucl. Eng. Dept., October 1966
(Thesis Supervisors: I. Kaplan and T. J. Thompson)

2. M.S. THESES ON MITR HEAVY WATER LATTICE PROJECT

Quinteiro Blanco, Manuel
Design and Construction of an Automatic Neutron Flux Scanner for the M. I. T. Heavy Water Lattice Facility
M.S. Thesis, M. I. T. Nucl. Eng. Dept., February 1962
(Thesis Supervisor: T. J. Thompson)

Kielkiewicz, Marian S.
A Study of the Fast Fission Effect for Single Natural Uranium Rod
M.S. Thesis, M. I. T. Nucl. Eng. Dept., September 1962
(Thesis Supervisor: T. J. Thompson)

Kim, Hichull
Measurements of the Material Buckling of Lattice of Enriched Uranium Rods in Heavy Water
M.S. Thesis, M. I. T. Nucl. Eng. Dept., June 1963
(Thesis Supervisor: T. J. Thompson)

Harrington, Joseph
Measurement of the Material Buckling of a Lattice of Slightly Enriched Uranium Rods in Heavy Water
M.S. Thesis, M. I. T. Nucl. Eng. Dept., July 1963
(Thesis Supervisor: T. J. Thompson)

Bliss, Henry E.
Measurements of the Fast Effect in Heavy Water, Partially Enriched Uranium Lattices
M.S. Thesis, M. I. T. Nucl. Eng. Dept., May 1964
(Thesis Supervisor: D. D. Lanning)

Goebel, David M.
Return Coefficient Measurements for the M. I. T. Enriched Uranium-D_2O Lattice
M.S. Thesis, M. I. T. Nucl. Eng. Dept., May 1965
(Thesis Supervisor: D. D. Lanning)

Papay, Lawrence T.
Fast Neutron Fission Effect for Single Slightly Enriched Uranium Rods in Air and Heavy Water
M.S. Thesis, M. I. T. Nucl. Eng. Dept., June 1965
(Thesis Supervisor: D. D. Lanning)

Robertson, Cloin G.
Measurements of Neutron Utilization for Lattices of Slightly Enriched Uranium Rods.
M.S. Thesis, M. I. T. Nucl. Eng. Dept., June 1965
(Thesis Supervisor: D. D. Lanning)

Hellman, Sanford P.
Measurements of δ_{28} and ρ_{28} in a 2.5-Inch Triangular Lattice of 0.75-Inch Metallic Uranium Rods (0.947 wt% U^{235}) in a Heavy Water Moderator
M.S. Thesis, M.I.T. Nucl. Eng. Dept., September 1965
(Thesis Supervisor: T. J. Thompson)

Johnson, Malvin G.
A Radiation Detector for Noise Analysis on the MITR Subcritical Assembly
S.M. Thesis, M.I.T. Electrical Eng. Dept., September 1966
(Thesis Supervisor: F. M. Clikeman)

Hauck, Frederick H.
Investigation of Noise Analysis Techniques for the M.I.T. Heavy Water Lattice
S.M. Thesis, M.I.T. Nucl. Eng. Dept., August 1966
(Thesis Supervisors: F. M. Clikeman and M. J. Driscoll)

Ricketts, Robert L.
Development of Equipment Design, Experimental Procedures and Materials for Studying Lattices of UO_2 Fuel Rods in the M.I.T. Exponential Facility
S.M. Thesis, M.I.T. Nucl. Eng. Dept., August 1966
(Thesis Supervisor: M. J. Driscoll)

Price, Lee N.
A Systematic Study of Foil Correction Factors in the Measurement of δ_{28}, δ_{25}, ρ_{28} and C^* in Slightly Enriched, D_2O-Moderated Lattices
S.M. Thesis, M.I.T. Nucl. Eng. Dept., August 1966
(Thesis Supervisor: M. J. Driscoll)

Harper, Thomas L.
Analysis of Lattice Fuel Using Ge(Li) Gamma-Ray Spectrometry
S.M. Thesis, M.I.T. Nucl. Eng. Dept., August 1966
(Thesis Supervisors: N. C. Rasmussen and M. J. Driscoll)

Bowles, Kenneth D.
Investigations of the Void Effect in a Heavy Water Moderated, Organic-Cooled Assembly by the Pulsed Neutron Source Technique
S.M. Thesis, M.I.T. Nucl. Eng. Dept., September 1966
(Thesis Supervisors: T. J. Thompson and M. J. Driscoll)

3. LATTICE PROJECT PUBLICATIONS

3.1 Prior to September 30, 1965

J. T. Madell, T. J. Thompson, A. E. Profio, and I. Kaplan
Spatial Distribution of the Neutron Flux on the Surface of a Graphite-Lined Cavity
NYO-9657, MITNE-18, April 1962

A. Weitzberg, I. Kaplan, and T. J. Thompson
Measurements of Neutron Capture in U-238 Lattices of Uranium Rods in Heavy Water
NYO-9659, MITNE-11, January 8, 1962

P. F. Palmedo, I. Kaplan, and T. J. Thompson
Measurements of the Material Bucklings of Lattices of Natural Uranium Rods in D_2O
NYO-9660, MITNE-13, January 20, 1962

J. R. Wolberg, T. J. Thompson, and I. Kaplan
A Study of the Fast Fission Effect in Lattices of Uranium Rods in Heavy Water
NYO-9661, MITNE-15, February 21, 1962

J. Peak, I. Kaplan and T. J. Thompson
Theory and Use of Small Subcritical Assemblies for the Measurement of Reactor Parameters
NYO-10204, MITNE-16, April 9, 1962

P. S. Brown, T. J. Thompson, I. Kaplan and A. E. Profio
Measurements of the Spatial and Energy Distribution of Thermal Neutrons in Uranium, Heavy Water Lattices
NYO-10205, MITNE-17, August 20, 1962

K. F. Hansen
Multigroup Diffusion Methods
NYO-10206, MITNE-19, April 1962

I. Kaplan
Measurements of Reactor Parameters in Subcritical and Critical Assemblies: A Review
NYO-10207, MITNE-25, August 1962

I. Kaplan, D. D. Lanning, A. E. Profio and T. J. Thompson
Summary Report on Heavy Water, Natural Uranium Lattice Research
NYO-10209, MITNE-35, July 1963
(Presented at the IAEA Symposium on Exponential and Critical Experiments, Amsterdam, September 2-6, 1963)

J. R. Wolberg, T. J. Thompson and I. Kaplan
Measurement of the Ratio of Fissions in U-238 to Fissions in U-235 Using 1.60-Mev Gamma Rays of the Fission Product LA-140
NYO-10210, MITNE-36, 1963
(Presented at the IAEA Symposium on Exponential and Critical Experiments, Amsterdam, September 2-6, 1963)

R. Simms, I. Kaplan, T. J. Thompson and D. D. Lanning
Analytical and Experimental Investigations of the Behavior of Thermal Neutrons in Lattices of Uranium Metal Rods in Heavy Water
NYO-10211, MITNE-33, October 1963

B. K. Malaviya, I. Kaplan, T. J. Thompson and D. D. Lanning
Studies of Reactivity and Related Parameters in Slightly Enriched Uranium Heavy Water Lattices
MIT-2344-1, MITNE-49, May 1964

W. H. D'Ardenne, T. J. Thompson, D. D. Lanning and I. Kaplan
Studies of Epithermal Neutrons in Uranium, Heavy Water Lattices
MIT-2344-2, MITNE-53, August 1964

T. J. Thompson, I. Kaplan and A. E. Profio
Heavy Water Lattice Project Annual Report
NYO-9658, September 30, 1961

I. Kaplan, A. E. Profio and T. J. Thompson
Heavy Water Lattice Project Annual Report
NYO-10208, MITNE-26, September 30, 1962

I. Kaplan, D. D. Lanning and T. J. Thompson
Heavy Water Lattice Project Annual Report
NYO-10212, MITNE-46, September 30, 1963

D. D. Lanning, I. Kaplan and F. M. Clikeman
Heavy Water Lattice Project Annual Report
MIT-2344-3, MITNE-60, September 30, 1964

J. T. Madell, T. J. Thompson, A. E. Profio and I. Kaplan
Flux Distribution in the Hohlraum Assembly
Trans. Am. Nucl. Soc. 3, 420 (December 1960)

A. Weitzberg and T. J. Thompson
Coincidence Technique for U-238 Activation Measurements
Trans. Am. Nucl. Soc. 3, 456 (December 1960)

J. T. Madell, T. J. Thompson, I. Kaplan and A. E. Profio
Calculation of the Flux Distribution in a Cavity Assembly
Trans. Am. Nucl. Soc. 5, 85 (June 1962)

A. Weitzberg, J. R. Wolberg, T. J. Thompson, A. E. Profio and I. Kaplan
Measurements of U-238 Capture and Fast Fission in Natural Uranium, Heavy Water Lattices
Trans. Am. Nucl. Soc. 5, 86 (June 1962)

P. S. Brown, P. F. Palmedo, T. J. Thompson, A. E. Profio and I. Kaplan
Measurements of Microscopic and Macroscopic Flux Distributions in Natural Uranium, Heavy Water Lattices
Trans. Am. Nucl. Soc. 5, 87 (June 1962)

B. K. Malaviya and A. E. Profio
Measurement of the Diffusion Parameters of Heavy Water by the Pulsed-Neutron Technique
Trans. Am. Nucl. Soc. 6, 58 (June 1963)

B. K. Malaviya, T. J. Thompson and I. Kaplan
Measurement of the Linear Extrapolation Distance of Black Cylinders in Exponential Experiments
Trans. Am. Nucl. Soc. 6, 240 (November 1963)

P. S. Brown, I. Kaplan, A. E. Profio and T. J. Thompson
Measurements of the Spatial and Spectral Distribution of Thermal Neutrons in Natural Uranium Heavy Water Lattices
BNL-719, Vol. 2, 305-17, 1962

R. Simms, I. Kaplan, T. J. Thompson and D. D. Lanning
The Failure of the Cell Cylindricalization Approximation in Closely Packed Uranium, Heavy Water Lattices
Trans. Am. Nucl. Soc. 7, 9 (June 1964)

B. K. Malaviya, D. D. Lanning, A. E. Profio, T. J. Thompson and I. Kaplan
Measurement of Lattice Parameters by Means of the Pulsed-Neutron Technique
Paper presented at the ANS Winter Meeting, San Francisco, November 1964

B. K. Malaviya, I. Kaplan, D. D. Lanning and T. J. Thompson
Studies of the Reactivity Worth of Control Rods in Far Subcritical Assemblies
Trans. Am. Nucl. Soc. 8, 282 (June 1965)

3.2 Publications (Including Theses) Since September 30, 1965

T. J. Thompson, I. Kaplan, F. M. Clikeman and M. J. Driscoll
Heavy Water Lattice Project Annual Report
MIT-2344-4, MITNE-65, September 30, 1965

H. E. Bliss, D. D. Lanning, J. Harrington, I. Kaplan, B. K. Malaviya and T. J. Thompson
Studies of Subcritical Lattices with Distributed Neutron Absorbers by Means of the Pulsed Neutron Source Technique
Trans. Amer. Nucl. Soc. 8, 533 (November 1965)

E. E. Pilat, H. Gueron and D. D. Lanning
Measurement of Diffusion Coefficient in a Highly Anisotropic Medium
Trans. Amer. Nucl. Soc. 8, 446 (November 1965)

W. H. D'Ardenne, I. Kaplan, D. D. Lanning and T. J. Thompson
Reactor Physics Measurements in Slightly Enriched Uranium D_2O Lattices
Trans. Amer. Nucl. Soc. 8, 447 (November 1965)

M. J. Driscoll
The Heavy Water Lattice Program at M. I. T.
(Paper presented at June 1966 ASEE Meeting)

G. L. Woodruff, T. J. Thompson, I. Kaplan, and D. D. Lanning
A Kernel Method for Calculating the Spatial Distribution of Uncollided Neutrons Around Fuel Rods
Trans. Amer. Nucl. Soc. 9, 116 (June 1966)

B. K. Malaviya, I. Kaplan, T. J. Thompson and D. D. Lanning
Studies of Lattice Parameters in Pulsed and Steady-State Experiments on Subcritical Systems
Trans. Amer. Nucl. Soc. 9, 175 (June 1966)

M. G. Johnson
A Radiation Detector for Noise Analysis on the MITR Subcritical Assembly
S.M. Thesis, M.I.T. Elec. Eng. Dept., September 1966
(Thesis Supervisor: F. M. Clikeman)

F. H. Hauck
Investigation of Noise Analysis Techniques for the M. I. T. Heavy Water Lattice
S.M. Thesis, M.I.T. Nucl. Eng. Dept., August 1966
(Thesis Supervisors: F. M. Clikeman and M. J. Driscoll)

R. L. Ricketts
Development of Equipment Design, Experimental Procedures and Materials for Studying Lattices of UO_2 Fuel Rods in the M.I.T. Exponential Facility
S.M. Thesis, M.I.T. Nucl. Eng. Dept., August 1966
(Thesis Supervisor: M. J. Driscoll)

L. N. Price
A Systematic Study of Foil Correction Factors in the Measurement of δ_{28}, δ_{25}, ρ_{28} and C^* in Slightly Enriched, D_2O-Moderated Lattices
S.M. Thesis, M.I.T. Nucl. Eng. Dept., August 1966
(Thesis Supervisor: M. J. Driscoll)

T. L. Harper
Analysis of Lattice Fuel Using Ge(Li) Gamma-Ray Spectrometry
S.M. Thesis, M.I.T. Nucl. Eng. Dept., August 1966
(Thesis Supervisors: N. C. Rasmussen and M. J. Driscoll)

K. D. Bowles
Investigations of the Void Effect in a Heavy Water Moderated, Organic-Cooled Assembly by the Pulsed Neutron Source Technique
S.M. Thesis, M.I.T. Nucl. Eng. Dept., September 1966
(Thesis Supervisors: T. J. Thompson and M. J. Driscoll)

G. L. Woodruff, I. Kaplan and T. J. Thompson
A Study of the Spatial Distributions of Fast Neutrons in Lattices of Slightly Enriched Uranium Rods Moderated by Heavy Water
MIT-2344-5, MITNE-67, November 1965

J. Harrington, D. D. Lanning, I. Kaplan and T. J. Thompson
Use of Neutron Absorbers for the Experimental Determination of Lattice Parameters in Subcritical Assemblies
MIT-2344-6, MITNE-69, February 1966

H. E. Bliss, I. Kaplan and T. J. Thompson
Use of a Pulsed Neutron Source to Determine Nuclear Parameters of Lattices of Partially Enriched Uranium Rods in Heavy Water
MIT-2344-7, MITNE-73, September 1966

E. Sefchovich, I. Kaplan and T. J. Thompson
The Measurement of Reactor Parameters in Slightly Enriched Uranium, Heavy Water Moderated Miniature Lattices
MIT-2344-8, MITNE-76, October 1966